Peter Uppstu

Bioresorbable Polymer–Bioactive Glass Composite Scaffolds for Bone Regeneration

Åbo Akademi University

Bioresorbable Polymer–Bioactive Glass Composite Scaffolds for Bone Regeneration

Peter Uppstu

Polymer Technology
Faculty of Science and Engineering
Åbo Akademi University
Turku, Finland, 2024

Supervisors

Professor Carl-Eric Wilén
Laboratory of Molecular Science and Engineering
Åbo Akademi University
Turku, Finland

Dr Saara Inkinen
Nordic Catalyst e.U.
Vienna, Austria

Pre-examiner and opponent

Professor Emeritus Jukka Seppälä
Department of Chemical and Metallurgical Engineering
Aalto University
Helsinki, Finland

Pre-examiner

Dr Timothy E.L. Douglas
School of Engineering
Lancaster University
Lancaster, United Kingdom

ISBN 978-952-12-4337-0 (printed)
ISBN 978-952-12-4338-7 (digital)
Painosalama; Turku, Finland 2023

Till Ida, Aron och Iris

Acknowledgements

The work presented in this book was carried out at Polymer Technology, Faculty of Science and Engineering, Åbo Akademi University.

I would like to express my sincere gratitude to my supervisors Prof Carl-Eric Wilén and Dr Saara Inkinen. Calle, thank you for your strong support in my research, for letting me do a lot of teaching, and for your deep insights in all polymer-related aspects that you have shared over the years. Thank you also for giving me the opportunity to work with many different projects. Saara, thank you for your thoughtful views, your endless enthusiasm, and for your invaluable guidance in my research. I am super happy for your continued support and friendship, even though your own life has drifted away from our labs. I am also very grateful to my former supervisor Dr Ari Rosling who introduced me to the fascinating world of medical biomaterials.

I would like to thank the pre-examiners, Prof Jukka Seppälä and Dr Timothy Douglas, for all their insightful comments and suggestions to improve the scientific quality of this work. I am also deeply grateful to Jukka Seppälä for serving as the opponent for the thesis. Tack så mycket båda två!

This work would not have been possible to conduct without the contributions of my supervisees Charlotta Paakki and Simon Engblom, who were responsible for important steps in the synthesis and characterisation of scaffolds. You were great to work with, and you did great work. And you worked a lot. A huge thank you to you both!

The research work for three of the articles within this thesis was conducted within a project together with Tampere University and the University of Helsinki. Anne-Marie Haaparanta and Eve Salonius, thank you very much for your comprehensive research work with the different kinds of scaffolds *in vitro* and *in vivo* that is presented in this thesis. It was awesome to work with you, as well as with the whole group, including Virpi Muhonen, Ilkka Kiviranta, Minna Kellomäki, and others! Anne-Marie and Virpi, congratulations for your continuation with Askel Healthcare, and all the success to you to the remaining clinical trials. Eve and Ilkka, I admire you for your work with one of the most stubborn tissues in the human body. Minna, a warm thank you for your collaboration and all the expertise that you have shared.

Over the years, I have learned to appreciate the potential that bioactive glasses offer for tissue regeneration. For what I have learned of glass, I would most warmly want to thank Leena Hupa for always instructing in a knowledgeable and friendly manner, both regarding glass and also science in general. In the glass labs, I had the fortune to work with Laura Aalto-Setälä. Laura, thank you for all the discussions about glass and its inner life and for all your peer support! Minna Siekkinen, Polina Sinitsyna and Adrian Stiller, a big thank you for your collaboration and overwhelming kindness. Hopefully we can do nice research together in the future! Through the years I have got

multiple times invaluable help with syntheses and measurements – Jaana, Jalle, and Linus, thank you, you have been so nice to work with!

I would like to thank Nina Lindfors, Robert Björkenheim, Gustav Strömberg, Elin Eriksson, and Jukka Pajarinen for your collaboration in our fascinating induced membrane research, which for me has been running alongside my thesis project. It has been a pleasure to work with you, and we have got really interesting results! Thank you also to Jimmy Lucchesi and Fredrik Ollila from Bonalive for your contributions to the project.

Over the years, I have had the honour to be working with so many talented people in our lab: Timo, Amira, Ana, Yury, Kuldeep, Vishal, Ilona, Adèle, Mélanie, Mo, Chen, Marco, Tatu, Humayun, Kamran, Haolin, Xue (and Wenyang!), Anton, Pernilla, Maria, Weronika, Yanxi, Virpi, Mia, Kalle, Roger, and all others. Thank you all for your friendship and joy! Especially I would like to thank Teija (see, I did not forget you), thank you so much for all the help and knowledge that you have shared over the years in so many different matters. Thank you also to Mia Mäkinen, Annika Fougstedt, Eva Harjunkoski, Linda Nisula, and Paula Ojala for patiently responding to all kinds of questions and requests that usually arrive more or less in a hurry.

I would also like to thank our organic tigers, especially Tiina, Patrik, Reko, Janne, Robert, Denys, Jani, Magnus, Filip, and others for being so good neighbours over the years. Thank you to Niko Moritz, Julia Kulkova, and Artem Plyusnin for the insightful journeys into the multifaceted field of biomaterial startups, and best of luck with all future challenges! I am grateful to Pekka Vallittu, Chunlin Xu, and Sufyan Garoushi for hosting all the biomaterial-related events in Turku. Jessica Rosenholm, thank you for leading the Madness, I very much look forward to our future collaboration, together with Hongbo, Tappi, Kuldeep, Xiaoju, Chunlin, Ivan, Sébastien, Calle, and others!

For my scientific work I have received many smaller and some bigger grants, and I am very grateful for all the support from The Swedish Cultural Foundation in Finland, Waldemar von Frenckells stiftelse, Medicinska Understödsföreningen Liv och Hälsa, The Åbo Akademi University Foundation, Finnish Academy of Science and Letters, Rector of Åbo Akademi, The Finnish Foundation for Technology Promotion, and Business Finland.

I would like to thank my Mom, Dad, and my brother Andreas, for always being there for me and supporting me in all kinds of ways. Thank you also to Sami, Hannele, and Arto, for all your assistance and friendship.

My biggest gratitude goes to my family. Ida, Aron, and Iris, thank you for making every day exciting and colourful, and for being exactly the ones that you are. Päivi, my sincerest gratitude for all the support, understanding, and knowledge that you have contributed with, and thank you immensely for being there with me. I love you all.

Turku, December 2023

Peter Uppstu

Abstract

Bone defects, caused by disease or trauma, pose a significant challenge in medical care. Bone tissue transplants are commonly used for their treatment, and bone is the second most transplanted tissue in the world. Because of inherent issues relating to the transplants, synthetic materials are investigated for use as bone graft substitutes. In the research covered in this thesis, we studied synthetic three-dimensional scaffolds for bone regeneration. The aim of these scaffolds is to fill bone defects, allow cells from nearby tissues to enter their pores, and promote new tissue formation as they degrade. Ideally, as the scaffold is completely degraded, the defect site will be filled with newly formed bone. Using different methods, we manufactured porous scaffolds with either a polymer matrix or a bioactive glass matrix and studied their degradation *in vitro* in aqueous degradation media. We also tested two of the scaffolds for their ability to support bone formation in an *in vivo* model.

In the first two articles, we manufactured poly(lactide-co-glycolide) (PLGA)-based scaffolds with the gas foaming and freeze drying techniques, with or without incorporation of bioactive glass or magnesium hydroxide, and evaluated their degradation *in vitro*. Several scaffolds underwent unwanted shrinkage, and their pore structure was not satisfactory. However, the innovative approach of integrating bioactive glass fibres into freeze-dried structures resulted in dimensionally stable scaffolds featuring well-interconnected porosity. We also studied the magnesium ion release from gas-foamed scaffolds. As the role of magnesium in bone regeneration may vary in time during the healing process, it may be beneficial to regulate the magnesium release temporally, with a higher initial release followed by rapidly decreasing release concentrations. Scaffolds with magnesium-containing bioactive glasses released low concentrations of magnesium, whereas scaffolds with magnesium hydroxide provided a significantly higher and more immediate release, which may be particularly beneficial for the bone healing process.

In the third article, two scaffolds, one gas-foamed PLGA scaffold and one freeze-dried PLGA scaffold with bioactive glass fibres, were tested in a bone regeneration model *in vivo* and compared with commercial bone graft substitutes. Whereas bone healed well with the commercial materials, the tissue regeneration with the experimental scaffolds was not equally good. The unsatisfactory performance of the experimental scaffolds was likely due to their pore size and pore interconnectivity. Pore interconnectivity of the gas-foamed PLGA scaffolds was presumably too low to allow for efficient bone ingrowth, and the pore size of the freeze-dried PLGA–bioactive glass scaffolds was probably too small to allow for dense vascularisation within the scaffold structure, thus inhibiting extensive bone ingrowth.

In the last study, we manufactured porous bioactive glass scaffolds with different polylactide (PLA) coating stereochemistries. The aim was to find out similarities and differences in the mechanical and degradation properties of

amorphous, homocrystalline, and stereocomplex crystalline PLA. Although the coatings were only 3 wt.% of the glass scaffold mass, scaffolds coated with PLA had an approximately four-fold higher compressive toughness before immersion and a two-fold higher toughness after immersion in simulated body fluid. Both homocrystalline and stereocomplex crystalline PLA had significantly higher toughness than the amorphous coatings. The coatings also moderated the initial pH peak caused by the bioactive glass, which may be beneficial in an *in vivo* setting.

Overall, the results in this thesis provide insights into the feasibility of scaffold materials and structures for bone regeneration and the biological requirements for bone growth within the scaffolds. An optimised pore structure should be sought with methods that have a high repeatability and require minimal manual work, such as additive manufacturing techniques. By making informed choices of bioresorbable polymers, for example through variations in the polymer stereochemistry, or by optimisation of the release pattern of biologically active substances, it could be possible to produce scaffolds tailored to exhibit specific properties essential for effective bone regeneration.

Sammanfattning

Benskador som orsakats av sjukdomar eller olyckor är vanligt förekommande och utgör en betydande utmaning inom medicinsk behandling. Transplantat av benvävnad används ofta i behandlingen, och benvävnad är den näst mest transplanterade vävnaden i världen. På grund av problem och begränsningar med transplantaten undersöks syntetiska material som substitut för dem. I den här avhandlingen undersökte vi syntetiska tredimensionella stödstrukturer, så kallade scaffolds, för återbildning av benvävnad. Syftet med stödstrukturerna är att fylla bendefekterna, låta celler från omkringliggande vävnader tränga in i deras porer, och understöda återbildningen av vävnad när de nedbryts. Idealt fylls defekterna slutligen helt och hållet med nybildad vävnad. Vi använde olika metoder för att framställa stödstrukturer, som bestod av en kontinuerlig struktur av endera bionedbrytbar polymer eller bioaktivt glas, och undersökte deras nedbrytning *in vitro* i vattenlösningar som simulerar kroppsförhållanden. Vi testade även två typer av stödstrukturer för att utvärdera deras förmåga till benåterbildning i en *in vivo*-modell.

I de två första artiklarna framställde vi stödstrukturer av poly(laktid-sam-glykolid) (PLGA) med gasskumning och frystorkning, endera med eller utan tillsats av bioaktivt glas eller magnesiumhydroxid. I nedbrytningstesterna krympte flera av de framställda stödstrukturerna, med en olämplig porstruktur som följd. Genom att integrera fibrer av bioaktivt glas i frystorkade stödstrukturer lyckades vi åstadkomma en öppen porstruktur och god dimensionsstabilitet. Vi undersökte även magnesiumfrisättningen från gasskummade stödstrukturer. Eftersom funktionen av magnesium i benåterbildningen varierar i olika stadier av återbildningsprocessen, kan det vara fördelaktigt att reglera frisättningen tidsmässigt, med en hög frisättning i början och med snabbt avtagande nivåer därefter. Stödstrukturer med magnesiuminnehållande bioaktivt glas frisatte magnesium i låga och relativt stadiga koncentrationer, medan stödstrukturer med tillsatt magnesiumhydroxid uppvisade en mycket högre men snabbare avtagande frisättning, vilket kan vara fördelaktigt för benåterbildningen.

I den tredje artikeln undersöktes benåterbildningsförmågan *in vivo* för stödstrukturer framställda av gasskummat PLGA och frystorkat PLGA med fibrer av bioaktivt glas. Dessa experimentella stödstrukturer jämfördes med två kommersiella bensubstitut. Benvävnaden återbildades väl med de kommersiella materialen, medan vävnadstillväxten inte var lika bra för de experimentella implantaten. De otillfredsställande resultaten för de experimentella stödstrukturerna berodde troligtvis på porstrukturen och porstorleken, vilka inte var optimala för benåterbildningen. Porstrukturen hos gasskummade stödstrukturer var troligtvis för instängd, med för få öppna porer, och porstorleken hos de frystorkade stödstrukturerna var troligtvis för liten för att möjliggöra en tillräcklig blodkärlsåterbildning.

I den sista studien framställde vi porösa stödstrukturer av bioaktivt glas med beläggningar av polylaktid (PLA) med olika stereokemier. Syftet var att karakterisera mekaniska egenskaper och nedbrytningsegenskaper hos amorf, homokristallin och stereokomplext kristallin PLA. Fastän beläggningarna utgjorde enbart 3 vikt-% av glasstrukturens massa, hade stödstrukturerna med polymerbeläggning ungefär fyra gånger högre kompressionsseghet före immersion och två gånger högre seghet efter immersion i simulerad kroppsvätska. De båda delkristallina beläggningarna uppvisade högre seghet än de amorfa beläggningarna. Beläggningarna även begränsade den initiala pH-ökningen som förorsakas av det bioaktiva glaset, vilket kan vara fördelaktigt *in vivo*.

Generellt ger resultaten i den här avhandlingen insikter om möjligheterna för material och strukturer att återbilda benvävnad, samt om de biologiska betingelserna som möjliggör benåterbildning inne i stödstrukturerna. En optimerad porstruktur bör eftersträvas med metoder som har hög upprepbarhet och kräver minimalt av manuellt arbete, till exempel genom användning av additiv tillverkning. Genom välgrundade val av biologiskt nedbrytbara polymerer, såsom genom variationer i polymerens stereokemi eller genom optimering av frisättningsmönstret för biologiskt aktiva ämnen, kan det vara möjligt att framställa stödstrukturer som är anpassade för att uppvisa specifika egenskaper som är väsentliga för effektiv benåterbildning.

List of original publications

I. **Uppstu P**, Paakki C, Rosling A. In vitro hydrolysis and magnesium release of poly(D,L-lactide-co-glycolide)-based composites containing bioresorbable glasses and magnesium hydroxide. *Journal of Applied Polymer Science*. 2015;132:42646.

II. Haaparanta AM, **Uppstu P**, Hannula M, Ellä V, Rosling A, Kellomäki M. Improved dimensional stability with bioactive glass fibre skeleton in poly(lactide-co-glycolide) porous scaffolds for tissue engineering. *Materials Science and Engineering: C*. 2015;56:457–66.

III. Salonius E, Muhonen V, Lehto K, Järvinen E, Pyhältö T, Hannula M, Aula AS, **Uppstu P**, Haaparanta AM, Rosling A, Kellomäki M, Kiviranta I. Gas-foamed poly(lactide-co-glycolide) and poly(lactide-co-glycolide) with bioactive glass fibres demonstrate insufficient bone repair in lapine osteochondral defects. *Journal of Tissue Engineering and Regenerative Medicine*. 2019;13(3):406–15.

IV. **Uppstu P**, Engblom S, Inkinen S, Hupa L, Wilén C-E. Influence of polylactide coating stereochemistry on mechanical and in vitro degradation properties of porous bioactive glass scaffolds for bone regeneration. *Journal of Biomedical Materials Research Part B*. 2024; 112(1):e35328.

List of related publications

V. Björkenheim R, Strömberg G, Pajarinen J, Ainola M, **Uppstu P**, Hupa L, Böhling TO, Lindfors NC. Polymer-coated bioactive glass S53P4 increases VEGF and TNF expression in an induced membrane model in vivo. *Journal of Materials Science*. 2017;52(15):9055–65.

VI. Xu W, Pranovich A, **Uppstu P**, Wang X, Kronlund D, Hemming J, Öblom H, Moritz N, Preis M, Sandler N, Willför S, Xu C. Novel biorenewable composite of wood polysaccharide and polylactic acid for three dimensional printing. *Carbohydrate Polymers*. 2018;187:51–8.

VII. Björkenheim R, Strömberg G, Ainola M, **Uppstu P**, Aalto-Setälä L, Hupa L, Pajarinen J, Lindfors NC. Bone morphogenic protein expression and bone formation are induced by bioactive glass S53P4 scaffolds in vivo. *Journal of Biomedical Materials Research Part B: Applied Biomaterials*. 2019;107(3):847–57.

VIII. Plyusnin A, Kulkova J, Arthurs G, Jalava N, **Uppstu P**, Moritz N. Biological response to an experimental implant for tibial tuberosity advancement in dogs: A pre-clinical study. *Research in Veterinary Science*. 2020;128:183–96.

IX. Björkenheim R, Jämsen E, Eriksson E, **Uppstu P**, Aalto-Setälä L, Hupa L, Eklund KK, Ainola M, Lindfors NC, Pajarinen J. Sintered S53P4 bioactive glass scaffolds have anti-inflammatory properties and stimulate osteogenesis in vitro. *European Cells & Materials*. 2021;41:15–30.

X. Eriksson E, Björkenheim R, Strömberg G, Ainola M, **Uppstu P**, Aalto-Setälä L, Leino V-M, Hupa L, Pajarinen J, Lindfors NC. S53P4 bioactive glass scaffolds induce BMP expression and integrative bone formation in a critical-sized diaphysis defect treated with a single-staged induced membrane technique. *Acta Biomaterialia*. 2021;126:463–76.

XI. Aalto-Setälä L, **Uppstu P**, Sinitsyna P, Lindfors NC, Hupa L. Dissolution of Amorphous S53P4 Glass Scaffolds in Dynamic In Vitro Conditions. *Materials*. 2021;14(17):4834.

XII. Strömberg G, Aalto-Setälä L, **Uppstu P**, Björkenheim R, Pajarinen J, Eriksson E, Lindfors NC, Hupa L. Development and Characterization of Non-coated and PLGA-Coated S53P4 and S59 Bioactive Glass Scaffolds for Treatment of Load-Bearing Defects. *Biomedical Materials & Devices*. 2023:https://doi.org/10.1007/s44174-023-00099-4

Patent application

I. Ollila F, Lindfors N, Björkenheim R, Strömberg G, Hupa L, **Uppstu P**, Pajarinen J. A bone implant. WO2018065665A1, 2018.

The author's contributions

Publication I	The author participated in the planning of the work and conducted all laboratory work together with C. Paakki. The author was responsible for the interpretation of the results and for writing the paper.
Publication II	The author polymerised and purified the polymers and was responsible for part of their characterisation. The author participated in the interpretation of the results and in the review of the manuscript.
Publication III	The author participated in the planning of the material-related aspects of the work, polymerised and purified the polymers and was responsible for their characterisation. The author participated in the review of the manuscript.
Publication IV	The author planned the work together with the supervisors. The author conducted all laboratory work and analyses together with S. Engblom. The author was responsible for the interpretation of the results and for writing the paper.

Definitions

Bioabsorption	Absorption and elimination of substances from the body through natural pathways (in practice often synonymous with bioresorption)
Bioactivity	The ability of a glass to form a hydroxycarbonate apatite layer on its surface after implantation in the body
Biocompatibility	The ability of a material to perform with an appropriate host response in a specific application
Biodegradation	Breakdown of a material mediated within a biological system
Biomaterial	A material designed to take a form that can direct, through interactions with living systems, the course of any therapeutic or diagnostic procedure
Bioresorption	Degradation and elimination of substances from the body through natural pathways (in practice often synonymous with bioabsorption)
Implant	A medical device made from one or more biomaterials that is intentionally placed, either totally or partially, within the body
Scaffold	A biomaterial structure that serves as a substrate and guide for tissue repair and regeneration

Abbreviations

ACP	Amorphous calcium phosphate
ANOVA	Analysis of variance
BMP	Bone morphogenetic protein
β-TCP	β-tricalcium phosphate
Đ	Dispersity (M_w/M_n)
DBM	Demineralised bone matrix
EDX	Energy dispersive X-ray
EMA	European Medicines Agency (EU)
FDA	Food and Drug Administration (US)
GPC	Gel permeation chromatography
HCA	Hydroxycarbonate apatite
ICP-OES	Inductively coupled plasma optical emission spectroscopy
μCT	X-ray microtomography
M_n	Number average molecular weight
MSC	Mesenchymal stem cell
M_w	Weight average molecular weight
PBS	Phosphate-buffered saline
PCL	Polycaprolactone
PDLA	Poly(D-lactide)
PDLLA	Poly(D,L-lactide)
PGA	Polyglycolide
PLA	Polylactide or poly(lactic acid)
PLLA	Poly(L-lactide)
PLGA	Poly(lactide-co-glycolide)
PTFE	Polytetrafluoroethylene
ROP	Ring-opening polymerisation
RT	Room temperature
SBF	Simulated body fluid
SEM	Scanning electron microscopy
TGA	Thermogravimetric analysis
Tris	Tris(hydroxymethyl)aminomethane

Table of contents

1. Introduction

Bone defects may originate from disease, trauma, or congenital issues. Each year, 160–190 million new bone fractures occur globally (1), with 5–10% of all fractures resulting in non-union or otherwise incomplete healing (2). The defects may have long-standing effects on the health and quality of life for the patient, and they cause significant costs to society.

Bone defects may be treated with various methods, depending on factors such as the cause, size, and location of the injury, the patient's age, the risk of infection, or complications from other treatments. Depending on their situation, the patients have also personal preferences and recovery goals. Minor bone defects may heal spontaneously over time without any interventions, and simple fractures with minimal bone loss can recover with proper temporary stabilisation, for instance by casting. Extensive bone defects, on the other hand, usually require surgical intervention, and in many cases, follow-up surgeries are necessary. Fractures may be stabilised with the help of screws, plates, or pins, and defects with significant bone loss may require a bone void filler which promotes regeneration of the tissue. Defects that require graft material for healing are termed critical-sized defects (3). In long bones, such as the tibia, a segmental defect may be considered critical-sized if it exceeds 2.5 cm in length (4,5).

Bone grafts are used to fill the defect site and promote bone ingrowth. Over time, they degrade or are remodelled, allowing the defect site to be completely filled with newly formed bone. While biological grafts, such as bone autografts taken from another part of the patient's body, are effective, they have limitations regarding graft availability and donor site morbidity. Therefore, synthetic materials and structures for bone regeneration are being developed (6). The materials, which are in the shape of granules, pastes, or putties, are commonly inorganic, such as calcium sulphate, β-tricalcium phosphate (β-TCP), hydroxyapatite, or different kinds of bioactive glasses (7). These synthetic bone graft substitutes can be used either as such, or in combination with biological grafts, and they are efficient in the treatment of small defects.

In contrast to small defects, the treatment of large bone defects is often demanding. These defects are characterised by a significantly disrupted vascularisation and are frequently associated with extensive soft tissue damage. Treatment options range from different kinds of bone grafts, staged bone grafting (with the induced membrane technique), and distraction osteogenesis, to limb shortening, or even amputation as a last option (8). To overcome limitations with existing treatment modalities, three-dimensional porous scaffolds are being developed as a potential solution. The scaffolds are used to fill the defect site, with cells from the surrounding tissue entering the pores of the scaffold. Assisted by the favourable environment within the scaffold, the cells proliferate and begin to produce new tissue. Ideally, when the

entire scaffold has completely degraded, the defect site becomes filled with newly formed bone tissue.

Various resorbable biomaterials have been developed and tested for use in scaffolds for bone regeneration, such as bioresorbable polymers and bioactive glasses. Many bioresorbable polymers are biocompatible, they can easily be processed into desired shapes, and they have highly tuneable properties. Bioactive glasses have unique properties that are beneficial for bone growth, including release of biologically active ions, and formation of a bone mineral-like layer on the glass surface after implantation. With polymer–bioactive glass composite scaffolds, it is possible to combine the mechanical properties and processability of the polymers with the bioactive properties of the glasses (9–13). However, for various reasons, synthetic scaffolds for large bone defects are not yet widely used in the clinics (8).

In this thesis work, we developed and tested synthetic three-dimensional scaffolds for bone regeneration *in vitro* and *in vivo*. We produced porous structures of bioresorbable polymers and bioactive glasses with gas foaming, freeze drying, or foam replication techniques. We evaluated their properties before and after immersion in simulated body fluids, and in an *in vivo* bone regeneration model. The aim with these studies was to develop and test new materials and structures for bone regeneration. Where applicable, the definitions of specific terms used in this thesis follow recent consensus definitions within the field (14,15).

2. Bone tissue

Bone tissue defines the shape and structure of vertebrate bodies. Bones serve as attachment sites for muscles and tendons, protect vital organs, and serve as reservoirs for minerals such as calcium and phosphorus. Bone marrow, which is found in cavities inside bones, contains multipotent stem cells and produces blood cells. Bone is a vascularised tissue and one of the few tissues in the body that has the inherent ability to regenerate even during adulthood.

To effectively design synthetic materials for bone regeneration, a thorough understanding of the structure and growth of bone tissue is required. In this chapter, the fundamental components of bone structure and its healing mechanisms are presented.

2.1. Structure of bone

There are four general types of bones in the human skeleton: long bones, short bones, flat bones, and irregular bones (16). Long bones, such as the tibia and femur, are located mainly in the extremities, and short bones in the hands and feet. Flat bones include the ribs and several bones in the head, and irregular bones are found, for example, in the vertebrae. Approximately 80% of the bone matrix in humans is composed of dense cortical bone, with the remaining 20% consisting of spongy trabecular bone, also called cancellous bone. Cortical bone forms the cortex, or outer shell, of the bones. Trabecular bone consists of a porous network of bone trabeculae inside bones. All bone tissue is vascularised, and it is periodically renewed through the action of bone cells. Cancellous bone is metabolically more active and remodelled more often than cortical bone (17).

Long bones are macroscopically structured as long shafts with bulbous rounded ends. The shaft, called diaphysis, consists of a cylindrical hollow channel of cortical bone. The medullary cavity inside of the channel contains yellow bone marrow which is a source of mesenchymal stem cells (MSCs) that are able to differentiate into several kinds of mature cells. The ends of long bones, epiphyses, consist of trabecular bone enveloped by a thin surface layer of cortical bone. The red bone marrow is located inside pores within trabecular bone, and produces red blood cells, white blood cells, and platelets. The region between the diaphysis and the epiphysis is called metaphysis.

The ends of long bones are covered with articular cartilage, which acts as a cushioning layer between adjacent bones and facilitates smooth joint movement by reducing friction. A dense layer of well-vascularised connective tissue containing osteoblast precursor cells, the periosteum, covers the remaining bone surface, facilitating nutrient delivery to the bone (18).

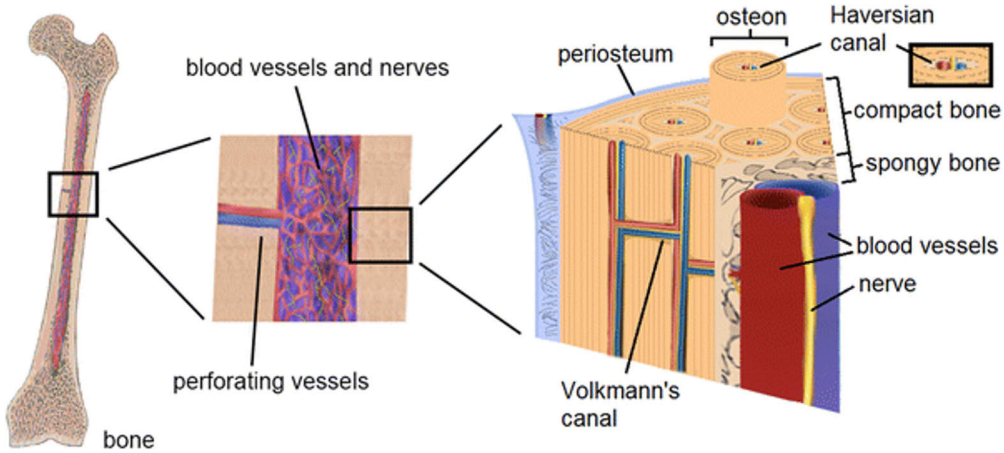

Figure 1. Structure of bone displaying magnified cross-sectional areas of the femur. Reprinted with permission from (18). © Springer Nature 2015.

Microscopically, remodelled compact bone tissue is composed of osteons comprising longitudinal lamellae of mineralised bone matrix encircling a central Haversian canal (19). Blood vessels within the Haversian canals are central for the nutrient supply of the bone tissue. Haversian canals are connected by transversally oriented Volkmann's canals. The macroscopic and microscopic appearance of bone tissue is depicted in Figure 1.

On a molecular level, bone tissue is an inorganic–organic composite material. Its main constituents are the bone mineral, i.e. carbonated apatite (approximately 65 wt.%), the organic phase mainly consisting of fibrous collagen type I protein (25 wt.%), and water (10 wt.%) (20). The primary structural unit is the mineralised collagen fibril, where apatite nanocrystals are dispersed within and around an oriented matrix of crosslinked collagen. Bone mineral is often approximated as the composition of pure hydroxyapatite $Ca_{10}(PO_4)_6(OH)_2$. However, its composition varies due to the presence of different cationic and anionic species, such as CO_3^{2-}, which can make up more than 5% of the total weight (21). Due to these significant impurities, bone mineral has a lower degree of crystallinity than pure synthetic hydroxyapatite (22). The mineral phase makes bone tissue strong, the organic phase gives ductility and toughness, and water is believed to have a plasticizing effect for increased toughness (22). Therefore, bone exhibits exceptional mechanical properties, such as high rigidity and toughness, in relation to its weight (23).

2.2. Bone growth and healing

Bone is a dynamic, vascularised tissue that constantly remodels. Along with skin, epithelial tissue, and liver, bone is one of the few tissues in the body which have the natural capability to regenerate, although to a limited extent, even in adult life.

The three types of bone cells are osteoblasts, osteoclasts, and osteocytes. Bone tissue is constantly remodelled by resorption of old bone by osteoclasts and formation of new bone tissue by osteoblasts. The osteoblasts eventually become trapped within the bone matrix that they secrete, and mature into osteocytes (24). Through the remodelling activity, bone tissue adapts to changing mechanical conditions according to Wolff's law (25). With increased loading on the bone, the tissue may become denser or change orientation according to the load. In the inverse event of decreased bone loading, bone resorption with a decrease in bone tissue density may occur. However, Wolff's law is not universally applicable. Bone adaptation is biologically comprised of a variety of different processes, and there are also other signals than mechanical strains that trigger bone deposition or resorption (26). If a very stiff implant is used to stabilise bone tissue, it may not allow the bone to be stressed properly. As the bone does not receive sufficient mechanical stimulus, stress shielding with a loss of bone tissue may lead to loosening of the implant and a new bone fracture (27). An imbalance in the action of osteoblasts and osteoclasts may result in diseases such as osteoporosis (28).

Bone growth may occur via two osteogenic pathways: endochondral ossification and intramembranous ossification. During the growth of a child, most bones in the face and skull are formed via intramembranous ossification, whereas long bones are formed through endochondral ossification. Both pathways begin with recruitment of MSCs and their differentiation directed by growth factors and cytokines (29). In intramembranous ossification, the MSCs differentiate to osteoblasts to directly form new bone. In endochondral ossification, MSCs differentiate into chondrocytes to form a cartilaginous template, which is calcified, and osteoblasts begin to form bone around the template. Although the pathways that form the bone are different, the formed bone tissue will be similar irrespective of the pathway that led to its formation. The type of bone regeneration pathway in fractures depends, among other factors, on the amount of strain in the fracture gap: small strains below 2–5% promote intramembranous ossification, strains smaller than 15% promote endochondral ossification, and larger strains promote the formation of connective tissue (30,31). It has been found that endosteal stem cells drive endochondral ossification, and periosteal stem cells drive bone formation through the intramembranous ossification pathway (32). Both endochondral and intramembranous ossification pathways may be active within the same fracture (2).

With a minimal fracture gap and a rigid fixation, such as when a locking plate is used, bone may be healed directly through primary fracture healing. In these conditions, the healing resembles normal bone remodelling. Bone resorbs at the fracture line by osteoclasts and new bone tissue is deposited by osteoblasts, with a re-establishment of the Haversian system (33).

In most cases, bone fractures heal through secondary fracture healing, which may involve both the endochondral and intramembranous ossification pathways. The multi-stage process has earlier been divided into three

consecutive phases, involving inflammation, repair, and remodelling (34), but in recent literature, a more refined view with five interdependent and overlapping phases has been proposed (35). The first stage is pro-inflammatory and characterised by the formation of a blood clot, or haematoma, resulting from the breakage of blood vessels when the bone fractures. This proinflammatory stage is seen as critical for the tissue regeneration process and is complete within seven days (36). An anti-inflammatory stage follows, with a disturbed oxygen supply because of the broken vessels. The traumatised area is hypoxic, which stimulates new vessel formation (35,37). During the repair phase, at first, a soft callus is formed by hyaline cartilage, after which the matrix is mineralised into a hard callus with immature randomly oriented woven bone. Finally, the bone tissue is reorganised by remodelling of the bone into highly oriented lamellar bone to match the mechanical stimuli. Throughout the bone healing cascade, the chemical, mechanical, and biological properties of the bone healing environment are constantly evolving (35).

3. Materials and scaffolds for bone regeneration

Both natural and synthetic materials may be used for promoting bone regeneration. They have different biological properties based on their origin, chemical composition, and structure. The materials can be divided into osteoconductive, osteoinductive, and osteogenic materials (38,39). Osteoconductive materials, such as synthetic calcium sulphates and calcium phosphates, provide a favourable environment and suitable surfaces for hosting MSCs, osteoblasts, and osteoclasts for bone growth. Osteoinductive materials have the capability to induce bone formation in extraskeletal sites (sites outside of the native bone tissue) by recruitment of undifferentiated and pluripotent cells and stimulating them to develop into bone forming cells. For example, both bone morphogenetic proteins (BMPs) and synthetic biphasic calcium phosphate, composed of hydroxyapatite and β-TCP, are often considered to be osteoinductive (40,41). Osteogenic materials are defined as materials that contain viable cells that can differentiate into bone. Biological bone grafts may be osteogenic if they contain living cells. Synthetic tissue engineered grafts, in which porous scaffolds have been seeded with bone forming cells, may also be osteogenic. Osteostimulation is an additional term that has been coined to describe the potential of bioactive glasses to activate progenitor cells via their dissolution products into producing more bone (42). Interestingly, intrinsic osteoinduction has been proposed to be triggered through the action of calcium phosphate precipitation within the material, leading to calcium and phosphate deficiency, promoting bone growth in ectopic sites from within the template material (43).

3.1. Biological bone grafts

The most commonly used material for bone regeneration is transplanted bone tissue. After blood, bone is the most transplanted tissue, with several million transplants performed worldwide each year (44,45). Bone can be transplanted as cancellous or cortical bone grafts and as bone marrow aspirate (46). Vascularised grafts are transplanted with an intact structure, whereas morselised grafts have been ground into small pieces which can be used to fill irregularly shaped defects.

The gold standard among graft materials is the autologous bone graft, which is derived from another part of the patient's body. It is typically harvested from the iliac crest, manually morselised, and inserted into the defect site. Cancellous bone autografts are osteoinductive, due to the presence of growth factors, osteogenic, as they contain viable bone-forming cells, and osteoconductive, because of their natural matrix structure. Autologous grafts do not suffer from problems relating to graft rejection and disease transmission. Morselised cancellous bone autografts are commonly used in orthopaedic surgery for filling cavitary defects and in specialised procedures such as in the induced membrane technique (47). However, some significant

drawbacks relate to the use of autologous bone grafts. When the bone graft is harvested, a new lesion is created at the harvest site, and donor site morbidity is a frequent problem affecting a significant proportion of patients (48–50). However, with the modern reamer-irrigator-aspirator method for graft collection, the incidence rate may be reduced (51). Additionally, with autologous bone grafts, there may be issues with the quantity and the quality of the available bone tissue. The volume of available bone may not be sufficient, and for patients with lower quality bone, such as for those who suffer from osteoporosis, the autologous bone graft may not function adequately.

When it is deemed unsuitable to use autograft bone tissue, a second option is to use allograft tissue which may be derived from hip replacement surgery or from a deceased donor. Allograft bone is regarded as osteoconductive and, depending on how it is processed, it may be osteoinductive due to growth factors that may still be present (52). The sterilisation of the allografts degrades the quality of the tissue, and despite sterilisation, disease transmission is a known risk factor (53). Regardless of its potential drawbacks, allograft bone in the form of demineralised bone matrix (DBM) is a commonly used bone graft product (54). DBM is produced by cleaning and sterilising donor bone, after which it is morselised into finer particles and demineralised in a hydrochloric acid solution. After freeze-drying, a powder is obtained that contains mostly collagen, some non-collagenous proteins and growth factors, and a small amount of residual calcium phosphate mineral as well as cellular debris (55). Viscous carrier materials, such as glycerol, gelatin, or alginate, are used to formulate the DBM powder into a mouldable paste or putty for easier administration. A third biological option is xenograft bone that has been derived from another species, typically a pig. As with allograft bone, there are risks of disease transmission with xenograft bone. There may also be an immune response to allograft and xenograft tissues, which affects the outcome of the operation negatively.

For large defects in long bones, a vascularised autologous bone graft may be used, which is commonly performed with a fibular graft where a part of the patient's fibula is transplanted to the defect site (56). Fibular grafts are effective in treating large defects, owing to their intact bone structure and blood supply. However, fibular grafts used to treat long-bone defects have a complication rate of approximately 40%, resulting from issues including fractures, non-unions, thrombosis, and donor-site morbidity (57).

3.2. Synthetic scaffolds

Due to the drawbacks and limitations of autograft bone and bone grafts from other individuals, synthetic bone grafts, also called synthetic bone graft substitutes, have been developed (58). The synthetic materials may be in the form of granules, pastes, or putties, which are used to fill bone cavities, or as three-dimensional scaffolds, which may be used for the treatment of larger bone defects. Regardless of their form, the goal of these synthetic bone graft substitutes is to fill a defect site, promote bone growth into the defect, slowly

degrade as the bone grows, and, finally, enable filling of the entire defect site with the body's own bone tissue.

Small bone defects, which are well contained within surrounding load-bearing healthy bone, can be treated by filling with a synthetic granule- or paste-like substance without a predefined three-dimensional shape. These substances are typically used for filling of the entire defect cavity to facilitate bone growth throughout the defect volume. Pastes and putties are often regarded as easier to apply than granules, and there are several synthetic products that are clinically available (7). They often contain a quickly dissolving polymeric carrier to facilitate the application of the material into the defect, and more slowly degrading materials with the desired biological functionality. Some materials may harden after insertion, providing mechanical strength to the defect area. The functional materials that are used for bone regeneration may be inorganic materials such as calcium sulphates, calcium phosphates, hydroxyapatite, or bioactive glasses, or organic materials, such as BMPs (6). Also bone growth enhancing drugs may be added, such as bisphosphonates, which are commonly used to treat osteoporosis (59,60). In addition to improving bone growth, the materials can offer added functionalities such as antimicrobial activity for infection control and radioactive irradiation for cancer treatment (61–63). A granule- or paste-like substance can be introduced into the bone cavity via minimally invasive surgery, promoting lesion healing.

Three-dimensional bone regeneration scaffolds are typically intended for the treatment of large bone defects, or defects which are not sufficiently surrounded by bone tissue. These implants may be stacked or carved from standard-size pieces to fill a defect, the defect may be shaped to suit the implant, or the scaffold may be fabricated as a personalised implant according to the shape of the patient's defect.

There are probably no universally applicable materials or structures for bone scaffolds, but instead different solutions may be needed for different patients and different locations in the body. In addition to the biological requirements presented below, there are a number of other factors that need to be fulfilled before a scaffold can be translated from concept to clinic (64–68). The scaffold should be targeted at a specific clinical indication with a clear clinical need and offer a meaningful benefit over existing treatment modalities. It must be possible to produce it in sufficient quantities in a reproducible and economically feasible manner, and with minimal batch-to-batch inconsistency. For safe use, the scaffold should be either sterilisable or produced under sterile conditions, and it should have a sufficient shelf-life.

Medical devices for bone regeneration are heavily regulated. Due to the extensive requirements, purely material-based strategies without any biological components may be preferred (58). For a successful clinical translation of a scaffold, there must be significant financial investment made into a project which, ultimately, may fail because of a number of various reasons.

3.2.1. Biological requirements for scaffolds

The diamond concept illustrates the fundamental requirements for scaffolds designed for bone fracture healing (69). According to the concept, there are four essential requirements that have to be met for bone restoration: a supply of osteogenic cells, sufficient numbers of growth factors, an osteoconductive scaffold material, and a suitable mechanical environment. Later, the hexagon concept was introduced, adding two additional requirements for successful fracture healing: the presence of inflammatory cells and sufficient vasculature (33). Each of these requirements has specific implications for scaffold design and application.

To ensure infiltration of osteogenic cells into the scaffolds, cells which have been isolated from the patient can be pre-seeded within the scaffold prior to surgery. This approach, known as bone tissue engineering, holds potential for improved bone tissue development, but has the drawbacks of increased cost and difficulty in meeting with regulatory requirements (70). Cell-free scaffolds may therefore be preferred. As the scaffold is placed next to intact bone tissue, a source for osteogenic cells is present. Pre-seeding of cells may therefore not be necessary, as long as the scaffolds are able to recruit bone-forming cells and provide them with a suitable environment to produce new tissue.

Growth factors that promote bone formation may be added to scaffolds in the production phase. However, concerns have been raised regarding the correct dosing of growth factors, with too high doses believed to be able to cause over-growth of tissue, or potentially cancer (71). A natural supply of growth factors may be achieved with sufficient vascularisation within the scaffold. Vascularisation is also required for oxygen and nutrient transport, as well as waste exchange, when the distance to existing tissue exceeds 100–300 μm, and lack of adequate vascularisation has been seen as one of the major factors contributing to bone scaffold failure (18,72–76). Vascularisation develops to some degree naturally in many kinds of scaffold materials and structures. Incorporation of trace quantities of copper or cobalt in the scaffold structure has been used to promote vascularisation (77–79). However, the toxicity of especially cobalt is a limiting factor to utilizing this strategy.

Another strategy for improved vascularisation potential and supply of growth factors is the utilisation of an induced membrane, which is a concept that our team has been developing in the related contributions V, VII, IX, X, and XII of this thesis. By coating scaffolds with quickly degrading polymers, it is possible to cause beneficial short-term tissue irritation. As a response, the body induces a membrane which is naturally rich in growth factors around the scaffold, and our hypothesis is that the membrane promotes bone growth inside of the scaffold. The early results of this strategy seem promising, but more work is needed to establish optimised scaffold structures.

An osteoconductive scaffold material promotes bone growth along the surface of the scaffold. A number of materials are regarded as osteoconductive, including ceramics, glasses, and polymers (80). For osteoconduction, the porosity of the scaffold has to be suitable to facilitate both entrance of cells into

the scaffold and vascularisation within the scaffold structure. Often-quoted ranges of suitable pore sizes are approximately 100–400 μm (81,82) or even up to approximately 700 μm (83), but depending on the scaffold material and structure, bone growth may occur also in smaller and larger pores (84–86). The minimum requirement for pore size is that osteoblast cells, which are approximately 20–50 μm in size, should be able to enter the pores. However, vascularisation will probably be a limiting factor for the smallest pore sizes (82) as blood vessel growth requires larger pores, and bone can only grow in the vicinity of the vessels (87,88). For very large pore sizes, the supporting effect of the scaffold to facilitate bone regeneration diminishes. Scaffolds have also been produced with gradient structures for improved biological response (89), and microporosity in the range of 1–100 μm may be of high importance especially for the early stage bone formation (88). A high overall porosity, significantly above 50%, has been suggested to be preferable, but the drawback of a higher porosity is compromised mechanical properties (9,90).

Bone regeneration occurs only in a mechanically stable environment. The loads that the scaffold may have to withstand differ from case to case, depending for example on the size, shape, and location of the injury. The fracture healing capacity largely depends on the mechanical environment. Both a loosely fixed environment with significant strains and a perfectly stable one without any micromotion can be detrimental to the tissue healing process (33). It has been speculated that within environments shielded by overly rigid fixations, the bone forming cells are not sufficiently stressed to obtain the required stimulus for advancing bone growth (91). The need for the scaffold to support mechanical stresses varies. In some cases, the primary load may be borne by fixation devices like external casts, internal plates, or intramedullary nails, reducing the mechanical burden on the scaffold (69,76). However, bone should grow quickly into soft biomaterials to enable full mobilisation of the patient, as bone should form before the implant becomes loose or fails because of fatigue (76). To stimulate MSC differentiation into bone-forming cells, also macroscopically soft materials should have sufficient microscale stiffness (92).

Inflammation of the fracture site is necessary in the early stages of bone regeneration, but chronic inflammation has been shown to have detrimental effects on the healing of the tissue (33). Chronic inflammation may for example be caused by repeated mechanical trauma at the regeneration site, exceeding the durability of the provisional tissue, or by a material-induced sustained action of inflammatory macrophage cells. To reduce inflammation, a sufficiently rigid fixation is required. Additionally, modulation of the inflammatory signalling pathways may induce a positive effect on the healing process (33).

3.2.2. Scaffold fabrication techniques

Porous scaffolds for bone regeneration have been manufactured for research purposes using a number of different methods. Polymer-based scaffolds have been manufactured via particulate leaching (93), freeze drying (94), gas

foaming (95–97), electrospinning (98,99), and, more recently, via a number of additive manufacturing (three-dimensional printing) techniques, such as powder bed fusion and material extrusion (100). The techniques and their suitability for creating scaffolds for research and clinical use have been extensively examined in a number of review articles (80,101–111). In this thesis, the gas foaming, freeze drying, and foam replication techniques were used.

In gas foaming, a solid polymer block is subjected to a gas, typically carbon dioxide, at a high pressure. The gas saturates the polymer during the course of hours or days and plasticises the polymer. The pressure is then rapidly decreased, which causes foaming and expansion of the polymer. The method provides a solvent-free approach to scaffold manufacturing, enabling high porosities and relatively consistent pore structures between scaffolds. The processing can also be performed without significant heating, which allows for the use of heat-sensitive materials. However, gas-foamed scaffolds may have somewhat small pore sizes with regard to bone regeneration applications, the porosity may not be well interconnected, and the stretched polymer chains may relax when subjected to higher temperatures, causing shrinkage of the structure.

Freeze drying of scaffolds is performed by dissolving a polymer into a solvent, freezing the solution to below its triple point, and sublimating the solvent. Finally, a drying step is applied. The resulting pore structure may be altered by modifying the cooling procedure. Like gas foaming, freeze drying is a relatively replicable method that enables high porosities.

In the foam replication method, a sacrificial foam with interconnected porosity is used to give the structure to the scaffold. A slurry is prepared with a binder polymer and particles of glass or ceramic mixed into a solvent. The foam is immersed in a slurry and squeezed repeatedly to infiltrate the entire foam with the slurry, after which the structure is thoroughly dried. The foam is thereafter heat-treated to burn away the sacrificial foam and the binder, and to sinter the particles together into a porous three-dimensional structure (112,113). With the choice of foam, it is possible to create different kinds of architectures. However, the manual processing that is required especially for the coating of the sacrificial foam with the prepared slurry limits the scaffold-to-scaffold consistency (114).

3.3. Materials for bone scaffolds

Bone regeneration scaffolds are typically designed to be degradable, which offers multiple advantages. As scaffolds degrade, they allow the body's own tissue to grow. A gradual degradation enables a progressive transfer of mechanical loads from the scaffold to the growing bone tissue, and, in some cases, the scaffold degradation products may promote bone growth. Ultimately, once the scaffold has fully degraded, no foreign materials remain, which reduces the potential for infections or other adverse reactions.

Degradable materials can be characterised by their degradation behaviour in biological environments. Biodegradation can be strictly defined as degradation that occurs through enzymatic catalysis (115,116), or, more broadly, as any degradation that occurs in biological environments (66,117–121). Bioresorption and bioabsorption have been defined as elimination and absorption of substances from the body through natural pathways (116,122). In practice, the terms biodegradable, bioresorbable, and bioabsorbable have often been used interchangeably, and for synthetic polymers, they most often refer to polymers that by any pathway are degraded and metabolised in the body.

The degradation of biomaterials can be examined in aqueous media *in vitro*, and inside of vertebrates *in vivo*. For *in vitro* testing, different kinds of buffered solutions that mimic body conditions, such as simulated body fluid (SBF), tris(hydroxymethyl)aminomethane (Tris) solution, and phosphate-buffered saline (PBS) are commonly used. These solutions provide an environment which to some extent is intended to resemble the conditions inside the body. The experimental degradation or dissolution results vary depending on the medium that is chosen (123,124). Tris solution is a buffered water solution, without additional ions that would mimic *in vivo* conditions. PBS is designed to mimic the concentrations of four ions in blood plasma (Na^+, K^+, Cl^-, and HPO_4^{2-}), and SBF is designed to mimic the concentrations of seven ions in blood plasma (Na^+, K^+, Mg^{2+}, Ca^{2+}, Cl^-, HCO_3^-, and HPO_4^{2-}). Like human blood, all three solutions are buffered, but they lack the biological cues found in body fluids. Especially SBF has been used very widely for *in vitro* degradation testing of biomaterials, as it is the solution that most closely resembles the ion concentrations in the blood plasma. However, the use of SBF has been criticised for the intricate preparation process, which leaves little room for error, and for the potential of false negative and false positive results regarding the apatite forming ability of materials (125). *In vitro* testing may give valuable information regarding the degradation and dissolution behaviour of biomaterials. However, the biological environment for bone regeneration is different from the ion-containing solutions and from *in vitro* cell cultures. As long as there are no synthetically created life-like models for bone tissue (126), *in vivo* testing with a biologically relevant test setup is the only comprehensive method to test the performance of materials and scaffolds for bone regeneration (127). The model selection for *in vivo* testing is important, because the tissue regeneration can vary substantially both within and, especially, between species (128).

Materials used for scaffolds, including their degradation products, must be biocompatible, indicating that they elicit an appropriate host response without causing inadvertent tissue damage or inducing cell death. Biocompatibility is not a universal property of a material, but instead biocompatibility varies from one application to the other, and should be determined on a case-by-case basis (15,129,130). The materials must also be sterilisable, as sterility is a fundamental requirement for surgical implants. Commonly used materials for

synthetic bone regeneration scaffolds include degradable polymers, bioactive glasses, and their composites.

3.3.1 Synthetic bioresorbable polymers

Polymers are large molecules composed of repeating covalently bound monomeric units. Many polymers exist as long chains, but they can occur in many other configurations as well, such as star-shaped, comb-shaped, or cross-linked. When combined with additives, synthetic and semi-synthetic polymers are processed into various types of plastics. Due to their large molecular weight, entanglements, and repetitive inter- and intrachain interactions, the properties of polymeric materials differ significantly from chemically similar small molecules.

Several kinds of synthetic polymers for biomedical purposes can be obtained commercially, but for research purposes, they are often synthesised and characterised in the laboratory. Commercial polymers have a good batch-to-batch consistency, and they may already be certified for clinical use. However, commercially produced high-purity polymers are often very expensive, especially on a small scale. The choices of for example molecular weights and comonomer ratios are limited, unless the polymers are produced in even more expensive customer-specific processes. Additionally, their impurities may not be disclosed properly and challenging to analyse. In contrast, self-made polymer synthesis enables manufacturing of materials according to the case-specific requirements, with a better control over the contents of the final material. With self-made polymers, the tuning of properties, such as the molecular weight distribution, is possible. However, it may be time-consuming to produce varieties of polymers, and their clinical translation may be troublesome because of the regulatory requirements. Irrespective of the origin of the polymer, thorough characterisation is beneficial, in order to be able to predict and understand the behaviour of the polymer under different conditions.

Polymers with hydrolytically or enzymatically cleavable groups in their backbone may degrade in biological environments, such as inside the human body (131). In medical contexts, hydrolytic degradation is often preferred to minimise variability in degradation behaviour between different sites and different patients (66). The properties of the hydrolytically degrading polymer are heavily influenced by its degradation mechanism. Depending on the rate of water absorption into the polymer matrix compared with the degradation rate of the chains, the polymers may undergo either bulk degradation or surface erosion, as presented in Figure 2 (132,133).

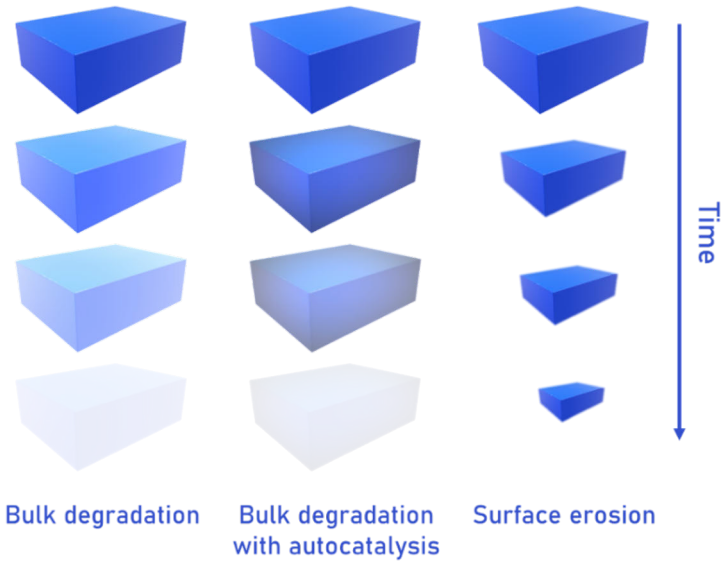

Figure 2. Schematic illustration of bulk degradation, bulk degradation with autocatalysis, and surface erosion of bioabsorbable polymers as a function of time. Lighter colour indicates decrease in molecular weight.

Surface erosion occurs for materials that degrade faster than they absorb water or other erosive agents, such as enzymes (134). In surface erosion, the mass loss is linear with respect to the surface area of the polymer. Molecular weight changes of the bulk polymer are minimal, as the degradation products are directly leached into the environment. Surface erosion may therefore be a desirable degradation mechanism in controlled drug release applications, where a steady and predictable release of the pharmaceutical substance is preferred. However, if hydrolytic surface erosion is the result of a strongly hydrophobic polymer surface, the material may be less suitable for tissue regeneration, as bone-forming cells may be less likely to adhere to hydrophobic surfaces (135–137).

In cases where water or other degrading substances are absorbed inside the polymer matrix before the polymer is degraded, concurrent degradation throughout the material occurs, called bulk degradation. In bulk degradation, the average molecular weight of the polymer decreases early due to degrading chains throughout the polymer bulk. Contrastingly, significant mass loss only happens later, after a substantial decrease in molecular weight, and leaching of the low-molecular-weight degradation products into the surrounding environment.

In thick sections of the material, the formation of degradation products within the polymer matrix may occur at a higher rate than their leaching out of the material. This leads to the accumulation of degradation products within the material, which in the case of degradable polyesters are acidic. As the cleavage of polymer chains is catalysed in acidic conditions (138), the bulk degradation

is autocatalysed. Accumulated degradation products cause a more rapid degradation inside of the polymer bulk than near the surface of the material, where degradation products more easily leach out from the polymer. The autocatalytic process may turn a seemingly slow degradation process into a quickly occurring loss of molecular weight and polymer mass, with an accompanying steep decline in the mechanical properties of the material. An autocatalysed process may therefore cause acidification of the environment during the late stages of degradation, potentially leading to an inflammatory reaction, with a negative impact on the surrounding tissues (139,140).

By replacing the ester end groups of aliphatic polyesters with carboxylic acid end groups, it is possible to accelerate the degradation rate by increasing both the hydrophilicity and the acidity of the polymer (117). To compensate for the pH decrease during the degradation of polyesters, they have been combined with pH increasing materials, such as bioactive glasses and metallic magnesium (141).

In practice, degradable polymers can rarely be described as purely bulk degradable or purely surface erodible, but they often exhibit a somewhat mixed behaviour intermediate to the two idealised models.

Aliphatic polyesters such as polylactide (PLA), polyglycolide (PGA), polycaprolactone (PCL), and their copolymers, are a commonly used group of bioresorbable polymers for medical purposes. Polyesters contain an ester bond which is created through a reaction between a carboxylic acid and an alcohol, as water is removed. The esterification reaction is reversible, and a water molecule can therefore split an ester bond. Many aliphatic polyesters are biocompatible, they can be degraded in aqueous environments, their degradation products are metabolised and removed by the body, and the polymer properties can be modified with various methods.

Polylactide

PLA is a widely used and researched biodegradable synthetic poly(α-hydroxyester) derived from renewable resources. It has mechanical properties that are close to those of many traditional plastics such as polystyrene (142), and it has garnered a lot of interest within the biomedical field. PLA is listed as generally recognised as safe by the US Food and Drug Administration (FDA), and it is permitted for food contact and several biomedical applications also by the European Medicines Agency (EMA) (143).

PLA is commonly produced either via ring-opening polymerisation (ROP) or via polycondensation (Figure 3). Lactic acid is first fermented from starch, for example from corn or sugarcane. For ROP, a lactide dimer is created by oligomerising and subsequently depolymerising the lactic acid. The lactide is thereafter polymerised in dry conditions using for example stannous octoate (tin(II) 2-ethylhexanoate) and an alcohol as polymerisation initiating agents (144,145). In polycondensation, PLA is produced directly from lactic acid with removal of water during the polymerisation reaction (146). When polymerised from the lactic acid monomer, the polymer is typically referred to

as poly(lactic acid) instead of polylactide. The polymer backbone is chemically identical between poly(lactic acid) and polylactide, and both are abbreviated PLA, but the polymer obtained through polycondensation of the lactic acid monomer typically has a lower molecular weight with a higher dispersity compared to the polymer produced through ROP (142,146,147). Polylactide, produced with ROP, is preferred for medical products due to possibilities for higher molecular weight, narrower molecular weight distribution, and better batch-to-batch consistency.

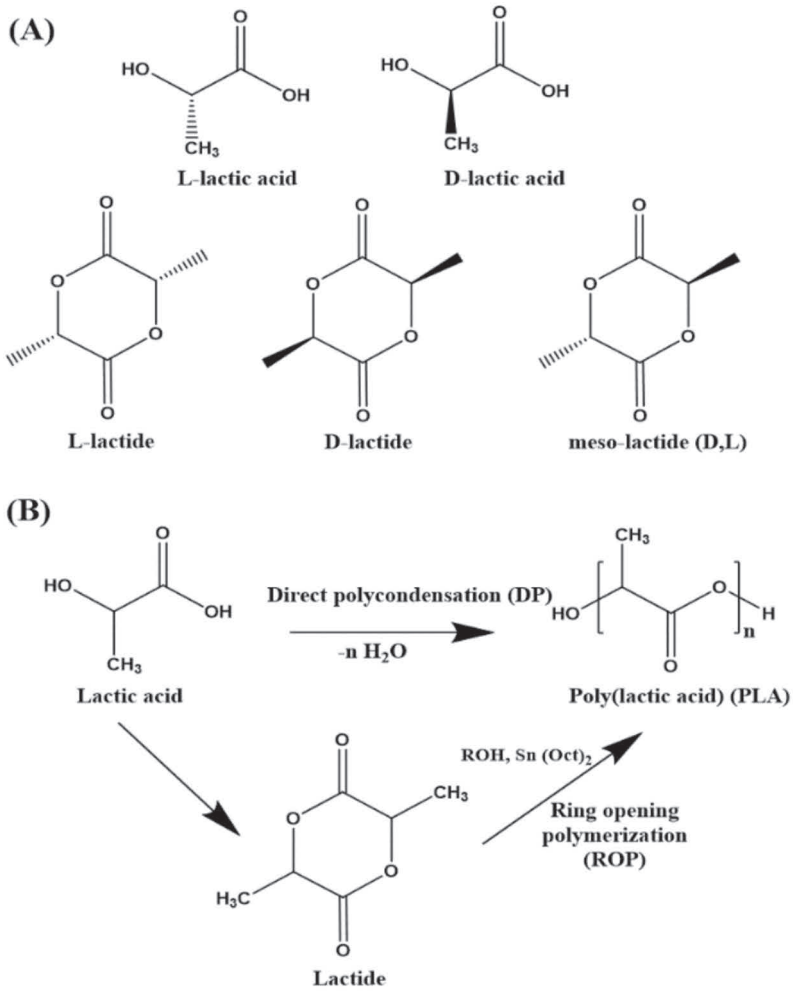

Figure 3. (a) The different stereochemical forms of lactic acid and lactide. (b) Polycondensation of lactic acid and ROP of lactide into PLA. Image reproduced with permission from (148).

Lactic acid contains a chiral carbon atom and can exist as two enantiomers, commonly referred to as L-lactic acid and D-lactic acid. Lactide is a dimer of

lactic acid, containing two chiral carbon atoms which enable three stereoisomeric forms: L,L-lactide, D,D-lactide, and the meso-form D,L-lactide. A 50:50 mixture of L,L-lactide and D,D-lactide is called racemic lactide (146). The chirality of the used monomers determines the ability of the polymer to crystallise: PLA which to a large extent contains only L- (PLLA) or D-units (PDLA) may crystallise, whereas PLA chains which contain significant amounts of randomly ordered L- and D-units (PDLLA) are not able to crystallise and will remain amorphous irrespective of their thermal history. An optical purity of at least 72–75% is required for crystallisation to occur (146,147). In medical applications, PLLA is more often utilised than PDLA, because the hydrolysis of PLLA yields L-lactic acid, which is the naturally occurring stereoisomer.

The melting point of well-crystallised optically pure PLLA and PDLA is theoretically above 200°C, but due to imperfect crystallites, slight racemisation, and impurities, the melting point of PLA is typically measured at 170–180°C (146,149,150). The crystallinity of PLA has a significant effect on its mechanical, thermal, and degradation properties. Crystalline regions are more resistant to water absorption than amorphous regions and hydrolyse therefore slower. By modifying the crystallinity with, for example, heat treatments and by choice of optical purity of the polymers, it is therefore possible to adjust the degradation rate of PLA in the body (151).

The glass transition temperature (T_g) of PLA is typically in the range of 50–65°C (152). When implanted into the body, PLA is therefore always in the glassy state below its T_g, which increases both its mechanical properties and its degradation time.

By blending PDLA with PLLA, it is possible to form stereocomplex crystallites (PLA SC) consisting of a 1:1 ratio between PDLA and PLLA units (153,154). PLA SC has a significantly higher melting temperature, approximately 220–230°C, than crystallites of either PDLA or PLLA. The melting enthalpy of PLA SC crystallites is 142 J/g, which is significantly higher than for homocrystalline PLA (93 J/g) (146). PLA SC is often stated to have higher strength than homocrystalline PLA (147,155–158), but in several studies, there have been little or no observed differences between homocrystalline and stereocomplex PLA (159–161). Additionally, the compressive properties of PLA SC have not yet been well characterised, and there is an apparent lack of knowledge with regard to the mechanical behaviour of PLA SC as compared with amorphous and semicrystalline PLA.

PLA is easily melt-processed into desired structures. Common processing methods include extrusion and injection moulding, and PLA can also be processed into films and fibres. PLA is also suitable for 3D printing processes, such as fused deposition modelling, where it is commonly used by hobbyists and by researchers.

Like most polymers, it is possible to modify PLA with a multitude of methods. In the polymerisation process, the stereochemistry of the monomers can be chosen to attain the desired crystallisation properties. It is also possible to impact the molecular weight and its dispersity by choosing suitable

polymerisation conditions. In melt processing, the polymer chain orientation can be affected by controlling the flow conditions, and the crystallinity may be adjusted based on the cooling rate or subsequent heat treatments. PLA can be copolymerised with other monomers into random and block copolymers, and it can be grafted. Blends with other polymers may give desired properties or lower the cost of the material. It is also possible to functionalise PLA with groups that are covalently attached to the backbone, and to cross-link functionalised PLA (162). With regard to medical applications, even the sterilisation method impacts the properties of the polymer, and can be used to modify the polymer in a desired manner (163).

The degradation of PLA occurs mainly through bulk degradation, with amorphous regions being more susceptible to degradation than crystalline regions. The degradation rate is relatively slow because of the steric hindrance of the methyl group that is present on the α-carbon (147). PLA is degraded hydrolytically in the body into lower molecular weight fragments of approximately 5000 g/mol or less, which are leached into the surrounding fluids and further metabolised by cells via the Krebs cycle into water and carbon dioxide (145,164,165). During the degradation, the crystalline regions may support the mechanical properties of the polymer, even when the molecular weight of the amorphous regions has decreased (117). The degradation may be accelerated with lower crystallinity, more acidic end groups, higher ambient temperature, and by applying mechanical stresses on the polymer (140,147,166).

PLA, often in the form of PLLA, is used clinically in medical devices where relatively high mechanical stability and slow degradation are preferred. Commercialised products include bone fixation systems by DePuy Synthes, screws by Stryker, soft-tissue fixation systems by Zimmer, screws and darts by Arthrex, and screws and fixation systems by Conmed (167). PLA-based medical devices developed by Finnish companies include orthopaedic fixation screws and plates (bioabsorbable systems by Inion), joint spacers for small joint arthroplasties (RegJoint™ by Scaffdex), and composite templates for cartilage regeneration (COPLA® Scaffold by Askel Healthcare). PLA SC, as a medical biomaterial, has been predominantly studied for drug release applications, with limited research in areas emphasizing mechanical properties (168).

Poly(lactide-co-glycolide)

Poly(lactide-co-glycolide) (PLGA) is a copolymer of lactide and glycolide, typically synthesised with ROP (Figure 4). The mechanical and degradation properties of the material can be adjusted with different glycolide-to-lactide ratios. Glycolide lacks the methyl group that is present on the α-carbon in lactide, and PLGA is therefore more hydrophilic than PLA. Like PLA, PLGA degrades predominantly through bulk degradation, but PLGA degrades faster and has lower strength (169).

With approximately 25–70% of glycolide co-monomer, PLGA is completely amorphous, and compositions closer to either pure polymer (PLA and PGA)

may crystallise (150). The degree of crystallisation may be tuned also with the choice of the lactide monomer, and the use of D,L-lactide prevents crystallisation (170). PLGA has a lower T_g than PLA, typically between 30°C and 55°C, depending on the lactide-to-glycolide ratio and the molecular weight of the polymer (171). The degradation rate can be tuned by changing the glycolide-to-lactide ratio, with compositions higher in lactide content degrading more slowly (172). The degradation of PLGA in the body occurs generally in weeks or months, compared to years for semicrystalline PLA (173). As the T_g value of PLGA is close to the body temperature, small changes in the copolymer ratio or molecular weight affecting the T_g value may have a significant impact on the *in vivo* degradation properties of the polymer.

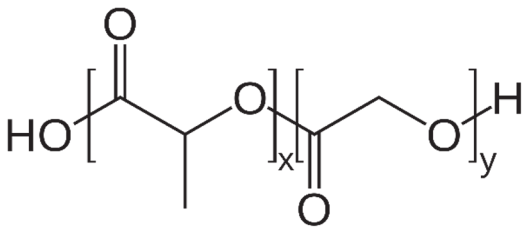

Figure 4. The structure of PLGA.

PLGA is commercially available in different grades, with varying molecular weights and comonomer ratios. Like PLA, it is approved for medical use by EMA and FDA, and it can be used for largely similar purposes as PLA. Due to the faster degradation profile, the focus in PLGA applications is on controlled drug delivery, with a number of drug release applications already in clinical use (174–178). For drug release, PLGA is often used as nanoparticles with a polyethylene glycol surface, commonly called PEGylated nanoparticles. With this modification, their hydrophilicity is increased, which reduces their uptake in the liver, and increases their time in the blood circulation (179). PLGA has been widely studied also for orthopaedic applications (169), and it is clinically used for example in orthopaedic fixation in a self-reinforced form (as a Finnish example, the Activa series by Bioretec).

PLGA is typically produced as random copolymers. With sequencing, it is possible to obtain highly ordered polymer chains that exhibit slower, more controlled hydrolytic degradation and a linear decrease in molecular weight (180).

3.3.2. Bioactive glasses

Glasses are non-crystalline solids that are typically transparent and brittle. Silica-based glasses are commonly encountered in everyday life in windowpanes as well as in glass bottles and jars. Silicon dioxide or silica (SiO_2) is the network forming agent, and the network structure consists of silica tetrahedra connected by bridging oxygens in Si-O-Si-bonds (Figure 5). With a silica content of approximately 70–75% and a high number of bridging

oxygens, these so-called soda-lime glasses are chemically very durable. Silica-based glasses may also contain network modifying agents, such as Na and Ca, which open the glass network structure by introducing non-bridging oxygens. Pure SiO_2 glass, called quartz glass, only contains bridging oxygens, with each silica tetrahedra connecting to four other silica tetrahedra.

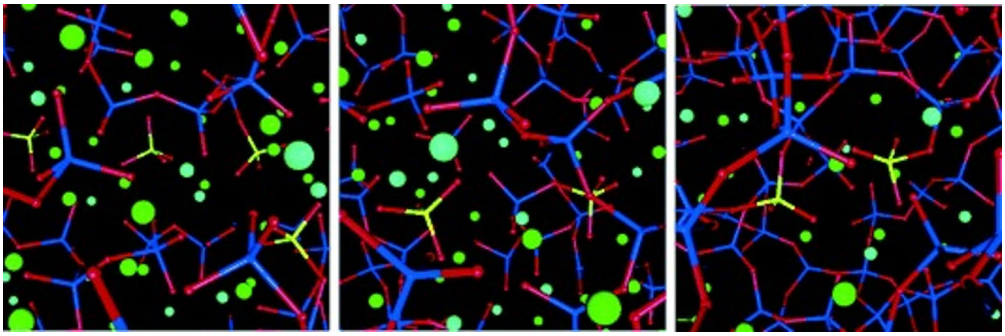

Figure 5. The simulated network structure of three bioactive glasses with 46.1 mol.% SiO_2 (Bioglass® 45S5, left), 56.5 mol.% SiO_2 (BG55, center), and 66.9 mol.% SiO_2 (BG65, right). Red = oxygen, blue = silicon, yellow = phosphorus, dark green = sodium, cyan = calcium. Reprinted with permission from (181). © American Chemical Society 2007.

Silicate glasses which contain less than 60% SiO_2 are chemically less durable and can dissolve in aqueous environments. Glasses with low silica content within a certain compositional range may exhibit significant biological activity when implanted into the body, and are commonly referred to as bioactive glasses (10,182,183).

The bioactivity of a glass has typically been defined by its ability of the glass to form a hydroxycarbonate apatite (HCA) layer on the glass surface after subjecting the glass to an *in vivo* environment, or an environment which mimics the *in vivo* conditions (184,185). The HCA layer is a surface to which bone can bond (186–188). *In vivo*, bioactive glasses are characterised by bone growth in direct contact with the glass surface. In addition to silicate glasses, also borate- and phosphate-based glasses have been found to have bioactive properties (189–191). In broader terms, bioactivity can also be defined as the general ability of the material to induce a positive host tissue response (15).

The SiO_2 content of melt-derived silica-based bioactive glasses is approximately 40–60% (187,192). Compositions having a silica content of less than 40% do not form a glass, and glasses with a higher silica content react and dissolve very slowly. Bone bonding is generally higher with a decreased molar fraction of SiO_2 (192), but it has been shown that bone bonds to borate-containing glasses even at high SiO_2 fractions (193). Silica-based bioactive glasses are commonly characterised by high Na_2O and CaO contents, as well as a high CaO/P_2O_5 ratio (10). Even though phosphate can be classified as a glass network former on its own (11), the phosphate in bioactive glasses has been

suggested not to enter the silica network and significantly affect network connectivity, but to exist as a separate orthophosphate species (194,195). Phosphate is not required for bioactivity, as the phosphate required for HCA layer formation can be adsorbed also from the environment (196). However, with a higher phosphate content, the rate of HCA development on the glass surface is increased (197).

For melt-derived glasses, different elements can relatively easily be incorporated in small quantities to modify the thermal, chemical, or biological properties of the glass. Commonly included therapeutic elements in bioactive glasses for bone regeneration include magnesium, boron, zinc, copper, and strontium (11,198). In addition to conducting *in vitro* and *in vivo* tests, the properties and reactivity of glasses with different compositions can be predicted by mathematical models (199–203).

Bioactive glasses are clinically mostly used in the form of granules and pastes as bone graft substitutes in the treatment of non-load-bearing defects. Bioactive glass compositions for which marketing authorisation has been approved for clinical use include 45S5 (Bioglass®), S53P4 (Bonalive®), and 13–93 (183). The compositions of these glasses, and the compositions of three less studied experimental glasses used in this thesis, labelled BG1, BG2, and NC–5, are shown in Table 1.

Table 1. Compositions of bioactive glasses S53P4, 13–93, BG1, BG2, NC–5, and 45S5, in wt.% and in mol.%.

Glass (wt.%)	**SiO_2**	**CaO**	**Na_2O**	**P_2O_5**	**K_2O**	**MgO**	**B_2O_3**	**Al_2O_3**
S53P4	53	20	23	4	-	-	-	-
13–93	53	20	6	4	12	5	-	-
BG1	69.1	12.5	12.4	1.4	-	3.0	1.1	0.5
BG2	69.6	8.8	13.1	1.4	-	4.9	2.1	-
NC–5	62	13	17	2	-	4	2	-
45S5	45	24.5	24.5	6	-	-	-	-
Glass (mol.%)	**SiO_2**	**CaO**	**Na_2O**	**P_2O_5**	**K_2O**	**MgO**	**B_2O_3**	**Al_2O_3**
S53P4	53.9	21.8	22.7	1.7	-	-	-	-
13–93	54.6	22.1	6.0	1.7	7.9	7.7	-	-
BG1	68.7	13.3	11.9	0.6	-	4.4	0.9	0.3
BG2	68.6	9.3	12.5	0.6	-	7.2	1.8	-
NC–5	61.4	13.8	16.3	0.8	-	5.9	1.7	-
45S5	46.1	26.9	24.4	2.6	-	-	-	-

Glass 45S5 contains a relatively low amount of Si, with a high concentration of non-bridging oxygens. Compared with the other bioactive glasses presented here, it exhibits a higher bioactivity and a more rapid dissolution. S53P4

contains a significantly higher amount of Si, with fewer non-bridging oxygens, and exhibits a somewhat lower bioactivity and slower dissolution. Glass 13–93 is similar to S53P4 with respect to the content of Si, Ca, and P, but by replacing some of the Na in the S53P4 composition with K and Mg, it has been designed for versatile hot-working properties (187,204). The difference between T_g and T_m of 13–93 is approximately 200°C, which allows for viscous flow enabling sintering without crystallisation. It is also possible to draw 13–93 into fibres. The experimental glasses BG1, BG2, and NC–5 have a silica content of higher than 60%, but they are still bioactive owing to the network altering effect of boron in their structure.

A rapid cascade of reactions occurs when bioactive glasses are immersed in aqueous solutions or implanted into the body. The reactions can be described with the incongruent dissolution model (10,205). Initially, the leaching of network modifying ions dominates, with ions such as Ca^{2+} and Na^{+} dissolving from the glass surface through ion exchange reactions with H^{+} and H_3O^{+}. The solution pH therefore increases, and a silica-rich layer depleted in network-modifying ions is formed on the glass surface. In the silica-rich layer, neighbouring silanol groups may polycondensate into an amorphous silica-rich gel. Si dissolution is facilitated by the pH increase. The dissolution of Ca, Na and P ions proceeds, and as the concentration of Ca and P increases, amorphous calcium phosphate (ACP) begins to precipitate on the surface of the silica-rich gel. If the solution inherently contains Ca and P ions, also they may be incorporated in the ACP precipitate on the surface of the silica-rich gel. These reactions occur quickly, with ACP formation observed *in vivo* already within 1 h of implantation. Thereafter, the ACP layer crystallises into HCA with addition of OH^{-}, CO_3^{2-}, or F^{-} ions from the environment.

When implanted in bone, subsequent reactions occur, as biological moieties, such as collagen fibres and macrophages, are adsorbed onto the HCA layer. Osteoblast precursor cells differentiate into osteoblasts and secrete collagen into the growing HCA matrix, and bone which is bound to the glass surface is formed (10).

Bioactive glass was the first synthetic material found to be able to undergo chemical bonding with living tissue without fibrous tissue formation. The main applications of bioactive glasses still focus on bone regeneration, although focus has also been put on, for example, soft tissue and cartilage healing (206). In bone regeneration, bioactive glasses that activate osteoprogenitor cells in the body and encourage the body to build more bone may be characterised as osteostimulative (42). The bone regeneration capability of bioactive glasses has been shown in both short-term (207,208) and long-term clinical studies (209).

The ions that dissolve from bioactive glasses have significant biological impacts on angiogenesis and bone growth (198,210), and their impact has been likened to that of growth factors (42). Dissolved Si and Ca species may upregulate and activate a multitude of genes in osteoprogenitor cells, and Si is known to be an essential component for bone formation and calcification. The

ion concentrations are critical. For instance, low (2–4 mmol) and medium (6–8 mmol) concentrations of calcium ions are favourable for osteoblast differentiation, whereas high (>10 mmol) concentrations are cytotoxic to osteoblast cells (211). The cellular effects of released silicate species have been extensively quantified, with evidence of silicate concentrations below 52 ppm being the most probable to show favourable cellular responses (212).

The ionic dissolution products from bioactive glasses may have similar activity as drugs that are used to treat diseases such as osteoporosis. However, drugs are commonly used systemically, and they may induce unwanted side effects. Ions dissolving from the established, clinically used bioactive glasses exist naturally in the body, and typically have mainly local effects within the body.

The long-term delivery of ions from bioactive glasses can be significantly modified by altering the silica content, and therefore the degradation rate, of the glass. Slowly dissolving glasses with a high silica content may dissolve more congruently, producing a steadier and more predictable release of ions. The dissolution behaviour is also strongly dependent on the size of the glass particles and the flow rate of the fluids (213,214).

Bioactive glasses may exhibit significant antibacterial activity (215,216). The antimicrobial activity is thought to result from the rapid initial release of ions when the glass is immersed in a biological environment, which causes an increase in the osmotic pressure on the cells. The antimicrobial activity is probably enhanced by the rapidly increased pH. Bioactive glass S53P4 may therefore be used also to treat infected bone (osteomyelitis) (217). However, the environment that is effective against microbes may also negatively affect the patient's own cells, with potentially cytotoxic effects to the host tissue (127,218).

In thermal processing, for instance into porous scaffolds, bioactive glasses crystallise easily. The crystallisation typically commences at temperatures slightly higher than the T_g value of the glass due to the high content of network modifying ions. Partly crystallised glasses, commonly called glass-ceramics, can also be used in medical applications, but they have different properties compared with their fully amorphous counterparts, exhibiting for instance retarded hydroxyapatite layer formation (10). Depending on the sintering conditions, varying amounts of crystallinity may be induced, and the compositions of the crystallites may differ. To obtain materials with a good batch-to-batch consistency, and that are relatively easy to characterise, it may be desirable to avoid crystallisation and only work with fully amorphous bioactive glasses. Recently, we have shown that under carefully controlled conditions, sintering of S53P4 particles into porous cylinders is possible without any crystalline phase formation (219).

3.3.3. Polymer–bioactive glass composites

As discussed above, bioactive glass has several beneficial properties for bone regeneration applications compared with bioresorbable polymers, such as the

formation of a HCA layer on the glass surface after implantation, the release of biologically active ions that promote bone formation, and in some cases also antimicrobial properties. However, glass also has drawbacks, such as difficulty in forming mechanically robust three-dimensional porous structures and the inherent brittleness of glass. In addition, the initial burst release of ions, accompanied by a strong pH increase, contribute to the antimicrobial effect but may simultaneously cause damage to the surrounding cells and tissues.

Composites of bioresorbable polymers and bioactive glass are produced to combine their desirable properties (12,13,102,169,220). For composites with a continuous polymer phase, the polymer provides design freedom and increased ductility, whereas bioactive glasses may enhance the biological properties by providing a release of ions and potentially HCA formation on the scaffold surface. Composites with a continuous bioactive glass phase may benefit from polymer coating through an improvement in the mechanical properties of the scaffolds and by moderation of the initial pH and ion release peaks. It has been shown that the biological activity of bioactive glass may be promoted through addition of PLGA (221).

Polyester–bioactive glass composites affect pH by the glass dissolution, which increases the pH, and by the degradation of the polyester, which lowers the pH. For composite scaffolds, the initial pH peak of the glass may be strongly reduced or even eliminated, which may be beneficial for host cell survival. The pH lowering effect may continue for prolonged periods of time (221). In very low pH environments, the dissolution of the glass is significantly affected, with a more rapid ion release and potentially inhibited calcium phosphate layer formation (222). However, such pH values (pH 4 and below) may be outside of what is applicable for *in vivo* bone regeneration.

4. Objectives of the thesis

The overall objective of this thesis was to develop and study scaffold designs and materials for bone regeneration. More precisely, the aims were:

i. To produce highly porous polymer-based scaffolds with gas foaming and freeze drying techniques, with incorporation of bioactive glasses and magnesium hydroxide, and test their degradation *in vitro* (Publications I and II)

ii. To evaluate the *in vivo* bone regeneration capability of gas-foamed and freeze-dried scaffolds (Publication III)

iii. To compare the mechanical and *in vitro* degradation properties of bioactive glass scaffolds coated with polylactide stereocomplexes with amorphous and homocrystalline polylactide coatings (Publication IV)

5. Materials and methods

5.1. Materials

PLGA (Publications I–III) was polymerised from D-lactide (>99.5%) and glycolide (>99.5%) from Corbion/Purac and L-lactide (>99%) from Futerro.

PDLLA, PLLA, and PDLA (Publication IV) were polymerised from D,L-lactide, L-lactide, and D-lactide monomers of pharmaceutical grade from Corbion/Purac.

Bioactive glasses 13–93 and NC–5 (Publication I), BG1 (Publication II), BG2 (Publications II, III), and S53P4 (Publication III) were supplied by Bonalive Biomaterials Ltd. The glasses BG1 and BG2 were supplied as fibres with a diameter of 13 µm and with a sizing layer of 3-glycidoxypropyltriethoxysilane and low molecular weight PCL. Bioactive glass 13–93 (Publication IV) was melted at the Laboratory of Inorganic Chemistry, ÅAU, from Belgian quartz sand and analytical-grade reagents Na_2CO_3, K_2CO_3, MgO, $CaCO_3$, and $CaHPO_4 \cdot 2(H_2O)$.

Porous β-TCP granules with a porosity of 60% (chronOS®) were obtained from Synthes (Publication III).

Other reagents and solvents were of analytical or equivalent grade.

5.2. Methods

5.2.1. Polymerisation (I–IV)

ROP was used to prepare PLGA (Publications I–III) and PLA (Publication IV). The dry monomers L-lactide, D-lactide, D,L-lactide, and glycolide, and the initiator stannous octoate and co-initiator 1-decanol, were weighed in a glove box in inert nitrogen atmosphere. The polymerisation was carried out in an argon atmosphere by heating the monomers in a round flask at 120°C, inserting the initiator and co-initiator through a septum, and polymerising at 150°C for 3–5 h with initial stirring. After the polymer had cooled, it was dissolved in a 7-fold amount of dichloromethane (w/v) and precipitated in a 6-fold amount of ethanol (v/v) to remove unreacted monomers and obtain a polymer precipitate. The polymer was thereafter thoroughly dried to remove any residual solvent and manually cut to smaller particles. The PLGA was manufactured with a D-lactide-to-L-lactide ratio of 1:1 and a lactide-to-glycolide ratio of 70:30.

5.2.2. Scaffold fabrication (I–IV)

Porous scaffolds were fabricated with gas foaming (Publications I, III), freeze drying (Publications II, III), or foam replication techniques (Publication IV).

Gas-foamed scaffolds were prepared by extruding PLGA into compact rods with either 10%, 20%, or 35% of 13–93, NC–5, $Mg(OH)_2$, or low-molecular weight PLA mixed into the structure (Publication I), or with PLGA only (Publication III). Prior to use, bioactive glass fibres of 13–93 and NC–5

(Publication I) were ground into particles of up to 50 μm in size using a ball mill (Philips MiniMill). All materials were dried overnight in vacuum at 40°C before extrusion and extruded with a single-screw extruder using the temperature profile 75–85–95°C. The rods, with a thickness of approximately 5.0 mm (Publication I) or 2.8 mm (Publication III), were cut into 16–17 mm long pieces and placed in cylindrical polytetrafluoroethylene (PTFE) moulds with an inner diameter of 1.5 times the diameter of the rod and with open ends. The moulds were placed inside of a pressure-resistant chamber which was filled with carbon dioxide at a pressure of 55 bar for a minimum of 10 h. The polymer foams were formed as the pressure was quickly released. To complete the expansion, the moulds with the expanded rods were placed for 45 s at 80°C and kept thereafter inside the moulds for one hour at room temperature (RT).

Freeze-dried scaffolds (Publications II, III) were manufactured by dissolving PLGA in 1,4-dioxane, stirred vigorously overnight, and poured into custom-made PTFE moulds with a diameter of 15 mm and a height of 3 mm. Pure PLGA foams were prepared from a 5% solution. Composite foams of PLGA and bioactive glass were prepared by placing a carded mesh of glass fibres into the moulds and immersing them in a 3% polymer solution. The solutions were frozen at −30°C for 24 h, freeze-dried for 24 h, and held under vacuum at RT for 48 h. The scaffolds were cut in half prior to *in vitro* analyses. In total, four different scaffolds were analysed: two different PLGA-only scaffolds, with different molecular weights (M_w 76 300 g/mol and 48 300 g/mol, denoted as PLGA1 and PLGA2), and two different composites (PLGA1 with BG1 and PLGA2 with BG2).

Bioactive glass scaffolds (Publication IV) were manufactured with the foam replication technique. A slurry was formed by dissolving 5 wt.% polyethylene glycol (35 000 g/mol) in ethanol at 40°C and adding 7.5 wt.% 13–93 granules of the size fraction 32–45 μm. The slurry was ball-milled for 30 min to ensure homogeneity. After milling, the mean glass granule size was measured as 20.2 μm with laser light scattering. Cylindrical polyurethane foams with a height of 20 mm and a diameter of 18 mm with an open interconnected porosity (15 pores per inch) were dipped into the slurry, manually squeezed and released to remove any entrapped air, and to completely infiltrate the foam with slurry. After removing the foams from the slurry, they were gently blown with air to remove excess slurry and to open clogged pores. The foams were dried in fume hoods at RT for a minimum of 3 days. The resulting green bodies were thereafter heat-treated under nitrogen flushing to burn the polymer and sinter the glass according to the following heating scheme: heating from RT to 300°C at 1°C/min, heating to 450°C at 0.8°C/min, 30 min hold at 450°C, heating to 670°C at 0.8°C/min, and 120 min hold at 670°C. After this, the heating was turned off, and the furnace was let to cool to RT. The sintered scaffolds were stored in a desiccator. A sacrificial polyurethane foam, a green body, and a sintered bioactive glass scaffold are shown in Figure 6.

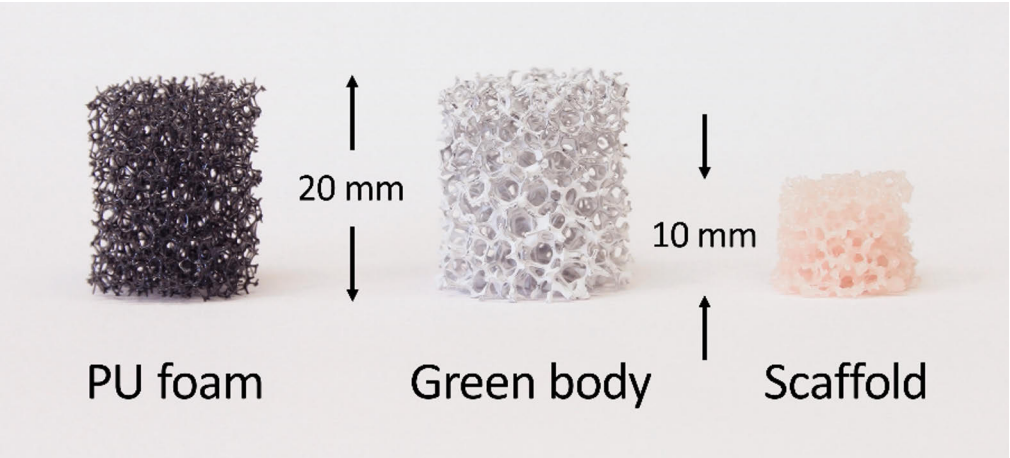

Figure 6. Photograph of different stages in the foam replication technique (Publication IV): A sacrificial polyurethane foam, a green body, and a sintered bioactive glass scaffold. The figure illustrates the size change of the scaffold in the sintering step.

For the coating of the glass scaffolds manufactured with the foam replication method, solutions of 25 g $CHCl_3$ and either 1.5 g PDLLA, 1.5 g PLLA, or a mixture of 0.75 g PDLA with 0.75 g PLLA were prepared. The glass scaffolds were fully immersed in the coating solution for 3 min, during which they were placed in a vacuum chamber at 600 mbar for 60 s to remove air bubbles. The coated scaffolds were then dried overnight in a fume hood at RT, and subsequently overnight at RT in <50 mbar pressure. For improved polymer crystallisation, the scaffolds were heat-treated under nitrogen atmosphere at 180°C for 60 min.

5.2.3. Analysis of molecular weight (I–IV)

The molecular weight of the polymers was analysed with gel permeation chromatography (GPC) with an LC-10ATVP HPLC-pump (Shimadzu Corp.), an AM GPC Gel 10 µm Linear Column (American Polymer Standards), and a Sedex 85 light scattering detector (Sedere). All measurements were performed at 40°C with a tetrahydrofuran flow of 1 mL/min and a sample concentration of 1 mg/mL. The samples were filtered with 0.22 µm PTFE filters prior to analysis. Calibration was carried out with polystyrene standards with a narrow molecular weight distribution (Polymer Standards Service).

The molecular weight analyses with GPC gave information on the number average molecular weight (M_n), weight average molecular weight (M_w), and the dispersity (Đ), where Đ is defined as M_w/M_n.

5.2.4. Analysis of scaffold structure (I, II, IV)

Scanning electron microscopy (SEM) was used to analyse the structure of the scaffold cross-sections, with LEO Gemini 1530 by Zeiss (Publications I, IV) or with SEM by JEOL Ltd (Publication II), at a 30× to 250× magnification. To

preserve the scaffold microstructure, the foam-replicated scaffolds were embedded in epoxy resin prior to analysis.

X-ray microtomography (μCT) was used to analyse the three-dimensional structure of the scaffolds with MicroXCT-400 by Zeiss X-ray Microscopy, Inc. (Publications II, III) or with SkyScan 1072 by SkyScan (Publication IV).

5.2.5. *In vitro* studies (I, II, IV)

In vitro degradation studies were performed in Tris (Publication I), PBS (Publication II), or SBF (Publication IV) solution. Tris was manufactured as a 0.1 M solution, and PBS and SBF were prepared with commonly used protocols (223,224). Briefly, precisely weighed amounts of salts were dissolved in ultrapure water in a predefined order, and the pH was adjusted with hydrochloric acid to 7.4 at 37°C. The amount of solution was 1 mL per 3.5 mg of scaffold (Publication I), 10 mL per scaffold (Publication II), or 30 mL per 1 g of scaffold (Publication IV). The solution-to-scaffold ratios were chosen based on the matrix material (polymer or bioactive glass), international standards, and practical limitations in the laboratory.

The immersion times were 4 h, 1 d, 3 d, 1 w, 2 w, 3 w, 5 w, 7 w, and 10 w (Publication I), 2 w, 4 w, 6 w, 8 w, and 10 w (Publication II), or 2 w, 4 w, 6 w, and 10 w (Publication IV). The buffer solution was changed weekly (Publications I, IV) or fortnightly (Publication II), unless pH exceeded the given limits of 7.35–7.45 when the solution was changed weekly. Three (Publication I), six (Publication II), or eight (Publication IV) parallel scaffolds were used in the *in vitro* studies per time point.

Mass loss was defined as the decrease in mass during the course of the experiment as a percentage of the original mass. To determine the dimensional change of soft scaffolds (Publications I, II), the length and diameter were measured both before and after the *in vitro* experiments.

5.2.6. Thermal and mechanical characterisation (I, II, IV)

Differential scanning calorimetry (DSC) was used to determine the T_g, crystallisation (T_c), and melting (T_m) temperatures. Heating rates were 20°C/min (Publication II) or 10°C/min (Publication IV). The value for T_g was determined by the half-height between the onset and endset of the transition, while the values for T_c and T_m were identified at the peak of their respective transitions.

Thermogravimetric analysis (TGA) was used to analyse polymer and glass ratios in composite scaffolds (Publication II). Analyses were conducted with 10 mg samples that were heated to 800°C with Q500 (TA Instruments).

Compressive testing (Publication IV) was conducted with an L&W Crush Tester (Lorentzen & Wettre), with five parallel scaffolds per time point compressed at a rate of 2 mm/min. After the *in vitro* degradation study, the scaffolds were compressed in their wet state immediately after removal from the SBF solution, while 0-week scaffolds were compressed in their dry state. The value for compressive strength was determined as the peak value up to 33%

strain, whereas the toughness was calculated as the integral of the stress-strain curve up to 33% strain. The 33% threshold value was chosen to enable a sufficient amount of data to be included to account for any variations between the parallel scaffolds.

5.2.7. Bioactivity and magnesium ion release (I, IV)

The bioactivity of scaffolds manufactured with the foam replication method (Publication IV) was studied with SEM coupled with energy dispersive X-ray analysis (EDX). The appearance of silica-rich and calcium phosphate reaction layers on the glass surface were considered indicative of glass dissolution, as well as calcium phosphate precipitation on the coating polymer.

Magnesium ion release from scaffolds (Publication I) was studied with inductively coupled plasma optical emission spectroscopy (ICP-OES) with an Optima 5300 instrument (PerkinElmer). The solutions were diluted at a 1:1 ratio before analysis, with addition of 4 drops of nitric acid per sample.

5.2.8. *In vivo* bone regeneration (III)

For the *in vivo* study, gas-foamed pure PLGA scaffolds with a diameter of 4 mm and a length of 8 mm were manufactured according to Publication I. Freeze-dried PLGA–bioactive glass fibre composites of the same size were produced by first stacking meshes that had been fabricated as described in Publication II. These were then bonded together with an additional freeze-drying procedure with a 3 wt.% PLGA solution. Prior to the experiments, the scaffolds were sterilised with gamma irradiation at a dose of 25 kGy. The experimental scaffolds were compared with two commercial bone substitutes, namely S53P4 granules of size fraction 500–800 μm and β-TCP granules of size fraction 500–700 μm (Figure 7a).

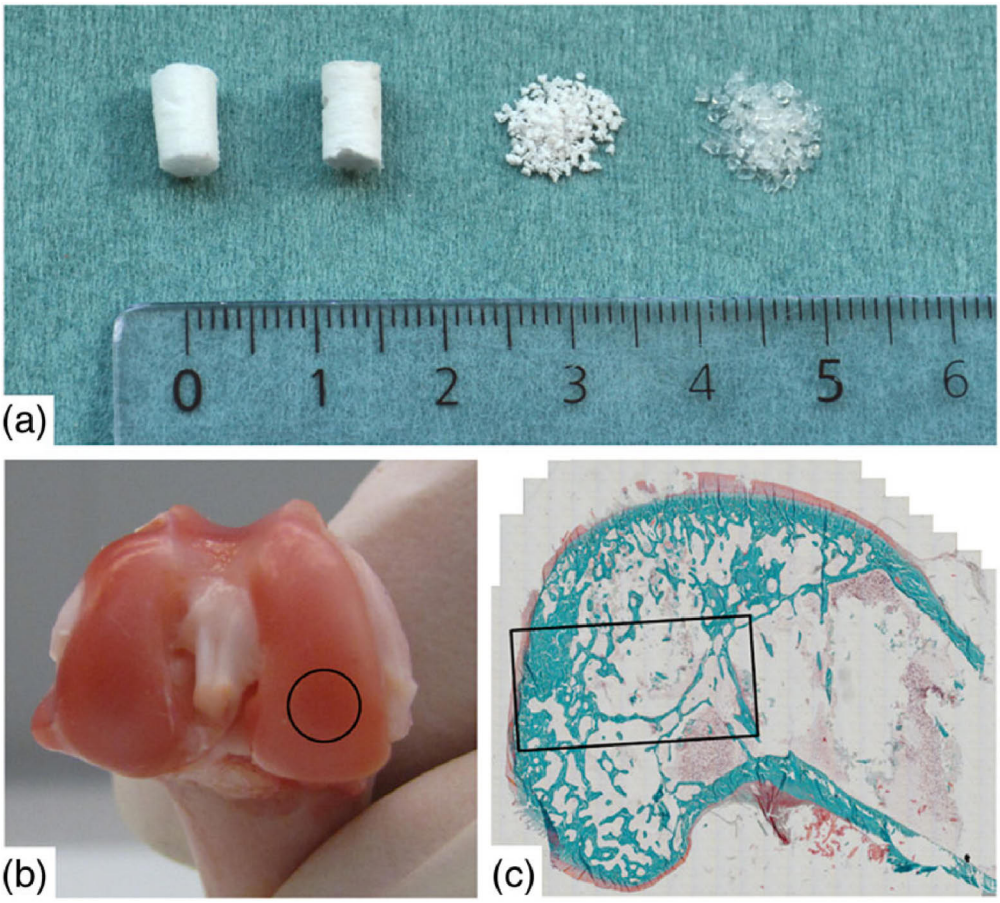

Figure 7. The operating procedure for the *in vivo* study (Publication III): (a) The materials used for filling of the osteochondral defect. From left to right: a gas-foamed PLGA scaffold, a freeze-dried PLGA scaffold with bioactive glass fibres, β-TCP granules, and S53P4 bioactive glass granules. (b) The defect site marked with a black circle in the medial condyle of the femur. (c) The depth of the defect marked with a black rectangle.

The fabricated scaffolds and commercial bone substitutes were studied *in vivo* in New Zealand white rabbits. The Finnish National Animal Experiment Board had authorised the study (ESAVI/3785/04.10.03/2011), which was conducted according to the ethical guidelines and regulations of the Finnish Act on Animal Experimentation (62/2006). Lesions of 4 mm in diameter and 8 mm deep were created in femoral condyles, with the defects extending into the bone marrow space (Figures 7b, 7c). The lesions were either filled with the experimental scaffolds, commercial materials (positive control), or left unfilled (negative control). The animals received both antibiotic prophylaxis as well as preoperative and postoperative analgesics. After 12 weeks, the animals were euthanised, and the operated and non-operated contralateral knees were photographed and evaluated macroscopically, imaged with μCT (Zeiss Xradia

MicroXCT–400), and thin slides were stained with Masson–Goldner trichrome stains for histological analysis of the tissue (Zeiss AxioImager Z1). For quantitative μCT analysis, the BoneJ plugin for Fiji software was used (225,226).

5.2.9. Statistical analysis (I–IV)

The data are presented as average values ± standard deviations. Statistical analyses were performed to find differences between groups, and differences were considered significant at p values <0.05. Statistical tests that were used included analysis of variance (ANOVA) with linear models (Publication I), the Mann–Whitney U test (Publication II), permutation ANOVA with Holm adjustment (Publication III), and ANOVA with linear and mixed models (Publication IV).

6. Results and discussion

The *in vitro* degradation of PLGA-based gas-foamed (Publication I) and freeze-dried (Publication II) scaffolds for bone regeneration was studied, followed by an *in vivo* study of chosen scaffolds (Publication III). Results from these three articles are presented and discussed in sections 6.1–6.5. The last study (Publication IV) was conducted to evaluate the mechanical properties and *in vitro* degradation in SBF of various PLA coatings with different stereochemistries, intended for use as coatings for bioactive glass scaffolds. Results from the last study are presented and discussed in section 6.6.

The purpose of Publication I was to create and characterise highly porous magnesium-releasing scaffolds to facilitate bone regeneration. The magnesium release especially from magnesium hydroxide was of high interest, as it is a slowly soluble salt in water, and there were few studies on its use in scaffolds before our experiment. The gas-foamed PLGA scaffolds contained 10%, 20%, or 35% of bioactive glass particles (NC–5 or 13–93) or magnesium hydroxide. 20% low-molecular weight PLA was used as an alternative filler. To allow for precise measurements of magnesium release, the degradation study was conducted in Tris solution.

Publication II was conducted to study the manufacturing and degradation properties of freeze-dried scaffolds of PLGA with embedded bioactive glass fibres, with focus on the dimensional stability. The scaffolds contained PLGA of two different molecular weights, with or without incorporation of bioactive glass fibres (BG1 or BG2) in their structures. Many porous polymer-based scaffolds manufactured with different techniques suffer from poor dimensional stability, and this research was an attempt to overcome that challenge.

In Publication III, a gas-foamed (pure PLGA) and a freeze-dried scaffold (PLGA with BG2 fibres) were compared with commercial bone graft substitutes (β-TCP and S53P4 granules) and spontaneous bone repair *in vivo*. An osteochondral defect model was introduced for this purpose. The experimental scaffolds were chosen based on older data and on results in Publications I and II. Direct comparisons of commercially available bone substitutes are surprisingly rare in the literature, which added value to this study.

In Publication IV, we performed mechanical and degradation testing for different PLA stereochemistries as coatings on bioactive glass scaffolds. There were few previous reports on the compressive properties of PLA SC, and with this study we aimed at providing a thorough comparison between PLA SC and amorphous as well as homocrystalline PLA. The reaction layer formation within the polymer-coated glass scaffolds was also of special interest.

The choice of PLGA as scaffold material in the first three articles was based on extensive previous knowledge and clinical use of the material. In exploring modifications to established manufacturing methods, it is advantageous to employ the most suitable material for the intended purpose, rather than introducing uncertainty with a new material. Additionally, one of the main hindrances in bringing new scaffolds to the market has been the use of novel

materials, which have a significantly longer regulatory path before potential acceptance. We chose PLA for the last article as we wanted to address a lack of knowledge in some of the fundamental aspects of the different stereochemical forms of the polymer.

6.1. Structure of polymer-based scaffolds (I, II)

The gas-foamed (Publication I) and freeze-dried (Publication II) PLGA-based scaffolds were highly porous with an overall porosity of >90%. A high porosity provides ample volume for bone growth and reduces the amount of scaffold material that the tissue must metabolise during the degradation. The pore wall thickness of the freeze-dried scaffolds was higher for composite scaffolds containing bioactive glass fibres compared with plain PLGA-based scaffolds.

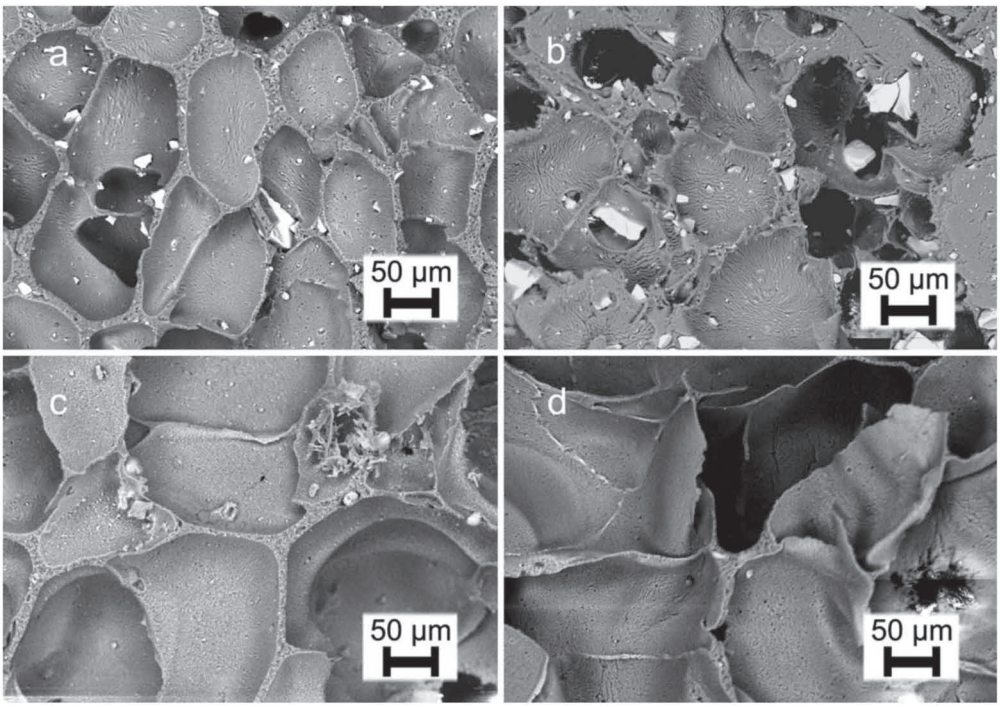

Figure 8. The structure of gas-foamed scaffolds with different fillers after 1 day of immersion in Tris buffer solution at 37°C (Publication I) as visualised with SEM : (a) 13–93 20%, (b) NC–5 20%, (c) $Mg(OH)_2$ 20%, and (d) PLA 20%.

The soft PLGA-based scaffolds enabled manual elastic compression of the structure, allowing the scaffolds to be press-fitted into the lesions created in the *in vivo* study (Publication III). The bioactive glass and magnesium hydroxide fillers were well distributed within the scaffolds.

The structure of the gas-foamed scaffolds varied based on the type of filler used (Figure 8). After the initial shrinkage that occurred as the scaffolds were immersed in SBF, the scaffolds with bioactive glass particles contained pores

which were mostly 50–150 μm in diameter. Both the purely polymer-based and the magnesium hydroxide-containing scaffolds had larger pores, mostly in the range of 100–500 μm. For all gas-foamed scaffolds, the pore interconnectivity was rather low, with a majority of the pores appearing closed in the cross-sectional analysis, with only approximately one-third of the pores being open. Similar pore structures have been obtained with gas foaming of PLGA-based materials (227).

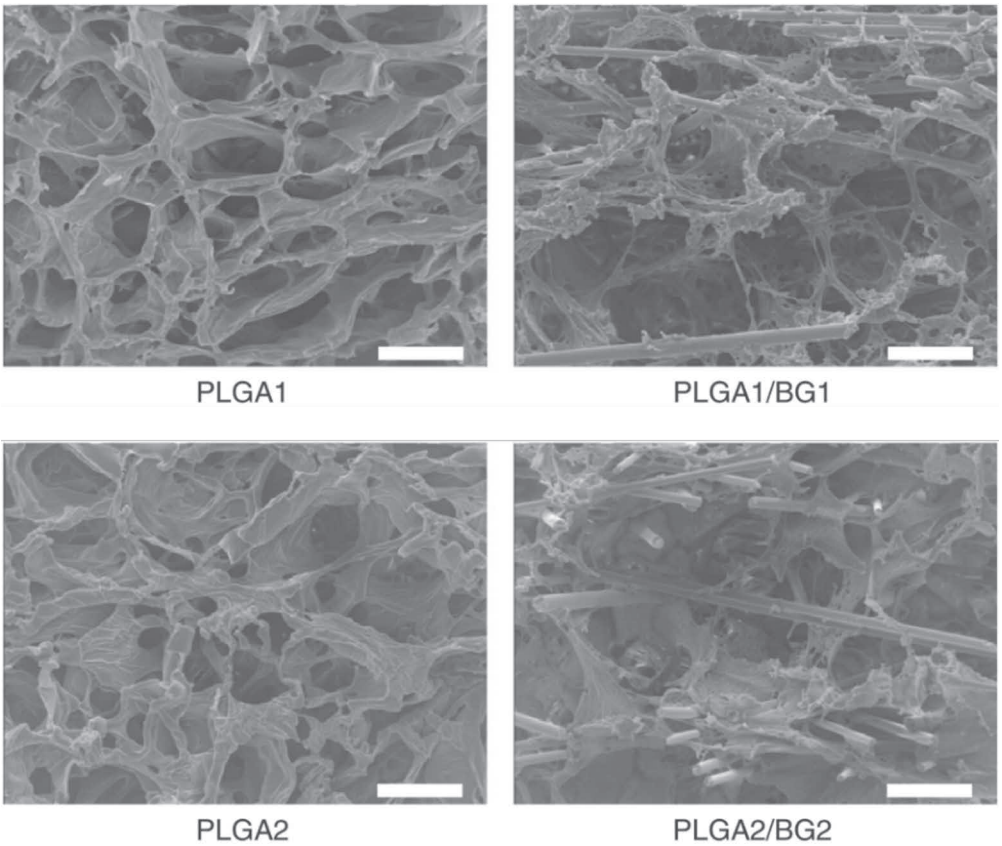

Figure 9. The structure of freeze-dried PLGA scaffolds before degradation tests as visualised with SEM (Publication II). Scale bars 100 μm.

In contrast to the gas-foamed scaffolds, the freeze-dried scaffolds primarily exhibited interconnected open porosity, as visualised with SEM (Figure 9) and μCT (Figure 10). However, the pores were significantly smaller, with the majority of pores less than 100 μm in diameter. The average pore size of the composite scaffold containing BG2 fibres was the largest, with a fraction of the pores as large as 250 μm.

Pore size and interconnectivity are critical factors that influence the potential for bone tissue ingrowth. It is commonly believed that pore sizes above 100 μm support bone ingrowth, while larger pores, approximately 300–700 μm, are thought to be essential for efficient vascularisation within the

scaffold structure (81–83). However, in some experimental setups, bone growth has been observed even in smaller pores, as low as 50 µm (84), whereas others propose significantly larger pore sizes of 700–1200 µm to be optimal for bone regeneration (228). As the transport of nutrients and oxygen further into the scaffold structure is dependent on vascularisation, it is necessary that the scaffold enables, and preferentially promotes, rapid blood vessel formation.

Given that the pores in the gas-foamed scaffolds were primarily larger than 100 µm in size, the pore size should be sufficient to support bone ingrowth. However, the largely closed-cell porosity is not preferable, as the pore structure would limit the possibilities for bone tissue to grow into the scaffold structure until the pore walls were degraded. In contrast, for the freeze-dried scaffolds, while the pore interconnectivity was good, the pore size might be considered somewhat small in terms of its potential to support bone tissue growth.

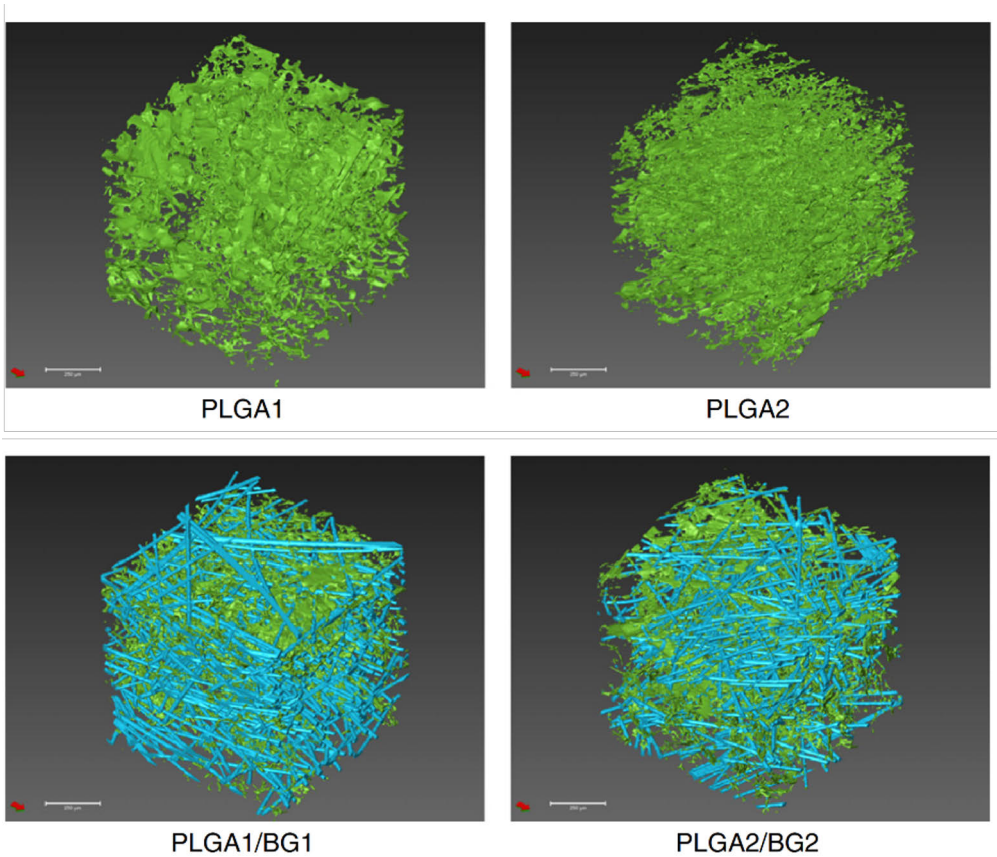

Figure 10. The structure of freeze-dried PLGA scaffolds before degradation tests as visualised with µCT (Publication II). Green colour = PLGA, blue colour = bioactive glass fibres. Scale bars 250 µm.

6.2. Dimensional stability of polymer-based scaffolds (I, II)

When the gas-foamed and purely PLGA-based freeze-dried scaffolds were immersed in the degradation media at 37°C, they underwent significant shrinkage, with a decrease in diameter of approximately 20–40% (Figure 11). The decrease was smaller for the scaffolds with bioactive glass fillers compared with the magnesium hydroxide-containing scaffolds. This shrinkage aligns with previously reported findings for fibrous and gas-foamed scaffolds, as well as for foams produced by particulate leaching (227,229,230). However, the addition of bioactive glass fibres yielded scaffolds which were dimensionally stable when immersed in the degradation medium.

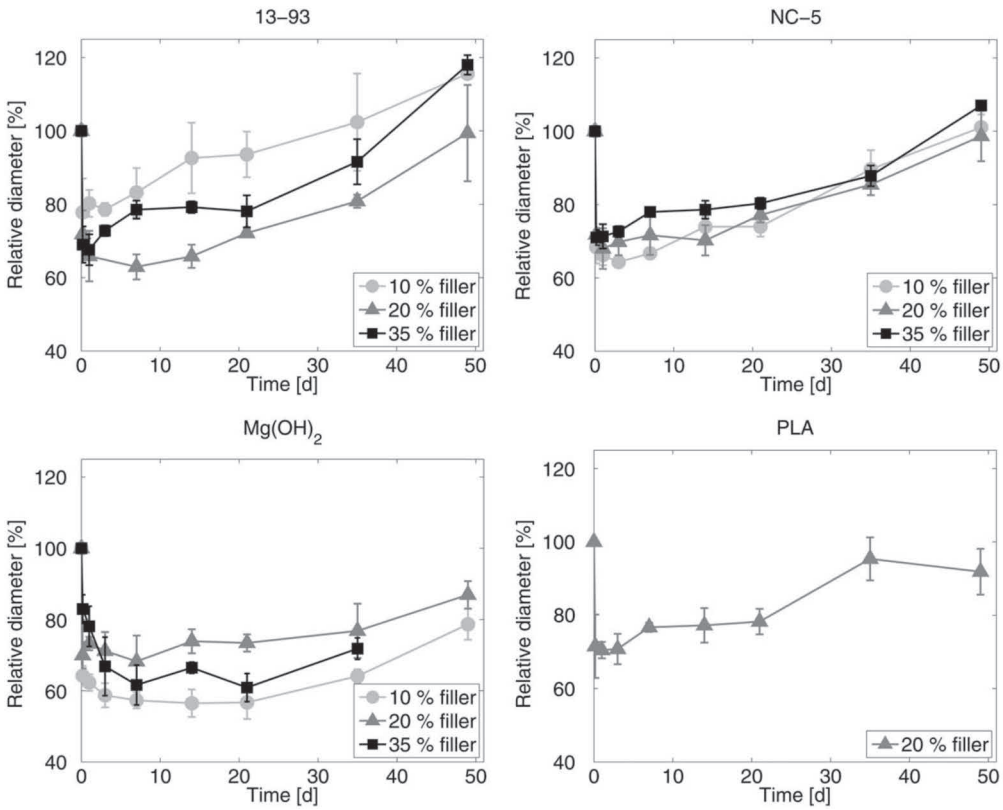

Figure 11. Change in normalised diameter of gas-foamed PLGA scaffolds after immersion in Tris buffer solution (Publication I). Error bars indicate standard deviations.

Maintaining the dimensional stability of scaffolds for tissue regeneration is desirable. Biologically, scaffold shrinkage after implantation may result in displacement, which could negatively affect its tissue regeneration potential. From a regulatory perspective, significant dimensional changes present challenges because of their unpredictable behaviour.

The shrinkage of the porous scaffold structures may be associated with their T_g. If the transition occurs close to 37°C, the mobility of the polymer chains may drastically increase at that temperature, which would enable relaxation of the polymer structure and shrinkage of the scaffold. Initially, the measured T_g values of the PLGA polymers were approximately 51°C. During the freeze-drying and gamma irradiation procedures (Publication II), the T_g values decreased by approximately 10°C, reaching close to body temperature. A polymer with a higher molecular weight, and therefore a higher T_g, may exhibit improved dimensional stability because of reduced chain relaxation at body temperatures. Cross-linking the polymers after processing them into porous structures may also prevent shrinkage, but the cross-linking would have a significant impact on the degradation rate and degradation behaviour of the polymers. Another potential approach to reduce shrinkage is to heat-treat the scaffolds before use, even though this may result in the formation of warped scaffold structures, without precise control of the outcome. Both pre-heating and cross-linking methods are associated with uncertainties, which may affect the regulatory approval processes negatively.

After the initial shrinkage in the degradation medium, the gas-foamed scaffolds experienced significant swelling. After seven weeks of immersion in Tris, the purely polymeric and the bioactive glass-containing scaffolds had either regained their original dimensions or exceeded them. In contrast, the scaffolds containing magnesium hydroxide did not regain their original dimensions. This may have resulted from the significantly higher mass loss that was observed for the magnesium hydroxide-containing scaffolds, which could limit the swelling potential. The freeze-dried scaffolds also swelled, showing an increase in height of 45–100% after 8 weeks of immersion, with no substantial differences between purely PLGA-based and PLGA–bioactive glass composite scaffolds.

The swelling of the polymer-based scaffolds results from the absorption of water into their structure. However, within an *in vivo* environment, surrounding tissue would likely obstruct such an expansion.

6.3. *In vitro* degradation of polymer-based scaffolds (I, II)

PLGA degrades rapidly in water. Additionally, its molecular weight decreases during both melt processing and sterilisation by gamma irradiation. In the gas-foaming study (Publication I), the M_w of as-polymerised PLGA was approximately 110 000 g/mol, and either 76 000 g/mol (PLGA1) or 48 000 g/mol (PLGA2) in the freeze-drying study (Publication II). During extrusion processing of PLGA into rods for gas-foaming, the M_w decreased by approximately 25–50%. In the freeze-drying process, the decrease was approximately 10–20%, with an additional 25–30% reduction during sterilisation by gamma irradiation. The gas-foamed scaffolds were not sterilised prior to the *in vitro* degradation tests.

The molecular weight of both the gas-foamed and freeze-dried scaffolds decreased during the immersion in the buffer solutions. The M_w of gas-foamed

scaffolds with magnesium hydroxide decreased less than that of scaffolds with bioactive glass granules. This difference may stem from the smaller granule size of magnesium hydroxide, which leads to the creation of a large number of small pores within the scaffold structure as it is dissolved. This may enable easier leaching of low-molecular-weight PLGA fragments into the solution. Measurement of the remaining solid polymer would therefore not correctly reflect all degradation phenomena of the polymer, because the solubilised low-molecular-weight components are not included in the analysis.

The inclusion of bioactive glasses into the polymer neutralises the acidic degradation products of PLGA. The effect was observed in both gas-foamed and freeze-dried scaffolds containing bioactive glass. This probably contributed to the slower molecular weight decrease and lower mass loss of the bioactive glass-containing freeze-dried scaffolds (Publication II). Neutralising the environment of degrading PLGA, or other polymers with acidic degradation products, may be beneficial for the biological efficacy of bone regeneration scaffolds. Acidic pH can be detrimental to bone healing, especially after the initial inflammatory phase, whereas slightly alkaline conditions may favour bone regeneration processes (231–234).

Over the first 7 weeks of immersion in Tris solution (Publication I), the mass loss of bioactive glass-containing gas-foamed scaffolds was small (Figure 12). After that, the mass loss accelerated markedly, with the highest losses for scaffolds with the least amount of bioactive glass. This may be partly explained by the slower dissolution of the glass compared with the degradation rate of the polymer. However, the mass loss for NC–5-containing scaffolds was higher than for 13–93 scaffolds, even though 13–93 dissolves more rapidly. The difference may be explained by the stronger pH-neutralising effect caused by the higher rate of dissolution. This effect reduces the degradation rate of the PLGA and delays the autocatalytic degradation process. Therefore, the higher bioactive glass content also protects the polymer from degrading.

There was a substantial difference in mass loss between magnesium hydroxide-containing gas-foamed scaffolds and those containing bioactive glass. The scaffolds with magnesium hydroxide experienced a rapid initial mass loss, which was higher than the amount of magnesium hydroxide that they contained. Magnesium hydroxide has a rather low solubility in water, but with the high surface area and in the low concentrations present in this study, it was expected that most of the salt would dissolve quickly. The strong increase in local pH and the increased surface area created by the dissolution of the magnesium hydroxide were probably significant contributing factors to the mass loss of the polymer.

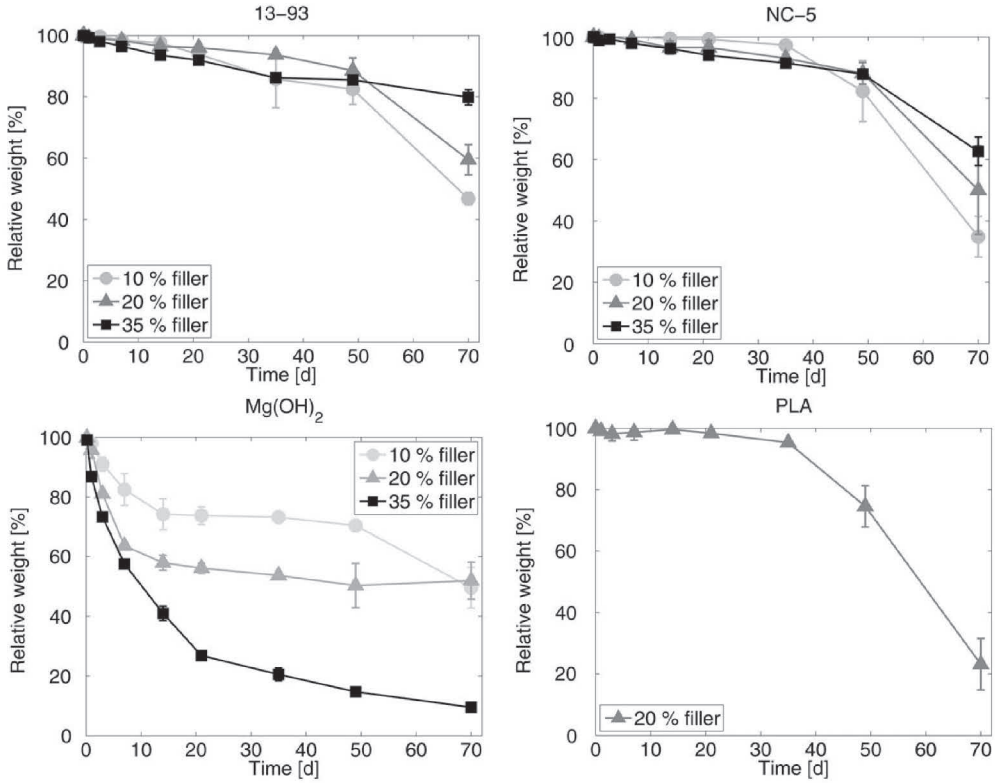

Figure 12. Mass loss of gas-foamed PLGA scaffolds with different filler content after immersion in Tris buffer solution (Publication I). Error bars indicate standard deviations.

6.4. Magnesium release from gas-foamed scaffolds (I)

Magnesium ion release from the magnesium-containing gas-foamed scaffolds was studied with ICP-OES (Publication I). Largely dose-dependent levels of magnesium ions were released into the Tris buffer from scaffolds with magnesium hydroxide or magnesium-containing bioactive glass (Figure 13). The release from scaffolds containing 13–93 was initially two to three times higher than from scaffolds containing NC–5, despite their largely similar magnesium content (5 wt.% vs 4 wt.%), indicating a significantly higher dissolution rate for glass 13–93. The magnesium release from scaffolds containing magnesium hydroxide occurred initially at a rapid rate, with substantially lower release levels after the first three weeks of degradation.

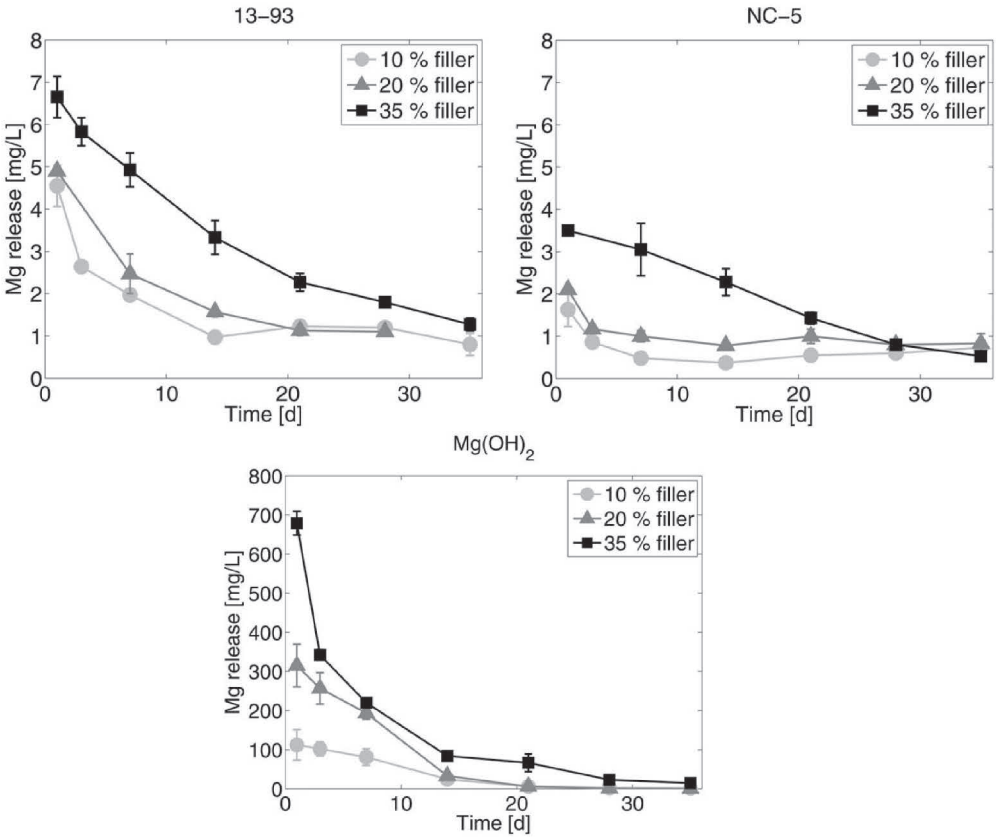

Figure 13. Magnesium release from gas-foamed PLGA scaffolds with magnesium-containing fillers into Tris buffer solution (Publication I). Error bars indicate standard deviations.

The reason for the addition of magnesium into the scaffold structure was to promote bone healing in an environment where it may be compromised by antibiotic use. Quinolones, which are a commonly used class of antibiotics for prevention of bacterial infections (prophylaxis), can lower magnesium levels in bone tissues by forming magnesium complexes. This may have an adverse effect on bone regeneration (235). To compensate, magnesium may be administered either systemically or locally, and magnesium supplementation has been found to be favourable for chondrocytes treated with quinolones (235). In our study, magnesium was readily released with different release profiles, indicating that the negative effects of quinolone prophylaxis may be countered. However, the use of quinolones in surgical prophylaxis is decreasing because of the growing concerns of antimicrobial resistance (236).

According to previous studies, magnesium is beneficial for bone healing by promoting bone marrow stromal cell proliferation and by increasing bone cell adhesion and stability (237–239). The role of magnesium ions in the bone healing cascade appears to be complex, with a favourable effect during the

early inflammatory stage, and possibly an inhibiting effect later in the regeneration process (240). The rapid early release of magnesium from magnesium hydroxide-containing scaffolds could therefore be particularly beneficial for the bone regeneration process, with a strongly diminishing release later during the scaffold degradation.

In this study, the initial concentrations of released magnesium in the degradation medium were in the order of 100–700 mg/L for scaffolds with magnesium hydroxide and approximately 2–7 mg/L for those with bioactive glass. These concentrations translate to roughly 4–30 mM and 0.1–0.3 mM, respectively. A magnesium concentration of approximately 10 mM may be beneficial for bone forming cells, but significantly higher concentrations than that may be detrimental (238,239). Although the concentrations released from magnesium hydroxide-containing scaffolds seem superficially to have the correct order of magnitude, the *in vivo* conditions for cells and scaffolds differ significantly from *in vitro* experiments with simulated body fluids, and direct comparisons are challenging.

6.5. Tissue regeneration *in vivo* (III)

The capability of gas-foamed PLGA- and freeze-dried PLGA–bioactive glass scaffolds to repair osteochondral defects in comparison with commercial β-TCP and S53P4 bioactive glass granules was studied *in vivo*, with empty defects as negative controls (Publication III). The synthetic bone graft substitutes were inserted into rabbit femoral condyles for 12 weeks. The defect model was designed to provide information on the repair of bone tissue within an osteochondral defect, with a possibility to also study the potential (but unlikely) repair of cartilage tissue. The volume and structure of bone were examined with μCT, and histological analysis enabled identification of the quality of the tissues (Figure 14).

Macroscopically, all defects appeared filled after the 12-week implantation time, with no significant depressions appearing at or near the defect site. The surface was uneven and differed in colour from the surrounding cartilage.

Based on μCT analysis, the bone tissue seemed to grow from the edges towards the middle of the defect, with the volume between newly formed bone trabeculae consisting of connective tissue and bone marrow. The defects filled with gas-foamed PLGA or left empty exhibited growth of both bone and fibrous tissue, whereas the defects filled with freeze-dried PLGA–bioactive glass exhibited substantial fibrous tissue formation.

Commercial β-TCP displayed the highest bone volume fraction, exceeding that of the non-operated contralateral knee by 14 percentage points. The μCT results for the trabecular thickness, trabecular spacing, and trabecular number, as well as the histological examination, indicate that there was ample bone growth within β-TCP and S53P4 granules, whereas the results for gas-foamed PLGA were largely similar to the defects left empty. The worst bone regeneration was surprisingly observed for the freeze-dried PLGA–bioactive glass scaffolds.

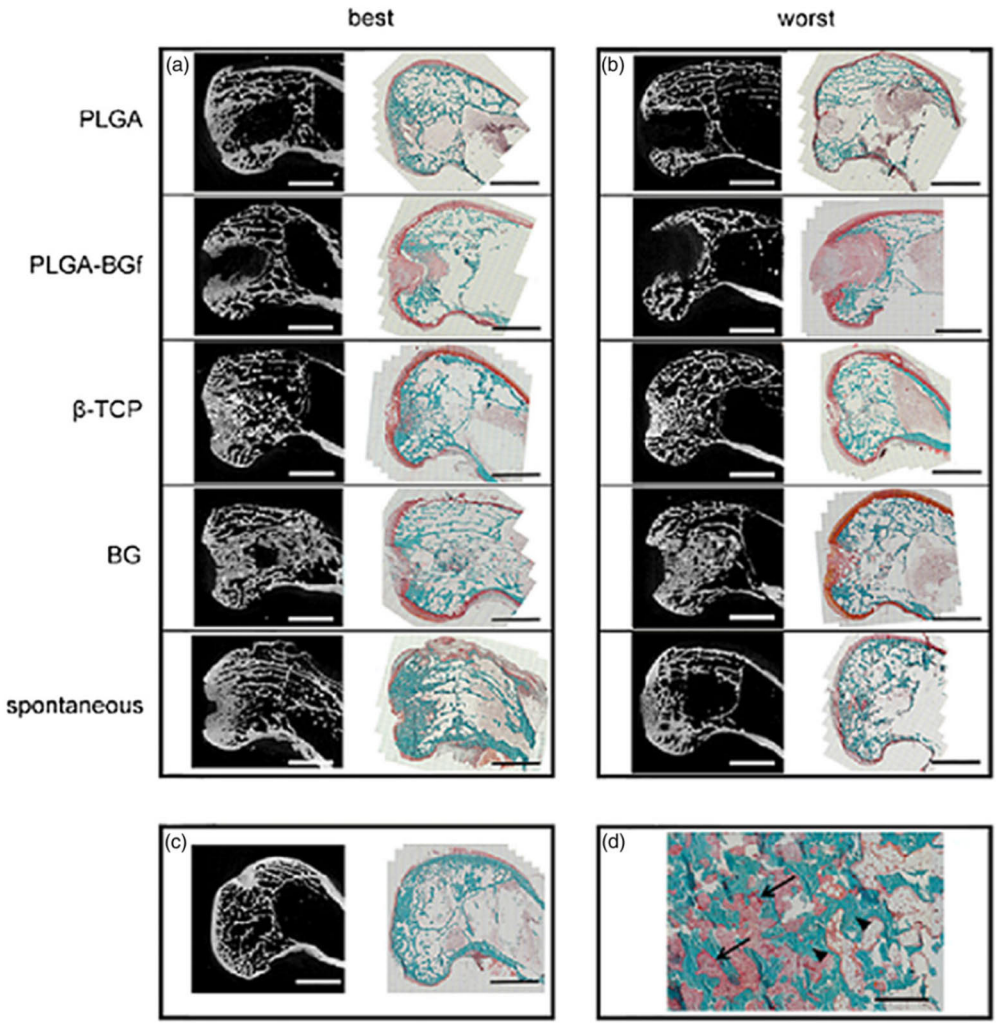

Figure 14. Best (a) and worst (b) tissue regeneration with different bone graft substitutes or with spontaneous repair after 12 weeks of *in vivo* implantation (Publication III), as visualised with μCT or through histological staining. A non-operated contralateral control is also shown (c), as well as a close-up of bone growth for β-TCP substitute (d) with osteoids (arrows) and mineralised bone (arrowheads) marked. Scale bars 4 mm in (a)–(c) or 500 μm (d).

The predominantly closed-cell porosity of the gas-foamed PLGA scaffolds probably contributed significantly to the unsatisfactory results, as the bone-forming cells would have limited possibilities to enter inside of the scaffold. The significant shrinkage of the scaffold after implantation may also have contributed, as it may have detached the scaffold from the defect edges. These gas-foamed PLGA scaffolds with suboptimal pore structure and without any biologically active materials such as bioactive glasses were used because of the allegedly promising results in an earlier *in vivo* study with similar scaffolds.

However, the results of that study had not been published, and in later analysis it was found that the tissue regeneration results were not on the level as originally thought, and the regenerated tissue mainly consisted of fibrous scar tissue (results not published).

Our initial hypothesis was that the freeze-dried PLGA scaffolds with bioactive glass fibres would be well suited for bone growth, due to their highly interconnected porosity and the bioactive properties of the glass fibres. Although the pore sizes were not optimal, there was previous *in vivo* evidence that bone growth within pores in this size range should be possible. Despite that, the unsatisfactory results may have mostly resulted from lack of suitable porosity. The porosity would probably not allow for vascularisation throughout the scaffold structure, which would inhibit tissue growth inside the scaffold. Additionally, absorption of water by PLGA would cause swelling of the structure, followed by an additional decrease in pore size, which could have a further negative impact on the tissue regeneration process.

It was not confirmed whether there was significant HCA layer formation on the scaffold surfaces. The sizing of the glass fibres with polycaprolactone at least initially limits their dissolution rate, with a further limiting contribution from embedding the fibres in a freeze-dried PLGA matrix. It is possible that the reactivity of the glass was slow, with a delayed or possibly even totally inhibited formation of an osteoconductive HCA-layer on the scaffold surface. This would significantly reduce the biological benefits of incorporating bioactive glass in the polymer structure.

The substantial bone growth within the defects that were left empty indicates that the defects were potentially close to the critical size limit. Over time, it is possible that the empty defects would have healed fully, at least with regard to bone tissue. The inadequate bone formation within the experimental scaffolds, coupled with the long 12-week repair time, should therefore not have resulted from the employed surgical technique.

None of the tested materials adequately regenerated cartilage, which is consistent with previous studies on similar materials (241,242). To heal the entire osteochondral defect, a distinct layer for cartilage regeneration seems necessary.

6.6. Influence of PLA stereochemistry (IV)

Foam-replicated 13–93 bioactive glass scaffolds with interconnected porosity coated with amorphous PDLLA, semicrystalline PLLA, or stereocomplex PLA SC were investigated *in vitro* (Publication IV). The aim of the experiment was to explore differences in the degradation and mechanical properties of the coatings over a time period of 10 weeks.

The porosity of the scaffolds was on average 76%, consisting of open interconnected porosity. The pore sizes were highly variable, with the majority of pores between 500 µm and 1500 µm (Figure 15). The polymer coating on the scaffolds was mostly located inside of the scaffold structure, with less coating closer to the outer edges. This was due to the coating technique that involved

gentle blowing of the scaffolds after the coating to open clogged pores, but simultaneously decreasing the amount of polymer close to the scaffold surface. The uncoated scaffolds seem to have smaller pore size than the coated ones, as the smallest pores of the coated scaffolds may have been obstructed by the polymer coating.

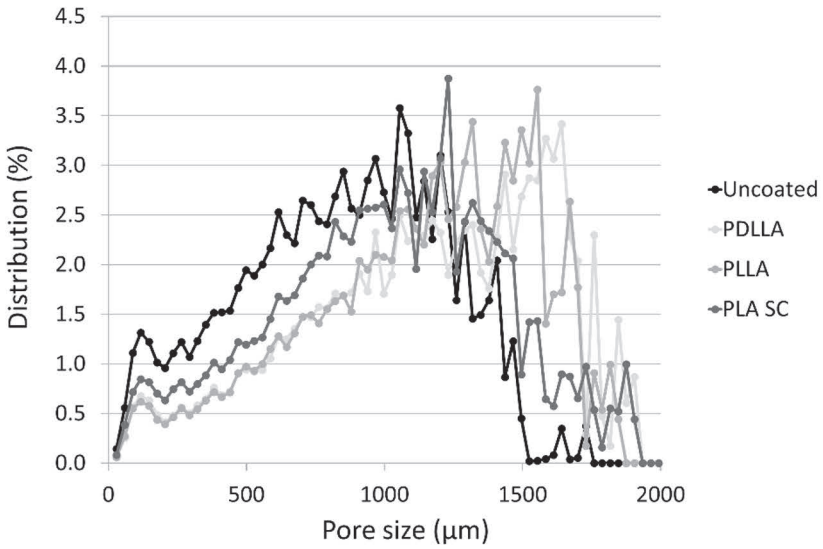

Figure 15. Pore size distribution of foam-replicated bioactive glass scaffolds (Publication IV) as analysed with µCT.

The PLA coating morphology was studied with DSC both before and after a 10-week immersion in SBF. For PDLLA, the only transformation that could be observed was the T_g, indicating the purely amorphous nature of the polymer. For PLLA and PLA SC, both glass transition peaks and melting peaks were apparent, indicating their semicrystalline nature (Figure 16). The melting peak for PLLA before immersion at 183°C indicated homocrystallinity, whereas the melting peak for PLA SC before immersion at 225°C indicated stereocomplex crystallinity. For most PLA SC scaffolds, no peaks indicating homocrystal melting could be detected. The only exception was a melting peak for one 10-week PLA SC scaffold at 176°C, indicating a small quantity of homocrystallinity. Because the polymers were studied as coatings on glass scaffolds, no quantitative analysis could be made from the melting enthalpies with regard to the amount of crystallinity, as a significant and unmeasured amount of glass was present in the analysed samples.

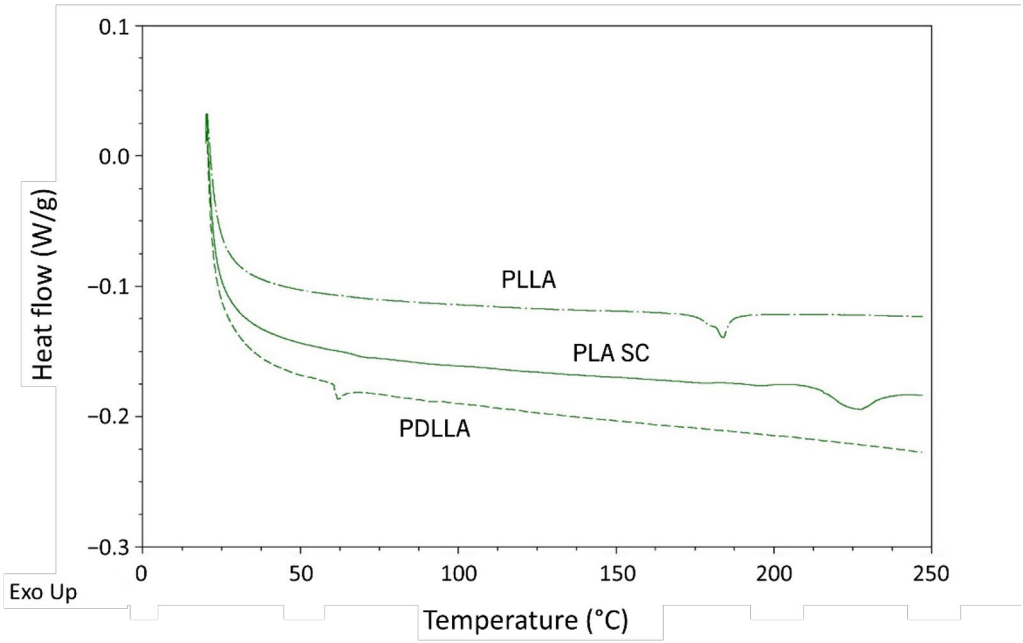

Figure 16. DSC analysis results of 0-week foam-replicated bioactive glass scaffolds for PDLLA, PLLA, and PLA SC coatings (Publication IV). The curves illustrate the phase transitions of the different polymers.

The pH of the solution peaked during the first three weeks of immersion (Figure 17), because of the ion exchange reactions at the glass surface that caused a decrease in the H^+ concentration. The initial pH peak was significantly stronger for the uncoated scaffolds than for the coated scaffolds. While the pH peak is believed to contribute to the antimicrobial properties of the glass (216), it may also have harmful effects for the surrounding tissue (127). After the initial weeks, the pH values remained between pH 7.3 and 7.6. As the immersion solution was replenished every week to fresh SBF, the deviations from pH 7.4 were not cumulative in nature.

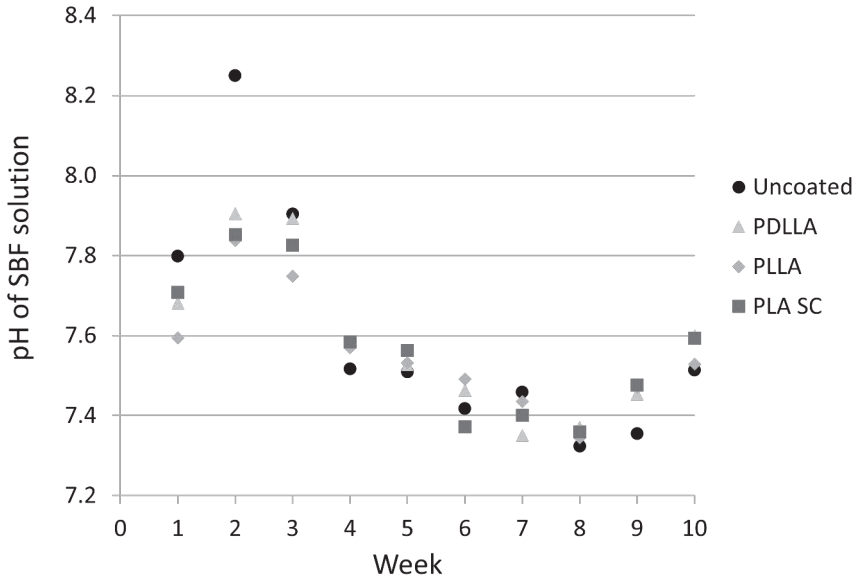

Figure 17. The evolution of pH of SBF solution for foam-replicated bioactive glass scaffolds with different PLA coatings or without coating (Publication IV). As the immersion solutions were replenished weekly, any deviations from the original pH 7.4 are not cumulative.

Bioactive glass dissolution layers were observed with SEM-EDX (Figure 18). Calcium phosphate and silica-rich reaction layers on the bioactive glass surface were apparent for both uncoated and PLA-coated scaffolds at all time points, with significant thickening and increase in coverage of the layers over time. Notably, for coated scaffolds, the calcium phosphate precipitation formed mostly on the polymer surface. This phenomenon, which has been observed also in earlier studies (243–246), should provide a favourable surface for bone growth even where the bioactive glass would not be directly exposed to its surroundings.

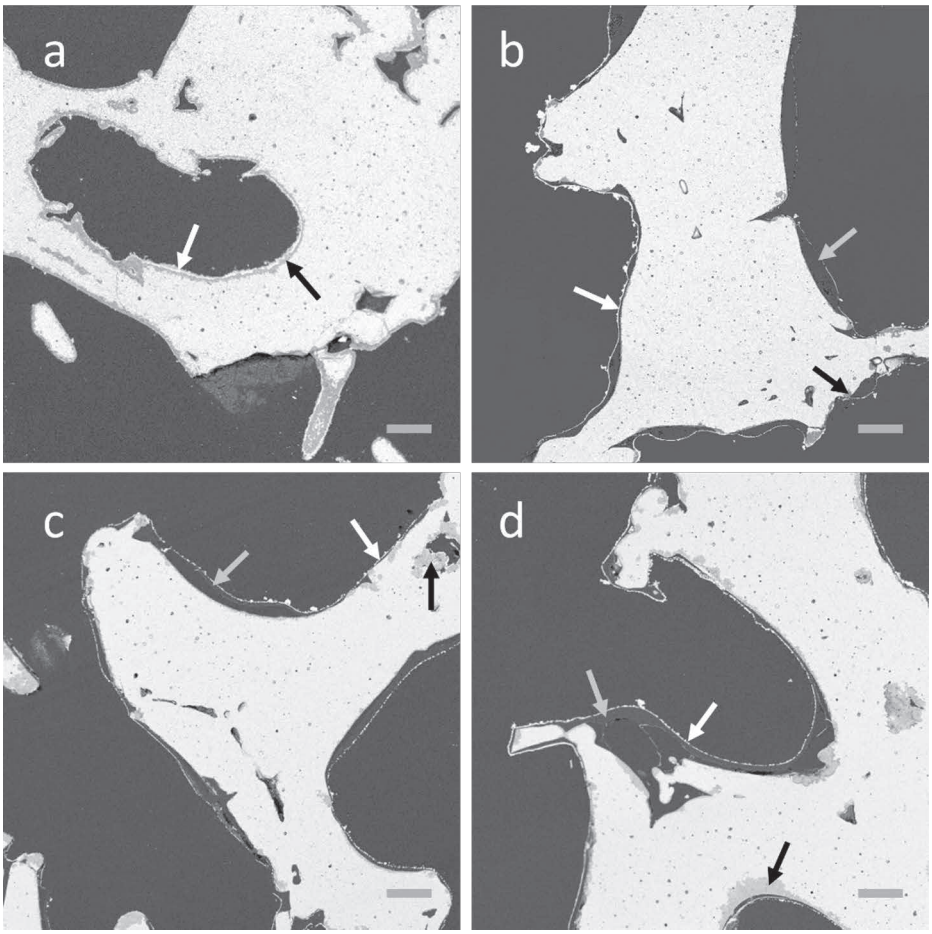

Figure 18. Reaction layers on foam-replicated bioactive glass scaffolds after 10 weeks of immersion in SBF solution (Publication IV) as cross-sectional SEM images: (a) uncoated glass scaffold, (b) glass scaffold with PDLLA coating, (c) glass scaffold with PLLA coating, and (d) glass scaffold with PLA SC coating. Arrows of different colours indicate calcium phosphate layer (white), silica-rich layer (black), and polymer coating (grey). Scale bars 200 μm.

The scaffolds were compression tested both before immersion in their dry state and after immersion in their wet state (Figures 19a, 19b). The uncoated glass scaffolds were brittle. The coatings improved the toughness of the glass scaffolds, with an approximately four-fold increase in toughness for coated scaffolds compared with uncoated scaffolds before immersion, and a two-fold increase after immersion. The coated scaffolds had also higher compressive strength than the uncoated scaffolds, but the difference was not as pronounced. Among the different PLA coatings, the toughness of PLA SC coatings was similar to the homocrystalline PLLA coatings, but significantly higher than for the amorphous PDLLA coatings.

The decrease in toughness and strength after wetting of the coated scaffolds may have resulted from two concurrent phenomena. The absorption of water into the polymer structure may have contributed with a plasticising effect on the amorphous part of the polymer chains, and water entering between the coating and the glass surface may have detached the coating from the glass.

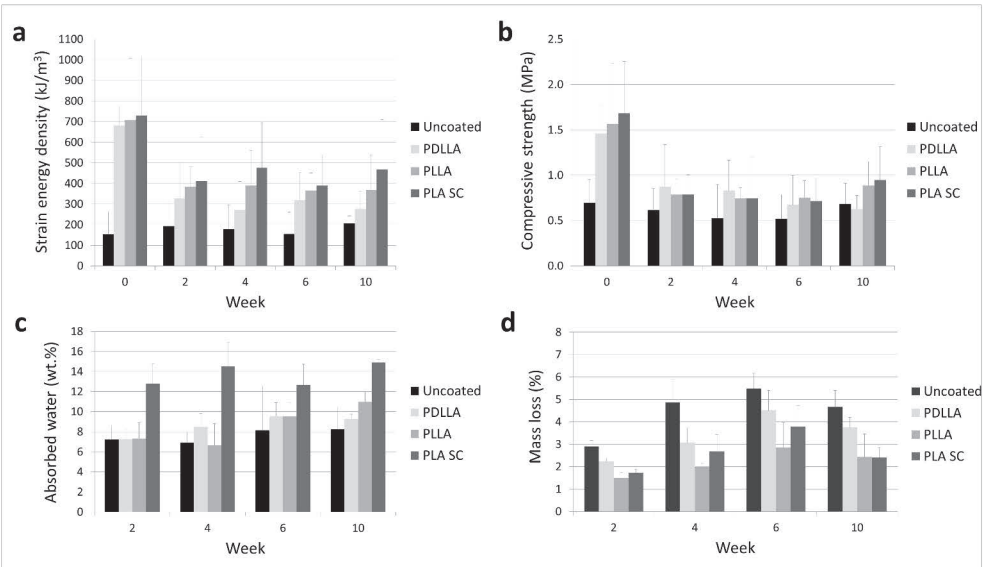

Figure 19. Properties of the PLA-coated bioactive glass scaffolds after immersion in SBF solution (Publication IV): (a) compressive toughness, (b) compressive strength, (c) absorbed water, and (d) mass loss. Error bars indicate standard deviations.

It would have been possible to produce glass scaffolds with higher strength, for instance, by extending the sintering time, or by using sacrificial polymer templates with a different architecture. However, this could have reduced the porosity of the scaffolds. Additionally, the purpose of the tests was to evaluate differences between the different PLA morphologies, and stronger scaffolds could have overshadowed these differences.

Water absorption levels differed between PLA SC and the other scaffolds (Figure 19c), with a significantly higher absorption for PLA SC. The mass loss was small for all scaffolds throughout the study duration, with the highest mass loss measured for uncoated scaffolds (Figure 19d).

Stereocomplexation has not yet been widely utilised in medical device research outside of drug delivery applications (247). PLA SC has good mechanical strength and a significantly higher melting temperature than that of homocrystalline PLA, with potential for creating purely PLA-based highly crystalline mechanically robust structures with spatially varied properties. With well-tuned processing conditions and by utilizing, for instance, additive

manufacturing techniques, this could enable manufacturing of single- or multi-material constructs with finely tuned mechanical properties.

The modulus, strength, and ductility are central parameters to consider when designing scaffolds for bone regeneration. A soft scaffold can be easy to operate and fit into a defect, but it does not allow for weight-bearing after the operation. A stiff and strong scaffold may allow some load-bearing, but it may be more demanding to shape it to fit the defect, unless it is manufactured as a patient-specific implant according to three-dimensional imaging of the defect.

The findings in this study demonstrate the potential for modification of scaffold properties with suitable coatings, not only with regard to the polymer type, but also to the stereochemical characteristics of the polymer. Already a small amount of coating, in this case approximately 3% compared to the glass scaffold mass, brought substantial differences to the scaffold properties.

7. Conclusions and future perspectives

In the first two articles within the thesis, we studied the dimensional stability of PLGA-based gas-foamed and freeze-dried scaffolds *in vitro*. All gas-foamed and the purely polymeric freeze-dried scaffolds experienced significant shrinkage. However, embedded bioactive glass fibres acted as a skeleton within the structure of freeze-dried scaffolds and provided good dimensional stability without any substantial shrinkage. For both gas-foamed and freeze-dried polymer scaffolds, a pH stabilizing effect was achieved by adding bioactive glass into the scaffold structure.

Local administration of magnesium into a bone defect site may promote bone regeneration. We studied the magnesium release from polymer-based gas-foamed scaffolds with a relatively easily soluble magnesium salt, magnesium hydroxide, and with two different magnesium-containing slowly resorbable bioactive glasses. The release of magnesium was up to two orders of magnitude higher and more rapidly decreasing for magnesium hydroxide than for the bioactive glasses. As there is evidence that magnesium supplementation may enhance bone growth especially early in the regeneration process, magnesium hydroxide may be a suitable, slowly dissolving salt for use in bone regeneration scaffolds.

To study the ability of the developed PLGA-based scaffolds to heal osteochondral defects *in vivo*, we compared gas-foamed purely PLGA-containing scaffolds and freeze-dried PLGA–bioactive glass composite scaffolds with clinically used β-TCP and bioactive glass S53P4. While the commercial materials efficiently regenerated bone tissue, the results from the experimental scaffolds were unsatisfactory. The largely closed porosity of the gas-foamed PLGA scaffolds, coupled with significant shrinkage of the structure, probably contributed negatively to the performance of these scaffolds. In contrast, the freeze-dried scaffolds with bioactive glass fibres had well interconnected porosity, and they were dimensionally stable. However, the pore sizes of these scaffolds were probably too small to enable vascularisation throughout the scaffold structure, which may be the explanation for their performance. With an improved pore size range, which may be possible to achieve by modification of the manufacturing parameters, the freeze-drying method could be an efficient method for producing highly porous bone regeneration scaffolds.

PLA is an interesting biomaterial because, despite having the same chemical formula, different stereoisomeric forms of PLA can exhibit markedly different properties. In the final publication, we investigated these properties by coating porous foam-replicated bioactive glass scaffolds with either fully amorphous, homocrystalline, or stereocomplex PLA, and studied their mechanical properties and *in vitro* degradation behaviour. Despite constituting only 3 wt.% of the glass scaffold mass, the coatings significantly enhanced the toughness and strength of the scaffolds, with a four-fold difference for the dry scaffolds prior to their immersion in SBF. The coated scaffolds would therefore be significantly easier to handle during surgery. The polymeric coating was

found to moderate the initial basic pH peak caused by glass dissolution, which would potentially reduce any negative impact to the surrounding host cells and tissues *in vivo*. Furthermore, the calcium phosphate layer resulting from the dissolution of the bioactive glass was primarily formed on the surface of the polymer coating, creating a favourable substrate for the adhesion of bone-forming cells.

It is important to consider the manufacturing techniques for medical devices such as scaffolds for tissue regeneration. While certain methods are well suited for research work, they may not be equally well suited for clinical use due to the regulatory requirements. For example, the foam replication method is an innovative process for manufacturing scaffolds with desirable porosity. However, the manual work that is required in the manufacturing of the green bodies, and the shifting of the dimensions during the sintering step, led to significant individual variation in the final scaffolds. This may be challenging to overcome from a regulatory perspective. Consistency in the production process, with minimal variation among parallels, is beneficial even in basic research.

For potential clinical translation, focusing on the biological requirements for bone regeneration and conducting research with simple, reproducible structures is important. Thorough evaluation of the implants in clinically relevant *in vivo* models is also crucial. For instance, various additive manufacturing techniques, recently adopted for scaffold manufacturing, allow for precise control over the scaffold structure and even enable the creation of individually tailored implants based on the size and shape of the defects. Additive manufacturing also offers a better repeatability than several other manufacturing methods. Although promising, very few products are currently clinically available, and optimization of both design and material choices is necessary. With continued research and innovation, advanced bone regeneration implants have the potential to significantly improve the treatment of clinically demanding bone defects.

References

1. Wu AM, Bisignano C, James SL, Abady GG, Abedi A, Abu-Gharbieh E, et al. Global, regional, and national burden of bone fractures in 204 countries and territories, 1990–2019: a systematic analysis from the Global Burden of Disease Study 2019. Lancet Healthy Longev. 2021;2(9):e580–92.

2. Ghiasi MS, Chen J, Vaziri A, Rodriguez EK, Nazarian A. Bone fracture healing in mechanobiological modeling: A review of principles and methods. Bone Rep. 2017;6:87–100.

3. Keating JF, Simpson AHRW, Robinson CM. The management of fractures with bone loss. J Bone Joint Surg Br. 2005;87-B(2):142–50.

4. Schemitsch EH. Size Matters: Defining Critical in Bone Defect Size! J Orthop Trauma. 2017;31:S20.

5. Nauth A, Schemitsch E, Norris B, Nollin Z, Watson JT. Critical-Size Bone Defects: Is There a Consensus for Diagnosis and Treatment? J Orthop Trauma. 2018;32:S7.

6. Sohn HS, Oh JK. Review of bone graft and bone substitutes with an emphasis on fracture surgeries. Biomater Res. 2019;23(1):9.

7. Fernandez de Grado G, Keller L, Idoux-Gillet Y, Wagner Q, Musset AM, Benkirane-Jessel N, et al. Bone substitutes: a review of their characteristics, clinical use, and perspectives for large bone defects management. J Tissue Eng. 2018;9:2041731418776819.

8. Schulze F, Lang A, Schoon J, Wassilew GI, Reichert J. Scaffold Guided Bone Regeneration for the Treatment of Large Segmental Defects in Long Bones. Biomedicines. 2023;11(2):325.

9. Fu Q. Chapter 15 - Bioactive Glass Scaffolds for Bone Tissue Engineering. In: Kaur G, editor. Biomedical, Therapeutic and Clinical Applications of Bioactive Glasses. Woodhead Publishing; 2019. p. 417–42.

10. Hupa L, Wang X, Eqtesadi S. Bioactive Glasses. In: Musgraves JD, Hu J, Calvez L, editors. Springer Handbook of Glass. Springer International Publishing; 2019. p. 813–49.

11. Kaur G, Pandey O p., Singh K, Homa D, Scott B, Pickrell G. A review of bioactive glasses: Their structure, properties, fabrication and apatite formation. J Biomed Mater Res A. 2014;102(1):254–74.

12. Gerhardt LC, Boccaccini AR. Bioactive Glass and Glass-Ceramic Scaffolds for Bone Tissue Engineering. Materials. 2010;3(7):3867–910.

13. He L, Yin J, Gao X. Additive Manufacturing of Bioactive Glass and Its Polymer Composites as Bone Tissue Engineering Scaffolds: A Review. Bioengineering. 2023;10(6):672.

14. Zhang X, Williams D. Definitions of Biomaterials for the Twenty-First Century. Elsevier; 2019. 292 p.

15. Williams DF. Biocompatibility pathways and mechanisms for bioactive materials: The bioactivity zone. Bioact Mater. 2022;10:306–22.

16. Clarke B. Normal Bone Anatomy and Physiology. Clin J Am Soc Nephrol. 2008;3(Supplement_3):S131.

17. Rho JY, Kuhn-Spearing L, Zioupos P. Mechanical properties and the hierarchical structure of bone. Med Eng Phys. 1998;20(2):92–102.

18. Mercado-Pagán ÁE, Stahl AM, Shanjani Y, Yang Y. Vascularization in Bone Tissue Engineering Constructs. Ann Biomed Eng. 2015;43(3):718–29.

19. Wegst UGK, Bai H, Saiz E, Tomsia AP, Ritchie RO. Bioinspired structural materials. Nat Mater. 2015;14(1):23–36.

20. Boskey AL. Bone composition: relationship to bone fragility and antiosteoporotic drug effects. BoneKEy Rep. 2013;2:447.

21. Von Euw S, Wang Y, Laurent G, Drouet C, Babonneau F, Nassif N, et al. Bone mineral: new insights into its chemical composition. Sci Rep. 2019;9(1):8456.

22. Olszta MJ, Cheng X, Jee SS, Kumar R, Kim YY, Kaufman MJ, et al. Bone structure and formation: A new perspective. Mater Sci Eng R Rep. 2007;58(3):77–116.

23. Metzger CE, Burr DB, Allen MR. Anatomy and Structural Considerations. In: Zaidi M, editor. Encyclopedia of Bone Biology. Oxford: Academic Press; 2020. p. 218–32.

24. Dallas SL, Bonewald LF. Dynamics of the transition from osteoblast to osteocyte. Ann N Y Acad Sci. 2010;1192(1):437–43.

25. Wolff J. Das Gesetz der Transformation der Knochen. DMW - Dtsch Med Wochenschr. 1893;19(47):1222–4.

26. Pearson OM, Lieberman DE. The aging of Wolff's "law": Ontogeny and responses to mechanical loading in cortical bone. Am J Phys Anthropol. 2004;125(S39):63–99.

27. Sumner DR. Long-term implant fixation and stress-shielding in total hip replacement. J Biomech. 2015;48(5):797–800.

28. Föger-Samwald U, Dovjak P, Azizi-Semrad U, Kerschan-Schindl K, Pietschmann P. Osteoporosis: Pathophysiology and therapeutic options. EXCLI J. 2020;20(19):1017–37.

29. Fu R, Liu C, Yan Y, Li Q, Huang RL. Bone defect reconstruction via endochondral ossification: A developmental engineering strategy. J Tissue Eng. 2021;12:20417314211004211.

30. Claes LE, Heigele CA, Neidlinger-Wilke C, Kaspar D, Seidl W, Margevicius KJ, et al. Effects of Mechanical Factors on the Fracture Healing Process. Clin Orthop Relat Res. 1998;355:S132.

31. McKibbin B. The biology of fracture healing in long bones. J Bone Joint Surg Br. 1978;60-B(2):150–62.

32. Debnath S, Yallowitz AR, McCormick J, Lalani S, Zhang T, Xu R, et al. Discovery of a periosteal stem cell mediating intramembranous bone formation. Nature. 2018;562(7725):133–9.

33. Loi F, Córdova LA, Pajarinen J, Lin T hua, Yao Z, Goodman SB. Inflammation, fracture and bone repair. Bone. 2016;86:119–30.

34. LaStayo PC, Winters KM, Hardy M. Fracture healing: Bone healing, fracture management, and current concepts related to the hand. J Hand Ther. 2003;16(2):81–93.

35. Duda GN, Geissler S, Checa S, Tsitsilonis S, Petersen A, Schmidt-Bleek K. The decisive early phase of

bone regeneration. Nat Rev Rheumatol. 2023;19(2):78–95.

36. Marsell R, Einhorn TA. The biology of fracture healing. Injury. 2011;42(6):551–5.

37. Schmidt-Bleek K, Schell H, Lienau J, Schulz N, Hoff P, Pfaff M, et al. Initial immune reaction and angiogenesis in bone healing. J Tissue Eng Regen Med. 2014;8(2):120–30.

38. Fillingham Y, Jacobs J. Bone grafts and their substitutes. Bone Jt J. 2016;98-B(1_Supple_A):6–9.

39. Roberts TT, Rosenbaum AJ. Bone grafts, bone substitutes and orthobiologics. Organogenesis. 2012;8(4):114–24.

40. Fellah BH, Gauthier O, Weiss P, Chappard D, Layrolle P. Osteogenicity of biphasic calcium phosphate ceramics and bone autograft in a goat model. Biomaterials. 2008;29(9):1177–88.

41. Miron RJ, Sculean A, Shuang Y, Bosshardt DD, Gruber R, Buser D, et al. Osteoinductive potential of a novel biphasic calcium phosphate bone graft in comparison with autographs, xenografts, and DFDBA. Clin Oral Implants Res. 2016;27(6):668–75.

42. Hench LL, Jones JR. Bioactive Glasses: Frontiers and Challenges. Front Bioeng Biotechnol. 2015;3.

43. Bohner M, Miron RJ. A proposed mechanism for material-induced heterotopic ossification. Mater Today. 2019;22:132–41.

44. Giannoudis PV, Dinopoulos H, Tsiridis E. Bone substitutes: An update. Injury. 2005;36(3, Supplement):S20–7.

45. Shegarfi H, Reikeras O. Review Article: Bone Transplantation and Immune Response. J Orthop Surg. 2009;17(2):206–11.

46. Baldwin P, Li DJ, Auston DA, Mir HS, Yoon RS, Koval KJ. Autograft, Allograft, and Bone Graft Substitutes: Clinical Evidence and Indications for Use in the Setting of Orthopaedic Trauma Surgery. J Orthop Trauma. 2019;33(4):203.

47. Masquelet A, Kanakaris NK, Obert L, Stafford P, Giannoudis PV. Bone Repair Using the Masquelet Technique. JBJS. 2019;101(11):1024.

48. Younger EM, Chapman MW. Morbidity at Bone Graft Donor Sites. J Orthop Trauma. 1989;3(3):192.

49. Tonk G, Yadav PK, Agarwal S, Jamoh K. Donor site morbidity in autologous bone grafting – A comparison between different techniques of anterior iliac crest bone harvesting: A prospective study. J Orthop Trauma Rehabil. 2022;29(1):22104917221092163.

50. Kim DH, Rhim R, Li L, Martha J, Swaim BH, Banco RJ, et al. Prospective study of iliac crest bone graft harvest site pain and morbidity. Spine J. 2009;9(11):886–92.

51. van de Wall BJM, Beeres FJP, Rompen IF, Link BC, Babst R, Schoeneberg C, et al. RIA versus iliac crest bone graft harvesting: A meta-analysis and systematic review. Injury. 2022;53(2):286–93.

52. Campana V, Milano G, Pagano E, Barba M, Cicione C, Salonna G, et al. Bone substitutes in orthopaedic surgery: from basic science to clinical practice. J Mater Sci Mater Med. 2014;25(10):2445–61.

53. Välimäki VV, Aro HT. Molecular Basis for Action of Bioactive Glasses as Bone Graft Substitute. Scand J Surg. 2006;95(2):95–102.

54. Zhang H, Yang L, Yang X gang, Wang F, Feng J tao, Hua K chi, et al. Demineralized Bone Matrix Carriers and their Clinical Applications: An Overview. Orthop Surg. 2019;11(5):725–37.

55. Gruskin E, Doll BA, Futrell FW, Schmitz JP, Hollinger JO. Demineralized bone matrix in bone repair: History and use. Adv Drug Deliv Rev. 2012;64(12):1063–77.

56. Bumbasirevic M, Stevanovic M, Bumbasirevic V, Lesic A, Atkinson HDE. Free vascularised fibular grafts in orthopaedics. Int Orthop. 2014;38(6):1277–82.

57. Feltri P, Solaro L, Errani C, Schiavon G, Candrian C, Filardo G. Vascularized fibular grafts for the treatment of long bone defects: pros and cons. A systematic review and meta-analysis. Arch Orthop Trauma Surg. 2023;143(1):29–48.

58. Koons GL, Diba M, Mikos AG. Materials design for bone-tissue engineering. Nat Rev Mater. 2020;5(8):584–603.

59. Cattalini JP, Boccaccini AR, Lucangioli S, Mouriño V. Bisphosphonate-Based Strategies for Bone Tissue Engineering and Orthopedic Implants. Tissue Eng Part B Rev. 2012;18(5):323–40.

60. Cui Y, Zhu T, Li D, Li Z, Leng Y, Ji X, et al. Bisphosphonate-Functionalized Scaffolds for Enhanced Bone Regeneration. Adv Healthc Mater. 2019;8(23):1901073.

61. Chew SA, Danti S. Biomaterial-Based Implantable Devices for Cancer Therapy. Adv Healthc Mater. 2017;6(2):1600766.

62. Baino F, Fiume E, Ciavattini S, Kargozar S, Borges R, Genova LA, et al. Biomedical Radioactive Glasses for Brachytherapy. Materials. 2021;14(5):1131.

63. Mariano LC, Fernandes MHR, Gomes PS. Antimicrobial Biomaterials for the Healing of Infected Bone Tissue: A Systematic Review of Microtomographic Data on Experimental Animal Models. J Funct Biomater. 2022;13(4):193.

64. Hollister SJ, Murphy WL. Scaffold Translation: Barriers Between Concept and Clinic. Tissue Eng Part B Rev. 2011;17(6):459–74.

65. Volk HD, Stevens MM, Mooney DJ, Grainger DW, Duda GN. Key elements for nourishing the translational research environment. Sci Transl Med. 2015;7(282):282cm2-282cm2.

66. Nair LS, Laurencin CT. Biodegradable polymers as biomaterials. Prog Polym Sci. 2007;32(8):762–98.

67. Puppi D, Chiellini F, Piras AM, Chiellini E. Polymeric materials for bone and cartilage repair. Prog Polym Sci. 2010;35(4):403–40.

68. Bayon Y, Bohner M, Eglin D, Thérin M, Montali A, Procter P, et al. Progressing innovation in biomaterials. From the bench to the bed of patients. J Mater Sci Mater Med. 2015;26(9):228.

69. Giannoudis PV, Einhorn TA, Marsh D. Fracture healing: The diamond concept. Injury. 2007;38:S3–6.

70. Bara JJ, Herrmann M, Evans CH, Miclau T, Ratcliffe A, Richards RG. Improving translation success of cell-based therapies in orthopaedics. J Orthop Res. 2016;34(1):17–21.

71. Oliveira ÉR, Nie L, Podstawczyk D, Allahbakhsh A, Ratnayake J, Brasil DL, et al. Advances in Growth Factor Delivery for Bone Tissue Engineering. Int J Mol Sci. 2021;22(2):903.

72. Simunovic F, Finkenzeller G. Vascularization Strategies in Bone

Tissue Engineering. Cells. 2021;10(7):1749.

73. Sathy BN, Mony U, Menon D, Baskaran VK, Mikos AG, Nair S. Bone Tissue Engineering with Multilayered Scaffolds—Part I: An Approach for Vascularizing Engineered Constructs In Vivo. Tissue Eng Part A. 2015;21(19–20):2480–94.

74. Lienau J, Schmidt-Bleek K, Peters A, Haschke F, Duda GN, Perka C, et al. Differential regulation of blood vessel formation between standard and delayed bone healing. J Orthop Res. 2009;27(9):1133–40.

75. Schmidt-Bleek K, Petersen A, Dienelt A, Schwarz C, Duda GN. Initiation and early control of tissue regeneration – bone healing as a model system for tissue regeneration. Expert Opin Biol Ther. 2014;14(2):247–59.

76. Winkler T, Sass FA, Duda GN, Schmidt-Bleek K. A review of biomaterials in bone defect healing, remaining shortcomings and future opportunities for bone tissue engineering: The unsolved challenge. Bone Jt Res. 2018;7(3):232–43.

77. Alasvand N, Simorgh S, Malekzadeh Kebria M, Bozorgi A, Moradi S, Hosseinpour Sarmadi V, et al. Copper / cobalt doped strontium-bioactive glasses for bone tissue engineering applications. Open Ceram. 2023;14:100358.

78. Wang Y, Zhang W, Yao Q. Copper-based biomaterials for bone and cartilage tissue engineering. J Orthop Transl. 2021;29:60–71.

79. Glenske K, Donkiewicz P, Köwitsch A, Milosevic-Oljaca N, Rider P, Rofall S, et al. Applications of Metals for Bone Regeneration. Int J Mol Sci. 2018;19(3):826.

80. Polo-Corrales L, Latorre-Esteves M, Ramirez-Vick JE. Scaffold Design for Bone Regeneration. J Nanosci Nanotechnol. 2014;14(1):15–56.

81. Karageorgiou V, Kaplan D. Porosity of 3D biomaterial scaffolds and osteogenesis. Biomaterials. 2005;26(27):5474–91.

82. Abbasi N, Hamlet S, Love RM, Nguyen NT. Porous scaffolds for bone regeneration. J Sci Adv Mater Devices. 2020;5(1):1–9.

83. Bružauskaitė I, Bironaitė D, Bagdonas E, Bernotienė E. Scaffolds and cells for tissue regeneration: different scaffold pore sizes—different cell effects. Cytotechnology. 2016;68(3):355–69.

84. Itälä AI, Ylänen HO, Ekholm C, Karlsson KH, Aro HT. Pore diameter of more than 100 μm is not requisite for bone ingrowth in rabbits. J Biomed Mater Res. 2001;58(6):679–83.

85. Sicchieri LG, Crippa GE, de Oliveira PT, Beloti MM, Rosa AL. Pore size regulates cell and tissue interactions with PLGA–CaP scaffolds used for bone engineering. J Tissue Eng Regen Med. 2012;6(2):155–62.

86. Lu X, Wang Y, Jin F. Influence of a non-biodegradable porous structure on bone repair. RSC Adv. 2016;6(84):80522–8.

87. Mishra S, Knothe Tate ML. Effect of lacunocanalicular architecture on hydraulic conductance in bone tissue: Implications for bone health and evolution. Anat Rec - Part Discov Mol Cell Evol Biol. 2003;273(2):752–62.

88. Bohner M, Baroud G, Bernstein A, Döbelin N, Galea L, Hesse B, et al. Characterization and distribution of mechanically competent mineralized tissue in micropores of β-tricalcium phosphate bone substitutes. Mater Today. 2017;20(3):106–15.

89. Pattnaik A, Sanket AS, Pradhan S, Sahoo R, Das S, Pany S, et al. Designing of gradient scaffolds and their applications in tissue regeneration. Biomaterials. 2023;296:122078.

90. Jodati H, Yılmaz B, Evis Z. A review of bioceramic porous scaffolds for hard tissue applications: Effects of structural features. Ceram Int. 2020;46(10, Part B):15725–39.

91. Glatt V, Evans CH, Tetsworth K. A Concert between Biology and Biomechanics: The Influence of the Mechanical Environment on Bone Healing. Front Physiol. 2017;7.

92. Burke DP, Kelly DJ. Substrate Stiffness and Oxygen as Regulators of Stem Cell Differentiation during Skeletal Tissue Regeneration: A Mechanobiological Model. PLOS ONE. 2012;7(7):e40737.

93. Prasad A, Sankar MR, Katiyar V. State of Art on Solvent Casting Particulate Leaching Method for Orthopedic ScaffoldsFabrication. Mater Today Proc. 2017;4(2):898–907.

94. Fereshteh Z. 7 - Freeze-drying technologies for 3D scaffold engineering. In: Deng Y, Kuiper J, editors. Functional 3D Tissue Engineering Scaffolds. Woodhead Publishing; 2018. p. 151–74.

95. Mathieu LM, Montjovent MO, Bourban PE, Pioletti DP, Månson J a. E. Bioresorbable composites prepared by supercritical fluid foaming. J Biomed Mater Res A. 2005;75A(1):89–97.

96. Salerno A, Oliviero M, Di Maio E, Iannace S, Netti PA. Design of porous polymeric scaffolds by gas foaming of heterogeneous blends. J Mater Sci Mater Med. 2009;20(10):2043–51.

97. Pitkänen S, Paakinaho K, Pihlman H, Ahola N, Hannula M, Asikainen S, et al. Characterisation and in vitro and in vivo evaluation of supercritical-CO2-foamed β-TCP/PLCL composites for bone applications. Eur Cell Mater. 2019;38:35–50.

98. Zhou H, Green TB, Joo YL. The thermal effects on electrospinning of polylactic acid melts. Polymer. 2006;47(21):7497–505.

99. Fang J, Zhang L, Sutton D, Wang X, Lin T. Needleless Melt-Electrospinning of Polypropylene Nanofibres. J Nanomater. 2012;2012:e382639.

100. Yang Y, Wang G, Liang H, Gao C, Peng S, Shen L, et al. Additive manufacturing of bone scaffolds. Int J Bioprinting. 2018;5(1):148.

101. Liu X, Ma PX. Polymeric Scaffolds for Bone Tissue Engineering. Ann Biomed Eng. 2004;32(3):477–86.

102. Rezwan K, Chen QZ, Blaker JJ, Boccaccini AR. Biodegradable and bioactive porous polymer/inorganic composite scaffolds for bone tissue engineering. Biomaterials. 2006;27(18):3413–31.

103. Ge Z, Jin Z, Cao T. Manufacture of degradable polymeric scaffolds for bone regeneration. Biomed Mater. 2008;3(2):022001.

104. Eltom A, Zhong G, Muhammad A. Scaffold Techniques and Designs in Tissue Engineering Functions and Purposes: A Review. Adv Mater Sci Eng. 2019;2019:e3429527.

105. Amiryaghoubi N, Fathi M, Pesyan NN, Samiei M, Barar J, Omidi Y. Bioactive polymeric scaffolds for osteogenic repair and bone regenerative medicine. Med Res Rev. 2020;40(5):1833–70.

106. Lu T, Li Y, Chen T. Techniques for fabrication and construction of three-dimensional scaffolds for tissue engineering. Int J Nanomedicine. 2013;8(1):337–50.

107. Haider A, Haider S, Rao Kummara M, Kamal T, Alghyamah AAA, Jan Iftikhar F, et al. Advances in the scaffolds fabrication techniques using biocompatible polymers and their biomedical application: A technical and statistical review. J Saudi Chem Soc. 2020;24(2):186–215.

108. Kim HD, Amirthalingam S, Kim SL, Lee SS, Rangasamy J, Hwang NS. Biomimetic Materials and Fabrication Approaches for Bone Tissue Engineering. Adv Healthc Mater. 2017;6(23):1700612.

109. Chocholata P, Kulda V, Babuska V. Fabrication of Scaffolds for Bone-Tissue Regeneration. Materials. 2019;12(4):568.

110. Wubneh A, Tsekoura EK, Ayranci C, Uludağ H. Current state of fabrication technologies and materials for bone tissue engineering. Acta Biomater. 2018;80:1–30.

111. Abdelaziz AG, Nageh H, Abdo SM, Abdalla MS, Amer AA, Abdal-hay A, et al. A Review of 3D Polymeric Scaffolds for Bone Tissue Engineering: Principles, Fabrication Techniques, Immunomodulatory Roles, and Challenges. Bioengineering. 2023;10(2):204.

112. Chen QZ, Thompson ID, Boccaccini AR. 45S5 Bioglass®-derived glass–ceramic scaffolds for bone tissue engineering. Biomaterials. 2006;27(11):2414–25.

113. Park YS, Kim KN, Kim KM, Choi SH, Kim CK, Legeros RZ, et al. Feasibility of three-dimensional macroporous scaffold using calcium phosphate glass and polyurethane sponge. J Mater Sci. 2006;41(13):4357–64.

114. Fiume E, Ciavattini S, Verné E, Baino F. Foam Replica Method in the Manufacturing of Bioactive Glass Scaffolds: Out-of-Date Technology or Still Underexploited Potential? Materials. 2021;14(11):2795.

115. Nagel B, Dellweg H, Gierasch LM. Glossary for chemists of terms used in biotechnology (IUPAC Recommendations 1992). Pure Appl Chem. 1992;64(1):143–68.

116. Vert M, Doi Y, Hellwich KH, Hess M, Hodge P, Kubisa P, et al. Terminology for biorelated polymers and applications (IUPAC Recommendations 2012). Pure Appl Chem. 2012;84(2):377–410.

117. Middleton JC, Tipton AJ. Synthetic biodegradable polymers as orthopedic devices. Biomaterials. 2000;21(23):2335–46.

118. Ulery BD, Nair LS, Laurencin CT. Biomedical applications of biodegradable polymers. J Polym Sci Part B Polym Phys. 2011;49(12):832–64.

119. Sheikh Z, Najeeb S, Khurshid Z, Verma V, Rashid H, Glogauer M. Biodegradable Materials for Bone Repair and Tissue Engineering Applications. Materials. 2015;8(9):5744–94.

120. Wei S, Ma JX, Xu L, Gu XS, Ma XL. Biodegradable materials for bone defect repair. Mil Med Res. 2020;7(1):54.

121. Yu H, Liu H, Shen Y, Ao Q. Synthetic biodegradable polymer materials in the repair of tumor-associated bone defects. Front Bioeng Biotechnol. 2023;11.

122. Khan H, Barkham B, Trompeter A. The use of bioabsorbable materials in orthopaedics. Orthop Trauma. 2021;35(5):289–96.

123. Fagerlund S, Hupa L, Hupa M. Comparison of Reactions of Bioactive Glasses in Different Aqueous Solutions. In: Advances in

Bioceramics and Biotechnologies. John Wiley & Sons, Ltd; 2010. p. 101–13.

124. Varila L, Fagerlund S, Lehtonen T, Tuominen J, Hupa L. Surface reactions of bioactive glasses in buffered solutions. J Eur Ceram Soc. 2012;32(11):2757–63.

125. Bohner M, Lemaitre J. Can bioactivity be tested in vitro with SBF solution? Biomaterials. 2009;30(12):2175–9.

126. Kim MK, Paek K, Woo SM, Kim JA. Bone-on-a-Chip: Biomimetic Models Based on Microfluidic Technologies for Biomedical Applications. ACS Biomater Sci Eng. 2023;9(6):3058–73.

127. El-Rashidy AA, Roether JA, Harhaus L, Kneser U, Boccaccini AR. Regenerating bone with bioactive glass scaffolds: A review of in vivo studies in bone defect models. Acta Biomater. 2017;62:1–28.

128. Dienel K, Abu-Shahba A, Kornilov R, Björkstrand R, van Bochove B, Snäll J, et al. Patient-Specific Bioimplants and Reconstruction Plates for Mandibular Defects: Production Workflow and In Vivo Large Animal Model Study. Macromol Biosci. 2022;22(4):2100398.

129. Williams DF. On the mechanisms of biocompatibility. Biomaterials. 2008;29(20):2941–53.

130. Crawford L, Wyatt M, Bryers J, Ratner B. Biocompatibility Evolves: Phenomenology to Toxicology to Regeneration. Adv Healthc Mater. 2021;10(11):2002153.

131. Williams DF. Enzymic Hydrolysis of Polylactic Acid. Eng Med. 1981;10(1):5–7.

132. Göpferich A. Mechanisms of polymer degradation and erosion. Biomaterials. 1996;17(2):103–14.

133. Laycock B, Nikolić M, Colwell JM, Gauthier E, Halley P, Bottle S, et al. Lifetime prediction of biodegradable polymers. Prog Polym Sci. 2017;71:144–89.

134. Woodruff MA, Hutmacher DW. The return of a forgotten polymer—Polycaprolactone in the 21st century. Prog Polym Sci. 2010;35(10):1217–56.

135. Zhang Y, Andrukhov O, Berner S, Matejka M, Wieland M, Rausch-Fan X, et al. Osteogenic properties of hydrophilic and hydrophobic titanium surfaces evaluated with osteoblast-like cells (MG63) in coculture with human umbilical vein endothelial cells (HUVEC). Dent Mater. 2010;26(11):1043–51.

136. Lotz EM, Olivares-Navarrete R, Berner S, Boyan BD, Schwartz Z. Osteogenic response of human MSCs and osteoblasts to hydrophilic and hydrophobic nanostructured titanium implant surfaces. J Biomed Mater Res A. 2016;104(12):3137–48.

137. Oliveira DP de, Micocci KC, Almeida GFB de, Otuka AJG, Mendonça CR, Selistre-de-Araujo HS, et al. Comparison of hydrophilic and hydrophobic nano topographic surfaces of titanium alloys on pre-osteoblastic cell interaction. Biomed Phys Eng Express. 2023;9(4):045020.

138. Paakinaho K, Heino H, Väisänen J, Törmälä P, Kellomäki M. Effects of lactide monomer on the hydrolytic degradation of poly(lactide-co-glycolide) 85L/15G. J Mech Behav Biomed Mater. 2011;4(7):1283–90.

139. Bergsma JE, de Bruijn WC, Rozema FR, Bos RRM, Boering G. Late degradation tissue response to poly(l-lactide) bone plates and screws. Biomaterials. 1995;16(1):25–31.

140. Athanasiou K, Agrawal C, Barber F, Burkhart S. Orthopaedic applications for PLA-PGA biodegradable polymers. Arthrosc J Arthrosc Relat Surg. 1998;14(7):726–37.

141. Wang X, Sun H, Song M, Yan G, Wang Q. The Biodegradability and in Vitro Cytological Study on the Composite of PLGA Combined With Magnesium Metal. Front Bioeng Biotechnol. 2022;10.

142. Gupta AP, Kumar V. New emerging trends in synthetic biodegradable polymers – Polylactide: A critique. Eur Polym J. 2007;43(10):4053–74.

143. Jamshidian M, Tehrany EA, Imran M, Jacquot M, Desobry S. Poly-Lactic Acid: Production, Applications, Nanocomposites, and Release Studies. Compr Rev Food Sci Food Saf. 2010;9(5):552–71.

144. Okada M. Chemical syntheses of biodegradable polymers. Prog Polym Sci. 2002;27(1):87–133.

145. Dechy-Cabaret O, Martin-Vaca B, Bourissou D. Controlled Ring-Opening Polymerization of Lactide and Glycolide. Chem Rev. 2004;104(12):6147–76.

146. Inkinen S, Hakkarainen M, Albertsson AC, Södergård A. From Lactic Acid to Poly(lactic acid) (PLA): Characterization and Analysis of PLA and Its Precursors. Biomacromolecules. 2011;12(3):523–32.

147. Farah S, Anderson DG, Langer R. Physical and mechanical properties of PLA, and their functions in widespread applications — A comprehensive review. Adv Drug Deliv Rev. 2016;107:367–92.

148. Singha S, Hedenqvist MS. A Review on Barrier Properties of Poly(Lactic Acid)/Clay Nanocomposites. Polymers. 2020;12(5):1095.

149. Rasal RM, Janorkar AV, Hirt DE. Poly(lactic acid) modifications. Prog Polym Sci. 2010;35(3):338–56.

150. Gilding DK, Reed AM. Biodegradable polymers for use in surgery—polyglycolic/poly(actic acid) homo- and copolymers: 1. Polymer. 1979;20(12):1459–64.

151. Perego G, Cella GD, Bastioli C. Effect of molecular weight and crystallinity on poly(lactic acid) mechanical properties. J Appl Polym Sci. 1996;59(1):37–43.

152. Zaaba NF, Jaafar M. A review on degradation mechanisms of polylactic acid: Hydrolytic, photodegradative, microbial, and enzymatic degradation. Polym Eng Sci. 2020;60(9):2061–75.

153. de Jong SJ, van Dijk-Wolthuis WNE, Kettenes-van den Bosch JJ, Schuyl PJW, Hennink WE. Monodisperse Enantiomeric Lactic Acid Oligomers: Preparation, Characterization, and Stereocomplex Formation. Macromolecules. 1998;31(19):6397–402.

154. Rahaman MdH, Tsuji H. Synthesis and Characterization of Stereo Multiblock Poly(lactic acid)s with Different Block Lengths by Melt Polycondensation of Poly(L-lactic acid)/Poly(D-lactic acid) Blends. Macromol React Eng. 2012;6(11):446–57.

155. Garlotta D. A Literature Review of Poly(Lactic Acid). J Polym Environ. 2001;9(2):63–84.

156. Tsuji H. Poly(lactide) Stereocomplexes: Formation, Structure, Properties, Degradation, and Applications. Macromol Biosci. 2005;5(7):569–97.

157. Fukushima K, Kimura Y. Stereocomplexed polylactides (Neo-PLA) as high-performance bio-based polymers: their formation,

properties, and application. Polym Int. 2006;55(6):626–42.

158. Tsuji H. Poly(lactic acid) stereocomplexes: A decade of progress. Adv Drug Deliv Rev. 2016;107:97–135.

159. Takasaki M, Ito H, Kikutani T. Development of Stereocomplex Crystal of Polylactide in High-Speed Melt Spinning and Subsequent Drawing and Annealing Processes. J Macromol Sci Part B. 2003;42(3–4):403–20.

160. Sarasua J r., Arraiza AL, Balerdi P, Maiza I. Crystallinity and mechanical properties of optically pure polylactides and their blends. Polym Eng Sci. 2005;45(5):745–53.

161. Furuhashi Y, Kimura Y, Yoshie N, Yamane H. Higher-order structures and mechanical properties of stereocomplex-type poly(lactic acid) melt spun fibers. Polymer. 2006;47(16):5965–72.

162. Sakai R, John B, Okamoto M, Seppälä JV, Vaithilingam J, Hussein H, et al. Fabrication of Polylactide-Based Biodegradable Thermoset Scaffolds for Tissue Engineering Applications. Macromol Mater Eng. 2013;298(1):45–52.

163. Pérez Davila S, González Rodríguez L, Chiussi S, Serra J, González P. How to Sterilize Polylactic Acid Based Medical Devices? Polymers. 2021;13(13):2115.

164. Pachence JM, Bohrer MP, Kohn J. Chapter Twenty-Three - Biodegradable Polymers. In: Lanza R, Langer R, Vacanti J, editors. Principles of Tissue Engineering (Third Edition). Burlington: Academic Press; 2007. p. 323–39.

165. Hamad K, Kaseem M, Yang HW, Deri F, Ko YG. Properties and medical applications of polylactic acid: A review. EXPRESS Polym Lett. 2015;9(5):435–55.

166. Lunt J. Large-scale production, properties and commercial applications of polylactic acid polymers. Polym Degrad Stab. 1998;59(1):145–52.

167. Narayanan G, Vernekar VN, Kuyinu EL, Laurencin CT. Poly (lactic acid)-based biomaterials for orthopaedic regenerative engineering. Adv Drug Deliv Rev. 2016;107:247–76.

168. Jing Y, Quan C, Liu B, Jiang Q, Zhang C. A Mini Review on the Functional Biomaterials Based on Poly(lactic acid) Stereocomplex. Polym Rev. 2016;56(2):262–86.

169. Gentile P, Chiono V, Carmagnola I, Hatton PV. An Overview of Poly(lactic-co-glycolic) Acid (PLGA)-Based Biomaterials for Bone Tissue Engineering. Int J Mol Sci. 2014;15(3):3640–59.

170. Xu Y, Kim CS, Saylor DM, Koo D. Polymer degradation and drug delivery in PLGA-based drug–polymer applications: A review of experiments and theories. J Biomed Mater Res B Appl Biomater. 2017;105(6):1692–716.

171. Liu G, McEnnis K. Glass Transition Temperature of PLGA Particles and the Influence on Drug Delivery Applications. Polymers. 2022;14(5):993.

172. Wu XS, Wang N. Synthesis, characterization, biodegradation, and drug delivery application of biodegradable lactic/glycolic acid polymers. Part II: Biodegradation. J Biomater Sci Polym Ed. 2001;12(1):21–34.

173. Vert M, Mauduit J, Li S. Biodegradation of PLA/GA polymers: increasing complexity. Biomaterials. 1994;15(15):1209–13.

174. Garner J, Skidmore S, Park H, Park K, Choi S, Wang Y. A protocol for assay of poly(lactide-co-glycolide) in clinical products. Int J Pharm. 2015;495(1):87–92.

175. Ghitman J, Biru EI, Stan R, Iovu H. Review of hybrid PLGA nanoparticles: Future of smart drug delivery and theranostics medicine. Mater Des. 2020;193:108805.

176. Borandeh S, van Bochove B, Teotia A, Seppälä J. Polymeric drug delivery systems by additive manufacturing. Adv Drug Deliv Rev. 2021;173:349–73.

177. Rocha CV, Gonçalves V, da Silva MC, Bañobre-López M, Gallo J. PLGA-Based Composites for Various Biomedical Applications. Int J Mol Sci. 2022;23(4):2034.

178. Wan B, Bao Q, Burgess D. Long-acting PLGA microspheres: Advances in excipient and product analysis toward improved product understanding. Adv Drug Deliv Rev. 2023;198:114857.

179. Danhier F, Ansorena E, Silva JM, Coco R, Le Breton A, Préat V. PLGA-based nanoparticles: An overview of biomedical applications. J Controlled Release. 2012;161(2):505–22.

180. Li J, Stayshich RM, Meyer TY. Exploiting Sequence To Control the Hydrolysis Behavior of Biodegradable PLGA Copolymers. J Am Chem Soc. 2011;133(18):6910–3.

181. Tilocca A, Cormack AN, de Leeuw NH. The Structure of Bioactive Silicate Glasses: New Insight from Molecular Dynamics Simulations. Chem Mater. 2007;19(1):95–103.

182. Hench LL. The story of Bioglass®. J Mater Sci Mater Med. 2006;17(11):967–78.

183. Baino F, Hamzehlou S, Kargozar S. Bioactive Glasses: Where Are We and Where Are We Going? J Funct Biomater. 2018;9(1):25.

184. Kokubo T. Bioactive glass ceramics: properties and applications. Biomaterials. 1991;12(2):155–63.

185. Kokubo T, Takadama H. How useful is SBF in predicting in vivo bone bioactivity? Biomaterials. 2006;27(15):2907–15.

186. Hench LL, Paschall HA. Direct chemical bond of bioactive glass-ceramic materials to bone and muscle. J Biomed Mater Res. 1973;7(3):25–42.

187. Brink M. The influence of alkali and alkaline earths on the working range for bioactive glasses. J Biomed Mater Res. 1997;36(1):109–17.

188. Hench LL. Chronology of Bioactive Glass Development and Clinical Applications. New J Glass Ceram. 2013;3(2):67–73.

189. Liang W, Christian R, Day DE, Völksch G. Bioactive comparison of a borate, phosphate and silicate glass. J Mater Res. 2006;21(1):125–31.

190. Lepry WC, Nazhat SN. A Review of Phosphate and Borate Sol–Gel Glasses for Biomedical Applications. Adv NanoBiomed Res. 2021;1(3):2000055.

191. Ege D, Zheng K, Boccaccini AR. Borate Bioactive Glasses (BBG): Bone Regeneration, Wound Healing Applications, and Future Directions. ACS Appl Bio Mater. 2022;5(8):3608–22.

192. Brink M, Turunen T, Happonen RP, Yli-Urpo A. Compositional dependence of bioactivity of glasses in the system Na2O-K2O-MgO-CaO-B2O3-P2O5-SiO2. J Biomed Mater Res. 1997;37(1):114–21.

193. Brauer DS, Hupa L. Glass as a biomaterial: strategies for optimising bioactive glasses for clinical applications. Comptes Rendus Géoscience. 2022;354(S1):185–97.

194. Lockyer MWG, Holland D, Dupree R. NMR investigation of the structure of some bioactive and related glasses. J Non-Cryst Solids. 1995;188(3):207–19.

195. O'Donnell MD, Watts SJ, Law RV, Hill RG. Effect of P2O5 content in two series of soda lime phosphosilicate glasses on structure and properties – Part I: NMR. J Non-Cryst Solids. 2008;354(30):3554–60.

196. Hench LL, Andersson Ö. Bioactive glasses. In: An Introduction to Bioceramics. WORLD SCIENTIFIC; 1993. p. 41–62. (Advanced Series in Ceramics; vol. Volume 1).

197. O'Donnell MD, Watts SJ, Hill RG, Law RV. The effect of phosphate content on the bioactivity of soda-lime-phosphosilicate glasses. J Mater Sci Mater Med. 2009;20(8):1611–8.

198. Kargozar S, Baino F, Hamzehlou S, Hill RG, Mozafari M. Bioactive glasses entering the mainstream. Drug Discov Today. 2018;23(10):1700–4.

199. Vedel E, Zhang D, Arstila H, Hupa L, Hupa M. Predicting physical and chemical properties of bioactive glasses from chemical composition.Part 4: Tailoring compositions with desired properties. Glass Technol - Eur J Glass Sci Technol Part A. 2009;50(1):9–16.

200. Zhang D, Vedel E, Hupa L, Aro HT, Hupa M. Predicting physical and chemical properties of bioactive glasses from chemical composition.Part 3: In vitro reactivity. Glass Technol - Eur J Glass Sci Technol Part A. 2009;50(1):1–8.

201. Fagerlund S, Hupa L, Hupa M. Dissolution patterns of biocompatible glasses in 2-amino-2-hydroxymethyl-propane-1,3-diol (Tris) buffer. Acta Biomater. 2013;9(2):5400–10.

202. Brauer DS, Rüssel C, Kraft J. Solubility of glasses in the system P2O5–CaO–MgO–Na2O–TiO2: Experimental and modeling using artificial neural networks. J Non-Cryst Solids. 2007;353(3):263–70.

203. O'Donnell MD. Predicting bioactive glass properties from the molecular chemical composition: Glass transition temperature. Acta Biomater. 2011;7(5):2264–9.

204. Fagerlund S, Massera J, Hupa M, Hupa L. T–T–T behaviour of bioactive glasses 1–98 and 13–93. J Eur Ceram Soc. 2012;32(11):2731–8.

205. Jones JR. Review of bioactive glass: From Hench to hybrids. Acta Biomater. 2013;9(1):4457–86.

206. Kaou MH, Furkó M, Balázsi K, Balázsi C. Advanced Bioactive Glasses: The Newest Achievements and Breakthroughs in the Area. Nanomaterials. 2023;13(16):2287.

207. Lindfors NC, Heikkilä JT, Koski I, Mattila K, Aho AJ. Bioactive glass and autogenous bone as bone graft substitutes in benign bone tumors. J Biomed Mater Res B Appl Biomater. 2009;90B(1):131–6.

208. Lindfors NC. Treatment of a recurrent aneurysmal bone cyst with bioactive glass in a child allows for good bone remodelling and growth. Bone. 2009;45(2):398–400.

209. Lindfors NC, Koski I, Heikkilä JT, Mattila K, Aho AJ. A prospective randomized 14-year follow-up study of bioactive glass and autogenous bone as bone graft substitutes in benign bone tumors. J Biomed Mater

Res B Appl Biomater. 2010;94B(1):157–64.

210. Hoppe A, Güldal NS, Boccaccini AR. A review of the biological response to ionic dissolution products from bioactive glasses and glass-ceramics. Biomaterials. 2011;32(11):2757–74.

211. Maeno S, Niki Y, Matsumoto H, Morioka H, Yatabe T, Funayama A, et al. The effect of calcium ion concentration on osteoblast viability, proliferation and differentiation in monolayer and 3D culture. Biomaterials. 2005;26(23):4847–55.

212. Turner J, Nandakumar A, Anilbhai N, Boccaccini AR, Jones JR, Jell G. The effect of Si species released from bioactive glasses on cell behaviour: A quantitative review. Acta Biomater. 2023;170:39–52.

213. Sinitsyna P, Karlström O, Hupa L. In vitro dissolution of bioactive glass S53P4 microspheres. J Am Ceram Soc. 2022;105(3):1658–70.

214. Stiller A, Engblom M, Karlström O, Lindén M, Hupa L. Impact of fluid flow rate on the dissolution behavior of bioactive glass S53P4. J Non-Cryst Solids. 2023;607:122219.

215. Leppäranta O, Vaahtio M, Peltola T, Zhang D, Hupa L, Hupa M, et al. Antibacterial effect of bioactive glasses on clinically important anaerobic bacteria in vitro. J Mater Sci Mater Med. 2008;19(2):547–51.

216. Zhang D, Leppäranta O, Munukka E, Ylänen H, Viljanen MK, Eerola E, et al. Antibacterial effects and dissolution behavior of six bioactive glasses. J Biomed Mater Res A. 2010;93A(2):475–83.

217. Lindfors NC, Hyvönen P, Nyyssönen M, Kirjavainen M, Kankare J, Gullichsen E, et al. Bioactive glass S53P4 as bone graft substitute in treatment of osteomyelitis. Bone. 2010;47(2):212–8.

218. El-Ghannam A, Ducheyne P, Shapiro IM. Formation of surface reaction products on bioactive glass and their effects on the expression of the osteoblastic phenotype and the deposition of mineralized extracellular matrix. Biomaterials. 1997;18(4):295–303.

219. Aalto-Setälä L, Uppstu P, Sinitsyna P, Lindfors NC, Hupa L. Dissolution of Amorphous S53P4 Glass Scaffolds in Dynamic In Vitro Conditions. Materials. 2021;14(17):4834.

220. Hutmacher DW, Schantz JT, Lam CXF, Tan KC, Lim TC. State of the art and future directions of scaffold-based bone engineering from a biomaterials perspective. J Tissue Eng Regen Med. 2007;1(4):245–60.

221. Magri AMP, Fernandes KR, Assis L, Kido HW, Avanzi IR, Medeiros M da C, et al. Incorporation of collagen and PLGA in bioactive glass: in vivo biological evaluation. Int J Biol Macromol. 2019;134:869–81.

222. Björkvik L, Wang X, Hupa L. Dissolution of Bioactive Glasses in Acidic Solutions with the Focus on Lactic Acid. Int J Appl Glass Sci. 2016;7(2):154–63.

223. Kokubo T, Kushitani H, Sakka S, Kitsugi T, Yamamuro T. Solutions able to reproduce in vivo surface-structure changes in bioactive glass-ceramic A-W3. J Biomed Mater Res. 1990;24(6):721–34.

224. Shah SS, Cha Y, Pitt CG. Poly (glycolic acid-co-dl-lactic acid): diffusion or degradation controlled drug delivery? J Controlled Release. 1992;18(3):261–70.

225. Doube M, Kłosowski MM, Arganda-Carreras I, Cordelières FP, Dougherty RP, Jackson JS, et al. BoneJ: Free and extensible bone image analysis in ImageJ. Bone. 2010;47(6):1076–9.

226. Schindelin J, Arganda-Carreras I, Frise E, Kaynig V, Longair M, Pietzsch T, et al. Fiji: an open-source platform for biological-image analysis. Nat Methods. 2012;9(7):676–82.

227. Orava E, Korventausta J, Rosenberg M, Jokinen M, Rosling A. In vitro degradation of porous poly(dl-lactide-co-glycolide) (PLGA)/bioactive glass composite foams with a polar structure. Polym Degrad Stab. 2007;92(1):14–23.

228. Ghayor C, Weber FE. Osteoconductive Microarchitecture of Bone Substitutes for Bone Regeneration Revisited. Front Physiol. 2018;9.

229. Jose MV, Thomas V, Johnson KT, Dean DR, Nyairo E. Aligned PLGA/HA nanofibrous nanocomposite scaffolds for bone tissue engineering. Acta Biomater. 2009;5(1):305–15.

230. Holy CE, Cheng C, Davies JE, Shoichet MS. Optimizing the sterilization of PLGA scaffolds for use in tissue engineering. Biomaterials. 2000;22(1):25–31.

231. Galow AM, Rebl A, Koczan D, Bonk SM, Baumann W, Gimsa J. Increased osteoblast viability at alkaline pH in vitro provides a new perspective on bone regeneration. Biochem Biophys Rep. 2017;10:17–25.

232. Zhang Z, Lai Q, Li Y, Xu C, Tang X, Ci J, et al. Acidic pH environment induces autophagy in osteoblasts. Sci Rep. 2017;7(1):46161.

233. Han SH, Chae SW, Choi JY, Kim EC, Chae HJ, Kim HR. Acidic pH environments increase the expression of cathepsin B in osteoblasts: The significance of ER stress in bone physiology. Immunopharmacol Immunotoxicol. 2009;31(3):428–31.

234. Lee GH, Hwang JD, Choi JY, Park HJ, Cho JY, Kim KW, et al. An acidic pH environment increases cell death and pro-inflammatory cytokine release in osteoblasts: The involvement of BAX Inhibitor-1. Int J Biochem Cell Biol. 2011;43(9):1305–17.

235. Egerbacher M, Wolfesberger B, Gabler C. In Vitro Evidence for Effects of Magnesium Supplementation on Quinolone-treated Horse and Dog Chondrocytes. Vet Pathol. 2001;38(2):143–8.

236. Menz BD, Charani E, Gordon DL, Leather AJ, Moonesinghe SR, Phillips CJ. Surgical Antibiotic Prophylaxis in an Era of Antibiotic Resistance: Common Resistant Bacteria and Wider Considerations for Practice. Infect Drug Resist. 2021;14:5235–52.

237. Yamasaki Y, Yoshida Y, Okazaki M, Shimazu A, Uchida T, Kubo T, et al. Synthesis of functionally graded MgCO3 apatite accelerating osteoblast adhesion. J Biomed Mater Res. 2002;62(1):99–105.

238. Zreiqat H, Howlett CR, Zannettino A, Evans P, Schulze-Tanzil G, Knabe C, et al. Mechanisms of magnesium-stimulated adhesion of osteoblastic cells to commonly used orthopaedic implants. J Biomed Mater Res. 2002;62(2):175–84.

239. Yoshizawa S, Brown A, Barchowsky A, Sfeir C. Magnesium ion stimulation of bone marrow stromal cells enhances osteogenic activity, simulating the effect of magnesium alloy degradation. Acta Biomater. 2014;10(6):2834–42.

240. Qiao W, Wong KHM, Shen J, Wang W, Wu J, Li J, et al. TRPM7 kinase-mediated immunomodulation in macrophage plays a central role in magnesium ion-induced bone regeneration. Nat Commun. 2021;12(1):2885.

241. Fan W, Wu C, Miao X, Liu G, Saifzadeh S, Sugiyama S, et al. Biomaterial scaffolds in cartilage–subchondral

bone defects influencing the repair of autologous articular cartilage transplants. J Biomater Appl. 2013;27(8):979–89.

242. Matsuo T, Kita K, Mae T, Yonetani Y, Miyamoto S, Yoshikawa H, et al. Bone substitutes and implantation depths for subchondral bone repair in osteochondral defects of porcine knee joints. Knee Surg Sports Traumatol Arthrosc. 2015;23(5):1401–9.

243. Wang X, Molino BZ, Pitkänen S, Ojansivu M, Xu C, Hannula M, et al. 3D Scaffolds of Polycaprolactone/Copper-Doped Bioactive Glass: Architecture Engineering with Additive Manufacturing and Cellular Assessments in a Coculture of Bone Marrow Stem Cells and Endothelial Cells. ACS Biomater Sci Eng. 2019;5(9):4496–510.

244. Bochicchio B, Barbaro K, De Bonis A, Rau JV, Pepe A. Electrospun poly(d,l-lactide)/gelatin/glass-ceramics tricomponent nanofibrous scaffold for bone tissue engineering. J Biomed Mater Res A. 2020;108(5):1064–76.

245. Plyusnin A, Kulkova J, Arthurs G, Jalava N, Uppstu P, Moritz N. Biological response to an experimental implant for tibial tuberosity advancement in dogs: A pre-clinical study. Res Vet Sci. 2020;128:183–96.

246. Oudadesse H, Najem S, Mosbahi S, Rocton N, Refifi J, El Feki H, et al. Development of hybrid scaffold: Bioactive glass nanoparticles/chitosan for tissue engineering applications. J Biomed Mater Res A. 2021;109(5):590–9.

247. Im SH, Im DH, Park SJ, Chung JJ, Jung Y, Kim SH. Stereocomplex Polylactide for Drug Delivery and Biomedical Applications: A Review. Molecules. 2021;26(10):2846.

Appendix: Original publications

Uppstu P, Paakki C, Rosling A. In vitro hydrolysis and magnesium release of poly(D,L-lactide-co-glycolide)-based composites containing bioresorbable glasses and magnesium hydroxide. Journal of Applied Polymer Science. 2015;132:42646.

I

JOURNAL OF Applied Polymer SCIENCE

In vitro hydrolysis and magnesium release of poly(D,L-lactide-co-glycolide)-based composites containing bioresorbable glasses and magnesium hydroxide

Peter Uppstu, Charlotta Paakki, Ari Rosling
Laboratory of Polymer Technology, Centre of Excellence in Functional Materials at Biological Interfaces, Åbo Akademi University, Biskopsgatan 8, FI-20500, Åbo, Finland
Correspondence to: P. Uppstu (E-mail: peter.uppstu@abo.fi)

ABSTRACT: Magnesium is important for both bone growth and cartilage formation. However, the postoperative intake of antibiotics such as quinolones may cause a reduction in magnesium levels in tissue. The addition of magnesium to scaffolds may therefore be beneficial for the regeneration of osteochondral defects. In this study, porous composite scaffolds were produced by gas foaming of poly(D,L-lactide-co-glycolide) (PLGA) rods with magnesium-containing bioresorbable glasses and magnesium hydroxide as fillers. The *in vitro* hydrolytical degradation of the composite scaffolds in Tris buffer was followed over a 10-week period. Mg^{2+} was released in a controlled manner from the scaffolds with varying release profiles between the different materials. Higher glass content resulted in a reduced mass loss compared to scaffolds with lower glass content. As a result of the foaming method, the scaffolds shrank initially, without evidence that the addition of hydrophilic fillers would decrease the initial shrinkage. © 2015 Wiley Periodicals, Inc. J. Appl. Polym. Sci. **2015**, *132*, 42646.

KEYWORDS: biomedical applications; composites; porous materials; properties and characterization

Received 19 February 2015; accepted 23 June 2015
DOI: 10.1002/app.42646

INTRODUCTION

Poly(α-hydroxy acids) such as poly(D,L-lactide-co-glycolide) (PLGA) are biocompatible and biodegradable polymers, which can beneficially be used for the regeneration of bone tissue.[1,2] PLGA is hydrolytically unstable and the absorption of water into the polymer matrix causes scaffold degradation and gives space for tissue growth. The PLGA chains degrade in aqueous environments by random chain scission into acidic water-soluble low-molecular-weight fragments.[3,4] Bone growth is negatively impacted by acidic pH[5–7] and it has been suggested that it may be advantageous to reduce the acidity of PLGA scaffolds for bone regeneration.[8] It has even been suggested that increasing the pH from physiological values improves new bone formation.[9]

Composite materials of biodegradable aliphatic polyesters containing bioresorbable glasses generally exhibit improved mechanical properties compared to their constituents, and bioresorbable glasses also have a neutralizing effect on the acidity which is caused by the polyester degradation products.[2,10,11] Composites of biodegradable polymers containing bioresorbable glasses have been widely studied and they effectively combine the flexibility and degradation properties of polymers and the strength and potential bioactivity of the inorganic glass phase.[12,13]

Magnesium deficiency has been shown to negatively impact bone tissue and bone growth in animal models by increasing the osteoclast number,[14] reducing the bone mineral content and the volume of bone,[15,16] and inducing osteoporosis.[17,18] There is also clinical evidence of negative effects of magnesium deficiency on bone tissue.[18,19] In addition, magnesium deficiency has been proven to have a negative effect on bone tissue around osseointegrated implants.[20,21]

It has been found that the magnesium levels in tissue are decreased by certain antibiotics, quinolones, which potentially contributes to the formation of cartilage defects.[22] This is of special concern because quinolones are used in orthopedic surgery to reduce the risk of infection.[23] Supplementary magnesium reduces the quinolone-induced damage to chondrocytes.[22] The bioavailability of quinolones can be reduced by coadministration with magnesium, which may encourage the use of different administration routes for quinolones and magnesium.[24]

Magnesium and its alloys have been found to be suitable for the production of orthopedic implants.[25] Mesoporous magnesium silicate has enhanced the efficiency of new bone formation in bone defects in rabbits[26] and magnesium-containing alloys have been found to favor bone growth also in rats[27] and guinea

pigs.[28] Magnesium ions enhance the proliferation of human bone marrow stromal cells and support mineralization of the extracellular matrix.[29] Biomimetic scaffolds with added magnesium ions have been shown to favor osteochondral tissue regeneration in a clinical trial[30] and the beneficial effects of magnesium to chondrocyte proliferation and cartilage formation have been proven in several studies as well.[31–33] Pure magnesium corrodes to $Mg(OH)_2$ in aqueous environments.[34] The addition of $Mg(OH)_2$ to PLGA has been shown to neutralize the acidic environment inside the scaffold.[35] In several studies, it has been proven that magnesium-doped bioresorbable glasses are biocompatible, but because no undoped control groups have been used, the potential osteogenic effects of magnesium release from the glasses remain unproven.[36]

Shrinkage in physiological conditions is a typical but generally unwanted characteristic for several different types of polymeric structures and scaffolds used in biomedical applications. It has been reported for polylactic acid fibres,[37] microparticles,[38] and nanofibrous[39] and gas-foamed[40] scaffolds. Also foams produced by particulate leaching have been observed to shrink.[41,42] Shrinkage of polymeric scaffolds occurs when stretched amorphous polymer chains are able to relax when the internal energy of the polymer matrix increases, e.g., through an increase in the temperature or a decrease in the strength of intermolecular interactions.[43] Shrinkage of tissue regenerating scaffolds may result in displacement of the scaffold, which can possibly lead to a detrimental outcome of the regeneration process. Shrinkage also affects the pore structure of the scaffold, possibly obstructing cell infiltration, e.g., during *in vitro* cell culturing. In order to prevent these negative consequences, it would be desirable to inhibit the dimensional shrinkage of scaffolds under *in vitro* or physiological conditions.

The aim of this study was to analyze the *in vitro* degradation properties of porous scaffolds produced from PLGA in combination with magnesium-containing fillers. Mg^{2+} release from the scaffolds to the surrounding solution was studied because of its potential beneficial effects for tissue growth *in vivo*. The dimensional stability of the scaffolds was evaluated. Water absorption, weight loss, pH of the surrounding medium, and changes in molecular weight were also measured.

MATERIALS AND METHODS

Materials

Medical grade D-lactide and glycolide monomers were obtained from Corbion (Purac, Gorinchem, the Netherlands). L-lactide monomer (>99%) was purchased from Futerro (Escanaffles, Spain). Tin(II) 2-ethylhexanoate (approx. 95%) and 1-decanol (99%, distilled prior to use) were purchased from Sigma-Aldrich. Low molecular weight polylactic acid (PLA) polymerized by polycondensation was supplied by the Laboratory of Polymer Technology, Åbo Akademi, Finland. Magnesium hydroxide (≥99.0%) was purchased from Sigma-Aldrich (Helsinki, Finland). Bioresorbable glasses 13–93 and NC–5 were supplied by BonAlive Biomaterials Ltd (Turku, Finland), and their composition is shown in Table I.

Table I. The Composition (wt %) of Bioresorbable Glasses 13–93 and NC–5

Oxide	13-93	NC-5
Na_2O	6	17
SiO_2	53	62
CaO	20	13
P_2O_5	4	2
MgO	5	4
B_2O_3	0	2
K_2O	12	0

Polymerization

PLGA with a D-lactide-to-L-lactide ratio of 1 : 1 and a lactide-to-glycolide molar ratio of 7 : 3 was synthesized in inert atmosphere by ring-opening polymerization. Briefly, 100 g L-lactide (0.694 mol), 100 g D-lactide (0.694 mol), and 69 g glycolide (0.594 mol) that were freshly obtained and had been stored at −18°C were weighed in a round bottle. The bottle was heated at 120°C until all monomers were molten after which 803 mg tin(II) 2-ethylhexanoate (1.98 mmol) and 192 mg 1-decanol (1.21 mmol) were added. The temperature was then raised to 150°C for 5 h. After cooling to room temperature, the product was dissolved in altogether 2 L dichloromethane and precipitated in a sixfold amount of heavily stirred ethanol to remove unreacted monomers and other possible impurities. The polymer was dried in a vacuum oven (40°C, <50 mbar) for approximately 1 week until no residual solvent could be observed in ^{1}H-NMR. The dried polymer was manually cut to granules with a diameter of approximately 5 mm.

Extrusion

The bioresorbable glasses 13–93 and NC–5 were ground from fibers into particles of up to 50 μm in size with a Philips Mini-Mill ball mill. PLGA and PLA granules as well as the glass and the $Mg(OH)_2$ particles were dried in a vacuum oven (40°C, <50 mbar) overnight before extrusion. The blends containing PLGA and either PLA, 13–93, NC–5, or $Mg(OH)_2$ were extruded with a counter-rotating twin-screw extruder (Rheocord System 40, Haake Buchler) into rods. The temperature profile during extrusion was 75, 85, and 95°C and the die temperature was 95°C. The screw speed was 120 rpm.

Fabrication of Porous Scaffolds

The extruded rods, with a diameter generally between 4.0–5.5 mm, were cut into approximately 17-mm-long pieces and placed into cylindrical PTFE molds with a diameter of 1.5 times the diameter of the rod. The molds were placed in an autoclave and the foaming was performed at room temperature. A CO_2 pressure of 55 bar was applied on the rods for 22 h after which the excess pressure was quickly released during a time span of approximately 8 s. The molds with the expanded rods were placed in an oven (80°C, 45 s) after which the rods were kept inside of their molds for an hour at ambient temperature and pressure. The rods were stored in a desiccator until used in the hydrolysis experiments.

The degree of expansion was calculated according to eq. (1):

$$Volumetric\ expansion\,(\%) = \left[\left(V_{expanded} - V_{initial}\right)/V_{initial}\right] \times 100\% \quad (1)$$

Table II. The Theoretical and Measured Weight % of the Fillers and the Measured Weight % of PLGA

Filler	Theoretical filler content	Measured filler content	Measured PLGA content
13-93	10	11.5	88.5
13-93	20	20.9	79.1
13-93	35	35.0	65.0
NC-5	10	10.7	89.3
NC-5	20	20.3	79.7
NC-5	35	36.3	63.7
$Mg(OH)_2$	10	11.7	88.3
$Mg(OH)_2$	20	19.4	80.6
$Mg(OH)_2$	35	34.6	65.4
PLA	20	18.7	81.3

where $V_{expanded}$ is the volume of the sample after expansion and $V_{initial}$ is the volume of the scaffold before expansion.

The amount of bioresorbable glass in the glass composites was determined gravimetrically, based on the residual weight of a rod after burning it in open fire in a glass vial. The $Mg(OH)_2$ content was determined in a similar manner by burning, but corrected with the change in weight caused by the oxidation of Mg from $Mg(OH)_2$ to MgO. The amount of low-molecular-weight PLA was determined by ^{1}H NMR analysis.

In Vitro Hydrolysis

For *in vitro* tests, the foamed rods were cut into approximately 5-mm-long scaffolds which were measured to the nearest 0.01 mm using a caliper and weighed with an accuracy of 0.1 mg. The diameter of the foamed scaffolds varied approximately between 6 and 11 mm and the weight varied between 12 and 53 mg. The weight of the scaffolds was highly dependent on the filler content and on the volumetric expansion in the foaming process. The degradation tests of the porous scaffolds were carried out in 0.1 M tris(hydroxymethyl)aminomethane solution (Tris buffer) made from ultrapure (Millipore) water adjusted to pH 7.42 with hydrochloric acid. The scaffolds were immersed in syringes containing Tris buffer so that for each 3.5 mg of sample, 1 mL of buffer solution was added. The syringes were then stored in an incubating orbital shaker (Unimax 1010, Heidolph) at 37°C for predefined time periods (4 h, 1 d, 3 d, 7 d, 14 d, 21 d, 35 d, 49 d, and 70 d). At weekly intervals, the buffer solution was replaced with fresh solution. At the predefined time points, three samples of each scaffold type were removed from the syringes, dried superficially with moisture-absorbent paper, and characterized. The results shown in this article represent average values for the three parallel samples.

Scaffold Characterization

After removing the scaffolds from the Tris buffer, their dimensions and weight were measured. The scaffolds were subsequently freeze dried for 48 h. The dried scaffolds were weighed again and the molecular weight was determined for each scaffold.

The changes in diameter and length of the scaffolds were calculated according to eq. (2):

$$\textit{Change in dimension}\,(\%) = (D/D_0)\times 100\% \quad (2)$$

where D is the dimension in wet state after immersion and D_0 is the dimension before immersion in Tris buffer.

The weight loss of the scaffolds was calculated according to eq. (3):

$$\textit{Weight loss}\,(\%) = (W/W_0)\times 100\% \quad (3)$$

where W is the weight of the dried scaffold after immersion in Tris buffer and W_0 is the weight of the scaffold before immersion.

Water absorption was calculated according to eq. (4):

$$\textit{Water absorption}\,(\%) = \left[\left(m_{wet} - m_{dry}\right)/m_{dry}\right]\times 100\% \quad (4)$$

where m_{wet} is the mass of the sample in wet state after immersion in Tris buffer and m_{dry} is the mass of the sample after drying.

The determination of the molecular weight of the polymers was performed using gel permeation chromatography (GPC) with an LC-10ATVP HPLC-pump (Shimadzu Corporation), an AM GPC Gel 10 μm Linear colon (American Polymer Standards), and a Sedex 85 light scattering detector (Sedere). The GPC measurements were carried out at 40°C at a flow rate of 1 mL min^{-1} with tetrahydrofuran as solvent and a sample concentration of 1 mg mL^{-1}. Polystyrene standards from Polymer Standard Service were used for calibration. The samples were filtered with 0.22 μm PTFE filters before analysis.

The release of magnesium ions from the scaffolds was studied using an inductively coupled plasma optical emission spectrometer (ICP-OES) instrument (Optima 5300, PerkinElmer). The bestowed buffer solution was diluted with ultrapure water in a 1 : 1 ratio and 4 drops of nitric acid per sample were added. The samples were stored in closed vials in a refrigerator prior to analysis.

Statistical Analysis

Analysis of variance (ANOVA) was performed using general linear models with SAS 9.2 software (SAS Institute Inc.). Two-tailed linear models with an alpha-level of 0.05 were used. Assumptions of linear regressions were studied by observing normality of error distribution. Differences were considered significant at p values <0.05.

RESULTS AND DISCUSSION

Scaffold Fabrication and Characterization

The compositions of the studied composites are shown in Table II. In this study, the theoretical (aimed) composition values are used in the text for clarity, but the measured values were used in the statistical analysis.

The filler particles were uniformly distributed in the scaffold matrix, as is shown in the scanning electron microscope (SEM) images in Figure 1. The size distribution of the 13–93 and NC–5 glass particles was broad and especially the smaller glass particles were well-embedded into the matrix and pore walls. The shape of the pores varied from clearly elongated to almost

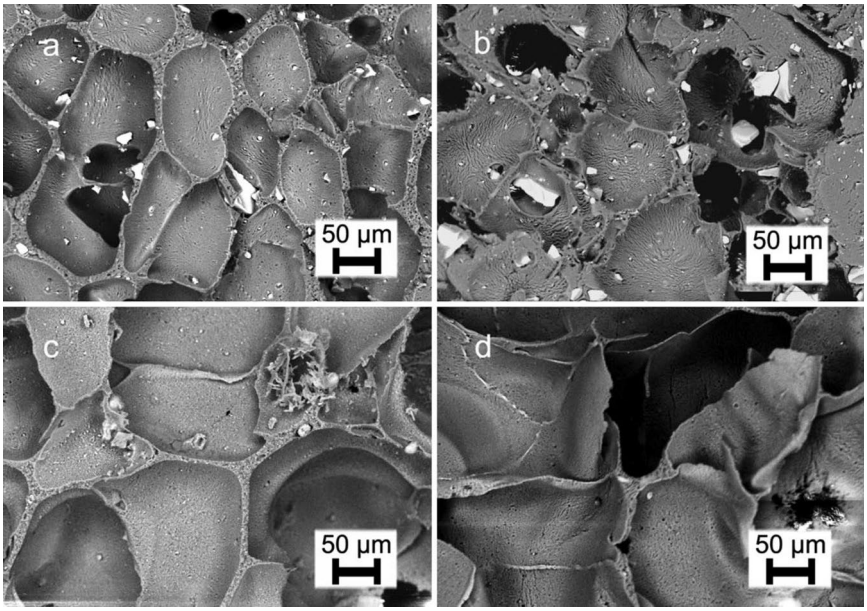

Figure 1. SEM images with 250× magnification of cross-sections of (a) 13–93 20%, (b) NC–5 20%, (c) $Mg(OH)_2$ 20%, and (d) PLA 20% scaffolds after 1 day of immersion in Tris buffer.

circular. The initial pore structure was predominantly closed and the pore diameter was mainly between 50 and 300 μm.

The average degrees of expansion of the prepared composites are shown in Figure 2. The volumetric expansion of the scaffolds in the foaming process varied from 460% to 2216%. The expansion in length was between 190% and 360% for most materials, whereas the diameter expansion was limited by the PTFE molds and was typically between 70% and 100%. A higher filler content (bioresorbable glasses or $Mg(OH)_2$) significantly decreased the degree of expansion ($p < 0.0001$, $n = 51$). The high expansion of PLA 20% scaffolds is explained by the fact that the filler (i.e., the low molecular weight PLA) is similar to the main matrix material (PLGA) and is in itself also expandable by gas foaming. Expansion of pure PLGA rods is comparable to the expansion of PLA 20% rods (approximately 2000% for similar samples).

Dimensional Change

The diameter of the scaffolds decreased significantly when they were immersed in Tris buffer at 37°C (Figure 3). The initial shrinkage for most materials was approximately 30%, with the range being from 22% to 44%. After the initial shrinkage, all materials started to expand. At the last time point (49 days), when the dimensions could reliably be measured, scaffolds containing bioresorbable glass and PLA were close to their original diameter or had exceeded it. At the same time point, the $Mg(OH)_2$-containing scaffolds had not regained their original diameter. The poor recovery of the original dimensions of the $Mg(OH)_2$-containing scaffolds may be linked to their considerable weight loss. Similar to the decrease in diameter, a significant reduction in length was observed for all samples when they were immersed in Tris solution (data not shown). For all 13–93- and NC–5-containing scaffolds, the maximum shrinkage in length was approximately 40%. At 49 days, they had regained their length to a large extent. Composite scaffolds with a filler content of $Mg(OH)_2$ 20% shrank noticeably less than those containing $Mg(OH)_2$ 10% and 35% and they also regained their dimensions to a much greater degree. No obvious explanation

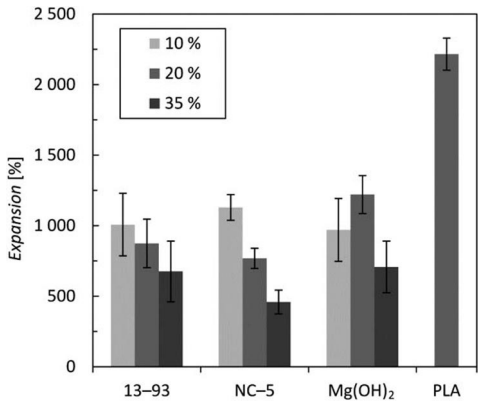

Figure 2. The average expansion percentages of the composite materials with different filler concentrations in the gas foaming process.

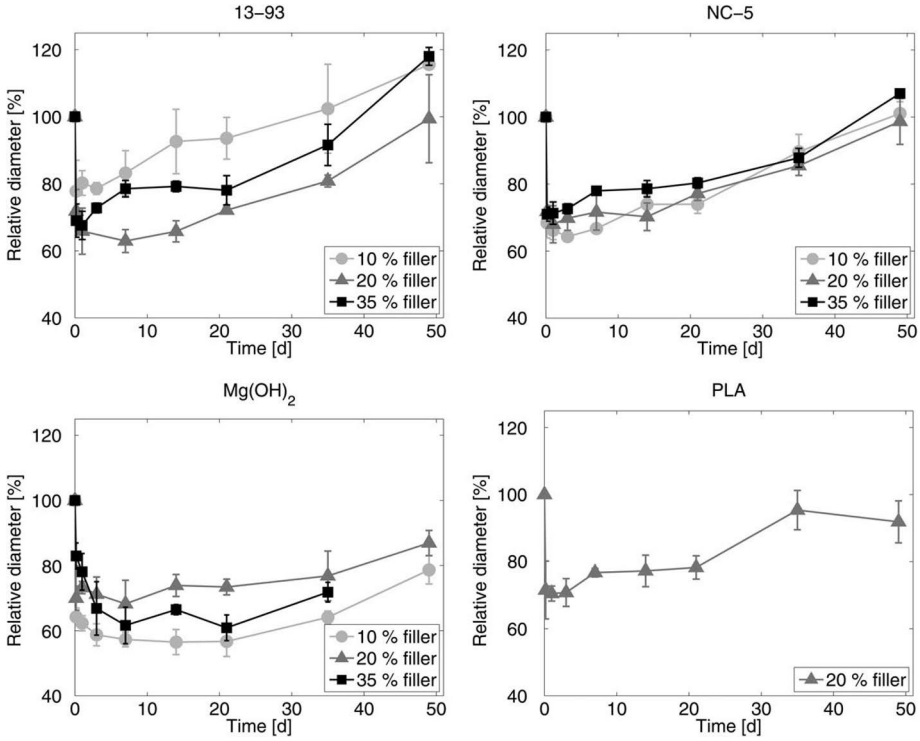

Figure 3. Change of normalized diameter of porous PLGA-based scaffolds with different amounts of magnesium-containing fillers.

to this phenomenon can be identified, as the expansion in the length dimension of the 20% scaffolds was similar to the 10% scaffolds and significantly greater than for the 35% scaffolds. The least initial length shrinkage was observed for PLA 20% scaffolds which showed a maximum shrinkage of 21%. At 49 days also they had regained their original length.

Regarding both diameter and length measurements, at 49 days many scaffolds were already very soft and the reliability of the measurements was worse than for scaffolds which had been immersed for shorter times in Tris buffer. The diameter and the length of the $Mg(OH)_2$ 35% scaffolds could not be measured at 49 days because all three parallel samples fell apart when removing them from the Tris buffer.

Gas foaming is a suitable method for the production of various types of porous scaffolds because it does not involve the use of solvents and the foaming process can be performed at ambient temperature. However, in the foaming process, the polymer chains become stretched. The initial shrinkage of the scaffolds seems to be caused by the stress relaxation of stretched polymer chains when they are exposed to elevated temperatures.[37] For the PLGA-based scaffolds used in this experiment, physiological temperatures were enough to induce the shrinkage. The initial shrinkage was not dependent on the expansion of the scaffolds when the type and amount of filler were controlled ($p = 0.82$, $n = 30$). PLA 20% scaffolds, which had the highest expansion percentage of all scaffolds by a wide margin, shrank less than all other types of scaffolds.

The volumetric changes for PLGA-based scaffolds with hydrophilic fillers are in line with gas-foamed scaffolds of pure PLGA having a similar physical structure tested earlier at our laboratory (results not shown here). It is evident that the addition of hydrophilic fillers did not significantly improve the dimensional stability of PLGA-based scaffolds. This may be attributable to the fact that the relaxation forces of the polymer chains appear higher than the countering forces induced by the water absorption of the scaffolds.

The shrinkage of porous scaffolds may at least partially be prevented by increasing the crystallinity of the polymer matrix[37,44] even though this could to some extent prevent expansion of the scaffolds during the processing and it also affects the rate of degradation.

Weight Loss

The degradation pattern of the scaffolds is important for the regeneration of bone because the degrading scaffold provides space for new tissue formation. Weight loss differed significantly between $Mg(OH)_2$-containing scaffolds and the other scaffolds

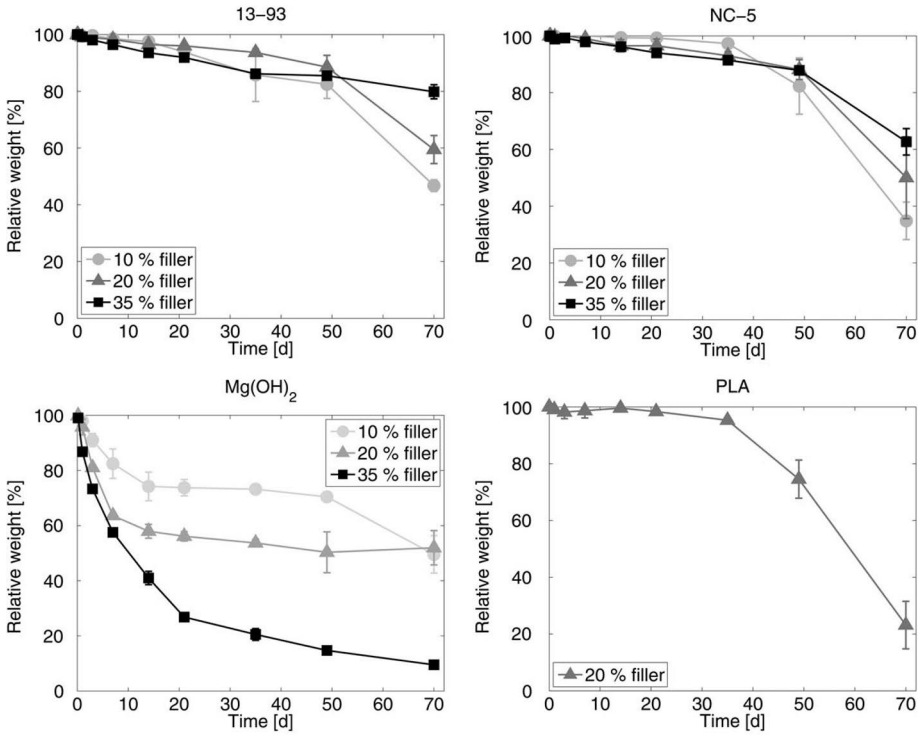

Figure 4. Change of normalized weight of porous PLGA-based scaffolds with different amounts of magnesium-containing fillers.

(Figure 4). The weight loss for $Mg(OH)_2$-containing scaffolds was very high during the first 2–3 weeks of immersion in Tris buffer, with a 25% loss for $Mg(OH)_2$ 10% scaffolds and a 73% loss for $Mg(OH)_2$ 35% scaffolds after 21 days. This is partly attributed to the quick dissolution of the $Mg(OH)_2$ particles, as shown below in the analysis of the Mg^{2+} release into the Tris buffer. However, as the early weight loss for the $Mg(OH)_2$-containing scaffolds was considerably higher than the total amount of $Mg(OH)_2$ in the scaffolds, it is evident that also the weight of the PLGA matrix decreased early during the immersion. A reason for this pattern may be that the rapid dissolution of $Mg(OH)_2$ resulted in a significant pH increase in the buffer solution (results not shown) which could increase the rate of degradation through alkaline hydrolysis. A similar degradation pattern has been observed in films consisting of poly(D,L-lactide) and 30% MgO.[45] The early weight reduction may also be attributable to the effect of an increased surface area because of dissolved $Mg(OH)_2$ particles originating from within the matrix. When the surface area increases, more of the soluble fragments may leach out into the solution. By replacing $Mg(OH)_2$ partly or fully by, e.g., magnesium chloride ($MgCl_2$), it may be possible to release similar amounts of magnesium and reduce the early increase in alkalinity, which would reduce the early degrading impact on the matrix.

The weight loss of the bioresorbable glass- and PLA-containing scaffolds followed a pattern reported earlier.[46] Weight loss was initially small until 35 days. At 49 days and 70 days, PLA 20% showed the most significant reduction in weight. Of 13–93- and NC–5-containing scaffolds, those with more glass had initially (during the first 21 days) a higher weight loss, but showed after that a slower reduction in weight than the scaffolds with a smaller amount of glass. The higher initial weight loss of scaffolds with a higher amount of glass has been attributed to the early leaching of glass from the scaffolds.[40,47] The reason for the slower weight loss later during the hydrolysis seems to be the subdued autocatalytic effect because of the higher pH induced by the neutralizing effect caused by the glasses. Scaffolds which contained the more rapidly resorbing 13–93 glass exhibited a smaller weight loss than NC–5-containing scaffolds, even though the more quickly dissolving 13–93 would intuitively elicit a higher weight loss. The bulk of the weight loss is, however, tied to the degradation of the polymer during the 70 day period, and as 13–93 is more quickly dissolving than NC–5, it also has more capacity to neutralize the medium and in that way possibly reduce the rate of polymer degradation.

It has been shown that the addition of a slightly alkaline component to PLGA decreases the rate of degradation of the

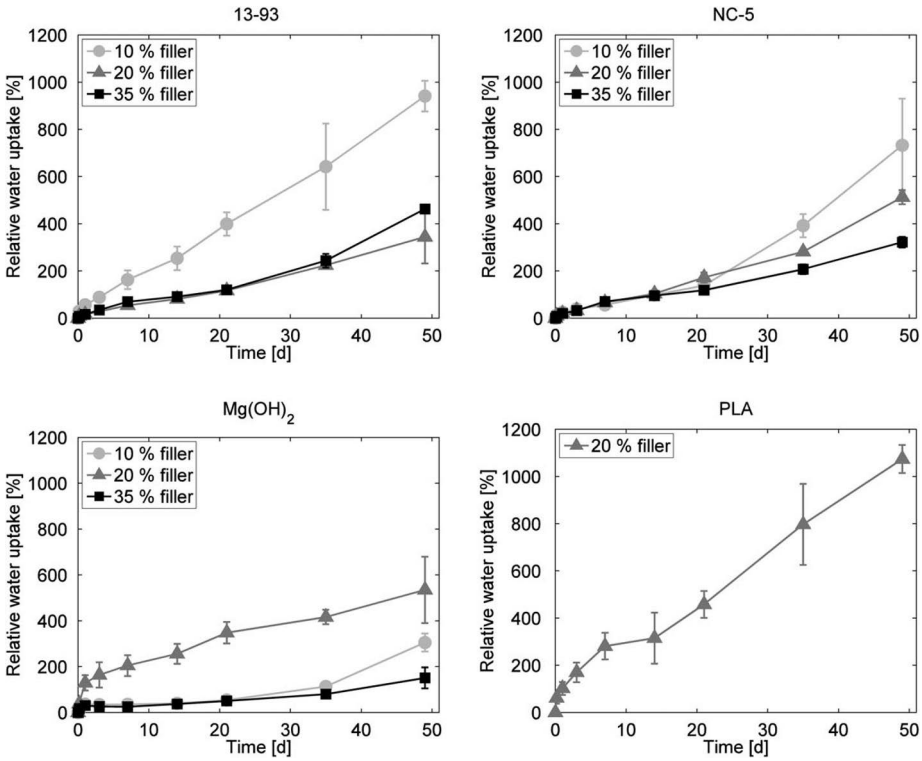

Figure 5. Change of normalized water uptake of porous PLGA-based scaffolds with different amounts of magnesium-containing fillers.

polymers, whereas the addition of acidic components accelerates the degradation process.[48] The dissolution process of bioresorbable glasses creates a slightly basic environment, which as expected slows down the degradation rate of aliphatic polyesters.[10] A drop in pH of 0.2 units has been shown not to affect bone healing negatively,[49] but greater changes significantly reduce osteoblast activity and affect bone growth negatively.[5–7] For bone regeneration, a pH-neutralizing filler in quickly degrading PLGA-based scaffolds may be a favorable solution.

Water Absorption

Water absorption, as shown in Figure 5, increased over time for all materials but did not show significant differences with regard to the amount of added filler ($p = 0.15$, $n = 259$). The highest rate of water absorption was observed for PLA 20% scaffolds, with relatively steadily increasing amount of absorbed water throughout the measurable 7-week period, with a maximum of 1074% at 49 days. The 13–93 10% scaffolds had an almost equally high water uptake, with a maximum of 941% at 49 days. Throughout the study, the water absorption of $Mg(OH)_2$ 10% and 35% scaffolds was at very low levels compared to the other materials. This correlates with the fact that their dimensions did not recover from their initial shrinkage as much as the other materials. The water absorption of the $Mg(OH)_2$ 20% scaffolds was initially very high but supposedly because of the considerable weight loss the water uptake increased relatively little over time.

The differences in the water uptake were partly a result of different porosities of the scaffolds. The scaffolds which contained 13–93 or NC–5 were initially denser than especially the PLA 20% scaffolds. In this work, we have not differentiated the water uptake in pores versus water uptake in the bulk matrix. This contributes to effect that the water uptake levels for PLA 20% appear higher than for the other scaffolds.

Mg^{2+} Release

Figure 6 shows the release of Mg^{2+} from the scaffolds into the Tris buffer. The highest rates of Mg^{2+} release were recorded during the first 1–2 weeks of immersion after which the rate leveled for most scaffolds. As the amount of magnesium in 13–93 and NC–5 is only a small fraction of the total mass of the glass, the Mg^{2+} release for 13–93- and NC–5-containing scaffolds was approximately two orders of magnitude smaller than for scaffolds with similar amounts of $Mg(OH)_2$. The fact that 13–93 contains more magnesium coupled with its higher resorption rate compared to NC–5 are the reasons for the higher Mg^{2+} release rate from 13–93 than from NC–5.

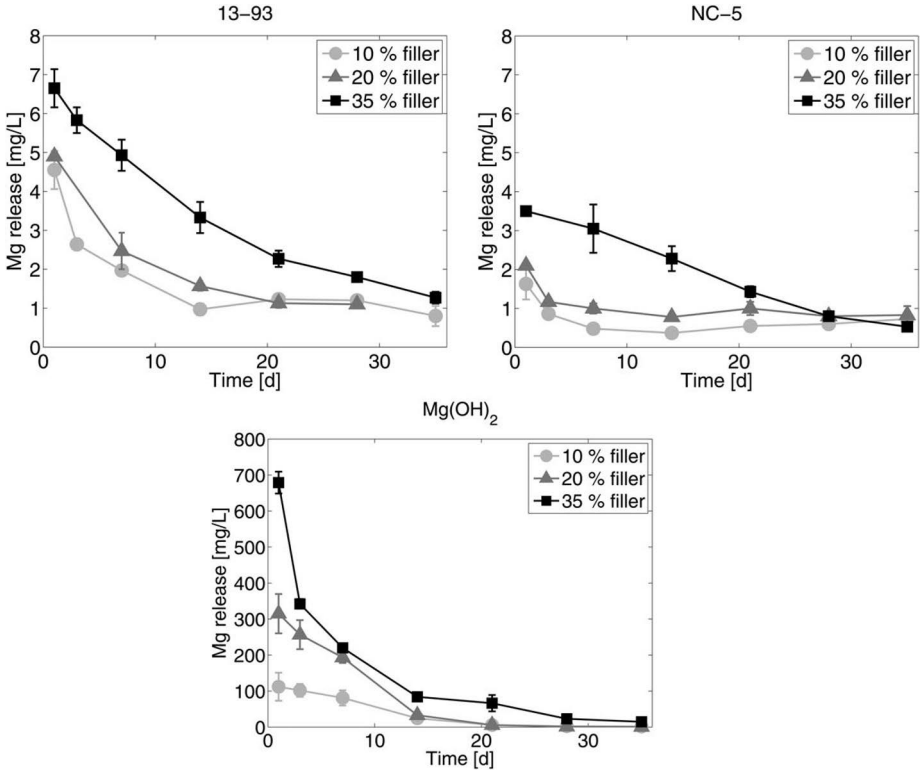

Figure 6. Normalized 7 day Mg^{2+} release rate (mg L^{-1}) into Tris buffer of porous PLGA-based scaffolds with different amounts of magnesium-containing fillers. Note different *Y*-axis scale for $Mg(OH)_2$.

With respect to antibiotics which cause magnesium deficiency in tissue, the rate of Mg^{2+} release may have the highest importance during the first weeks after the operation of the implant into the body. The tissue ingrowth into the scaffold may benefit from increased magnesium levels over longer periods of time. Janning *et al.*[50] demonstrated an enhanced bone growth using slowly dissolving nonporous cylinders of $Mg(OH)_2$ in a rabbit model. The effect is attributed either to the local magnesium

Table III. The Weight Average Molecular Weights (M_w) of the PLGA in the Composites Before and After Extrusion Processing (g mol^{-1}). Polydispersity indices (PDI) Before and After Extrusion are Also Shown

Filler	M_w before	M_w after	PDI before	PDI after
13-93 10%	107,000	58,000	1.95	1.99
13-93 20%	112,000	74,000	1.86	1.88
13-93 35%	112,000	65,000	1.86	1.91
NC-5 10%	107,000	74,000	1.95	1.93
NC-5 20%	107,000	79,000	1.95	1.73
NC-5 35%	112,000	69,000	1.86	1.84
$Mg(OH)_2$ 10%	107,000	71,000	1.95	1.69
$Mg(OH)_2$ 20%	107,000	51,000	1.95	1.72
$Mg(OH)_2$ 35%	112,000	84,000	1.86	1.61
PLA 20%	107,000	46,000	1.95	3.77

PDI = M_w/M_n, where M_n is the number average molecular weight. The values for PLA 20% reflect a mixture of PLGA and low molecular weight PLA.

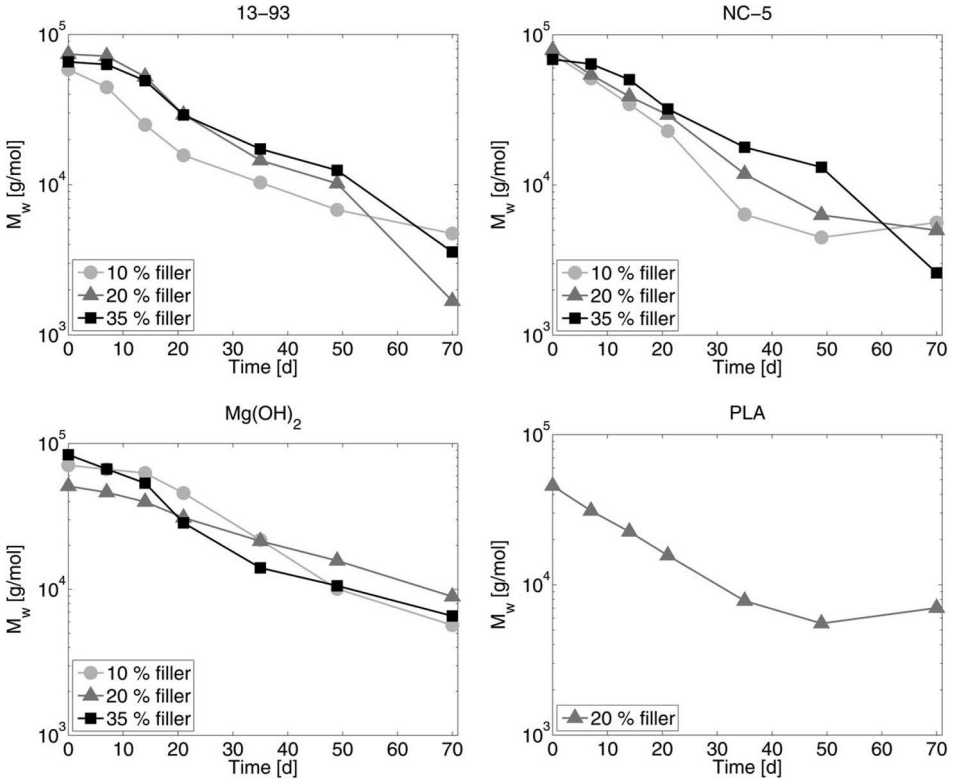

Figure 7. Change of weight average molecular weight (M_w) of porous PLGA-based scaffolds with different amounts of magnesium-containing fillers. The PLA 20% scaffolds have a lower initial M_w because of the low molecular weight PLA used in the blend.

concentration or to the local alkalosis. In that study, the release of magnesium into tissue was not directly measured. In another study, porous scaffolds, which were made of alloys containing 90% magnesium, were inserted in rabbit knees.[51] Three months after implantation, the scaffolds had largely degraded, and no significant harm was observed in the neighboring tissues. Actually, magnesium alloys have been shown to induce bone cell activation and increase bone mass around implants.[28] When compact magnesium scaffolds were immersed in cell culture medium in a previous study,[52] the release of magnesium from uncoated magnesium scaffolds into the medium during the first 7 days was approximately 110 mg L^{-1}, which is approximately equal to the release from $Mg(OH)_2$ 10% scaffolds during the first 7 days of immersion in this study. However, results from *in vitro* corrosion tests of magnesium alloys have been shown to correlate poorly with results from *in vivo* studies with the same materials.[53]

Feyerabend *et al.*[31] showed that $Mg(OH)_2$ release has a beneficial effect on chondrocyte proliferation, with an optimal concentration of magnesium at 10 mM, which corresponds to 243 mg L^{-1}. Magnesium levels equal to or higher than 15 mM were found to negatively affect chondrocytes. Yoshizawa *et al.*[29] showed osteogenic activity of bone marrow stromal cells to be at optimal levels at a magnesium concentration of 10 mM. In that study, the proliferation of the cells was slightly increased at a concentration of 10 mM compared to the base concentration of 0.8 mM, but the proliferation rate was low at a concentration of 100 mM. The deposition of extracellular matrix was enhanced at magnesium concentrations of 5 and 10 mM, and the protein expression which represented osteogenic activity was highest at 10 mM. *In vivo* tests with $Mg(OH)_2$ scaffolds show that even apparently high magnesium levels may improve bone formation.[50] The number of quinolone-treated chondrocytes decreased less when they were cultured in magnesium-containing medium as compared to culturing in a magnesium-free medium, and the effect was more pronounced when the amount of magnesium was tripled from the base amount of approximately 50–60 mg L^{-1},[22] where the tripled amount equaled roughly 6.8 mM.

On the basis of the studies mentioned above, a magnesium concentration of 10 mM seems to be favorable for osteogenesis and chondrocyte proliferation. This level is similar to the concentration in the Tris buffer of $Mg(OH)_2$ 20% and 35% scaffolds during the first week of immersion in this study. The concentration of magnesium is supposedly higher inside the scaffolds than in the Tris buffer, and even the lower concentrations of magnesium

ions released from the 13–93 and NC–5 scaffolds may therefore be of biological significance. The results of the above mentioned studies and this study are, however, not directly comparable, as neither the scaffold structure nor the quality and quantity of the immersion medium are standardized. Moreover, one cannot fully compare *in vitro* and *in vivo* conditions.

Molecular Weight

The weight average molecular weights (M_w) of the composites before and after extrusion processing are shown in Table III. M_w decreased considerably, by 26–52%, during the melt extrusion. The M_w of PLA 20% was notably low and the polydispersity index (PDI) was high after the extrusion because of the added low M_w PLA to PLGA during the extrusion.

The changes in M_w during the immersion in Tris buffer for 70 days are shown in Figure 7. For 13–93- and NC–5-containing scaffolds, the early degradation was slower for scaffolds with more glass, but toward the end of the immersion, their rate of degradation seemed to increase rapidly. The M_w of the $Mg(OH)_2$-containing scaffolds decreased less than the M_w of the glass-containing scaffolds, even though the $Mg(OH)_2$-containing scaffolds showed a more rapid weight loss. This implies that the early weight loss of the $Mg(OH)_2$-containing scaffolds was in addition to the $Mg(OH)_2$ dissolution mainly caused by the dissolution of fragments of the polymer matrix.

CONCLUSIONS

Mg^{2+} was released in a continuous and controlled manner from the scaffolds for an initial time span of at least 35 days. The release from all magnesium-containing scaffolds peaked in the beginning of the immersion in Tris buffer, which correlates with the time when postoperative antibiotics may reduce magnesium levels in tissue and affect tissue regeneration negatively. Comparisons to studies in the literature (see discussion and references above) indicate that the amount of released Mg^{2+} from the $Mg(OH)_2$ 20% and 35% scaffolds may be sufficient to elicit biological responses.

ACKNOWLEDGMENTS

The authors would like to thank the Finnish Funding Agency for Technology and Innovation (Tekes) for their financial support (Grant 3110/31/08). In addition, PU is grateful for the financial support from Medicinska Understödsföreningen Liv och Hälsa and the Swedish Cultural Foundation in Finland. Bioresorbable glasses were kindly provided by BonAlive Biomaterials Ltd. Jarl Hemming is thanked for his contribution to the molecular weight analysis. The contribution of materials and expertise from Dr Saara Inkinen is warmly acknowledged.

REFERENCES

1. Solchaga, L. A.; Temenoff, J. S.; Gao, J.; Mikos, A. G.; Caplan, A. I.; Goldberg, V. M. *Osteoarthritis Cartilage* **2005**, *13*, 297.
2. Puppi, D.; Chiellini, F.; Piras, A. M.; Chiellini, E. *Prog. Polym. Sci.* **2010**, *35*, 403.
3. Griffith, L. G. *Acta Mater.* **2000**, *48*, 263.
4. Siepmann, J.; Göpferich, A. *Adv. Drug Deliv. Rev.* **2001**, *48*, 229.
5. Kohn, D. H.; Sarmadi, M.; Helman, J. I.; Krebsbach, P. H. *J. Biomed. Mater. Res.* **2002**, *60*, 292.
6. Lee, G.; Hwang, J.; Choi, J.; Park, H.; Cho, J.; Kim, K.; Chae, H.; Kim, H. *Int. J. Biochem. Cell Biol.* **2011**, *43*, 1305.
7. Han, S.; Chae, S.; Choi, J.; Kim, E.; Chae, H.; Kim, H. *Immunopharmacol. Immunotoxicol.* **2009**, *31*, 428.
8. Bergsma, E. J.; Rozema, F. R.; Bos, R. R. M.; Bruijn, W. C. D. *Oral Maxillofac. Surg.* **1993**, *51*, 666.
9. Shen, Y.; Liu, W.; Wen, C.; Pan, H.; Wang, T.; Darvell, B. W.; Lu, W. W.; Huang, W. *J. Mater. Chem.* **2012**, *22*, 8662.
10. Li, H.; Chang, J. *Compos. Sci. Technol.* **2005**, *65*, 2226.
11. Zargar Kharazi, A.; Fathi, M. H.; Bahmani, F.; Fanian, H. *Polym. Degrad. Stab.* **2011**, *96*, 2055.
12. Rezwan, K.; Chen, Q. Z.; Blaker, J. J.; Boccaccini, A. R. *Biomaterials* **2006**, *27*, 3413.
13. Boccaccini, A. R.; Erol, M.; Stark, W. J.; Mohn, D.; Hong, Z.; Mano, J. F. *Compos. Sci. Technol.* **2010**, *70*, 1764.
14. Belluci, M. M.; Schoenmaker, T.; Rossa-Junior, C.; Orrico, S. R.; de Vries, T. J.; Everts, V. *J. Nutr. Biochem.* **2013**, *24*, 1488.
15. Rude, R.; Gruber, H.; Norton, H.; Wei, L.; Frausto, A.; Kilburn, J. *Osteoporosis Int.* **2006**, *17*, 1022–1032.
16. Rude, R. K.; Gruber, H. E.; Norton, H. J.; Wei, L. Y.; Frausto, A.; Kilburn, J. *Bone* **2005**, *37*, 211.
17. Rude, R. K.; Gruber, H. E.; Wei, L. Y.; Frausto, A.; Mills, B. G. *Calcif. Tissue Int.* **2003**, *72*, 32.
18. Rude, R. K.; Gruber, H. E. *J. Nutr. Biochem.* **2004**, *15*, 710.
19. Kanazawa, I.; Yamamoto, M.; Yamaguchi, T.; Yamauchi, M.; Yano, S.; Sugimoto, T. *Endocr. J.* **2007**, *54*, 935.
20. Belluci, M. M.; Giro, G.; del Barrio, R. A. L.; Pereira, R. M. R.; Marcantonio, E.; Orrico, S. R. P. *Clin. Oral Implants Res.* **2011**, *22*, 716.
21. Del Barrio, R. A.; Giro, G.; Belluci, M. M.; Pereira, R. M.; Orrico, S. R. *Int. J. Oral Maxillofac. Implants* **2010**, *25*, 1125.
22. Egerbacher, M.; Wolfesberger, B.; Gabler, C. *Vet. Pathol.* **2001**, *38*, 143.
23. Trampuz, A.; Zimmerli, W. *Drugs* **2006**, *66*, 1089.
24. Nichols, R. L. *Surg. Infect. (Larchmt)* **2000**, *1*, 65.
25. Staiger, M. P.; Pietak, A. M.; Huadmai, J.; Dias, G. *Biomaterials* **2006**, *27*, 1728.
26. He, D.; Dong, W.; Tang, S.; Wei, J.; Liu, Z.; Gu, X.; Li, M.; Guo, H.; Niu, Y. *J. Mater. Sci. Mater. Med.* **2014**, *25*, 1415.
27. Castellani, C.; Lindtner, R. A.; Hausbrandt, P.; Tschegg, E.; Stanzl-Tschegg, S. E.; Zanoni, G.; Beck, S.; Weinberg, A. *Acta Biomater.* **2011**, *7*, 432.
28. Witte, F.; Kaese, V.; Haferkamp, H.; Switzer, E.; Meyer-Lindenberg, A.; Wirth, C. J.; Windhagen, H. *Biomaterials* **2005**, *26*, 3557.
29. Yoshizawa, S.; Brown, A.; Barchowsky, A.; Sfeir, C. *Acta Biomater.* **2014**, *10*, 2834.

30. Kon, E.; Filardo, G.; Perdisa, F.; Di Martino, A.; Busacca, M.; Balboni, F.; Sessa, A.; Marcacci, M. *J. Mater. Sci. Mater. Med.* **2014**, *25*, 2437.
31. Feyerabend, F.; Witte, F.; Kammal, M.; Willumeit, R. *Tissue Eng.* **2006**, *12*, 3545.
32. Lee, C. H.; Wen, Z. H.; Chang, Y. C.; Huang, S. Y.; Tang, C. C.; Chen, W. F.; Hsieh, S. P.; Hsieh, C. S.; Jean, Y. H. *Osteoarthritis Cartilage* **2009**, *17*, 1485.
33. Shimaya, M.; Muneta, T.; Ichinose, S.; Tsuji, K.; Sekiya, I. *Osteoarthritis Cartilage* **2010**, *18*, 1300.
34. Witte, F.; Hort, N.; Vogt, C.; Cohen, S.; Kainer, K. U.; Willumeit, R.; Feyerabend, F. *Curr. Opin. Solid State Mater. Sci.* **2008**, *12*, 63.
35. Kang, J.; Schwendeman, S. P. *Biomaterials* **2002**, *23*, 239.
36. Hoppe, A.; Güldal, N. S.; Boccaccini, A. R. *Biomaterials* **2011**, *32*, 2757.
37. Aou, K.; Kang, S.; Hsu, S. L. *Macromolecules* **2005**, *38*, 7730.
38. Tran, V.; Benoît, J.; Venier-Julienne, M. *Int. J. Pharm.* **2011**, *407*, 1.
39. Jose, M. V.; Thomas, V.; Johnson, K. T.; Dean, D. R.; Nyairo, E. *Acta Biomater.* **2009**, *5*, 305.
40. Orava, E.; Korventausta, J.; Rosenberg, M.; Jokinen, M.; Rosling, A. *Polym. Degrad. Stab.* **2007**, *92*, 14.
41. Endres, S.; Hiebl, B.; Hagele, J.; Beltzer, C.; Fuhrmann, R.; Jager, V.; Almeida, M.; Costa, E.; Santos, C.; Traupe, H.; Jung, E. M.; Prantl, L.; Jung, F.; Wilke, A.; Franke, R. P. *Clin. Hemorheol. Microcirc.* **2011**, *48*, 29.
42. Holy, C. E.; Cheng, C.; Davies, J. E.; Shoichet, M. S. *Biomaterials* **2001**, *22*, 25.
43. Trznadel, M. and Kryszewski, M. *J Macromol. Sci. Polym. Rev.* **1992**, *3–4*, 259.
44. Smith, P. B.; Leugers, A.; Kang, S.; Hsu, S. L.; Yang, X. *J. Appl. Polym. Sci.* **2001**, *82*, 2497.
45. Meer, S. A. T.; Wijn, J. R.; Wolke, J. G. C. *J. Mater. Sci. Mater. Med.* **1996**, *7*, 359.
46. Holy, C. E.; Dang, S. M.; Davies, J. E.; Shoichet, M. S. *Biomaterials* **1999**, *20*, 1177.
47. Larrañaga, A.; Aldazabal, P.; Martin, F. J.; Sarasua, J. R. *Polym. Degrad. Stab.* **2014**, *110*, 121.
48. Ara, M.; Watanabe, M.; Imai, Y. *Biomaterials* **2002**, *23*, 2479.
49. Martin, C.; Winet, H.; Bao, J. Y. *Biomaterials* **1996**, *17*, 2373.
50. Janning, C.; Willbold, E.; Vogt, C.; Nellesen, J.; Meyer-Lindenberg, A.; Windhagen, H.; Thorey, F.; Witte, F. *Acta Biomater.* **2010**, *6*, 1861.
51. Witte, F.; Ulrich, H.; Rudert, M.; Willbold, E. *J. Biomed. Mater. Res. A* **2007**, *81A*, 748.
52. Xu, L.; Yamamoto, A. *Appl. Surf. Sci.* **2012**, *258*, 6353.
53. Witte, F.; Fischer, J.; Nellesen, J.; Crostack, H.; Kaese, V.; Pisch, A.; Beckmann, F.; Windhagen, H. *Biomaterials* **2006**, *27*, 1013.

Haaparanta AM, Uppstu P, Hannula M, Ellä V, Rosling A, Kellomäki M. Improved dimensional stability with bioactive glass fibre skeleton in poly(lactide-co-glycolide) porous scaffolds for tissue engineering. Materials Science and Engineering: C. 2015;56:457–66.

II

Materials Science and Engineering C 56 (2015) 457–466

Contents lists available at ScienceDirect

Materials Science and Engineering C

journal homepage: www.elsevier.com/locate/msec

Improved dimensional stability with bioactive glass fibre skeleton in poly(lactide-co-glycolide) porous scaffolds for tissue engineering

Anne-Marie Haaparanta [a,b,*], Peter Uppstu [c], Markus Hannula [a,b], Ville Ellä [a,b,1], Ari Rosling [c], Minna Kellomäki [a,b]

[a] Department of Electronics and Communications Engineering, Tampere University of Technology, Korkeakoulunkatu 3, 33720 Tampere, Finland
[b] BioMediTech, Institute of Biosciences and Medical Technology, Biokatu 10, 33520 Tampere, Finland
[c] Laboratory of Polymer Technology, Centre of Excellence in Functional Materials at Biological Interfaces, Åbo Akademi University, Biskopsgatan 8, 20500 Åbo, Finland

ARTICLE INFO

Article history:
Received 13 February 2015
Received in revised form 1 June 2015
Accepted 9 July 2015
Available online 15 July 2015

Keywords:
Poly(D,L-lactide-co-glycolide)
Bioactive glass
Composite
Freeze-drying
Bone
Tissue engineering

ABSTRACT

Bone tissue engineering requires highly porous three-dimensional (3D) scaffolds with preferable osteoconductive properties, controlled degradation, and good dimensional stability. In this study, highly porous 3D poly(D,L-lactide-co-glycolide) (PLGA) — bioactive glass (BG) composites (PLGA/BG) were manufactured by combining highly porous 3D fibrous BG mesh skeleton with porous PLGA in a freeze-drying process. The 3D structure of the scaffolds was investigated as well as *in vitro* hydrolytic degradation for 10 weeks. The effect of BG on the dimensional stability, scaffold composition, pore structure, and degradation behaviour of the scaffolds was evaluated. The composites showed superior pore structure as the BG fibres inhibited shrinkage of the scaffolds. The BG was also shown to buffer the acidic degradation products of PLGA. These results demonstrate the potential of these PLGA/BG composites for bone tissue engineering, but the ability of this kind of PLGA/BG composites to promote bone regeneration will be studied in forthcoming *in vivo* studies.

1. Introduction

Tissue engineering with highly porous three-dimensional (3D) biodegradable scaffolds has emerged as a promising method for bone tissue regeneration [1–4]. Especially polymer based scaffolds together with a ceramic phase acting as an osteoconductive component have been widely studied for bone regeneration [1,5]. A highly porous structure with open and interconnected pores is required for optimal tissue integration into the scaffolds after implantation [3]. For bone tissue engineering, the scaffold should also provide temporary mechanical support, osteoconductivity, controlled degradation rate, biocompatibility of the used materials and their degradation products, and be sterile [6].

Poly(lactide-co-glycolide) (PLGA) is the most studied biodegradable synthetic polymer for biomedical applications. It is widely used as sutures and drug delivery devices as it degrades rapidly compared to other biodegradable polyesters. Promising results have already been demonstrated with PLGA and it has also been approved by FDA (Food and Drug Administration) [7].

PLGA has been widely studied as tissue engineering scaffolds as well because it demonstrates favourable cell adhesion and proliferation properties [8,9]. Particularly, PLGA has been studied for use in porous tissue engineering scaffolds because of its tuneable degradation rate, good mechanical properties and processability [10]. Porous PLGA scaffolds often suffer from low mechanical strength and lack the osteoconductivity and hydrophilicity required for optimal bone tissue engineering [11].

Acidic by-products which result from PLGA degradation may lead to harmful pH decrease in the implantation site. Bioactive glass (BG), on the other hand, is hydrophilic by nature, possesses osteoconductive properties, and has good compression strength making it a good candidate for bone tissue engineering. Also, BG is shown to buffer the acidic degradation of PLGA [12]. This is why PLGA/BG composites are thought to overcome the limitations of plain PLGA scaffolds for improved bone regeneration.

Freeze-drying is a conventional method to fabricate porous tissue engineering scaffolds. Many of the previously studied freeze-dried polymer-bioactive ceramic scaffolds for bone tissue engineering have been prepared of bioactive ceramic filler particles and either natural polymers, such as collagen or chitosan [13–19], or synthetic polymers, such as PLGA or PDLLA [12,20–22]. The use of fibrous bioactive ceramic

* Corresponding author at: Department of Electronics and Communications Engineering, Tampere University of Technology, Korkeakoulunkatu 3, 33720 Tampere, Finland.
E-mail addresses: anne-marie.haaparanta@tut.fi (A.-M. Haaparanta), peter.uppstu@abo.fi (P. Uppstu), markus.hannula@tut.fi (M. Hannula), ville.ella@arcticbiomaterials.com (V. Ellä), ari.rosling@abo.fi (A. Rosling), minna.kellomaki@tut.fi (M. Kellomäki).
[1] Present address: Arctic Biomaterials OY, Osuusmyllynkatu 13, 33700 Tampere, Finland.

http://dx.doi.org/10.1016/j.msec.2015.07.013
0928-4931/

filler in a freeze-dried polymer matrix for bone tissue engineering scaffolds has as far as we know not been reported previously.

The potential of bioresorbable glass fibre-reinforced composites for load-bearing applications has been reported previously [23]. In the present study highly porous freeze-dried PLGA/BG composites for bone tissue engineering were prepared and studied. The aim was to develop highly porous three-dimensional composite scaffolds by incorporating porous PLGA with a highly porous BG fibre mesh skeleton in a freeze-drying process. Two PLGA–BG composite scaffolds were compared to two plain PLGA scaffolds. The manufactured scaffolds were studied 10 weeks *in vitro*. The dimensional stability, scaffold composition (TGA), scaffold pore structure (SEM, microCT), contact angle, ability of BG to buffer the acidic degradation products of PLGA, and degradation rates (GPC, DSC) of the scaffolds were studied.

2. Materials and methods

2.1. Materials

Medical grade D-lactide and glycolide monomers (purity of raw materials >99.5%) were purchased from PURAC Biochem bv (Gorinchem, the Netherlands) and L-lactide monomer (>99%) from Futerro (Escanaffles, Spain). Tin(II) 2-ethylhexanoate (approx. 95%), 1-decanol (99%, distilled prior to use), dichloromethane (≥99.9%), and 1,4-dioxane were purchased from Sigma-Aldrich (Helsinki, Finland).

Two compositions of bioresorbable melt-derived glass fibres (Vivoxid Ltd., Turku, Finland), denoted as BG1 and BG2 of a system Na_2O–CaO–MgO–Al_2O_3–B_2O_3–P_2O_5–SiO_2, were used as received as reinforcement for the composites. The fibres were coated fibres with a sizing layer constituted of 3-glycidoxypropyltriethoxysilane and low molecular weight polycaprolactone (PCL). The average diameter of the fibres was 13 μm. The compositions of BG1 and BG2 fibres are presented in Table 1.

2.2. Methods

2.2.1. Polymerization

PLGA with a rac-lactide-to-glycolide ratio of 70:30 was synthesized in an inert (argon) atmosphere by ring-opening polymerization. Briefly, 100 g L-lactide, 100 g D-lactide and 69 g glycolide were weighed into a round bottle at room temperature (RT). The monomers were freshly obtained and stored at −20 °C until use. The bottle was heated to 120 °C and kept at this temperature until all monomers were molten. After this, 0.1 mol-% of tin(II) 2-ethylhexanoate (initiator) and a molecular weight defining amount of 1-decanol (co-initiator) were added under initial heavy stirring. The temperature was raised to 150 °C and kept constant for 5 h. The reaction mixture was cooled to RT and subsequently dissolved in 2 L of dichloromethane and precipitated in a 6-fold amount of ethanol under vigorous stirring to remove unreacted monomers and other impurities. The polymer product was dried in vacuum at 40 °C for approximately one week until no residual solvent could be observed in ^{1}H-NMR. The dried polymers were cut to granules.

2.2.2. Scaffold fabrication

Two different molecular weight PLGAs, poly(D,L-lactide-co-glycolide) 70/30 were manufactured for matrix polymer. The weight average molecular weight (M_w) was 76 300 g/mol and 48 300 g/mol for PLGA1 and PLGA2, respectively.

BG1 and BG2 mesh were manufactured for the composite scaffolds. The glass fibres were cut to staple fibres (length of ~10 cm) and carded into mesh. The mesh was cut with a puncher to produce samples with a radius of 14 mm.

PLGA solutions of 3 and 5 wt.% were prepared by dissolving PLGA in 1,4-dioxane. The solutions were stirred vigorously overnight to form uniform solution. For plain PLGA scaffolds, 5 wt.% PLGA solution was poured into custom made Teflon sample moulds (diameter 15 mm, height 3 mm). For composite scaffolds, 3 wt.% PLGA solution was poured into moulds after which the BG mesh was thoroughly immersed into the solution. The samples were frozen at −30 °C for 24 h prior to 24 h freeze-drying. The samples were held under vacuum at RT for a minimum of 48 h and gamma sterilized at 25 kGy before characterization. Table 2 shows the different (fabricated) scaffold types.

2.2.3. Microstructure evaluation

The microstructure of the scaffolds was studied with a scanning electron microscope (SEM) (JEOL Ltd, Tokyo, Japan). The top surface and cross-section of the scaffolds were imaged. The samples were sputtered with gold prior to analysis. MicroCT imaging with MicroXCT-400 (Carl Zeiss X-ray Microscopy, Inc., Pleasanton, USA) was used to analyse the 3D structure of the scaffolds. To determine the pore structure (porosity, pore size, material thickness and pore size distribution) of the scaffolds, Fiji [24] with BoneJ [25] plugin, MATLAB (MathWorks Inc., Natick, MA, USA) and Avizo 9.0 software were used. BoneJ thickness function fits spheres inside the structure. The value of each voxel will be the diameter of the biggest sphere that includes the voxel. Obtained data can be used to calculate *e.g.* the mean thicknesses and porosities for certain size particles. Open porosities were calculated with a self-made MATLAB programme. Open porosity is considered as the pores that are accessible from outside of the scaffold. Open porosity has been calculated for particles of different sizes by using thickness data. Pore size distribution was determined by using Avizo. The tube voltage and voxel size were 40 kV and $2.2 \times 2.2 \times 2.2$ μm^3, respectively. No filters were used.

2.2.4. Contact angle measurements

Contact angle of the dry scaffolds prior to hydrolysis was examined with a Theta optical tensiometer (Biolin Scientific, Västra Frölunda, Sweden) device. The measurements were done with deionized water, phosphate-buffered saline (PBS, pH 7.40) and with bovine blood (commercially available) ($n = 6$ for each scaffold type with each different solutions).

2.2.5. In vitro studies

In vitro degradation studies, timed at weeks 0, 2, 4, 6, 8 and 10, were carried out using six parallel samples, each half the size of the original freeze-dried sample (weight ca. 15 mg). PBS prepared as described by Shah et al. [26], with the standard volume of 10 ml buffer per scaffold (according to International Standard, ISO 15814:1999 [27]) was used. The pH of the buffer was measured weekly, using a Mettler Toledo MP225 pH metre (Mettler-Toledo GmbH, Schwerzenbach, Switzerland). The buffer solution was changed fortnightly or weekly if pH exceeded the given limits (7.35–7.45).

Table 1
Oxide compositions (mol-%) of the bioactive glass fibres (BG1 and BG2).

Glass	SiO_2	CaO	MgO	B_2O_3	Al_2O_3	P_2O_5	Na_2O
BG1	68.7 ± 1.0	13.3 ± 0.2	4.4 ± 0.1	0.9 ± 0.1	0.3 ± 0.1	0.6 ± 0.1	11.9 ± 0.3
BG2	68.6 ± 1.0	9.3 ± 0.2	7.2 ± 0.1	1.8 ± 0.1		0.6 ± 0.1	12.5 ± 0.3

Table 2
The abbreviations of scaffolds (in bold) and their compositions (PLGA: poly(D,L-lactide-co-glycolide), BG: bioactive glass).

Polymer scaffolds		*Composites*	
PLGA1	PLGA1 (5 wt.%)	**PLGA1/BG1**	PLGA1 (3 wt.%) + BG1 mesh
PLGA2	PLGA2 (5 wt.%)	**PLGA2/BG2**	PLGA2 (3 wt.%) + BG2 mesh

2.2.6. Weight change

After the specified time intervals, the samples were weighed and the weight change was determined both for wet samples and after drying for dry samples. After weighing the wet samples, the samples were rinsed with deionized water and gently dried with tissue paper and then dried in a fume hood for two days and thereafter one week in a vacuum before the dry weighing. The difference in wet and dry weights after *in vitro* studies was calculated using the following equation:

$$\text{Weight change} = [(W_e - W_b)/W_b] \times 100\%,$$

where W_e is the sample weight after *in vitro* studies and W_b is the weight at the beginning of the *in vitro* studies. Due to the degradation of PLGA the plain PLGA scaffolds crumbled and were difficult to weigh accurately after the longest hydrolysis times.

2.2.7. Dimensional change

At the beginning of and after the *in vitro* studies the dimensions of the samples were measured and the diameter, radius, and thickness of the samples were determined.

2.2.8. Gel permeation chromatography

The molecular weight determination of the polymers was performed using gel permeation chromatography (GPC) with an LC-10ATVP HPLC-pump (Shimadzu Corporation, Kyoto, Japan), an AM GPC Gel 10 μm Linear colon (Mentor, Ohio, USA) and a Sedex 85 light scattering detector (Sedere SA, Alfortville, France). The GPC measurements were carried out at 40 °C at a flow rate of 1 ml min^{-1} with tetrahydrofuran as solvent. Polystyrene standards from Polymer Standard Service were used for calibration. The samples were filtered with 0.22 μm PTFE filters before analysis. The GPC analysis was conducted as average of parallel samples, as the remaining average mass of the studied scaffolds was too low for individual parallel measurements. Unfortunately, no data could be analysed from the week 10 scaffolds of the PLGA2 and PLGA2/BG2, as the remaining mass of those scaffolds was too low.

2.2.9. Differential scanning calorimetry

The glass transition temperature (T_g) of the samples was determined with differential scanning calorimetry (DSC). The used instrument was Q1000 (TA Instruments, New Castle, DE, USA) with the procedure: heat to 200 °C, 20 °C/min, cool to 0 °C, 50 °C/min, and heat to 200 °C, 20 °C/min. All samples were measured in standard aluminium pans under a dry N_2 atmosphere and the given results are from the second heating scan. The sample size was 5 mg ($n = 2$ for each scaffold at each time point).

2.2.10. Thermogravimetric analysis

Thermogravimetric analysis (TGA) was used for analytic measurement of component ratios of PLGA and BG in the composite scaffolds. Q500 (TA Instruments, New Castle, DE, USA) device was used with the method Hi-Res-Dynamic. The sample size was 10 mg and samples were heated to 800 °C ($n = 2$).

2.2.11. Statistical analysis

Majority of the data are presented as mean ± standard deviation (SD). The Mann–Whitney U test was conducted for the contact angle results to find out the statistical differences between the results. The significance level of $p \leq 0.05$ was used.

3. Results

3.1. Structure of the scaffolds

The structure of the PLGA/BG composites was more homogenous compared to the plain PLGA scaffolds (overall visual characterization). In addition, larger macropores were detected in the plain PLGA scaffolds. The more detailed characterization with microCT and SEM revealed highly similar overall pore structure of the PLGA component in the plain and composite scaffolds (Figs. 1 and 2).

MicroCT studies showed the highly porous structure of the scaffolds (Table 3) with porosity over 93%. The PLGA2/BG2 composites had the highest porosity, 96%. The material thickness (*i.e.* pore wall thickness) was higher for composite scaffolds than the parallel plain scaffolds. The mean pore sizes (Table 3) varied between different scaffolds and no clear difference could be noted between the parallel plain and composite scaffolds. The mean pore sizes of the studied scaffolds varied from 49 to 77 μm, and maximum pore sizes from 105 to 251 μm. The highest pore sizes with mean pore size of 77 μm and maximum pore size of 251 μm was detected for the PLGA2/BG2 composites. Furthermore, the PLGA2/BG2 composites showed broader pore size distribution (Fig. 3) and higher amount of pores over the size of 100 μm compared to the other scaffolds.

In Fig. 4 the total porosity and open porosity graphs for different scaffolds are shown. The majority of the pore structure in the scaffolds consists of open pores, as shown in the figure, indicating an interconnected pore structure. The PLGA1 and PLGA2/BG2 scaffolds had a considerable amount of open pores even at sizes exceeding 100 μm.

3.2. In vitro hydrolytic degradation of the scaffolds

The acidic degradation products of PLGA were noticed during the hydrolysis (as a decrease in pH value of the buffer). For PLGA1 and PLGA2 the pH started to decrease and the pH exceeded the given limits (7.35–7.45) after 4 weeks of hydrolysis (data not shown). After that point, the buffer of the plain scaffolds was changed weekly. The pH of the plain scaffolds reached the given limits (7.35–7.45) again at the end of the hydrolysis, at week 10. The pH of the composites, PLGA1/BG1 and PLGA2/BG2, stayed at the given limits. The pH values of the plain PLGA scaffolds were lower than the pH of the PLGA/BG composite scaffolds at all times. Therefore, the BG in the composites was shown to neutralize the acidic degradation products of PLGA.

Plain PLGA scaffolds lost their initial structure already at the beginning of the hydrolysis at week 2, due to severe collapse of their initial porous structure (Fig. 5). At week 2, PLGA1 scaffolds showed denser structure with shrunk pores, and the pore structure was completely lost in the PLGA2 scaffolds. Unlike the plain PLGA scaffolds, the BG fibres in the composites stabilized the structure of PLGA and the open porous structure was maintained in composites during the hydrolysis (10 weeks) (Fig. 5). However, the initial opaque appearance of the composites started to change into transparent after 2 weeks of hydrolysis, whereas the plain PLGA scaffolds retained their opaque appearance until the week 8 (visual characterization, data not shown).

Considerably better dimensional stability was shown for PLGA/BG composites than for plain PLGA scaffolds during the 10-week hydrolysis. The plain PLGA scaffolds suffered from severe shrinking and twisting (visual characterization) during the hydrolysis. No considerable change in radius of composite scaffolds was noticed during the hydrolysis, whereas the radius of plain PLGA scaffolds decreased to some extent (maximally −40%) (data not shown). The height of the scaffolds increased constantly during the hydrolysis until week 8, after which

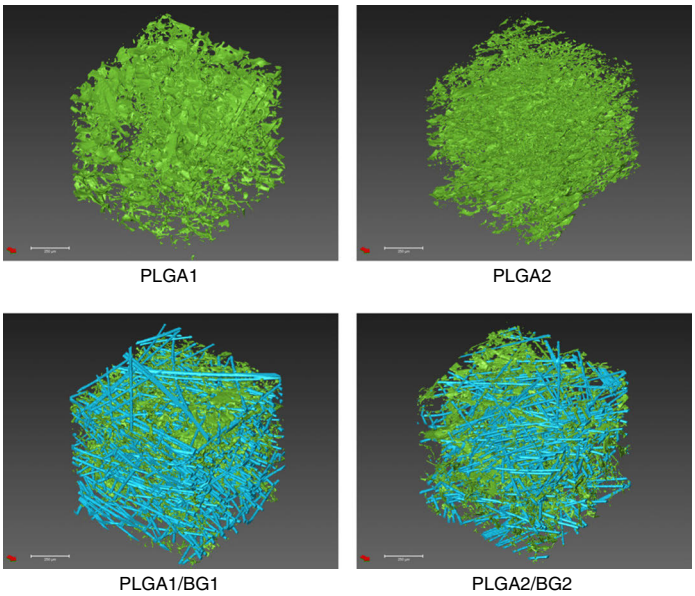

Fig. 1. 3D reconstructions of microCT images of different scaffolds. PLGA in green and BG in blue; scale bars 250 μm.

the increase was as high as 80% and 100% for PLGA1 and PLGA1/BG1 scaffolds, and 45% and 50% for PLGA2 and PLGA2/BG2 scaffolds, respectively. At week 10 the increase of height for PLGA1 and PLGA1/BG1 scaffolds were 40% and 60%, respectively, and 50% for PLGA2 scaffolds, whereas the height of PLGA2/BG2 composites had decreased to the initial values.

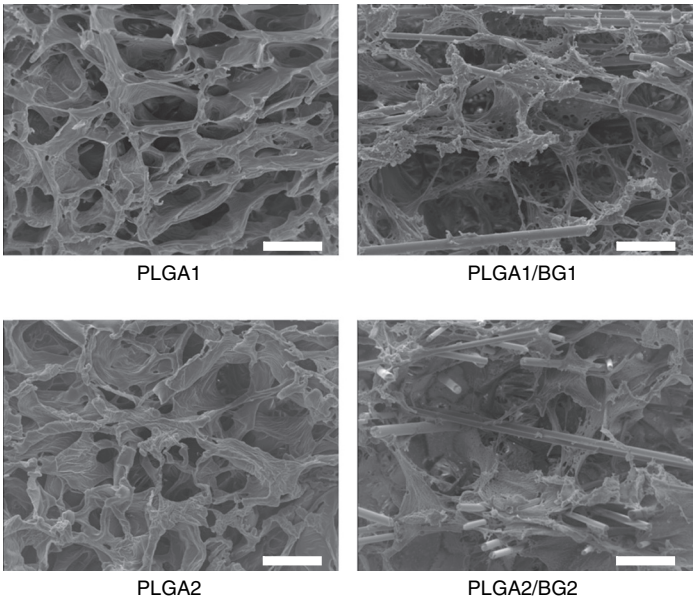

Fig. 2. SEM images of the initial structure of the different scaffolds. Scale bars 100 μm.

Table 3
Porosity, material thickness, and pore size of different scaffolds (microCT data).

	Porosity [%]	Material thickness [μm]	Material thickness max. [μm]	Pore size [μm]	Pore size max. [μm]
PLGA1	93	9 ± 3	24	69 ± 24	173
PLGA2	93	7 ± 2	18	49 ± 13	105
PLGA1/BG1	93	13 ± 5	30	53 ± 18	118
PLGA2/BG2	96	8 ± 3	20	77 ± 34	251

The weight of the scaffolds decreased gradually during the 10-week hydrolysis. The difference between composite PLGA/BG and plain PLGA scaffolds was moderate and the trend in weight loss was the same for parallel composite and plain scaffolds. After week 6 the weight loss of plain PLGA1 scaffolds was however higher than the corresponding composite (PLGA1/BG1). The overall weight loss after the 10-week hydrolysis was 63% for PLGA1 and 41% for PLGA1/BG1 scaffolds, whereas, the overall weight loss was 59% for PLGA2 and 63% for PLGA2/BG2 scaffolds.

A first order law can be used to describe the core-accelerated bulk degradation process by chain scission of ester bonds for poly(α-hydroxyesters), specifically, the M_n decrease during ester hydrolysis can be modelled as [28]:

$$1/M_n = 1/M_n^0 \ x \ exp^{kt}$$

or in its linearized form:

$$ln\left(M_n/M_n^0\right) = -kt,$$

where M_n (g/mol) is the number average molar mass of the polymer at any time point, $M^0{}_n$ is the initial number average molar mass (g/mol), k is the ester hydrolysis rate constant (per day) and t is the degradation time (day). Assuming that the above model is also applicable to composite degradation, the values of $ln(M_n/M^0{}_n)$ as a function of t can be described by a linear function. Both the plain PLGA scaffolds and the PLGA/BG composites showed M_n decrease according to the first order law during hydrolysis, with straight lines with good fits indicating core accelerated bulk degradation (Fig. 6).

Weight average molecular weight (M_w) and number average molecular weight (M_n) of the PLGA decreased constantly during the hydrolysis (Fig. 7). As seen in Fig. 7, the processing method and subsequently the sterilization of the scaffolds affected the most the molecular weight of the scaffolds. The PLGA1 with higher initial molecular weight lost its molecular weight more severely after the processing and sterilization, and the M_n of PLGA1 scaffolds decreased to the same level as that of the PLGA2. After the highest drop in M_n values (after processing and sterilization) the M_n values stayed relatively constant during the first two weeks of hydrolysis after which the values decreased gradually. The trend in the decrease of molecular weight (both M_w and M_n) was similar for all scaffolds.

3.3. Wettability properties of the scaffolds

Contact angle values of the studied scaffolds varied from 92° to 118° (Fig. 8), with only some variation between the different fluids. The PLGA1 scaffolds showed significant difference in contact angle values in water with respect to PLGA1/BG1 ($p < 0.05$), PLGA2 ($p = 0.05$) and PLGA2/BG2 ($p < 0.05$) scaffolds. Also, PLGA1 showed relatively significant difference with respect to PLGA2/BG2 scaffolds ($p = 0.055$) in blood. There was no significant difference in contact angle values between PLGA/BG and plain PLGA scaffolds when measured in PBS.

The studied scaffolds had constant water absorption until week 8 in hydrolysis (Fig. 9). The composites had a higher water absorption rate during the first hydrolysis weeks than the plain PLGA scaffolds. After week 4 the water absorption started to increase strongly for the plain PLGA scaffolds and the plain PLGA1 had the highest water absorption at the end of the hydrolysis.

3.4. Thermal properties of the scaffolds

The T_g values decreased the most during processing (from 51.9 to 42.0 °C for PLGA1), and during sterilization (from 47.3 to 37.5 °C for PLGA2) (Fig. 10). After 2 weeks of hydrolysis the T_g values of plain PLGA1 and PLGA2 scaffolds actually increased. After week 2, the T_g values remained relatively constant during the hydrolysis.

The TGA studies showed BG content of 50.7 ± 5.2% in the PLGA1/BG1 composites and 41.9 ± 3.0% in the PLGA2/BG2 composites (Fig. 11). The difference in BG content between parallel samples was moderate in the composites. Also, no major change in the BG content in composites was noticed during the 10-week hydrolysis. However, as the trend lines show in Fig. 11, the BG content was slowly increasing in PLGA1/BG1 composites during hydrolysis and slowly decreasing in PLGA2/BG2 composites.

4. Discussion

Freeze-drying is one of the most common techniques to prepare porous scaffolds for tissue engineering [29]. In this study, the combination of a highly porous BG fibre mesh skeleton inside a freeze-dried PLGA matrix led to a highly porous composite structure with good interconnection of BG fibres in the PLGA matrix. The overall pore structure of the studied scaffolds was highly similar for all the studied scaffolds (Figs. 1 and 2), except for the few larger macropores in the plain PLGA scaffolds. The higher material thickness in the composite scaffolds was most likely due to the embedded fibres in the structure (Table 3).

A highly porous scaffold structure is known to be important in tissue engineering applications for the tissue ingrowth and for flow transport of nutrients and metabolic waste. Natural bone tissue is highly porous

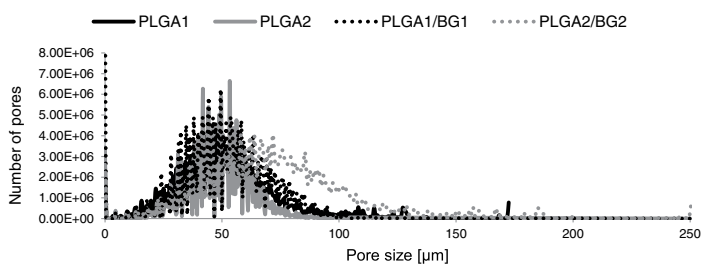

Fig. 3. Pore size distribution of PLGA1, PLGA2, PLGA1/BG1, and PLGA2/BG2 scaffolds.

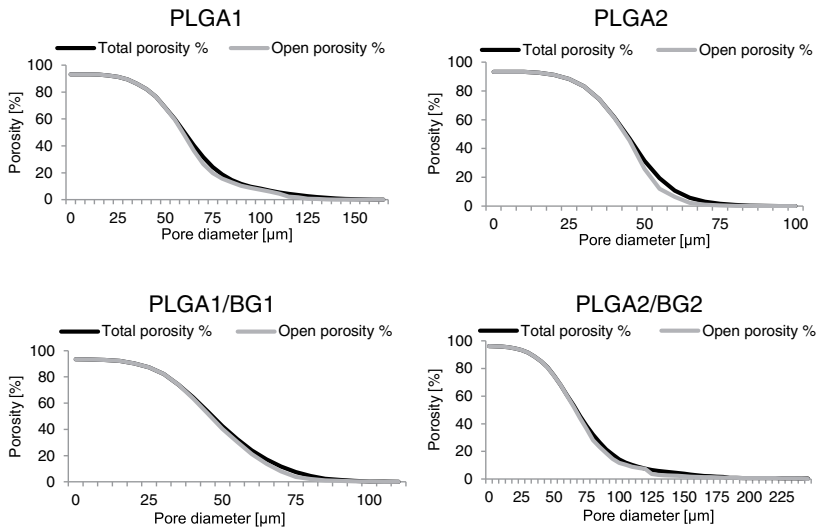

Fig. 4. Total porosity and open porosity graphs of the different scaffolds indicating highly interconnected pore structure in all scaffolds.

(50–90% porosity) depending on the type of bone [2]. Also, it is known that scaffold morphology affects the degradation of PLGA, as the scaffolds with higher porosity or smaller pores are found to degrade more slowly than those with lower porosity or larger pores [10]. The optimum pore size for bone tissue engineering scaffolds has been reported to be ~100 μm. However, lower porosity is thought to enhance osteogenesis *in vitro* due to cell aggregation and suppressed proliferation [3]. Therefore, the highly porous structure of the studied scaffolds with over 93% porosity and with lower mean pore size (lower than 100 μm) together with few larger pores (over 100 μm) could be a suitable structure for bone or osteochondral tissue engineering with an *in vitro* cell culture period before implantation.

It is known that the decrease in pH of biodegradable polyesters, like PLGA, is due to acidic by-products leached out from the polymer during degradation. The BG in aqueous solutions releases sodium, calcium, phosphate and magnesium ions, which forms basic hydroxides in the interphase, and therefore leads to higher local pH [23]. The acidic degradation products of PLGA scaffolds have been reported previously and bioceramics have been found to buffer the acidic degradation of PLGA [11,12,30]. This phenomenon was also shown with the studied PLGA/BG scaffolds as the BG was shown to buffer the acidic degradation products of PLGA as the pH of the plain PLGA scaffolds dropped under the given limit (7.35–7.45) after the week 4, unlike the pH of the composite scaffolds. The aliphatic polyesters are known to degrade hydrolytically by cleavage of the hydrolytically unstable ester bonds. All the studied scaffolds showed M_n decrease during hydrolysis with straight lines with good fits (Fig. 5). Therefore, unlike with solid poly(L-lactide-co-DL-lactide) (PLDLA)/BG composites reported previously [23], the studied porous scaffolds showed core-accelerated bulk degradation with chain scission of ester bonds as the rate limiting step. The presence of BG does not have significant influence on the degradation mechanism of PLGA in porous PLGA/BG composite scaffolds, as was seen both in the current study as well as reported previously [20], whereas the BG had an influence in PLDLA/BG scaffolds compared in that same study. The composite structure was found to affect the degradation rate of the scaffolds as the M_n, M_w and $\ln(M_n/M^0{}_n)$ figures show higher decrease in molecular weight values of plain PLGA scaffolds during the hydrolysis until the week 8. After week 8 the plain PLGA scaffolds had lost most of their mass and therefore the pH of the buffer solution also remained normal levels.

It is essential for tissue engineering scaffolds to hold initial dimensions during the time it takes the new tissue to form. The dimensional stability of plain PLGA scaffolds was found to be inadequate as the plain scaffolds lost their initial pore structure already at the beginning of the hydrolysis (Fig. 5), a phenomenon which was also detected previously in a study of porous PLGA scaffolds manufactured by solvent casting and pressure quenching with CO_2 [31]. However, in the present study the composite structure inhibited the dimensional changes of the scaffolds. The loose horizontally aligned fibre network, however, allowed some swelling of the PLGA component in the vertical direction during the hydrolysis. The porous structure of the PLGA/BG scaffolds remained intact until the end of the hydrolysis (Fig. 5).

Higher material thickness in porous PLGA scaffolds has been found to lead to higher degradation rate, because the thicker pore walls enhance acid-catalysed hydrolysis as the diffusion of acidic degradation products is inhibited [32]. Therefore, the higher material thickness in PLGA1/BG1 composites is most likely due to the BG content as the degradation of the PLGA component in PLGA1/BG1 composites is not enhanced when compared to PLGA1 scaffolds. The composite structure with BG inhibited the weight loss of PLGA1/BG1 scaffolds, even though the difference in weight loss between PLGA2 and PLGA2/BG2 scaffolds was much more moderate. This could be due to higher BG content in the PLGA1/BG1 compared to PLGA2/BG2 scaffolds (Fig. 11) and higher material thickness of PLGA1/BG1 scaffolds (microCT data, Table 3).

A porous structure and hydrophilic properties are crucial for successful cell seeding in tissue engineering scaffolds. The surface of the scaffold is the first component that comes into contact with the biological fluids. The contact angle of biomaterials is thought to affect the biocompatibility of the scaffolds. A material with contact angle values over 80° is considered hydrophobic [33]. PLGA is generally known to be hydrophobic and BG hydrophilic by nature. Therefore, BG can be thought to improve the wettability characteristics of PLGA scaffolds. However, the contact angles of the studied composite scaffolds were not improved compared to the plain PLGA scaffolds, and actually the plain PLGA1

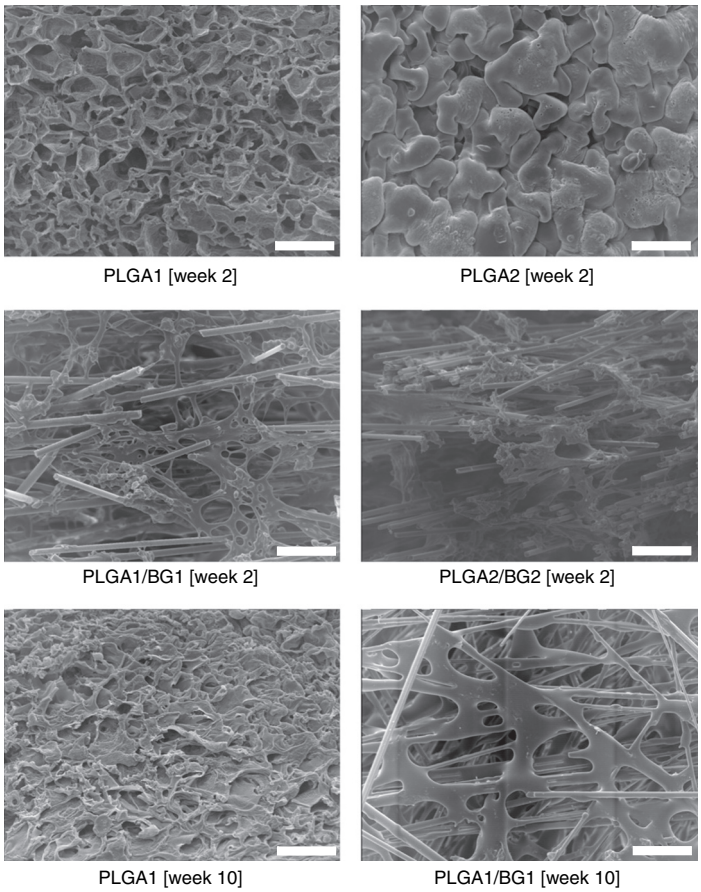

Fig. 5. SEM images of the scaffolds after 2 weeks in hydrolysis and PLGA1 and PLGA1/BG1 scaffolds after 10 weeks in hydrolysis. Scale bars 100 μm.

scaffolds showed improved wettability with significantly lower contact angle values ($p \leq 0.05$) in water, compared to PLGA1/BG1, PLGA2 and PLGA2/BG2. This was most likely due to the structure of the composites, as BG fibres were embedded into the PLGA matrix which covered the BG mesh thoroughly (as also detected from microCT studies). Also, the structure of the freeze-dried scaffolds was highly porous and

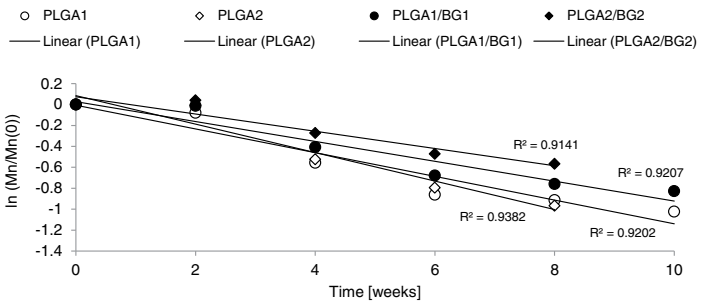

Fig. 6. Fitting the number average molecular weight decrease according to the first order law during ester hydrolysis.

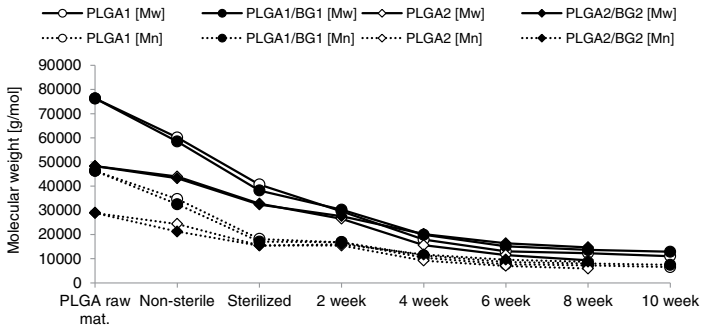

Fig. 7. Molecular weight change of the scaffolds during hydrolysis.

inhomogeneous which could have affected the contact angle results. Furthermore, the parallel contact angle results varied highly, more than 5° between the two measuring points of each droplet (the contact angle measured at right and at left in one droplet), indicating a highly uneven surface structure of the scaffolds. This might have also be the reason why the standard deviation in the contact angle results was high in almost all the results. The BG fibres made the scaffolds even denser (as detected from microCT studies with higher material thickness) which decreased the initial wettability and lead to higher contact angle values as well. Therefore, these results indicate that the scaffolds can be thought as hydrophobic and no improved hydrophilicity of the surface of the composite scaffolds was detected compared to plain PLGA scaffolds. To improve the initial wettability characteristics of the composite scaffolds the BG fibres should not be totally covered by polymer. However, a low contact angle (high wetting of the material surface) does not necessarily signify enhanced biocompatibility, as excessively hydrophobic surfaces enhance cell affinity and reduce biocompatibility, but highly hydrophilic surfaces are found to prevent cell–cell interactions [33].

Even though all studied scaffolds appeared to be equally hydrophobic in the contact angle measurements, the water absorption of the composites was higher than of the plain polymer scaffolds during the first weeks in hydrolysis. This phenomenon has also been reported by Boccaccini et al. [12], who presented that incorporation of BG filler into PLGA increases the capacity to absorb water during the initial incubation period.

The manufacturing method, freeze-drying, and sterilization affected the scaffolds' T_g and M_w values more than the 10-week hydrolysis. The BG in the composite structures stabilized the degradation of the PLGA component as T_g remained stable for PLGA/BG composites after processing and sterilization, and also during the 10 week hydrolysis. The gamma irradiation severely degrades the polymer component of the scaffolds, indicating that the sterilization mechanism should be re-evaluated.

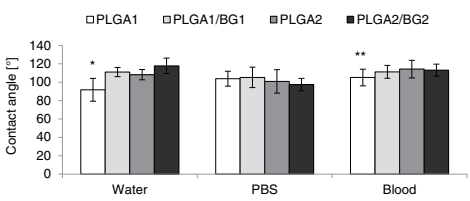

Fig. 8. Contact angle results in water, PBS, and bovine blood for the different dry scaffolds at week 0. *$p \leq 0.05$ with respect to PLGA1/BG1, PLGA2 and PLGA2/BG2. **$p = 0.055$ with respect to PLGA2/BG2.

The difference in BG content between the two different composites was as high as 8.8% as a result of the mesh fabrication procedure, where the amount of BG fibres in different meshes can vary due to heterogeneous mesh structure, which is typical for carded mesh. The larger amount of BG in the PLGA1/BG1 composites (compared to PLGA2/BG2) could explain the higher material thickness in the scaffolds (as stated in the weight change results), and lower pore size compared to plain PLGA1 scaffolds (Table 3). Interestingly, even though the BG content stayed relatively stable in composites during the 10-week hydrolysis, the BG content was shown to slowly increase in PLGA1/BG1 and to slowly decrease in PLGA2/BG2 composites. This indicates that the matrix polymer PLGA1 was degrading at a slightly higher pace and the PLGA2 at a slightly lower pace in the composites compared to the BG filler fibres. This was also shown in the weight change results, where the degradation of the scaffolds was decreasing in the rate of PLGA1 and PLGA2/BG2 > PLGA2 > PLGA1/BG1 between the different scaffolds. The glass fibre diameter is reduced during hydrolysis in composites (as also detected from SEM studies, Figs. 2 and 5). This can be explained by the resorption mechanism of the glass fibres BG1 and BG2, as they have previously been reported to go through surface erosion due to the high surface to volume ratio of these thin fibres [34]. Therefore, it can be assumed that the rate of degradation of PLGA and BG fibres was relatively equal as the amount of polymer and BG content is equal throughout the hydrolysis of 10 weeks.

We are subsequently performing *in vivo* studies with a rabbit model to substantiate the suitability of this kind of PLGA/BG composite scaffold for bone tissue regeneration. The *in vivo* results will be published in a separate forthcoming paper.

5. Conclusions

The manufactured PLGA/BG composites showed superior pore structure and dimensional stability during hydrolysis compared to plain

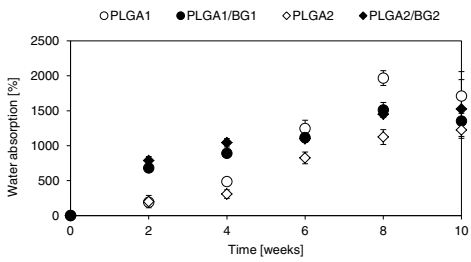

Fig. 9. Water absorption of the scaffolds during hydrolysis.

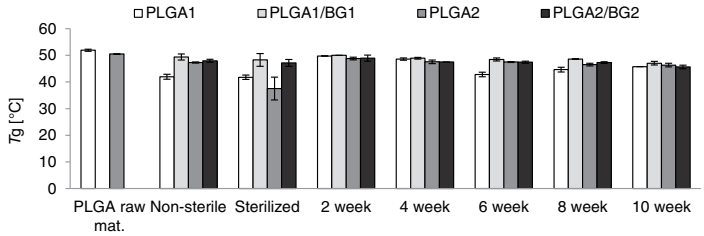

Fig. 10. Glass transition temperatures (T_g) of the scaffolds during hydrolysis (measured from the second heating scan).

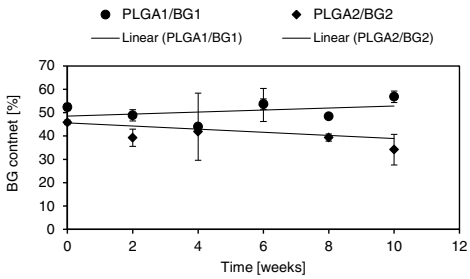

Fig. 11. Bioactive glass content of different scaffolds as function of time (TGA results).

PLGA scaffolds, which is essential for good tissue integration. The plain PLGA scaffolds were found to be unsuitable as tissue engineering scaffolds, as the porous structure of those scaffolds was lost already after the first weeks in hydrolysis. The buffering effect of BG in the composites improved the suitability of the PLGA/BG composites to be used in bone tissue engineering. In addition, the PLGA/BG composites demonstrated high water absorption already at the beginning of the hydrolysis.

Acknowledgments

Timo Lehtonen (Vivoxid Ltd., Finland) is greatly thanked for providing the glass fibres for the study and Prof. Jari Viik (Department of Electronics and Communications Engineering, Tampere University of Technology) for the assistance with the statistical analysis. Thanks are also due to Ms. Inari Lyyra and Ms. Linda Urbanski for their assistance in laboratory work. Funding from the Finnish Funding Agency for Technology and Innovation (TEKES) is greatly acknowledged (Grant no: 3110/31/08).

References

[1] D. Mohamad Yunos, O. Bretcanu, A. Boccaccini, Polymer–bioceramic composites for tissue engineering scaffolds, J. Mater. Sci. 43 (2008) 4433–4442.
[2] B. Stevens, Y. Yang, A. Mohandas, B. Stucker, K.T. Nguyen, A review of materials, fabrication methods, and strategies used to enhance bone regeneration in engineered bone tissues, J. Biomed. Mater. Res. B 85 (2008) 573–582.
[3] V. Karageorgiou, D. Kaplan, Porosity of 3D biomaterial scaffolds and osteogenesis, Biomaterials 26 (2005) 5474–5491.
[4] Q. Fu, E. Saiz, M.N. Rahaman, A.P. Tomsia, Bioactive glass scaffolds for bone tissue engineering: state of the art and future perspectives, Mater. Sci. Eng. C 31 (2011) 1245–1256.
[5] M. Navarro, C. Aparicio, M. Charles-Harris, M.P. Ginebra, E. Engel, J.A. Planell, Development of a biodegradable composite scaffold for bone tissue engineering: physicochemical, topographical, mechanical, degradation, and biological properties, Adv. Polym. Sci. 200 (2006) 209–231.
[6] A.S. Mistry, A.G. Mikos, Tissue engineering strategies for bone regeneration, Adv. Biochem. Eng./Biotechnol. 94 (2005) 1–22.
[7] A.R. Boccaccini, J.J. Blaker, V. Maquet, R.M. Day, R. Jerome, Preparation and characterisation of poly(lactide-co-grycolide) (PLGA) and PLGA/Bioglass® composite tubular foam scaffolds for tissue engineering applications, Mater. Sci. Eng. C 25 (2005) 23–31.
[8] L.S. Nair, C.T. Laurencin, Biodegradable polymers as biomaterials, Prog. Polym. Sci. 32 (2007) 762–798.
[9] B.D. Ulery, L.S. Nair LS, C.T. Laurencin CT, Biomedical applications of biodegradable polymers, J. Polym. Sci. B 49 (2011) 832–864.
[10] Z. Pan, J. Ding, Poly(lactide-co-glycolide) porous scaffolds for tissue engineering and regenerative medicine, Interface Focus 2 (2012) 366–377.
[11] E. Pamula, J. Kokoszka, K. Cholewa-Kowalska, M. Laczka, L. Kantor, L. Niedwiedzki, G.C. Reilly, J. Filipowska, W. Madej, M. Kolodziejczyk, G. Tylko, A.M. Osyczka, Degradation, bioactivity, and osteogenic potential of composites made of PLGA and two different sol–gel bioactive glasses, Ann. Biomed. Eng. 39 (2011) 2114–2129.
[12] A.R. Boccaccini, V. Maquet, Bioresorbable and bioactive polymer/Bioglass® composites with tailored pore structure for tissue engineering applications, Compos. Sci. Technol. 63 (2003) 2417–2429.
[13] G. Ciardelli, P. Gentile, V. Chiono, M. Mattioli-Belmonte, G. Vozzi, N. Barbani, P. Giusti, Enzymatically crosslinked porous composite matrices for bone tissue regeneration, J. Biomed. Mater. Res. A 92 (2010) 137–151.
[14] R.J. Kane, R.K. Roeder, Effects of hydroxyapatite reinforcement on the architecture and mechanical properties of freeze-dried collagen scaffolds, J. Mech. Behav. Biomed. Mater. 7 (2012) 41–49.
[15] G.M. Cunniffe, G.R. Dickson, S. Partap, K.T. Stanton, F.J. O'Brien, Development and characterisation of a collagen nano-hydroxyapatite composite scaffold for bone tissue engineering, J. Mater. Sci. Mater. Med. 21 (2010) 2293–2298.
[16] E.I. Oprita, L. Moldovan, O. Craciunescu, O. Zarnescu, In vitro behaviour of osteoblast cells seeded into a COL/β–TCP composite scaffold, Cent. Eur. J. Biol. 3 (2008) 31–37.
[17] Y. Zhang, M. Zhang, Microstructural and mechanical characterization of chitosan scaffolds reinforced by calcium phosphates, J. Non. Cryst. Solids 282 (2001) 159–164.
[18] J. Zhang, G. Liu, Q. Wu, J. Zuo, Y. Qin, J. Wang, Novel mesoporous hydroxyapatite/chitosan composite for bone repair, J. Bionic Eng. 9 (2012) 243–251.
[19] W.W. Thein-Han, R.D.K. Misra, Biomimetic chitosan–nanohydroxyapatite composite scaffolds for bone tissue engineering, Acta Biomater. 5 (2009) 1182–1197.
[20] V. Maquet, A.R. Boccaccini, L. Pravata, I. Notingher, R. Jerome, Porous poly(α-hydroxyacid)/Bioglass® composite scaffolds for bone tissue engineering. I: preparation and in vitro characterisation, Biomaterials 25 (2004) 4185–4194.
[21] J.A. Roether, J.E. Gough, A.R. Boccaccini, L.L. Hench, V. Maquet, R. Jerome, Novel bioresorbable and bioactive composites based on bioactive glass and polylactide foams for bone tissue engineering, J. Mater. Sci. Mater. Med. 13 (2002) 1207–1214.
[22] T. Miki, K. Masaka, Y. Imai, S. Enomoto, Experience with freeze-dried PGLA/HA/rhBMP-2 as a bone graft substitute, J. Cranio-Maxillofac. Surg. 28 (2000) 294–299.
[23] T.J. Lehtonen, J.U. Tuominen, E. Hiekkanen, Resorbable composites with bioresorbable glass fibers for load-bearing applications. In vitro degradation and degradation mechanism, Acta Biomater. 9 (2013) 4868–4877.
[24] J. Schindelin, I. Arganda-Carreras, E. Frise, V. Kaynig, M. Longair, T. Pietzsch, S. Preibisch, C. Rueden, S. Saalfeld, B. Schmid, J.-Y. Tinevez, D.J. White, V. Hartenstein, K. Eliceiri, P. Tomancak, A. Cardona, Fiji: an open-source platform for biological-image analysis, Nat. Methods 9 (2012) 676–682.
[25] M. Doube, M.M. Klosowski, I. Arganda-Carreras, F.P. Cordelieres, R.P. Dougherty, J.S. Jackson, B. Schmid, J.R. Hutchinson, S.J. Shefelbine, BoneJ: free and extensible bone image analysis in ImageJ, Bone 47 (2010) 1076–1079.
[26] S.S. Shah, Y. Cha, C.G. Pitt, Poly (glycolic acid-co-dl-lactic acid): diffusion or degradation controlled drug delivery? J. Control. Release 18 (1992) 261–270.
[27] ISO 15814, Implants for Surgery — Copolymers and Blends Based on Polylactide — In Vitro Degradation Testing, 1999.
[28] G.G. Pitt, M.M. Gratzl, G.L. Kimmel, J. Suries, A. Schindler, Aliphatic polyesters II. The degradation of poly (DL-lactide), poly (e-caprolactone), and their copolymers in vivo, Biomaterials 2 (1981) 215–220.
[29] C. Liu, Z. Xia, J.T. Czernuszka, Design and development of three-dimensional scaffolds for tissue engineering, Chem. Eng. Res. Des. 85 (2007) 1051–1064.
[30] F. Yang, W. Cui, Z. Xiong, L. Liu, J. Bei, S. Wang, Poly(l, l-lactide-co-glycolide)/tricalcium phosphate composite scaffold and its various changes during degradation in vitro, Polym. Degrad. Stab. 91 (2006) 3065–3073.
[31] E. Orava, J. Korventausta, M. Rosenberg, M. Jokinen, A. Rosling, In vitro degradation of porous poly(dl-lactide-co-glycolide) (PLGA)/bioactive glass composite foams with a polar structure, Polym. Degrad. Stab. 92 (2007) 14–23.

[32] L. Wu, J. Ding, Effects of porosity and pore size on in vitro degradation of three-dimensional porous poly(D, L-lactide-co-glycolide) scaffolds for tissue engineering, J. Biomed. Mater. Res. A 75 (2005) 767–777.
[33] K.L. Menzies, L. Jones, The impact of contact angle on the biocompatibility of biomaterials, Optom. Vis. Sci. 87 (2010) 387–399.
[34] T.J. Lehtonen, J.U. Tuominen, E. Hiekkanen, Dissolution behavior of high strength bioresorbable glass fibers manufactured by continuous fiber drawing, J. Mech. Behav. Biomed. Mater. 20 (2013) 376–386.

Anne-Marie Haaparanta (Dr. Tech.) is a postdoctoral researcher at Tampere University of Technology, Tampere, Finland. She is working in Biomaterials and Tissue Engineering group lead by professor Minna Kellomäki. Her research is focused on processing and characterization of natural and synthetic polymer-based composite scaffolds for tissue engineering. Main focus of her research is on cartilage, bone and osteochondral tissue engineering scaffolds.

Peter Uppstu (M.Sc. Tech) is a doctoral student at the Laboratory of Polymer Technology at Åbo Akademi University, Turku, Finland. In his doctoral thesis he combines biodegradable polymers with bioactive glasses to create mechanically strong composite scaffolds for bone regeneration.

Markus Hannula received his M.Sc. degree from the Department of Electrical Engineering, Tampere University of Technology (TUT), Finland in year 2004. He studied Biomedical Informatics during his M.Sc. and published his thesis about comparison of deformable models on medical image segmentation. Currently he is working in the Department of Electronics and Communications Engineering, TUT as a researcher. His main expertise is on μCT imaging and image analysis.

Ville Ellä (Dr. Tech.) is currently a Principal Investigator in Arctic Biomaterials OY. He worked for 15 years in Tampere University of Technology in the area of biomaterials and tissue engineering. His background is strong in the processing of bioresorbable medical polymers and composites to help and understand how to design preforms and implants for the future. Dr. Ellä has also long experience in teaching at the University level.

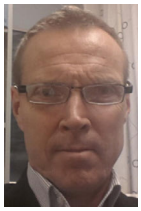

Ari Rosling is assistant professor at the Polymer Technology Department at Åbo Akademi University.
He obtained PhD in organic chemistry synthesis, then switched research focus towards biodegradable composites for biomedical and ecological applications. Main focus lies on synthesis and modification of aliphatic polyesters and polysaccharides for composite preparation with bioactive ceramics or natural fibres as reinforcement. In tissue engineering, material's bulk and surface properties and their influence on *e.g.* promotion of cell attachment to macroporous polymeric surfaces are of interest. Furthermore, dissolution and release rates of bioactive components are studied in together with the overall degradation rate of implant structures.

Dr. Tech. **Minna Kellomäki** is professor of Biomaterials and Tissue Engineering at Tampere University of Technology, Tampere, Finland. Her research interests are in biodegradable polymers and composites, both of natural and synthetic origin. The group is specialized in processing and characterization of the materials and devices developed. She has published appr. 160 original research articles and has h-index 21. She is actively involved in developing academic teaching in the areas representing.
(Picture taken by Petri Laitinen)

Salonius E, Muhonen V, Lehto K, Järvinen E, Pyhältö T, Hannula M, Aula AS, Uppstu P, Haaparanta AM, Rosling A, Kellomäki M, Kiviranta I. Gas-foamed poly(lactide-co-glycolide) and poly(lactide-co-glycolide) with bioactive glass fibres demonstrate insufficient bone repair in lapine osteochondral defects. Journal of Tissue Engineering and Regenerative Medicine. 2019;13(3):406–15.

III

Received: 5 July 2017 | Revised: 10 October 2018 | Accepted: 17 December 2018
DOI: 10.1002/term.2801

RESEARCH ARTICLE

WILEY

Gas-foamed poly(lactide-co-glycolide) and poly(lactide-co-glycolide) with bioactive glass fibres demonstrate insufficient bone repair in lapine osteochondral defects

Eve Salonius[1] | Virpi Muhonen[1] | Kalle Lehto[2] | Elina Järvinen[1] | Tuomo Pyhältö[3] | Markus Hannula[2] | Antti S. Aula[2,4] | Peter Uppstu[5] | Anne-Marie Haaparanta[2] | Ari Rosling[5] | Minna Kellomäki[2] | Ilkka Kiviranta[1,3]

[1] Department of Orthopaedics and Traumatology, Clinicum, Faculty of Medicine, University of Helsinki, Helsinki, Finland

[2] Department of Electronics and Communications Engineering, Tampere University of Technology, BioMediTech, Institute of Biosciences and Medical Technology, Tampere, Finland

[3] Department of Orthopaedics and Traumatology, Helsinki University Hospital, Helsinki, Finland

[4] Department of Medical Physics, Imaging Centre, Tampere University Hospital, Tampere, Finland

[5] Laboratory of Polymer Technology, Centre of Excellence in Functional Materials at Biological Interfaces, Åbo Akademi University, Turku, Finland

Correspondence
Ilkka Kiviranta, Department of Orthopaedics and Traumatology, Institute of Clinical Medicine, University of Helsinki, Haartmaninkatu 8, 00290, Helsinki, Finland.
Email: ilkka.kiviranta@helsinki.fi

Funding information
Tekes, Grant/Award Number: 3110/31/08

Abstract

Deep osteochondral defects may leave voids in the subchondral bone, increasing the risk of joint structure collapse. To ensure a stable foundation for the cartilage repair, bone grafts can be used for filling these defects. Poly(lactide-co-glycolide) (PLGA) is a biodegradable material that improves bone healing and supports bone matrix deposition. We compared the reparative capacity of two investigative macroporous PLGA-based biomaterials with two commercially available bone graft substitutes in the bony part of an intra-articular bone defect created in the lapine femur. New Zealand white rabbits (n = 40) were randomized into five groups. The defects, 4 mm in diameter and 8 mm deep, were filled with neat PLGA; a composite material combining PLGA and bioactive glass fibres (PLGA–BGf); commercial beta-tricalcium phosphate (β-TCP) granules; or commercial bioactive glass (BG) granules. The fifth group was left untreated for spontaneous repair. After three months, the repair tissue was evaluated with X-ray microtomography and histology. Relative values comparing the operated knee with its contralateral control were calculated. The relative bone volume fraction ($\Delta BV/TV$) was largest in the β-TCP group ($p \leq 0.012$), which also showed the most abundant osteoid. BG resulted in improved bone formation, whereas defects in the PLGA–BGf group were filled with fibrous tissue. Repair with PLGA did not differ from spontaneous repair. The PLGA, PLGA–BGf, and spontaneous groups showed thicker and sparser trabeculae than the commercial controls. We conclude that bone repair with β-TCP and BG granules was satisfactory, whereas the investigational PLGA-based materials were only as good as or worse than spontaneous repair.

KEYWORDS

animal model, biomaterial, bone repair, intra-articular, poly(lactide-co-glycolide)

1 | INTRODUCTION

Joint trauma may lead to deep osteochondral defects with severe subchondral bone loss (van Dijk, Reilingh, Zengerink, & van Bergen, 2010). The impairment of joint biomechanics and tissue metabolism leads to dysfunction of the joint and increases the risk of posttraumatic osteoarthritis and collapse of the joint structure (McKinley, Borrelli, D'Lima, Furman, & Giannoudis, 2010). These can lead to pain, swelling, and restricted movement of the joint (Jackson, Lalor, Aberman, & Simon, 2001).

Due to the poor intrinsic repair capacity of cartilage and osteoarthritis as the potential consequence of cartilage lesions, various

treatment options have been developed to preserve joints after damage (Huey, Hu, & Athanasiou, 2012). The current surgical methods to treat osteochondral defects include autologous osteochondral transfer, fresh osteochondral allografts, autologous chondrocyte implantation, and arthroplasty (Seo, Mahapatra, Singh, Knowles, & Kim, 2014). The choice of a treatment option depends on the size, depth, and location of the lesion as well as the age and previous treatments of the patient.

In intra-articular bone fractures and deep osteochondral defects, both the articular cartilage and the underlying bone should be taken into consideration when choosing the treatment method (Mano & Reis, 2007). Large bone voids should be filled with bone grafts to provide the healing defect site with sufficient structural support, which is a prerequisite for a successful cartilage repair. Autografts are the gold standard of bone grafting. Due to the limited availability, donor site morbidity, pain, and risk of infection and nerve injury (Arrington, Smith, Chambers, Bucknell, & Davino, 1996), allografts harvested from a cadaver have been used as an alternative source. However, allografts are associated with the risk of immune reaction and disease transmission. Tissue-engineered substitutes have been developed to overcome these limitations (Oryan, Alidadi, Moshiri, & Maffulli, 2014).

An advantageous bone filler that could be used together with a cartilage reparative construct remains to be developed. An optimal bone filler in a deep osteochondral defect would provide the tissue with mechanical support, be able to function as a carrier for reparative cells, degrade gradually as neotissue forms, and enable cartilage reparation (Oryan et al., 2014).

Several biomaterials have been studied for bone applications. Bioceramics, calcium phosphates, such as osteoconductive beta-tricalcium phosphate (β-TCP), have been used in clinical practice for over 20 years (Ghazal, Prein, & Müller, 1992; Stahl & Froum, 1986). β-TCP resorbs by osteoclastic activity and is replaced by new bone *in vivo* (Eggli, Muller, & Schenk, 1988). Friability and a limited osteogenic effect are the main problems encountered with β-TCP (Liu & Lun, 2012). Bioactive glasses (BGs) are silica-based materials that promote bone formation and have been in clinical use since the 1980s (Brauer, 2015; Keranen et al., 2011). Some BGs have shown antibacterial properties, thus mitigating the risk of surgical infections (Lindfors et al., 2010). BGs, like β-TCP, are brittle, and thus their mechanical properties are limited (Jones, 2013).

Bioabsorbable polymers have been actively studied as bone filler materials. Aliphatic polyesters of alpha-hydroxy acids are the most commonly used, and poly(lactide-co-glycolide) (PLGA) is often favoured in regenerative medicine due to its biocompatibility, relatively rapid and controllable degradation, and existing approval for clinical use by the U.S. Food and Drug Administration (Gentile, Chiono, Carmagnola, & Hatton, 2014,Serino, Rao, Iezzi, & Piattelli, 2008). Three-dimensional scaffolds made of PLGA have been shown to support cell attachment and bone matrix deposition on the scaffold surface and to promote bone healing compared with spontaneous repair (Karp, Shoichet, & Davies, 2003; Kleinschmidt, Marden, Kent, Quigley, & Hollinger, 1993). The acidic by-products that form during the degradation process as well as poor mechanical strength are the main limitations of synthetic polymers (Garcia-Gareta, Coathup, & Blunn, 2015).

Results of the use of porous PLGA scaffolds in the repair of bone defects have been promising (Pan et al., 2015). In our preliminary study in rats (unpublished), there was an island-like bone formation inside the implanted PLGA in the absence of inflammatory cells. Thus, we hypothesized that a porous plug-like PLGA rod could meet the requirements for a bone filler in osteochondral defects. We produced a cylindrical scaffold by gas foaming (CO_2) PLGA to be tested *in vivo* in a rabbit model.

Although polymer scaffolds are biocompatible, they lack sufficient bioactivity (Zeimaran et al., 2015). As BG has shown osteoconductive properties (Gunn, Rekola, Hirvonen, & Aho, 2013), we hypothesized that combining PLGA with bioactive glass fibres (BGf) would enhance the regenerative capacity of the biomaterial. Therefore, we also produced a rod-formed composite material combining PLGA with BGf in a freeze-drying process.

The purpose of this study was to evaluate the potential of two investigational PLGA-based biomaterials against two commercial biomaterials, and lesions left without treatment, in the repair of the bony part of deep osteochondral defects in a rabbit model.

2 | MATERIALS AND METHODS

A total of 40 female New Zealand white rabbits were obtained from a commercial supplier (Harlan Laboratories B.V., Venray, the Netherlands). The animals were 18 weeks old. They were housed in individual cages, acclimatized for 1 week before the operations, and their wellbeing was observed daily. The study was authorized by the Finnish National Animal Experiment Board (ESAVI/3785/04.10.03/2011) and conducted according to the ethical guidelines and regulations of the Finnish Act on Animal Experimentation (62/2006). The rabbits were randomized into five groups (n = 8 in each group). Four groups received PLGA, PLGA–BGf, commercial BG, or commercial β-TCP as a bone substitute material (Figure 1a). The fifth group was an untreated control group (spontaneous), which did not receive any bone substitute material.

2.1 | Preparation of the biomaterials

PLGA polymers were produced at Åbo Akademi University. Medical grade monomers of D-lactide and glycolide were acquired from Corbion (Corbion Purac, Gorinchem, the Netherlands) and L-lactide from Futerro (Escanaffles, Spain). The PLGA was polymerized in an argon atmosphere by ring-opening polymerization with 0.1mol-% stannous octoate as initiator and a molecular weight determining amount of 1-decanol as coinitiator. After polymerization, the polymer was purified by dissolution in dichloromethane and precipitation in ethanol. The PLGA had a lactide to glycolide ratio of 7:3 with equal amounts of D- and L-lactide and a weight average molecular weight of 48 000 g/mol.

PLGA scaffolds were produced at Åbo Akademi University with the gas foaming method. PLGA was first extruded into approximately 2.8 mm thick rods, which were cut to 16-mm long pieces. The PLGA pieces were then placed in custom-made Teflon molds with an inner diameter of 4.0 mm. The molds were placed in a chamber with a

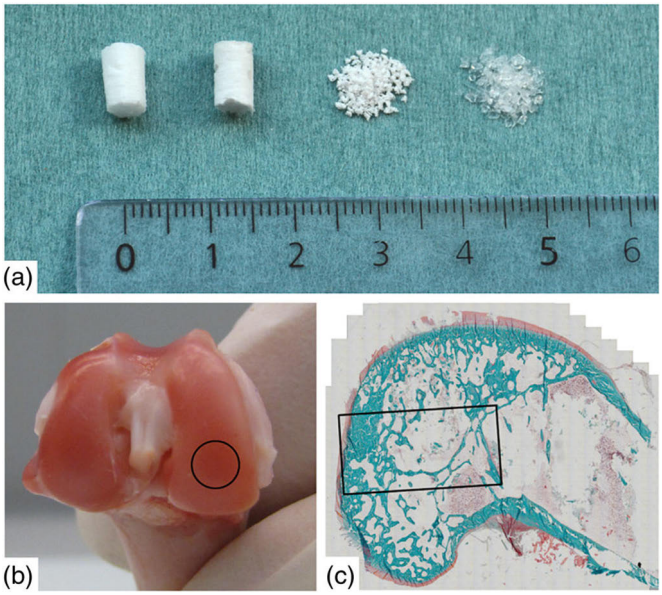

FIGURE 1 (a) A photograph of all the investigated bone substitutes from left to right: poly(lactide-co-glycolide) (PLGA), poly(lactide-co-glycolide)–bioactive glass fibres (PLGA–BGf), beta-tricalcium phosphate (β-TCP), and bioactive glass (BG). The site of the defect in the medial condyle of the femur (b) and its depth into the bone tissue (c) are indicated with a black line [Colour figure can be viewed at wileyonlinelibrary.com]

carbon dioxide pressure of 55 bar for 10 hr, then the pressure was released rapidly in 5 s. The rods were to some extent soft with a porosity of over 90%, which consisted of mainly closed pores. Scaffolds with the length of 8 mm and a mass of 24–27 mg were then cut from the foamed rods and sterilized with gamma irradiation with a dose of 25 kGy.

The PLGA–BGf composites were produced at Tampere University of Technology. Bioresorbable melt-derived glass fibres (Vivoxid Ltd., Turku, Finland), denoted as BGf, were composed of 68.6 SiO_2, 12.5 Na_2O, 9.3 CaO, 7.2 MgO, 1.8 B_2O_3, and 0.6 P_2O_5 (in mol-%). The average fibre diameter was 13 μm. The BGf was cut into staple fibres of approximately 10 cm in length and carded into mesh. The above described PLGA was dissolved in 1,4-dioxane as 3 wt-% solution. The 3 wt-% PLGA solution was immersed into BGf carded mesh, and the samples were frozen to −30°C for 24 hr prior to 24-hr freeze-drying. The freeze-dried PLGA–BGf composites were afterwards cut with a puncher into samples with diameter of 4 mm, and five parallel samples were placed on top of each other and glued together with 3 wt-% PLGA solution and freeze-dried again as described earlier. The height of the final sample was 8 mm, with a porosity of 96% (Haaparanta et al., 2015). The samples were held under vacuum at room temperature for a minimum of 48 hr and gamma sterilized at 25 kGy.

PLGA and PLGA–BGf were compared with two commercial bone substitutes, BG granules (BonAlive®, BonAlive Biomaterials Ltd, Turku, Finland) and β-TCP granules (Synthes® chronOS, Synthes GmbH, Oberdorf, Switzerland), and with spontaneous repair. BonAlive® granules are BG granules consisting of 53 SiO_2, 23 Na_2O, 20 CaO, and 4 P_2O_5 (in wt-%). The BG granules had a diameter of 0.5–0.8 mm. Synthes® chronOS granules are composed of β-TCP. The sizes of these granules were 0.5–0.7 mm, and the porosity of the material was 60%.

2.2 | Surgical procedure

The rabbits were operated under general anaesthesia induced with 0.5 mg/kg (sc) medetomidine and 25 mg/kg (sc) ketamine. Preoperative analgesia of 0.05 mg/kg (sc) of buprenorphine and 4 mg/kg (sc) of carprofen was administered. All the animals received 40 mg/kg (im) of cefuroxime preoperatively.

The animals were set on a supine position on the operating table. A medial parapatellar arthrotomy was made to the right hind leg. The patella was dislocated laterally, and the femoral condyles were exposed. A single lesion through the articular cartilage of the medial condyle was made with a hand-operated drill. The lesion covered almost the width of the femoral condyle, and the bony defect comprised a notable volume of the entire condyle with a diameter of 4 mm and a depth of 8 mm (as depicted in Figure 1b,c). The defect extended into the bone marrow space. The lesions were filled with the studied biomaterial or left empty for spontaneous repair. The granular materials BG and β-TCP were mixed with sterile water to create a paste-like composition prior to implantation. The PLGA and PLGA–BGf samples were semirigid plugs, which were press-fitted into the lesion (Figure 1a). The incisions were closed in layers. After the operation, 1 mg/kg (sc) of antipamexole was administered for reversal of the sedative effects of medetomidine.

The animals were allowed free weight-bearing and unrestricted movement after the operation. Antibiotic prophylaxis of 40 mg/kg (sc) of cefuroxime was continued three times a day for 3 days and postoperative analgesia of 0.01 mg/kg (sc) of buprenorphine and 4 mg/kg (sc) of carprofen for 4 days.

The follow-up time for each group was 12 weeks, whereafter the animals were anaesthetized as described above and euthanized with an overdose of pentobarbital (60 mg/kg, iv). The operated and nonoperated contralateral knees were photographed, evaluated for

gross macroscopic appearance, detached, and stored in 10% buffered formalin at +4°C for further processing.

2.3 | X-ray microtomography

Quantitative analyses of the operated femoral condyles were carried out with X-ray microtomography (μCT) imaging. Bone growth into the lesion and the subchondral bone morphology of the operated and nonoperated contralateral knees were analysed with Zeiss Xradia MicroXCT-400 (Zeiss, Pleasanton, CA, USA). The samples were transferred to the temperature of the μCT device (+29°C) for 30 min before the imaging to stabilize the set-up. The μCT imaging parameters were 100 kV source voltage (no filtering), 100 μA current, 0.4× macro objective, 2 binning, 800 projections, 360° projection angle, and 2.5 s exposure time. The cross-sectional image stacks were reconstructed using Zeiss Xradia XMReconstructor software (version 8.1, Zeiss), resulting in a 22.6-μm isotropic voxel size. The images were postprocessed and visualized using Avizo Fire 8.1 (FEI Visualization Sciences Group, Hillsboro, OR, USA) software. A cylindrical volume of interest (VOI) with a diameter of 5 mm and a depth of 8 mm was extracted. Subsequently, the VOI was denoised with the non-local means (NLM) filter (Buades, Coll, & Morel, 2005). The bone tissue and the implanted biomaterials were segmented by global thresholding. Manual correction was used to reduce segmentation over/under flow.

Quantitative analysis was performed using BoneJ plug-in (Doube et al., 2010) in Fiji (Schindelin et al., 2012) software. The analysed parameters were bone volume fraction (*BV/TV*), trabecular thickness (*Tb.Th*), trabecular spacing (*Tb.Sp*), and trabecular number (*Tb.N*).

2.4 | Histological analysis

The femurs were carefully split into two using a jig saw. Undecalcified samples were dehydrated in ethanol, cleared with xylene immersions, and subsequently embedded in methyl methacrylate. The hardened tissue blocks were cut into 5- to 10-μm thick sections with a Leica SM 2500 hard tissue slide microtome. The sections were stained with Masson–Goldner trichrome stain and mounted with permanent mounting medium. The sections were imaged with a Zeiss AxioImager Z1 microscope system equipped with an AxioCam MRc5 camera and Zen blue edition software (Carl Zeiss Microscopy GmbH, Göttingen, Germany) to acquire mosaic images of the entire histological sections.

For histomorphometry, the Masson–Goldner trichrome stained sections were imaged with an Olympus BX-60 microscope with an integrated Scion colour digital camera. ImageJ software was used for measurements, and scaling was performed with UKAS calibrated auxiliary object glass with a 1-mm scale. Semi-automatic image analysis with ImageJ was used for measuring the total surface area and the trabecular area of the defect. The qualitative assessment of the amount of osteoid and lymphocytes was carried out with the naked eye. Due to the low quantity of osteoid in the samples, quantitative assessment of the amount of osteoid could not be made.

2.5 | Statistical analyses

Relative μCT values, where each parameter for operated knees was compared with the corresponding nonoperated controls, were calculated and used to compare the groups with each other. Statistical analyses were carried out using the permutation analysis of variance test with Holm adjustment. The *p*-values under 0.05 were considered statistically significant.

3 | RESULTS

3.1 | Animal experiment

Three animals (one each from groups PLGA, β-TCP, and spontaneous) died during the induction of anaesthesia, probably due to respiratory arrest caused by the combination of ketamine and medetomidine (Calasans-Maia, Monteiro, Ascoli, & Granjeiro, 2009). Consequently, these three animals were not included in the analyses. Otherwise, the operations were carried out without complications, and all the animals recovered well.

3.2 | Macroscopic appearance

There were no signs of synovitis in the operated joints. All groups showed macroscopic lesion filling up to the joint surface (Figure 2). Repair tissue hypertrophy over the level of the surrounding cartilage was detected in two of eight samples in PLGA–BGf group, in one of six samples in PLGA group, and in one of eight samples in BG group. No overgrowth was detected in the spontaneously healed or in β-TCP-augmented groups. The surface of the neotissue in the defect areas in each group was uneven and differed by colour from healthy cartilage, but no deep tissue deficiencies were detected in the adjacent cartilage.

3.3 | Bone repair

Unresolved β-TCP and BG were still seen in μCT imaging. The bone and biomaterial could both be distinguished from the μCT images in all the test groups. The relative bone volume fraction between the operated and nonoperated knees ($\Delta BV/TV$) was greatly increased in the β-TCP group, where it was higher than in the other groups ($p \leq 0.012$, Figure 3a, Table 1, Table S1). The relative trabecular thickness ($\Delta Tb.Th$) was higher in groups PLGA, PLGA–BGf, and spontaneous than in the commercial controls β-TCP and BG ($p \leq 0.035$; Figure 3b). All groups differed from each other ($p \leq 0.048$) in relative trabecular spacing ($\Delta Tb.Sp$) with the exception of PLGA and spontaneous groups, which did not show a statistical difference from one another (Figure 3c). The trabeculae were sparsest in the PLGA–BGf group ($p \leq 0.014$).

The trabecular number (*Tb.N*) was close to the contralateral control in the β-TCP and BG groups (Figure 3d). These commercial groups did not differ from one another, but compared with the other groups, their relative trabecular number ($\Delta Tb.N$) was significantly higher ($p \leq 0.013$).

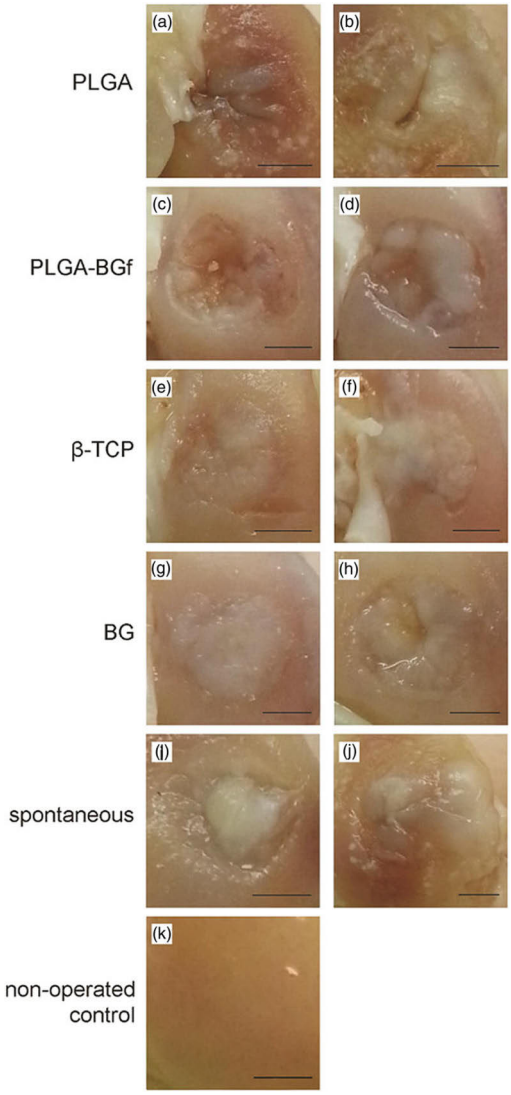

FIGURE 2 Photographs of two representative samples in each group, showing the macroscopic appearance of the cartilage surface where the drill hole was created. The groups are as follows: (a,b) poly(lactide-co-glycolide) (PLGA), (c,d) poly(lactide-co-glycolide)–bioactive glass fibres (PLGA–BGf), (e,f) beta-tricalcium phosphate (β-TCP), (g,h) bioactive glass (BG), (i,j) spontaneous, and (k) a nonoperated contralateral control. Scale bars: 2 mm (a–j) and 5 mm (k) [Colour figure can be viewed at wileyonlinelibrary.com]

Table 1 summarizes the results of the μCT imaging in each group in both the operated knees and the nonoperated contralateral control knees of the same animals. All statistically significant differences in $\Delta BV/TV$, $\Delta Tb.Th$, $\Delta Tb.Sp$, and $\Delta Tb.N$ are presented in Table S1.

3.4 | Repair tissue structure

The filling of the bony lesions seemed to migrate from the edges towards the middle of the defect. Histological assessment of the samples showed that the areas that appear empty in μCT images consist of connective tissue and bone marrow (Figure 4a,b).

In the PLGA and spontaneous groups, the defects were filled partly with fibrous tissue and partly with mineralized bone surrounded by scarce strands of osteoid (Figure 4a,b). The upper halves of the defects were well repaired, but the bone structure in the lower halves was sparse.

In the PLGA–BGf group, the bone defects were filled with fibrous tissue (Figure 4a,b). The perimeter of the defect site featured newly mineralized bone, but the surgically created defect itself showed no bone tissue formation.

Osteoid was seen in most of the samples, where it was located directly beneath the surface. Only one specimen in the spontaneously healed group and one in the PLGA–BGf group had no osteoid (Table 2). Osteoid was most abundant in the β-TCP group, where it encircled numerous small islands of mineralized bone (Figure 4d). Both commercial controls showed comprehensive lesion filling with tissue where mineralized bone and osteoid alternated with cell-rich fibrous tissue. Although the bone defect filling was satisfactory, there was a connective tissue-filled depression near the surface in β-TCP and BG groups (Figure 4a,b).

There was a low number of lymphocytes and macrophages in the histological sections (Table 2). Most inflammatory cells were seen in the PLGA group, where three of seven specimens showed 50–100 inflammatory cells on the slide, and in the PLGA–BGf group, where two of eight specimens showed 50–100 inflammatory cells. No other group showed an increase in the number of lymphocytes or macrophages.

4 | DISCUSSION

In this study, the use of bone defect fillers in intra-articular lesions was evaluated in a rabbit model. Our goal was to find out whether these fillers can be used in repairing the bony part of deep osteochondral defects. As PLGA-based scaffolds have been reported to produce favourable results when used to repair bone defects (Pan et al., 2015; Penk et al., 2013), we hypothesized that creating a rod-like PLGA-based bone filler would enhance the repair of the deep bony part of osteochondral defects and that combining BG with PLGA would further improve the scaffold.

We thought that the PLGA-based semi-rigid bone substitutes might have had additional advantage, as they could be constructed into a two-layer scaffold shaped to match the contours of the joint, with bone substituting material in the deeper part and regenerative cells for cartilage repair in the joint surface. This kind of a scaffold could be used as a bioprosthesis to fill the entire osteochondral defect.

Although the gas-foamed PLGA showed high porosity, the pores were collapsed (Uppstu, Paakki, & Rosling, 2015). As high porosity is needed for bone growth into the scaffold (Zeimaran et al., 2015), this might provide an explanation for the results that were worse than

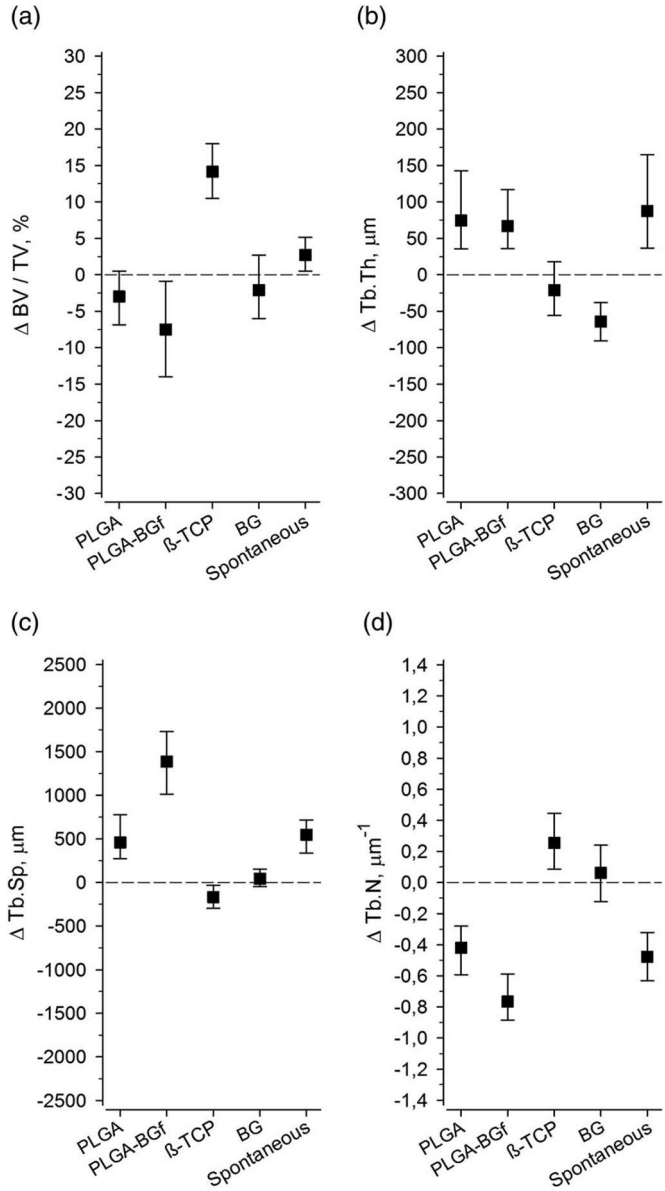

FIGURE 3 Quantitative results of X-ray microtomography showing the difference between the operated and the nonoperated contralateral knees in (a) bone volume fraction (Δ*BV/TV*, %), (b) trabecular thickness (Δ*Tb.Th*, µm), (c) trabecular spacing (Δ*Tb.Sp*, µm), (d) and trabecular number (Δ*Tb.N*, μm^{-1}) in each study group. The black square represents the average value of the operated knees, and the dash line represents the nonoperated knees. The whiskers represent 95% confidence intervals

expected. However, the use of gas-foamed PLGA produced repair tissue that did not differ from spontaneous healing, indicating that although it did not have a major overall impact on the healing process, the repair was not hampered by the material.

BG alone has been shown to work well in bone repair (Lindfors, Heikkila, Koski, Mattila, & Aho, 2009) and to promote bone formation in combination with polymers in vitro (Lu, El-Amin, Scott, & Laurencin, 2003). In the present study, BG alone resulted in adequate bone formation, but combining PLGA with BGf deteriorated the repair process. PLGA–BGf had initially small pores and compact structure with very little space for tissue ingrowth (Haaparanta et al., 2015). The BGfs were densely embedded in the PLGA, which probably impaired the interaction of BGf with the surrounding bone. As the composite material has a longer degradation time than the PLGA alone, it might lead to better structural support in load-bearing applications (Gentile et al., 2014) but delay the lesion repair (Haaparanta et al., 2015). We believe these factors explain why the bone defects treated with the PLGA–BGf composite scaffold were only filled with connective tissue and why the bone structure remained nearly unchanged throughout the 3-month long study period.

TABLE 1 Results of the X-ray microtomography imaging in each group in both the operated knees and the nonoperated contralateral control knees of the same animals

Operated	PLGA Mean ± SE *n* = 7	PLGA–BGf Mean ± SE *n* = 8	β-TCP Mean ± SE *n* = 7	BG Mean ± SE *n* = 8	Spontaneous Mean ± SE *n* = 7
BV/TV, %	33.6 ± 1.4	25.1 ± 3.6	46.0 ± 1.3	30.5 ± 1.7	37.1 ± 1.6
Tb.Th (μm)	354 ± 19	295 ± 18	225 ± 10	161 ± 9	364 ± 30
Tb.Sp (μm)	1050 ± 121	1984 ± 178	529 ± 26	632 ± 49	1144 ± 96
Tb.N (μm^{-1})	0.74 ± 0.05	0.46 ± 0.04	1.33 ± 0.04	1.30 ± 0.08	0.68 ± 0.05
Nonoperated	**PLGA Mean ± SE *n* = 7**	**PLGA–BGf Mean ± SE *n* = 8**	**β-TCP Mean ± SE *n* = 7**	**BG Mean ± SE *n* = 8**	**Spontaneous Mean ± SE *n* = 7**
BV/TV (%)	36.6 ± 0.8	32.6 ± 0.9	31.9 ± 1.5	32.6 ± 1.3	34.4 ± 2.0
Tb.Th (μm)	280 ± 10	228 ± 9	246 ± 12	226 ± 8	277 ± 19
Tb.Sp (μm)	589 ± 22	597 ± 27	695 ± 45	587 ± 19	595.0 ± 36.0
Tb.N (μm^{-1})	1.16 ± 0.04	1.22 ± 0.05	1.08 ± 0.05	1.24 ± 0.03	1.16 ± 0.05

Note. β-TCP: beta-tricalcium phosphate; BG: bioactive glass; *BV/TV*: bone volume fraction of the total tissue volume; PLGA: poly(lactide-co-glycolide); PLGA–BGf: poly(lactide-co-glycolide)–bioactive glass fibres; *Tb.N*, trabecular number; *Tb.Sp*, trabecular spacing; *Tb.Th*, trabecular thickness. The values are presented as mean ± standard error (SE).

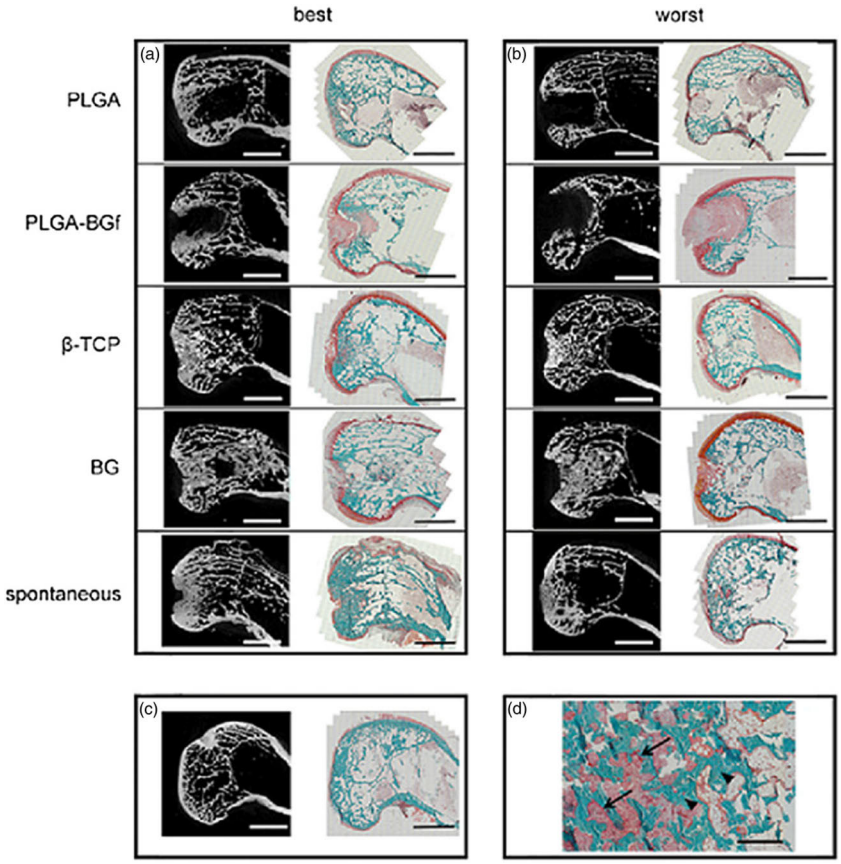

FIGURE 4 An X-ray microtomography (μCT) image and a Masson–Goldner trichrome-stained histological section of (a) the best and (b) the worst sample in each group, chosen according to the data obtained from the μCT imaging, as well as a nonoperated contralateral control (c). The close-up image of the best beta-tricalcium phosphate (β-TCP) section (d) shows the abundance of osteoid (arrow) in the perimeter of the mineralized bone (arrowhead). Scale bars: (a–c): 4 mm, (d) 500 μm [Colour figure can be viewed at wileyonlinelibrary.com]

TABLE 2 Number of animals (*n*) in each study group that presented with abundant, moderate, little, or no osteoid or 0–50, 50–100, and over 500 inflammatory cells in qualitative assessment of histology. None of the samples were classified to have abundant amounts of osteoid. Most inflammatory cells were seen in the PLGA and PLGA–BGf groups

		Osteoid (*n*)				Inflammatory cells (*n*)		
		Abundant	Moderate	Little	No osteoid	0–50	50–100	>500
Group	PLGA (*n* = 7)	0	2	5	0	4	3	0
	PLGA–BGf (*n* = 8)	0	0	7	1	6	2	0
	β–TCP (*n* = 7)	0	3	4	0	7	0	0
	BG (*n* = 8)	0	1	7	0	7	0	0
	spontaneous (*n* = 7)	0	1	5	1	7	0	0

Note. β-TCP: beta-tricalcium phosphate; BG: bioactive glass; PLGA: poly(lactide-co-glycolide); PLGA–BGf: poly(lactide-co-glycolide)–bioactive glass fibres. The values are presented as mean ± standard error (SE).

Degradation of PLGA occurs through hydrolysis, which produces lactic acid and glycolic acid, possibly lowering the pH of its surroundings (Gentile et al., 2014; Haaparanta et al., 2015). The inflammatory reaction and autocatalytic process caused by the acidic environment have been reported to promote bone reparative process (Mountziaris & Mikos, 2008; Zeimaran et al., 2015), although contradicting results have also been presented (Han et al., 2009,Shibutani & Heersche, 1993). In the present study, a slight increase in inflammatory cells was seen in the PLGA and PLGA–BGf-treated specimens but not in the spontaneously healed group or in the groups treated with the granular biomaterials. However, the minor inflammatory reaction seen in the PLGA-based treatment groups did not lead to enhanced bone repair.

In this study, the β-TCP group showed most osteoid, numerous thin trabeculae, and extensive bone formation at 12 weeks. In a previous study in sheep (Mayr et al., 2015), β-TCP resorption and bone formation continued for a long time, with only 12% of the biomaterial being resorbed after 24 weeks. In the present study in rabbits, the 12-week follow-up period shows bone repair in its early phase. It is probable that with time, the bone would have been exposed to remodelling to normalize the trabecular structure.

The bone volume fraction in the operated knees was close to that of the nonoperated controls in the spontaneously healed group. However, the trabeculae were thick and sparse in the spontaneously healed knees, unlike in the groups treated with the commercial granular bone substitutes β-TCP and BG, thus demonstrating a worse healing response than with the granular bone fillers. BG alone showed bone trabecular parameters that were closest to those of the nonoperated contralateral legs, indicating desirable overall repair tissue quality.

The β-TCP granules used in this study have been in clinical use in bone defect repair for over 20 years (Altermatt, Schwobel, & Pochon, 1992). The clinical use of granular β-TCP and BG in osteochondral defect filling, however, has been scanty (Hupa & Hupa, 2010). Granular structure enables easy and complete filling of misshapen osteochondral lesions, without a need to surgically enlarge the lesion to fit the shape of the scaffold. Granular bone fillers allow cell migration into the entire defect site, tissue ingrowth, vascularization, and well-functioning metabolism (Virolainen, Heikkila, Yli-Urpo, Vuorio, & Aro, 1997; Zerbo, Bronckers, de Lange, & Burger, 2005). In this study, the commercial materials BG and β-TCP showed satisfactory lesion filling and extensive bone formation, indicating that they have potential to be used in deep osteochondral defect repair. The potential downside of granular materials is that the granules might loosen from the surface. However, in this study, the articulating tibial surface showed no signs of abrasion by the granules. Adding a cartilage reparative scaffold on top of the bone repair would further secure the granules in place while restoring the cartilage surface.

There is emerging evidence of crosstalk between articular cartilage and underlying subchondral bone that emphasizes the importance of restoring the joint as a unit (Findlay & Kuliwaba, 2016). Survival of a whole tissue graft in osteochondral grafting depends largely on the integration of the graft bone into the host bone (Gross et al., 2008). Despite the favourable bone repair with the commercial bone substitute materials, the cartilage unit of the defect, which was left untreated, was inadequately repaired in the present study. Even though Masson–Goldner trichrome is not a cartilage staining method, it gives a general view of the tissue repair. For the tissue section analysed in the present study for detailed bone formation, it was evident that there was no or very minor cartilage formation over the bone regrowth. Thus, none of the studied materials alone were sufficient for the restoration of the entire osteochondral unit. Similar results were obtained in a study where PLGA was combined with hydroxyapatite-β-TCP (Fan et al., 2013) and in the work of Matsuo and colleagues (Matsuo et al., 2015) in which osteochondral repair was studied in a minipig model. A separate cartilage repair procedure on top of bone repair is therefore needed to restore the chondral part of the lesion.

The strength of this study is in its comparison of four different bone fillers with each other and with spontaneous repair. The bone defects were very large, creating a challenge both for the spontaneous repair and for the treatment groups. This study was limited by the lack of a healthy age-adjusted control group with no surgical procedures. In this study, it is possible that the operated limb carried less weight than the contralateral control limb. However, this animal-specific control was the same for every group, enabling comparison between the study groups.

5 | CONCLUSIONS

Filling of the bony part of a deep osteochondral lesion with a biodegradable gas-foamed PLGA scaffold resulted in insufficient repair. Combining PLGA with bioactive glass worsened the repair result.

The commercial controls with β-TCP and BG resulted in satisfactory bone defect filling with more abundant osteoid and mineralized bone tissue. Thus, these two bone substitute materials have the potential to be used in deep osteochondral defect repair, given that the cartilage unit of the defect is repaired with adequate techniques.

ACKNOWLEDGEMENTS

The authors wish to acknowledge the Finnish Funding Agency for Innovation (Tekes) for their financial support (3110/31/08). The authors express their gratitude to Hubert Häggman for photo documentation of the rabbit knees and for preparing Figure 2. The authors thank BioSiteHisto Oy (Tampere, Finland) for their technical expertise in histological sample preparation and histomorphometry, and Hannu Kautiainen (Medcare Oy) for his invaluable help with the statistical analyses. The authors would like to thank Timo Lehtonen (Vivoxid Ltd., Turku, Finland) for providing the glass fibres for the study. We thank the Biomedicum Imaging Unit (University of Helsinki) for technical support and microscopy services.

CONFLICT OF INTEREST

The authors have no financial or personal disclosures that would pose potential conflicts of interests.

AUTHOR CONTRIBUTIONS

Conception and design of the study: V.M., E.J., A.R., M.K., I.K.; providing study materials: P.U., A.M.H., A.R., M.K.; acquisition of data: E.S., V.M., K.L., E.J., T.P., M.H.; analysis and interpretation of data: E.S., V.M., K.L., M.H., A.A., I.K.; drafting the article: E.S., V.M., K.L., E.J., T.P., M.H., P.U., A.M.H.; critical revision of the article for important intellectual content: A.A., A.R., M.K., I.K.

All authors have read and approved the final submitted manuscript.

ORIGINAL PUBLICATION

This manuscript contains original unpublished work and it is not being submitted for publication elsewhere at the same time.

ORCID

Eve Salonius https://orcid.org/0000-0003-1988-2800

REFERENCES

Altermatt, S., Schwobel, M., & Pochon, J. P. (1992). Operative treatment of solitary bone cysts with tricalcium phosphate ceramic. A 1 to 7 year follow-up. *European Journal of Pediatric Surgery*, *2*, 180–182. https://doi.org/10.1055/s-2008-1063435

Arrington, E. D., Smith, W. J., Chambers, H. G., Bucknell, A. L., & Davino, N. A. (1996). Complications of iliac crest bone graft harvesting. *Clinical Orthopaedics and Related Research*, *329*, 300–309. https://doi.org/10.1097/00003086-199608000-00037

Brauer, D. S. (2015). Bioactive glasses-structure and properties. *Angewandte Chemie (International Ed. in English)*, *54*, 4160–4181. https://doi.org/10.1002/anie.201405310

Buades, A., Coll, B., & Morel, J. M. (2005). A non-logical algorithm for image denoising. *Computer Vision and Pattern Recognition*, *2*, 60–65.

Calasans-Maia, M. D., Monteiro, M. L., Ascoli, F. O., & Granjeiro, J. M. (2009). The rabbit as an animal model for experimental surgery. *Acta Cirúrgica Brasileira*, *24*, 325–328. https://doi.org/10.1590/S0102-86502009000400014

Doube, M., Klosowski, M. M., Arganda-Carreras, I., Cordelieres, F. P., Dougherty, R. P., Jackson, J. S., … Shefelbine, S. J. (2010). BoneJ: Free and extensible bone image analysis in ImageJ. *Bone*, *47*, 1076–1079. https://doi.org/10.1016/j.bone.2010.08.023

Eggli, P. S., Muller, W., & Schenk, R. K. (1988). Porous hydroxyapatite and tricalcium phosphate cylinders with two different pore size ranges implanted in the cancellous bone of rabbits. A comparative histomorphometric and histologic study of bony ingrowth and implant substitution. *Clinical Orthopaedics and Related Research*, *232*, 127–138.

Fan, W., Wu, C., Miao, X., Liu, G., Saifzadeh, S., Sugiyama, S., … Xiao, Y. (2013). Biomaterial scaffolds in cartilage-subchondral bone defects influencing the repair of autologous articular cartilage transplants. *Journal of Biomaterials Applications*, *27*, 979–989. https://doi.org/10.1177/0885328211431310

Findlay, D. M., & Kuliwaba, J. S. (2016). Bone–cartilage crosstalk: A conversation for understanding osteoarthritis. *Bone Research*, *4*, 16028. https://doi.org/10.1038/boneres.2016.28

Garcia-Gareta, E., Coathup, M. J., & Blunn, G. W. (2015). Osteoinduction of bone grafting materials for bone repair and regeneration. *Bone*, *81*, 112–121. https://doi.org/10.1016/j.bone.2015.07.007

Gentile, P., Chiono, V., Carmagnola, I., & Hatton, P. V. (2014). An overview of poly (lactic-co-glycolic) acid (PLGA)-based biomaterials for bone tissue engineering. *International Journal of Molecular Sciences*, *15*, 3640–3659. https://doi.org/10.3390/ijms15033640

Ghazal, G., Prein, J., & Müller, W. (1992). Knochendefektfüllungen in den Kieferknochen mit Tricalciumphosphat. *Swiss Dent*, *13*, 15–18.

Gross, A. E., Kim, W., Las Heras, F., Backstein, D., Safir, O., & Pritzker, K. P. (2008). Fresh osteochondral allografts for posttraumatic knee defects: Long-term followup. *Clinical Orthopaedics and Related Research*, *466*, 1863–1870. https://doi.org/10.1007/s11999-008-0282-8

Gunn, J. M., Rekola, J., Hirvonen, J., & Aho, A. J. (2013). Comparison of the osteoconductive properties of three particulate bone fillers in a rabbit model: Allograft, calcium carbonate (Biocoral(R)) and S53P4 bioactive glass. *Acta Odontologica Scandinavica*, *71*, 1238–1242. https://doi.org/10.3109/00016357.2012.757642

Haaparanta, A. M., Uppstu, P., Hannula, M., Ella, V., Rosling, A., & Kellomaki, M. (2015). Improved dimensional stability with bioactive glass fibre skeleton in poly (lactide-co-glycolide) porous scaffolds for tissue engineering. *Materials Science & Engineering. C, Materials for Biological Applications*, *56*, 457–466. https://doi.org/10.1016/j.msec.2015.07.013

Han, S. H., Chae, S. W., Choi, J. Y., Kim, E. C., Chae, H. J., & Kim, H. R. (2009). Acidic pH environments increase the expression of cathepsin B in osteoblasts: The significance of ER stress in bone physiology. *Immunopharmacology and Immunotoxicology*, *31*, 428–431. https://doi.org/10.1080/08923970902751651

Huey, D. J., Hu, J. C., & Athanasiou, K. A. (2012). Unlike bone, cartilage regeneration remains elusive. *Science*, *338*, 917–921. https://doi.org/10.1126/science.1222454

Hupa, L., & Hupa, M. (2010). Recent research on composition dependence of the properties of bioactive glasses. *Ceramic Transactions (Advances in Bioceramics and Biotechnologies)*, *218*, 145–156.

Jackson, D. W., Lalor, P. A., Aberman, H. M., & Simon, T. M. (2001). Spontaneous repair of full-thickness defects of articular cartilage in a goat model. A preliminary study. *Journal of Bone and Joint Surgery-American*, *83-A*, 53–64.

Jones, J. R. (2013). Review of bioactive glass: From Hench to hybrids. *Acta Biomaterialia*, *9*, 4457–4486. https://doi.org/10.1016/j.actbio.2012.08.023

Karp, J. M., Shoichet, M. S., & Davies, J. E. (2003). Bone formation on two-dimensional poly (DL-lactide-co-glycolide) (PLGA) films and three-dimensional PLGA tissue engineering scaffolds in vitro. *Journal of Biomedical Materials Research. Part a*, *64*, 388–396. https://doi.org/10.1002/jbm.a.10420

Keranen, P., Moritz, N., Alm, J. J., Ylanen, H., Kommonen, B., & Aro, H. T. (2011). Bioactive glass microspheres as osteopromotive inlays in macrotextured surfaces of Ti and CoCr alloy bone implants: Trapezoidal surface grooves without inlay most efficient in resisting torsional forces. *Journal of the Mechanical Behavior of Biomedical Materials*, *4*, 1483–1491. https://doi.org/10.1016/j.jmbbm.2011.05.018

Kleinschmidt, J. C., Marden, L. J., Kent, D., Quigley, N., & Hollinger, J. O. (1993). A multiphase system bone implant for regenerating the calvaria. *Plastic and Reconstructive Surgery*, *91*, 581–588. https://doi.org/10.1097/00006534-199304000-00002

Lindfors, N. C., Heikkila, J. T., Koski, I., Mattila, K., & Aho, A. J. (2009). Bioactive glass and autogenous bone as bone graft substitutes in benign bone tumors. *Journal of Biomedical Materials Research. Part B, Applied Biomaterials*, *90*, 131–136.

Lindfors, N. C., Hyvonen, P., Nyyssonen, M., Kirjavainen, M., Kankare, J., Gullichsen, E., & Salo, J. (2010). Bioactive glass S53P4 as bone graft substitute in treatment of osteomyelitis. *Bone*, *47*, 212–218. https://doi.org/10.1016/j.bone.2010.05.030

Liu, B., & Lun, D. X. (2012). Current application of beta-tricalcium phosphate composites in orthopaedics. *Orthopaedic Surgery*, *4*, 139–144. https://doi.org/10.1111/j.1757-7861.2012.00189.x

Lu, H. H., El-Amin, S. F., Scott, K. D., & Laurencin, C. T. (2003). Three-dimensional, bioactive, biodegradable, polymer-bioactive glass composite scaffolds with improved mechanical properties support collagen synthesis and mineralization of human osteoblast-like cells in vitro. *Journal of Biomedical Materials Research. Part a*, *64*, 465–474. https://doi.org/10.1002/jbm.a.10399

Mano, J. F., & Reis, R. L. (2007). Osteochondral defects: Present situation and tissue engineering approaches. *Journal of Tissue Engineering and Regenerative Medicine*, *1*, 261–273. https://doi.org/10.1002/term.37

Matsuo, T., Kita, K., Mae, T., Yonetani, Y., Miyamoto, S., Yoshikawa, H., & Nakata, K. (2015). Bone substitutes and implantation depths for subchondral bone repair in osteochondral defects of porcine knee joints. *Knee Surgery, Sports Traumatology, Arthroscopy*, *23*, 1401–1409. https://doi.org/10.1007/s00167-014-2853-4

Mayr, H. O., Suedkamp, N. P., Hammer, T., Hein, W., Hube, R., Roth, P. V., & Bernstein, A. (2015). beta-Tricalcium phosphate for bone replacement: Stability and integration in sheep. *Journal of Biomechanics*, *48*, 1023–1031. https://doi.org/10.1016/j.jbiomech.2015.01.040

McKinley, T. O., Borrelli, J. Jr., D'Lima, D. D., Furman, B. D., & Giannoudis, P. V. (2010). Basic science of intra-articular fractures and posttraumatic osteoarthritis. *Journal of Orthopaedic Trauma*, *24*, 567–570. https://doi.org/10.1097/BOT.0b013e3181ed298d

Mountziaris, P. M., & Mikos, A. G. (2008). Modulation of the inflammatory response for enhanced bone tissue regeneration. *Tissue Engineering. Part B, Reviews*, *14*, 179–186. https://doi.org/10.1089/ten.teb.2008.0038

Oryan, A., Alidadi, S., Moshiri, A., & Maffulli, N. (2014). Bone regenerative medicine: Classic options, novel strategies, and future directions. *Journal of Orthopaedic Surgery and Research*, *9*, 18. 799X-9-18, DOI: https://doi.org/10.1186/1749-799X-9-18

Pan, Z., Duan, P., Liu, X., Wang, H., Cao, L., He, Y., … Ding, J. (2015). Effect of porosities of bilayered porous scaffolds on spontaneous osteochondral repair in cartilage tissue engineering. *Regenerative Biomaterials*, *2*, 9–19. https://doi.org/10.1093/rb/rbv001

Penk, A., Forster, Y., Scheidt, H. A., Nimptsch, A., Hacker, M. C., Schulz-Siegmund, M., … Huster, D. (2013). The pore size of PLGA bone implants determines the de novo formation of bone tissue in tibial head defects in rats. *Magnetic Resonance in Medicine*, *70*, 925–935. https://doi.org/10.1002/mrm.24541

Schindelin, J., Arganda-Carreras, I., Frise, E., Kaynig, V., Longair, M., & Pietzsch, T. (2012). Fiji: An open-source platform for biological-image analysis. *Nature Methods*, *9*, 676–682. https://doi.org/10.1038/nmeth.2019

Seo, S. J., Mahapatra, C., Singh, R. K., Knowles, J. C., & Kim, H. W. (2014). Strategies for osteochondral repair: Focus on scaffolds. *Journal of Tissue Engineering*, *5*. 2041731414541850 DOI: https://doi.org/10.1177/2041731414541850

Serino, G., Rao, W., Iezzi, G., & Piattelli, A. (2008). Polylactide and polyglycolide sponge used in human extraction sockets: Bone formation following 3 months after its application. *Clinical Oral Implants Research*, *19*, 26–31.

Shibutani, T., & Heersche, J. N. (1993). Effect of medium pH on osteoclast activity and osteoclast formation in cultures of dispersed rabbit osteoclasts. *Journal of Bone and Mineral Research*, *8*, 331–336. https://doi.org/10.1002/jbmr.5650080310

Stahl, S. S., & Froum, S. (1986). Histological evaluation of human intraosseous healing responses to the placement of tricalcium phosphate ceramic implants. I. Three to eight months. *Journal of Periodontology*, *57*, 211–217. https://doi.org/10.1902/jop.1986.57.4.211

Uppstu, P., Paakki, C., & Rosling, A. (2015). In vitro hydrolysis and magnesium release of poly(d,l-lactide-co-glycolide)-based composites containing bioresorbable glasses and magnesium hydroxide. *Journal of Applied Polymer Science*, *132*, 41. 42646

van Dijk, C. N., Reilingh, M. L., Zengerink, M., & van Bergen, C. J. (2010). Osteochondral defects in the ankle: Why painful? *Knee Surgery, Sports Traumatology, Arthroscopy*, *18*, 570–580. https://doi.org/10.1007/s00167-010-1064-x

Virolainen, P., Heikkila, J., Yli-Urpo, A., Vuorio, E., & Aro, H. T. (1997). Histomorphometric and molecular biologic comparison of bioactive glass granules and autogenous bone grafts in augmentation of bone defect healing. *Journal of Biomedical Materials Research*, *35*, 9–17. https://doi.org/10.1002/(SICI)1097-4636(199704)35:1<9::AID-JBM2>3.0.CO;2-S

Zeimaran, E., Pourshahrestani, S., Djordjevic, I., Pingguan-Murphy, B., Kadri, N. A., & Towler, M. R. (2015). Bioactive glass reinforced elastomer composites for skeletal regeneration: A review. *Materials Science & Engineering. C, Materials for Biological Applications*, *53*, 175–188. https://doi.org/10.1016/j.msec.2015.04.035

Zerbo, I. R., Bronckers, A. L., de Lange, G., & Burger, E. H. (2005). Localisation of osteogenic and osteoclastic cells in porous beta-tricalcium phosphate particles used for human maxillary sinus floor elevation. *Biomaterials*, *26*, 1445–1451. https://doi.org/10.1016/j.biomaterials.2004.05.003

SUPPORTING INFORMATION

Additional supporting information may be found online in the Supporting Information section at the end of the article.

Table S1. Quantitative results of X-ray microtomography showing all statistically significant p values ($p \leq 0.05$) obtained with a permutation ANOVA test with Holm adjustment.

How to cite this article: Salonius E, Muhonen V, Lehto K, et al. Gas-foamed poly(lactide-co-glycolide) and poly(lactide-co-glycolide) with bioactive glass fibres demonstrate insufficient bone repair in lapine osteochondral defects. *J Tissue Eng Regen Med*. 2019;1–10. https://doi.org/10.1002/term.2801

Uppstu P, Engblom S, Inkinen S, Hupa L, Wilén C-E. Influence of polylactide coating stereochemistry on mechanical and in vitro degradation properties of porous bioactive glass scaffolds for bone regeneration. Journal of Biomedical Materials Research Part B. 2024; 112(1):e35328.

IV

Received: 8 April 2023 | Revised: 25 August 2023 | Accepted: 7 September 2023
DOI: 10.1002/jbm.b.35328

RESEARCH ARTICLE

Influence of polylactide coating stereochemistry on mechanical and in vitro degradation properties of porous bioactive glass scaffolds for bone regeneration

Peter Uppstu[1] | Simon Engblom[1] | Saara Inkinen[1,2] | Leena Hupa[1] | Carl-Eric Wilén[1]

[1]Laboratory of Molecular Science and Technology, Faculty of Science and Engineering, Åbo Akademi University, Turku, Finland

[2]Nordic Catalyst e.U., Vienna, Austria

Correspondence
Peter Uppstu, Laboratory of Molecular Science and Technology, Faculty of Science and Engineering, Åbo Akademi University, Turku, Finland.
Email: peter.uppstu@abo.fi

Funding information
Stiftelsen för Åbo Akademi; Svenska Kulturfonden; Tekniikan Edistämissäätiö

Abstract

The mechanical properties of polylactide stereocomplexes (PLA SC) have been primarily studied through tensile testing, with inconsistent results, and the compressive properties of PLA SC compared to homocrystalline or amorphous PLA remain poorly understood. In this study, we coated porous bioactive glass 13–93 scaffolds with amorphous, homocrystalline, or stereocomplex PLA to investigate their mechanical and degradation properties before and after immersion in simulated body fluid. The glass scaffolds had interconnected pores and an average porosity of 76%. The PLA coatings, which were 10–100 μm thick and approximately 3% of the glass scaffold mass, covered the glass to a large extent. The compressive strength and toughness of all PLA-coated scaffolds were significantly higher than those of uncoated scaffolds, with approximately a fourfold increase before immersion and a twofold increase after immersion. The compressive strength and toughness of PLA SC-coated scaffolds were similar to those of scaffolds with homocrystalline PLA coating, and significantly higher than for scaffolds with amorphous PLA coating. All PLA coatings moderated the initial pH increase caused by the glass, which could benefit surrounding cells and bone tissue in vivo after implantation.

KEYWORDS
bioactive glass, compressive testing, polylactide stereocomplex, scaffold, simulated body fluid

1 | INTRODUCTION

Polylactide (PLA) is a thermoplastic poly(α-hydroxyester) studied for various biomedical applications, including tissue regeneration and drug release.[1–3] It is widely used in orthopedic applications in porous scaffolds and composite implants both as a continuous and a non-continuous phase.[4,5] In orthopedic fixation, PLA is used clinically for example in plates, screws, and pins.[6]

The properties of PLA can be modified by altering its molecular weight, structure, and stereochemistry. Structural modifications include introducing branching, cross-linking, or tethering functional groups via copolymerization.[5] As the lactide dimer contains two chiral carbon atoms, it can exist in three forms: L,L-, D,D-, and D,L-lactide. The ability of PLA to crystallize and, therefore, its thermal and mechanical properties depend on the stereoform of the monomers. Crystallization generally occurs in PLA with an optical purity of at least 72%–75%, while PLA closer to a racemic mixture of the two forms remains amorphous.[7,8]

By blending poly(L-lactide) (PLLA) with poly(D-lactide) (PDLA), one can form stereocomplex crystallites with strong stereoselective

association between PLLA and PDLA.[9,10] Stereocomplex PLA (PLA SC) crystallites consist of PLLA and PDLA at a 1:1 ratio. PLA SC can be formed in the presence of chains or chain segments of PLLA and PDLA in solution, by cooling from melt, during polymerization, or during hydrolytic degradation.[11] Especially for PLA with a molecular weight higher than 100,000 g/mol, stereocomplex crystallization can be enhanced with synthesis of stereoblock-type PLA with blocks of PLLA and PDLA within the same chain.[12]

PLA SC has a higher melting point (220–230°C) than homocrystalline PLA (170–180°C)[13] and is hydrolytically[14–16] and thermally[17] more stable. However, its hydrolysis forms more acidic degradation products,[18] which may affect bone regeneration negatively.[1] Composites with bioactive glass neutralize acidic degradation products.[19,20] The degradation products of polyesters may even be used as positive irritation to stimulate the formation of growth factors for enhanced bone formation.[21–24]

PLA SC is often reported to have enhanced mechanical properties compared to isomerically pure PLLA or PDLA.[8,11,25,26] Although some studies support these claims,[27,28] others suggest similar or even inferior[29–31] tensile strength for stereocomplexes compared to other PLA forms. The compressive properties of PLA SC have not yet been extensively investigated. In one study, PLA with a small fraction of stereocomplex crystallites exhibited greater compressive strength than isomerically pure PLLA.[32] In other studies, PLLA and PDLA blended with D-mannitol[33] or ethylene-glycidyl methacrylate copolymer[34] exhibited higher compressive strength than pure PLLA. However, in these papers, the materials were studied as foams with different porosities for PLA SC compared to PLLA, complicating direct comparisons of material properties.

Scaffolds for bone regeneration are typically composed of biodegradable materials, such as PLA, processed into porous structures. When a scaffold is implanted into a bone defect, cells enter its pores, adhere to the pore walls, and generate new tissue. As the tissue grows, the scaffold degrades, ideally allowing the defect site to be filled with new bone as the scaffold completely degrades.[2] Although PLA is biocompatible, it lacks biologically active cues, and it is frequently combined with bioactive glasses for improved tissue growth.[6]

Bioactive glasses 45S5 and S53P4 can be favorably used to regenerate bone tissue.[35,36] They are clinically used as granules, pastes, plates, and discs. Despite intense research on creating porous three-dimensional (3D) scaffolds based on these glasses, no clinical products exist yet.[37] Several methods have been proposed for producing porous scaffolds from melt-derived bioactive glasses, including sintering of glass particles in a mold,[38,39] solid free-form fabrication techniques,[40,41] and the foam replication technique.[42] Each of these methods require a sintering step to consolidate the glass particles into the desired porous structure. The strong crystallization tendency during thermal treatment poses challenges when manufacturing porous scaffolds of 45S5 and S53P4. Extensive research has been conducted to adjust the composition of bioactive glasses to better suit various hot working processes. Bioactive glass 13–93 was found to allow versatile hot working[43,44] and is suitable for producing porous non-crystallized scaffolds for tissue regeneration.[39,45]

Low compressive strength and fracture toughness are main limitations of porous bioactive glass scaffolds.[46,47] Although 3D bioactive glass scaffolds have been designed for high compressive strength, this is generally achieved by compromising porosity, pore size, or pore interconnectivity.[48] The mechanical properties of bioactive glass scaffolds can be improved by coating them with biodegradable synthetic or naturally occurring polymers, such as PLA, poly(lactide-co-glycolide) (PLGA), polycaprolactone (PCL), poly(3-hydroxybutyrate) (P3HB), gelatin, silk, alginate, collagen, or chitosan.[49–51] Bioactive glass-based scaffolds produced with the foam replication method and coated with polymers typically exhibit compressive strength values of 1 MPa or below.[49]

In this study, we examined the impact of PLA coating morphology on the compressive and degradation properties of porous bioactive glass 13–93 scaffolds in a clinically relevant setting for bone regeneration, both before and after immersion in simulated body fluid (SBF). We used three types of PLA coatings with distinct morphologies: amorphous poly(D,L-lactide) (PDLLA), homocrystalline PLLA, and a 1:1 stereocomplex mixture of PLLA and PDLA. Pore morphology, total porosity, and the mass and thickness of the scaffold coatings were measured, and the polymer coatings were analyzed with differential scanning calorimetry (DSC). We immersed the scaffolds in SBF for 0, 2, 4, 6, or 10 weeks and measured mass loss, water absorption, pH, and compressive properties at each time point. The findings in this study provide insights into the selection of PLA-based coating stereochemistry for biomedical implants, with the aim to optimize their mechanical properties and degradation behavior.

2 | MATERIALS AND METHODS

2.1 | Materials

Medical-grade L-lactide, D-lactide, and D,L-lactide monomers (Corbion, Gorinchem, the Netherlands) were used to polymerize PLA. Bioactive glass 13–93, with a nominal composition of 53 SiO_2, 6 Na_2O, 12 K_2O, 5 MgO, 20 CaO, and 4 P_2O_5 (all in wt %), was prepared by mixing Belgian quartz sand with analytical-grade reagents Na_2CO_3, K_2CO_3, MgO, $CaCO_3$, and $CaHPO_4{\cdot}2(H_2O)$. The batch was melted in a platinum crucible at 1360°C for 3 h, cast, annealed, crushed, and remelted to ensure homogeneity. The annealed glass block was crushed, milled, and sieved to obtain a size fraction of 32–45 μm. All other chemicals used in this study were of analytical or equivalent grade.

2.2 | Polymerization

PLLA, PDLA, and racemic PDLLA were synthesized by ring-opening polymerization, following a previously reported procedure.[20] Briefly, 0.1 mol % stannous octoate was used as an initiator, and 1-decanol as a co-initiator. The polymerization was conducted in 200 g batches under an argon atmosphere for 3 h at 150°C with initial stirring. The polymer was subsequently dissolved in dichloromethane and carefully precipitated in ethanol.

2.3 | Production of glass scaffolds by foam replication

Polyethylene glycol (35,000 g/mol) was dissolved in ethanol at a concentration of 5 wt % at 40°C. Bioactive glass 13–93 particles (7.5 wt % compared to ethanol) were dispersed into the solution in a ball mill for 30 min. After milling, the mean particle size was 20.2 μm as measured with laser light scattering. Cylindrical PU foams (20 mm height, 18 mm diameter, and 15 pores per inch) were immersed in the slurry. To ensure full penetration of the slurry into the foam, the foams were manually compressed and released while still submerged in the slurry. Excess slurry was carefully removed with compressed air when removing the foams from the slurry. The slurry-coated foams were dried at room temperature (RT) for a minimum of 3 days to create green bodies. To burn out the polymer and sinter the glass, the green bodies were heated according to the following procedure: heating from RT to 300°C at 1°C min^{-1}, heating to 450°C at 0.8°C min^{-1}, 30 min hold at 450°C, heating to 670°C at 0.8°C min^{-1}, and 120 min hold at 670°C, after which the scaffolds were slowly cooled in the furnace to RT. The sintered glass scaffolds were stored in a desiccator until further use. Figure 1 shows the PU sacrificial foam before coating with the slurry, the slurry-coated green body, and the bioactive glass scaffold after sintering.

2.4 | Coating of glass scaffolds with PLA

The glass scaffolds were coated with PLA using a dip-coating technique. The stereocomplex solutions were prepared by dissolving 0.75 g PDLA and 0.75 g PLLA in 25 g $CHCl_3$ for a polymer concentration of 6 wt %. For the PDLLA and PLLA solutions, 1.5 g of either PDLLA or PLLA was dissolved in 25 g $CHCl_3$. The dry glass scaffolds were immersed in the polymer solution in beakers for 3 min, during which the beakers were placed in a vacuum oven, and the air pressure was reduced to 600 mbar for 60 s to remove bubbles from the scaffolds. The scaffolds were removed from the solution and gently blown with compressed air to open clogged pores. The polymer-coated scaffolds were dried overnight in a fume hood at RT, after which they were further dried overnight at RT at <50 mbar pressure. After coating and drying, the scaffolds were weighed again to determine the mass of the polymer coating.

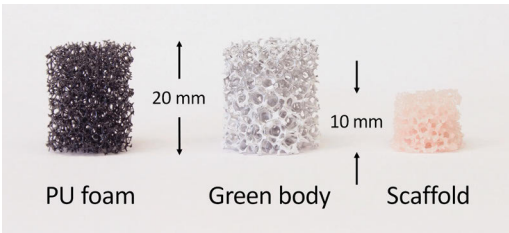

FIGURE 1 A polyurethane foam, a green body, and a final sintered bioactive glass scaffold. The figure illustrates the volume decrease of the scaffolds during the sintering step.

The crystallinity of the polymer was increased by heat-treating the scaffolds. Preliminary tests were conducted to determine the optimal conditions for stereocomplex formation. We found that heat treatment at temperatures equal to or exceeding the melt temperature of homocrystalline PLA at 180°C significantly enhanced stereocomplex formation compared to lower temperatures, which is in agreement with previous studies.[31,52] Consequently, the scaffolds were heated under nitrogen atmosphere at 180°C for 60 min.

2.5 | Characterization of microstructure

The microstructure of the glass scaffolds was analyzed with μ-CT (SkyScan 1072, SkyScan, Kontich, Belgium). Cross-sections of scaffolds were analyzed by SEM (LEO Gemini 1530, Carl Zeiss, Oberkochen, Germany) at a magnification of ×30. To preserve the macrostructure, scaffolds were embedded in epoxy resin before being ground and polished to expose the cross-section of the scaffold. EDX analysis (UltraDry X-ray detector, Thermo Fisher Scientific, WI, USA) was used to identify the reaction layers of the glass. The coverage of coating and reaction layers on the glass surface was estimated visually from the SEM images.

2.6 | In vitro degradation

The in vitro degradation properties of the polymer-coated scaffolds were studied in SBF using a 1:30 ratio of scaffold (in g) to SBF (in mL). SBF was prepared using a standard procedure.[53] The scaffolds, immersed in plastic containers, were placed in a shaking incubator at 100 rpm at 37°C for various durations (2, 4, 6, or 10 weeks). The 0-week scaffolds were analyzed without immersion in SBF. The pH of the immersion solution was measured every week for at least three parallel scaffolds. The solution for all scaffolds was replenished weekly to fresh SBF. The ratio between scaffold mass and SBF volume was chosen based on the low surface area of the scaffolds, the relatively slow reactivity of the 13–93 glass, and on the weekly replenishing of the SBF solution.

A total of eight parallel scaffolds were immersed in SBF for each time point and coating type. Five of the eight parallel scaffolds were randomly chosen for compressive testing. The remaining three scaffolds were superficially dried using tissue paper, weighed, freeze-dried, weighed again, and subjected to other analyses. The percentage of water absorption was calculated as the amount of water that was lost during scaffold drying divided by the dried mass after immersion. The mass loss was determined as the difference between the dry mass before and after immersion, divided by the pre-immersion dry mass.

2.7 | Compressive testing

Compression tests were performed using an L&W Crush Tester (Lorentzen & Wettre, Stockholm, Sweden). Five parallel scaffolds were

compressed along their axis at a rate of 2 mm/min. The 0-week scaffolds were compressed in their dry state, while the 2–10-week scaffolds were compressed in their wet state immediately after removal from the SBF. The toughness of each scaffold was estimated as the strain energy density calculated from the integral of the stress–strain curve up to 33% strain. The compressive strength was identified as the peak value up to 33% strain. The threshold level of 33% was chosen to allow for sufficient data to be collected to account for the slight variation in the structure and shape between parallel scaffolds.

2.8 | Analysis of the polymer coating

The thermal properties of the polymer coating were analyzed using DSC with a DSC Q1000 (TA Instruments) under a nitrogen atmosphere. The samples were heated from 10 to 250°C at a rate of 10°C min^{-1}. The glass transition temperature (T_g) was identified as the half-height value, and the melting temperature (T_m) was determined as the maximum value of the endothermic peak. As the samples for DSC analysis mainly consisted of bioactive glass with only a small, undefined amount of PLA, specific melting enthalpies could not be calculated. Thermal analysis was conducted in triplicate for all coated 0-week and 10-week scaffolds.

The number average molecular weight (M_n) and weight average molecular weight (M_w) of the polymers were measured using gel permeation chromatography (GPC) with an LC-10ATVP HPLC pump (Shimadzu Corporation, Kyoto Japan), an AM GPC Gel 10 μm linear column (Mentor, Ohio, USA), and a Sedex 85 light scattering detector (Sedere, Alfortville, France). Polystyrene samples with narrow molecular weight distributions were used as standards.

2.9 | Statistical analysis

Statistical analysis was performed using SAS 9.4 software (SAS Institute). Analysis of variance was conducted with linear and linear mixed models. Post hoc tests were employed to explore differences among the means of the coating groups while accounting for other explanatory factors in the model. In the statistical analysis of the pH of the immersion solution, the individual scaffold number was designated as a random factor to take into account multiple measurements per individual scaffold over time. Differences were considered statistically significant at p values <.05.

3 | RESULTS

3.1 | Structural analysis of the glass scaffolds

The foam replication method, using sacrificial polyurethane templates, produced scaffolds with high pore interconnectivity and an architecture resembling trabecular bone. The scaffolds had an average porosity of 76%. Figure 2 displays the pore size distribution of uncoated and coated glass scaffolds, measured with μCT as the average of two parallel scaffolds. Pore sizes were highly variable, predominantly between 100 and 1700 μm. On average, pore sizes of uncoated scaffolds were smaller than those of coated scaffolds. Coated scaffolds had fewer pores in the 50–1000 μm range and more pores in the 1300–1700 μm range compared to uncoated scaffolds. The cylindrical-shaped sintered glass scaffolds had an average height of 9.9 mm and an average mass of 746 mg.

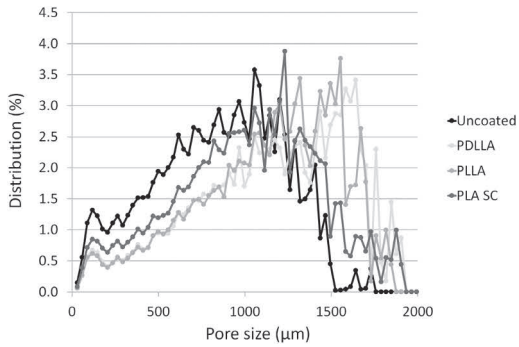

FIGURE 2 Pore size distribution of uncoated and coated bioactive glass scaffolds.

TABLE 1 Molecular weights and dispersity ($Đ$) of PLA polymers used in the coating of the 13–93 bioactive glass scaffolds as measured with GPC, and the average coating mass as a percentage of glass scaffold mass.

	M_n	M_w	$Đ$	Mass of coating (%)
PDLLA	33,000	56,000	1.7	2.6
PLLA	28,000	48,000	1.7	3.4
PDLA	26,000	43,000	1.7	3.2

Abbreviations: GPC, gel permeation chromatography; PDLLA, amorphous poly(D,L-lactide); PDLA, poly(D-lactide); PLA, polylactide; PLLA, poly(L-lactide).

3.2 | Properties of the polymer coating

Table 1 presents the molecular weight data of the precipitated and dried PDLLA, PLLA, and PDLA. The average mass of polymer coatings was approximately 3% of the glass scaffold mass for all coatings.

According to SEM analysis (Figure 6), the pores within the coated glass scaffolds were mostly covered with PLA coating, leaving approximately 20% of the glass surfaces uncoated. Most of the coating was located in the inner parts of the scaffolds, with less coating near the glass scaffold edges. The coating thickness varied, typically ranging between 10 and 100 μm.

DSC heating graphs for the scaffold coatings are shown in Figure 3, and thermal transition data from the DSC experiments is

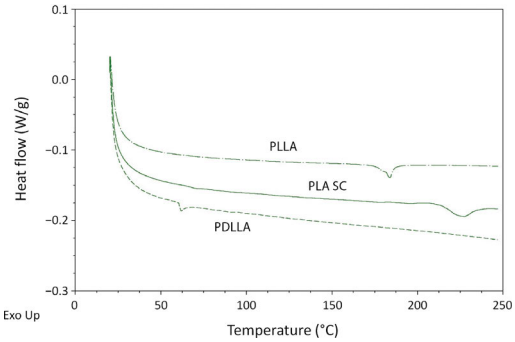

FIGURE 3 DSC curves illustrating phase transitions of PDLLA, PLLA, and PLA SC coatings before immersion in SBF. DSC, differential scanning calorimetry; PDLLA, amorphous poly(D,L-lactide); PLA, polylactide; PLLA, poly(L-lactide); SBF, simulated body fluid.

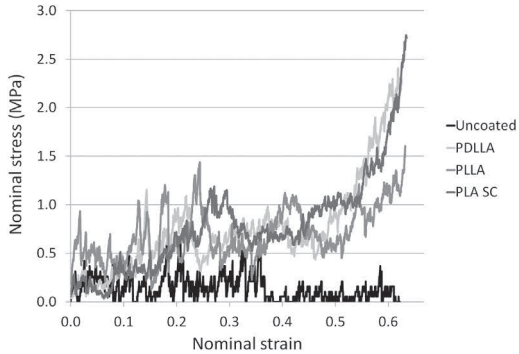

FIGURE 4 Compressive stress–strain graphs for 0-week scaffolds.

TABLE 2 Thermal transition points of PDLLA, PLLA, and PLA SC before immersion and after 10 weeks of immersion in SBF presented as averages ± SD.

Coating	Transition	0 weeks (°C)	10 weeks (°C)
PDLLA	T_g	60.5 ± 0.3	56.8 ± 0.7
PLLA	T_g	68.0 ± 0.5	68.3 ± 0.2
PLA SC	T_g	67.6 ± 0.6	71.5 ± 0.5
PLLA	T_m	183.2 ± 0.9	173.1 ± 0.7
PLA SC	T_m	225.2 ± 1.2	227.1 ± 0.7

Abbreviations: PDLLA, amorphous poly(D,L-lactide); PDLA, poly(D-lactide); PLA, polylactide; PLLA, poly(L-lactide); PLA SC, polylactide stereocomplexes; SBF, simulated body fluid.

summarized in Table 2. The thermal transition peaks in DSC were weak because the analyses were performed with crushed scaffolds, which primarily consisted of bioactive glass 13–93 (which does not undergo any transitions within the temperature range of the analyses) and only approximately 3 wt % of polymer. Distinct transitions in DSC occurred at the T_g for PDLLA (amorphous), the T_m for PLLA (homocrystalline), and the T_m for PLA SC (stereocomplex). Additionally, PLLA and PLA SC exhibited glass transitions, indicating their semi-crystalline nature. Besides the transitions reported in Table 2, melting of homocrystals for PLA SC scaffolds was detected in one 10-week scaffold, with a melting peak value of 176.1°C. Furthermore, there was a minor cold crystallization peak for all 10-week PLLA scaffolds at approximately 93°C.

3.3 | Compressive properties

Compressive stress–strain curves of representative 0-week scaffolds are presented in Figure 4. The toughness expressed as strain energy density during the initial 33% compression of the scaffold height before and after immersion in SBF is illustrated in Figure 5A. During compressive testing, all scaffolds experienced progressive failure, as parts of the scaffolds were continuously torn off, rather than the whole scaffold cracking at once. The size of the torn-off parts was smaller for uncoated scaffolds compared to coated scaffolds.

The toughness of the uncoated scaffolds remained unchanged from the dry state before immersion through the 10-week-long immersion in SBF ($p = .88$). In contrast, the toughness of all coated scaffolds was significantly higher before immersion than after immersion ($p < .0001$). Before immersion, no statistically significant difference was found between the three coatings ($p = .89$). The toughness of coated scaffolds remained constant throughout the immersion period, with no change from the 2-week time point until the 10-week time point ($p = .96$). After 2–10 weeks of immersion in SBF, the toughness of PLA SC-coated ($p = .0012$) and PLLA-coated ($p = .042$) scaffolds was significantly higher than that of PDLLA-coated scaffolds. The difference between PLA SC and PLLA coatings was not statistically significant ($p = .41$).

Figure 5B displays the compressive strength before and after immersing the scaffolds in SBF. The peak compressive strength in the dry state before immersion was 0.74 MPa for uncoated scaffolds, 1.46 MPa for PDLLA, 1.56 MPa for PLLA, and 1.68 MPa for PLA SC. After immersion, the compressive strength was slightly higher for coated scaffolds than for uncoated scaffolds.

3.4 | In vitro bioactivity and degradation properties

Figure 6 shows cross-sectional SEM images of 10-week scaffolds which were dried and cast in epoxy resin. Reaction layers of the bioactive glass, that is, silica-rich and calcium phosphate (CaP) layers, were visible for all scaffolds after immersion in SBF.

The abundance and thickness of the CaP reaction layer increased with immersion time in SBF. For uncoated scaffolds, a prominent CaP

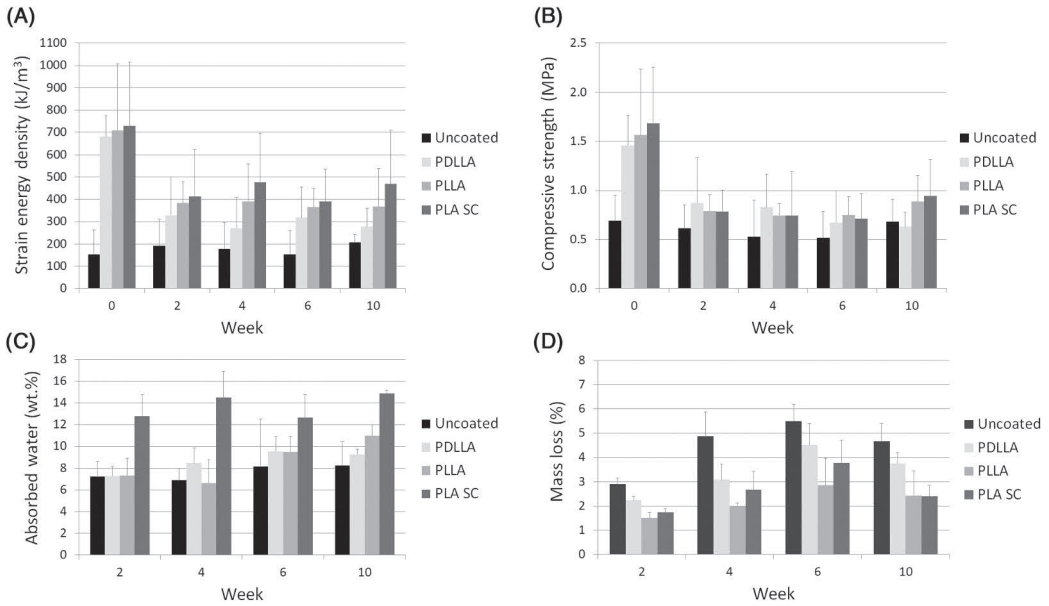

FIGURE 5 Properties of uncoated and coated glass scaffolds. (A) Strain energy density before and after immersion in simulated body fluid (SBF), calculated as the integral of the stress–strain curve for the initial 33% compression. (B) Compressive strength before and after immersion in SBF, measured as the peak value for the initial 33% of compression. (C) Water absorption after immersion in SBF. (D) Mass loss after immersion in SBF. Error bars in all graphs show standard deviations.

layer was visible on the glass surface. For coated scaffolds, the CaP layer primarily appeared on the polymer surface, with little CaP on the glass beneath the coating. This was clearly seen also in areas where the coating had detached from the glass surface: the CaP layer had mainly formed on the coating and to a lesser extent on the glass surface. The SEM images did not reveal any clear differences between the CaP layer on the different coatings.

The SBF solution was replenished weekly to simulate in vivo conditions in which released ions do not accumulate in the surrounding fluid over time. During the first 3 weeks, the pH values for the immersion solutions of all scaffolds were elevated due to the ion exchange reactions occurring on the bioactive glass surface (Figure 7). At weeks 1 and 2, the pH of the immersion solution of the uncoated scaffolds was significantly higher than that of coated scaffolds ($p < .005$). After the initial 3 weeks, pH values approached that of fresh SBF (7.4 at 37°C).

Figure 5C presents the water absorption of uncoated and coated scaffolds. The water absorption of uncoated scaffolds and PDLLA- and PLLA-coated scaffolds was between 5% and 11% at all time points with no differences between the coatings. In contrast, the water absorption of PLA SC scaffolds was significantly higher at all time points, with average values ranging from 12% to 15%. From the 2-week to 10-week time points, water absorption remained unchanged for all scaffold groups.

Mass loss for all scaffolds was small over the 10-week immersion time (Figure 5D). Uncoated scaffolds experienced the greatest mass

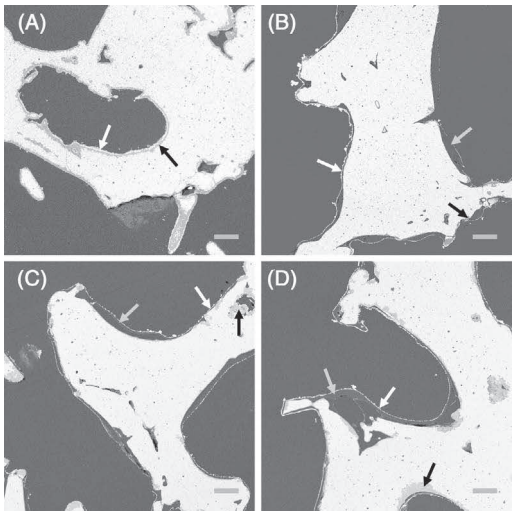

FIGURE 6 Cross-sectional SEM images of 10-week scaffolds: (A) uncoated, (B) PDLLA coating, (C) PLLA coating, and (D) PLA SC coating. Arrows indicate silica-rich layer (black arrow), CaP layer (white arrow), and PLA coating (gray arrow). Scale bar = 200 μm. PDLLA, amorphous poly(D,L-lactide); PLA, polylactide; PLLA, poly(L-lactide); PLA SC, polylactide stereocomplexes.

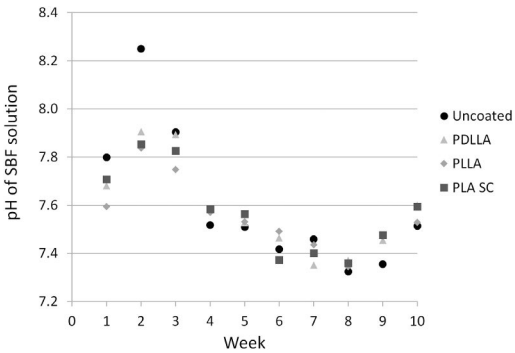

FIGURE 7 pH values of simulated body fluid (SBF) solution of uncoated and coated bioactive glass scaffolds. Immersion solutions were replenished weekly to fresh SBF and deviations from pH 7.4 are not cumulative. A total of 214 pH measurements were conducted for all scaffolds, with a standard deviation of ±0.16 between parallel samples.

loss at all time points, significantly differing from coated scaffolds ($p = .014$). After each immersion time, mass loss of PDLLA scaffolds was higher than that of PLLA ($p = .0027$) and PLA SC ($p = .024$) scaffolds. No statistically significant difference was found between PLLA and PLA SC ($p = .20$).

4 | DISCUSSION

The tensile properties of PLA SC have been reported by several authors,[27–31] but its compressive properties require further investigation. In this study, we used PLAs with varying stereocompositions as coatings for bioactive glass scaffolds in a clinically relevant bone regeneration setting. We compared the mechanical and short-term degradation properties of amorphous PDLLA, homocrystalline PLLA, and a mixture of PLLA and PDLA that resulted in stereocomplex crystallinity.

Compressive testing results showed significantly higher toughness and strength for PLA-coated scaffolds than for uncoated scaffolds. In the dry state before immersion in SBF, toughness differed approximately fourfold, and in the wet state after immersion, by approximately twofold. As the properties of uncoated scaffolds remained unchanged from dry to wet states, the observed differences in the coated scaffolds can be attributed to changes in the coating. PLA is a slowly degrading polymer,[54] and most changes in mechanical properties during the study timeframe can probably be explained by the plasticizing effect of water absorption into the polymer.[55] Additionally, scaffold wetting may have affected the adherence of the coating to the glass surface.

Scaffolds with semi-crystalline coating (PLLA and PLA SC) displayed greater toughness than those with amorphous coatings (PDLLA). Although PLA SC averages were higher than PLLA, there was no statistically significant difference between them. Earlier studies have shown PLA SC tensile strength to be similar or higher than that of isomerically pure PLLA, but wide variations in elongation-at-break have been recorded, with values for PLA SC both above and below PLLA.[27–31] More detailed studies should be conducted to determine the influence of factors such as crystal structure, percent crystallinity, and molecular weight on the mechanical properties of PLA SC compared to optically pure PLA.

It is crucial to optimize the mechanical properties of scaffolds for tissue regeneration to ensure that they are suitable for the surgical procedure. Surgically treated bone defects are often stabilized using intramedullary nails, screwed plates, or external fixators.[56] Even bone void fillers with lower mechanical properties may be utilized for the regeneration of load-bearing bone tissue, especially when the load is supported by the fixation devices.[57,58] In this study, the physical handling characteristics of coated scaffolds were improved compared to uncoated scaffolds, which were brittle and prone to breaking during experimental preparation.

Highly porous glass scaffolds were prepared using the template sintering technique. While creating glass scaffolds with lower overall porosity or smaller pore size could have significantly increased compressive strength,[48] it might have reduced their suitability for bone regeneration within the scaffold. Longer sintering times or higher sintering temperatures could have enhanced the compressive properties of the glass scaffolds by densifying the struts.[59] Additionally, a thicker coating or using a higher molecular weight polymer for the coating could have resulted in higher compressive properties. The compressive properties of the scaffolds analyzed in this study were comparable to previously reported values for polymer-coated, template-sintered scaffolds.[49,60]

The immersion solution was refreshed with new SBF weekly, allowing the measured pH values to reflect reactions that occurred during the previous week. The rate of ion exchange reactions in the bioactive glass was high during the first 3 weeks of immersion, resulting in increased pH values and mass loss of the scaffolds. The peak pH values were lower for coated scaffolds than for uncoated scaffolds. A pronounced pH peak immediately after immersion of bioactive glass into an aqueous solution has been reported to contribute to its antimicrobial effect.[61–63] However, an increase in pH can negatively impact cellular activity and potentially cause cytotoxic effects to the surrounding tissue.[64,65] It may therefore be beneficial to moderate the initial pH peak for example using coatings, such as those used in the present study. A slight increase in pH has been shown to positively influence osteoblast activity and contribute to new bone formation.[66,67] Throughout this study, differences between the PLA coatings were small. These findings are consistent with the results in an earlier study, where minor differences in pH were observed between films containing PLLA or a mixture of PLLA and PDLA during immersion at 37°C in a buffered solution for up to 39 weeks.[18]

The amorphous CaP layer that forms on bioactive glass progressively crystallizes into hydroxyapatite, promoting protein adsorption, cell attachment and differentiation, and new bone formation.[68] In this study, a CaP layer formed also on the surface of the PLA coating,

indicating that bone growth could be facilitated on the polymer surface similarly to uncoated bioactive glass. This phenomenon has been previously reported and is considered important for bone regeneration potential.[69–72]

Throughout the 10-week immersion period in SBF, mass loss of the scaffolds was small. Uncoated scaffolds consistently experienced the greatest mass loss, indicating that the coating prevented mass loss from the glass. However, the differences were small. Bioactive glass 13–93 is a slowly dissolving glass, and the rate of dissolution fits earlier reported data well.[73,74] The long degradation time of PLA also contributed to the limited mass loss observed in the scaffolds during the 10-week immersion.

DSC analysis revealed a high degree of stereocomplexation in PLA SC coatings, evidenced by the absence of homocrystal melting peaks for most PLA SC scaffolds. However, precise crystallinity measurements were unattainable, as bioactive glass present in the samples obscured the individual polymer masses. The T_g values of both PLLA and PLA SC were relatively high. For instance, the T_g value of 68°C for PLLA in both 0-week and 10-week scaffolds exceeded typical T_g values for PLA[11] but remained within the reported range.[75] The higher T_g values may result from the annealing process that was performed after scaffold coating. Comparable T_g values have been obtained by annealing[76–78] and physical aging at 40°C.[79] The 4°C T_g increase observed in PLA SC during the 10-week immersion in SBF may have resulted from volume relaxation leading to reduced segmental mobility of the polymer.[80] Conversely, the appearance of a crystallization peak at approximately 93°C for 10-week PLLA scaffolds may have resulted from increased polymer chain mobility caused by chain scission, resulting in a higher probability for crystal formation. Hydrolysis typically causes the degradation of amorphous regions first, increasing the mobility of undegraded chain segments and increasing crystallization potential.[81] These different behaviors may result from slower degradation of PLA SC compared to homocrystalline PLLA.[14] The T_m decrease of PLLA during hydrolysis and the unchanged T_m of stereocomplex crystallites have been reported previously.[14,82]

5 | CONCLUSIONS

We manufactured porous coated and uncoated bioactive glass scaffolds with potential applications in bone regeneration. Scaffolds with a PLA coating showed higher toughness than uncoated glass scaffolds, with an approximately fourfold increase in dry state and a twofold increase in wet state after up to 10-week immersion in SBF. Homocrystalline PLLA and stereocomplex PLA SC coatings had the highest average toughness with a significant difference to the amorphous PDLLA coating after immersion. Crucially, all coatings improved the handling characteristics of the scaffolds, which is essential for their potential clinical use.

CaP precipitation and subsequent hydroxyapatite formation are key indicators of glass bioactivity and important for cell attachment to scaffold surfaces. In our study, a CaP layer formed on the surface of all scaffolds after immersion in SBF. For uncoated scaffolds, the CaP layer was present on the glass surface, while for coated scaffolds, it had primarily formed on the surface of the PLA coating. Notably, the polymeric coating effectively moderated the initial potentially cytotoxic pH peak originating from the surface reactions of the bioactive glass.

Our findings indicate that the properties of bioactive glass scaffolds can be significantly enhanced using thin PLA-based coatings. In addition, using PLA stereocomplexes as coatings may offer additional benefits by increasing the overall toughness of the scaffold structure.

ACKNOWLEDGMENTS

The authors would like to thank Sara Kiran for her work on the foam replication method to produce glass scaffolds. We would also like to thank Dr. Tiina Saloranta-Simell for assistance with freeze drying, Jarl Hemming with the GPC measurements and Linus Silvander for the SEM analyses. Peter Uppstu is grateful for financial support from The Finnish Foundation of Technology Promotion, The Swedish Cultural Foundation in Finland, and the Åbo Akademi University Foundation.

DATA AVAILABILITY STATEMENT

Research data are not shared.

ORCID

Peter Uppstu https://orcid.org/0000-0002-6447-3355
Simon Engblom https://orcid.org/0000-0002-6460-5186
Leena Hupa https://orcid.org/0000-0001-7745-7779
Carl-Eric Wilén https://orcid.org/0000-0001-7720-3234

REFERENCES

1. Puppi D, Chiellini F, Piras AM, Chiellini E. Polymeric materials for bone and cartilage repair. *Prog Polym Sci*. 2010;35:403-440.
2. Lee S, Shin H. Matrices and scaffolds for delivery of bioactive molecules in bone and cartilage tissue engineering. *Adv Drug Deliv Rev*. 2007;59:339-359.
3. Tian H, Tang Z, Zhuang X, Chen X, Jing X. Biodegradable synthetic polymers: preparation, functionalization and biomedical application. *Prog Polym Sci*. 2012;37:237-280.
4. Tajbakhsh S, Hajiali F. A comprehensive study on the fabrication and properties of biocomposites of poly(lactic acid)/ceramics for bone tissue engineering. *Mater Sci Eng C*. 2017;70:897-912.
5. Lasprilla AJR, Martinez GAR, Lunelli BH, Jardini AL, Filho RM. Poly-lactic acid synthesis for application in biomedical devices — a review. *Biotechnol Adv*. 2012;30:321-328.
6. Narayanan G, Vernekar VN, Kuyinu EL, Laurencin CT. Poly (lactic acid)-based biomaterials for orthopaedic regenerative engineering. *Adv Drug Deliv Rev*. 2016;107:247-276.
7. Inkinen S, Hakkarainen M, Albertsson A, Sodergard A. From lactic acid to poly(lactic acid) (PLA): characterization and analysis of PLA and its precursors. *Biomacromolecules*. 2011;12:523-532.
8. Farah S, Anderson DG, Langer R. Physical and mechanical properties of PLA, and their functions in widespread applications—a comprehensive review. *Adv Drug Deliv Rev*. 2016;107:367-392.
9. Rahaman MH, Tsuji H. Synthesis and characterization of stereo multiblock poly(lactic acid)s with different block lengths by melt polycondensation of poly(L-lactic acid)/poly(D-lactic acid) blends. *Macromol React Eng*. 2012;6:446-457.
10. de Jong SJ, van Dijk-Wolthuis WNE, Kettenes-van dB, Schuyl PJW, Hennink WE. Monodisperse enantiomeric lactic acid oligomers:

preparation, characterization, and stereocomplex formation. *Macromolecules*. 1998;31:6397-6402.
11. Tsuji H. Poly(lactide) stereocomplexes: formation, structure, properties, degradation, and applications. *Macromol Biosci*. 2005;5:569-597.
12. Kakuta M, Hirata M, Kimura Y. Stereoblock polylactides as high-performance bio-based polymers. *Polym Rev*. 2009;49:107-140.
13. Bouapao L, Tsuji H. Stereocomplex crystallization and spherulite growth of low molecular weight poly(L-lactide) and poly(D-lactide) from the melt. *Macromol Chem Phys*. 2009;210:993-1002.
14. Tsuji H. In vitro hydrolysis of blends from enantiomeric poly(lactide)s. Part 1. Well-stereo-complexed blend and non-blended films. *Polymer*. 2000;41:3621-3630.
15. Tsuji H. In vitro hydrolysis of blends from enantiomeric poly(lactide)s. Part 4: well-homo-crystallized blend and nonblended films. *Biomaterials*. 2003;24:537-547.
16. Regnell Andersson S, Hakkarainen M, Inkinen S, Södergård A, Albertsson A. Customizing the hydrolytic degradation rate of stereocomplex PLA through different PDLA architectures. *Biomacromolecules*. 2012;13:1212-1222.
17. Tsuji H, Fukui I. Enhanced thermal stability of poly(lactide)s in the melt by enantiomeric polymer blending. *Polymer*. 2003;44:2891-2896.
18. Andersson SR, Hakkarainen M, Inkinen S, Södergård A, Albertsson A. Polylactide stereocomplexation leads to higher hydrolytic stability but more acidic hydrolysis product pattern. *Biomacromolecules*. 2010;11:1067-1073.
19. Haaparanta A, Uppstu P, Hannula M, Ellä V, Rosling A, Kellomäki M. Improved dimensional stability with bioactive glass fibre skeleton in poly(lactide-co-glycolide) porous scaffolds for tissue engineering. *Mater Sci Eng C*. 2015;56:457-466.
20. Uppstu P, Paakki C, Rosling A. In vitro hydrolysis and magnesium release of poly(d,l-lactide-co-glycolide)-based composites containing bioresorbable glasses and magnesium hydroxide. *J Appl Polym Sci*. 2015;132:42646.
21. Björkenheim R, Strömberg G, Ainola M, et al. Bone morphogenic protein expression and bone formation are induced by bioactive glass S53P4 scaffolds in vivo. *J Biomed Mater Res*. 2019;107:847-857.
22. Björkenheim R, Strömberg G, Pajarinen J, et al. Polymer-coated bioactive glass S53P4 increases VEGF and TNF expression in an induced membrane model in vivo. *J Mater Sci*. 2017;52:9055-9065.
23. Björkenheim R, Jämsen E, Eriksson E, et al. Sintered S53P4 bioactive glass scaffolds have anti-inflammatory properties and stimulate osteogenesis in vitro. *Eur Cell Mater*. 2021;41:15-30.
24. Eriksson E, Björkenheim R, Strömberg G, et al. S53P4 bioactive glass scaffolds induce BMP expression and integrative bone formation in a critical-sized diaphysis defect treated with a single-staged induced membrane technique. *Acta Biomater*. 2021;126:463-476.
25. Fukushima K, Kimura Y. Stereocomplexed polylactides (Neo-PLA) as high-performance bio-based polymers: their formation, properties, and application. *Polym Int*. 2006;55:626-642.
26. Garlotta D. A literature review of poly(lactic acid). *J Polym Environ*. 2001;9:63-84.
27. Tsuji H, Ikada Y. Stereocomplex formation between enantiomeric poly(lactic acid)s. XI. Mechanical properties and morphology of solution-cast films. *Polymer*. 1999;40:6699-6708.
28. López-Rodríguez N, Martínez de Arenaza I, Meaurio E, Sarasua JR. Improvement of toughness by stereocomplex crystal formation in optically pure polylactides of high molecular weight. *J Mech Behav Biomed Mater*. 2014;37:219-225.
29. Sarasua JR, Arraiza AL, Balerdi P, Maiza I. Crystallinity and mechanical properties of optically pure polylactides and their blends. *Polym Eng Sci*. 2005;45:745-753.
30. Takasaki M, Ito H, Kikutani T. Development of stereocomplex crystal of polylactide in high-speed melt spinning and subsequent drawing and annealing processes. *J Macromol Sci B*. 2003;42:403-420.
31. Furuhashi Y, Kimura Y, Yoshie N, Yamane H. Higher-order structures and mechanical properties of stereocomplex-type poly(lactic acid) melt spun fibers. *Polymer*. 2006;47:5965-5972.
32. Yan Z, Liao X, He G, et al. Green and high-expansion PLLA/PDLA foams with excellent thermal insulation and enhanced compressive properties. *Ind Eng Chem Res*. 2020;59:19244-19251.
33. Li W, Ren Q, Zhu X, et al. Enhanced heat resistance and compression strength of microcellular poly (lactic acid) foam by promoted stereocomplex crystallization with added D-mannitol. *J CO2 Util*. 2022;63:102118.
34. Cui W, Wei X, Luo J, Xu B, Zhou H, Wang X. CO2-assisted fabrication of PLA foams with exceptional compressive property and heat resistance via introducing well-dispersed stereocomplex crystallites. *J CO2 Util*. 2022;64:102184.
35. van Gestel NAP, Geurts J, Hulsen DJW, van Rietbergen B, Hofmann S, Arts JJ. Clinical applications of S53P4 bioactive glass in bone healing and osteomyelitic treatment: a literature review. *Biomed Res Int*. 2015;2015:684826.
36. Hench LL. Chronology of bioactive glass development and clinical applications. *New J Glass Ceram*. 2013;3:67-73.
37. Baino F, Hamzehlou S, Kargozar S. Bioactive glasses: where are we and where are we going? *J Funct Biomater*. 2018;9:25.
38. Fagerlund S, Massera J, Moritz N, Hupa L, Hupa M. Phase composition and in vitro bioactivity of porous implants made of bioactive glass S53P4. *Acta Biomater*. 2012;8:2331-2339.
39. Ylänen H, Karlsson KH, Itälä A, Aro HT. Effect of immersion in SBF on porous bioactive bodies made by sintering bioactive glass microspheres. *J Non Cryst Solids*. 2000;275:107-115.
40. Huang TS, Rahaman MN, Doiphode ND, et al. Porous and strong bioactive glass (13–93) scaffolds fabricated by freeze extrusion technique. *Mater Sci Eng C*. 2011;31:1482-1489.
41. Kolan KCR, Leu MC, Hilmas GE, Brown RF, Velez M. Fabrication of 13-93 bioactive glass scaffolds for bone tissue engineering using indirect selective laser sintering. *Biofabrication*. 2011;3:025004.
42. Chen QZ, Thompson ID, Boccaccini AR. 45S5 Bioglass®-derived glass–ceramic scaffolds for bone tissue engineering. *Biomaterials*. 2006;27:2414-2425.
43. Brink M. The influence of alkali and alkaline earths on the working range for bioactive glasses. *J Biomed Mater Res Part B: Appl Biomater*. 1997;36:109-117.
44. Fagerlund S, Massera J, Hupa M, Hupa L. T–T–T behaviour of bioactive glasses 1–98 and 13–93. *J Eur Ceram Soc*. 2012;32:2731-2738.
45. Brown RF, Day DE, Day TE, Jung S, Rahaman MN, Fu Q. Growth and differentiation of osteoblastic cells on 13–93 bioactive glass fibers and scaffolds. *Acta Biomater*. 2008;4:387-396.
46. Rezwan K, Chen QZ, Blaker JJ, Boccaccini AR. Biodegradable and bioactive porous polymer/inorganic composite scaffolds for bone tissue engineering. *Biomaterials*. 2006;27:3413-3431.
47. Fu Q, Saiz E, Rahaman MN, Tomsia AP. Bioactive glass scaffolds for bone tissue engineering: state of the art and future perspectives. *Mater Sci Eng C*. 2011;31:1245-1256.
48. Gerhardt L, Boccaccini AR. Bioactive glass and glass-ceramic scaffolds for bone tissue engineering. *Materials*. 2010;3:3.
49. Philippart A, Boccaccini AR, Fleck C, Schubert DW, Roether JA. Toughening and functionalization of bioactive ceramic and glass bone scaffolds by biopolymer coatings and infiltration: a review of the last 5 years. *Expert Rev Med Devices*. 2015;12:93-111.
50. Mohamad Yunos D, Bretcanu O, Boccaccini AR. Polymer-bioceramic composites for tissue engineering scaffolds. *J Mater Sci*. 2008;43:4433-4442.
51. Rahaman MN, Wei X, Wenhai H. Review—bioactive glass implants for potential application in structural bone repair. *Biomed Glass*. 2017;3:56.

52. Kokubo T, Kushitani H, Sakka S, Kitsugi T, Yamamuro T. Solutions able to reproduce in vivo surface-structure changes in bioactive glass-ceramic A-W3. *J Biomed Mater Res*. 1990;24:721-734.
53. Tsuji H. Poly(lactic acid) stereocomplexes: a decade of progress. *Adv Drug Deliv Rev*. 2016;107:97-135.
54. Danoux CB, Barbieri D, Yuan H, de Bruijn J, van Blitterswijk CA, Habibovic P. In vitro and in vivo bioactivity assessment of a polylactic acid/hydroxyapatite composite for bone regeneration. *Biomatter*. 2014;4:e27664.
55. Redondo FL, Giaroli MC, Ciolino AE, Ninago MD. Preparation of porous poly(lactic acid)/tricalcium phosphate composite scaffolds for tissue engineering. *Biointerface Res Appl Chem*. 2022;12:5610-5624.
56. Nieto H, Baroan C. Limits of internal fixation in long-bone fracture. *Orthop Traumatol Surg Res*. 2017;103:S61-S66.
57. Auregan J-C, Begue T. Induced membrane for treatment of critical sized bone defect: a review of experimental and clinical experiences. *Int Orthop*. 2014;38:1971-1978.
58. Bongio M, van den Beucken JJJP, Leeuwenburgh SCG, Jansen JJ. Development of bone substitute materials: from 'biocompatible' to 'instructive'. *J Mater Chem*. 2010;20:8747-8759.
59. Eqtesadi S, Motealleh A, Miranda P, Pajares A, Lemos A, Ferreira JMF. Robocasting of 45S5 bioactive glass scaffolds for bone tissue engineering. *J Eur Ceram Soc*. 2014;34:107-118.
60. Fiume E, Ciavattini S, Verné E, Baino F. Foam replica method in the manufacturing of bioactive glass scaffolds: out-of-date technology or still underexploited potential? *Materials*. 2021;14:2795.
61. Zhang D, Leppäranta O, Munukka E, et al. Antibacterial effects and dissolution behavior of six bioactive glasses. *J Biomed Mater Res*. 2010;93A:475-483.
62. Drago L, Toscano M, Bottagisio M. Recent evidence on bioactive glass antimicrobial and antibiofilm activity: a mini-review. *Materials*. 2018; 2:11.
63. Stoor P, Söderling E, Salonen JI. Antibacterial effects of a bioactive glass paste on oral microorganisms. *Acta Odontol Scand*. 1998;56: 161-165.
64. El-Ghannam A, Ducheyne P, Shapiro IM. Formation of surface reaction products on bioactive glass and their effects on the expression of the osteoblastic phenotype and the deposition of mineralized extracellular matrix. *Biomaterials*. 1997;18:295-303.
65. El-Rashidy AA, Roether JA, Harhaus L, Kneser U, Boccaccini AR. Regenerating bone with bioactive glass scaffolds: a review of in vivo studies in bone defect models. *Acta Biomater*. 2017;62: 1-28.
66. Kaysinger KK, Ramp WK. Extracellular pH modulates the activity of cultured human osteoblasts. *J Cell Biochem*. 1998;68:83-89.
67. Arnett TR. Extracellular pH Regulates Bone Cell Function. *J Nutr*. 2008;138:415S-418S.
68. Jones JR. Review of bioactive glass: from Hench to hybrids. *Acta Biomater*. 2013;9:4457-4486.
69. Wang X, Zhang Molino B, Pitkänen S, et al. 3D scaffolds of polycaprolactone/copper-doped bioactive glass: architecture engineering with additive manufacturing and cellular assessments in a coculture of bone marrow stem cells and endothelial cells. *ACS Biomater Sci Eng*. 2019;5:4496-4510.
70. Oudadesse H, Najem S, Mosbahi S, et al. Development of hybrid scaffold: bioactive glass nanoparticles/chitosan for tissue engineering applications. *J Biomed Mater Res Part A*. 2020;109:590-599.
71. Bochicchio B, Barbaro K, De Bonis A, Rau JV, Pepe A. Electrospun poly(D,L-lactide)/gelatin/glass-ceramics tricomponent nanofibrous scaffold for bone tissue engineering. *J Biomed Mater Res Part A*. 2020; 108:1064-1076.
72. Plyusnin A, Kulkova J, Arthurs G, Jalava N, Uppstu P, Moritz N. Biological response to an experimental implant for tibial tuberosity advancement in dogs: a pre-clinical study. *Res Vet Sci*. 2020;128:183-196.
73. Nommeots-Nomm A, Labbaf S, Devlin A, et al. Highly degradable porous melt-derived bioactive glass foam scaffolds for bone regeneration. *Acta Biomater*. 2017;57:449-461.
74. Sinitsyna P, Karlström O, Sevonius C, Hupa L. In vitro dissolution and characterisation of flame-sprayed bioactive glass microspheres S53P4 and 13–93. *J Non Cryst Solids*. 2022;591:121736.
75. Madhavan Nampoothiri K, Nair NR, John RP. An overview of the recent developments in polylactide (PLA) research. *Bioresour Technol*. 2010;101:8493-8501.
76. Park S, Todo M, Arakawa K. Effect of annealing on the fracture toughness of poly(lactic acid). *J Mater Sci*. 2004;39:1113-1116.
77. Tábi T, Sajó IE, Szabó F, Luyt AS, Kovács JG. Crystalline structure of annealed polylactic acid and its relation to processing. *Express Polym Lett*. 2010;4:659-668.
78. Dong T, Yu Z, Wu J, et al. Thermal and barrier properties of stretched and annealed polylactide films. *Polym Sci Ser A*. 2015;57:738-746.
79. Pan P, Zhu B, Inoue Y. Enthalpy relaxation and embrittlement of poly(l-lactide) during physical aging. *Macromolecules*. 2007;40:9664-9671.
80. Bergström J, Hayman D. An overview of mechanical properties and material modeling of polylactide (PLA) for medical applications. *Ann Biomed Eng*. 2016;44:330-340.
81. Södergård A, Stolt M. Properties of lactic acid based polymers and their correlation with composition. *Prog Polym Sci*. 2002;27:1123-1163.
82. Pekarek Leach KJ, Mathiowitz E. Degradation of double-walled polymer microspheres of PLLA and P(CPP:SA)20:80. I In vitro degradation. *Biomaterials*. 1998;19:1973-1980.

How to cite this article: Uppstu P, Engblom S, Inkinen S, Hupa L, Wilén C-E. Influence of polylactide coating stereochemistry on mechanical and in vitro degradation properties of porous bioactive glass scaffolds for bone regeneration. *J Biomed Mater Res*. 2024;112(1):e35328. doi:10.1002/jbm.b.35328

ISBN 978-952-12-4338-7